SPbGASU
1832

ARCHITECTURE & ENGINEERING

Volume 10
Issue 1
March, 2025

By Architects. For Architects.
By Engineers. For Engineers.

Architecture
Civil and Structural Engineering
Mechanics of Materials
Building and Construction
Urban Planning and Development
Transportation Issues in Construction
Geotechnical Engineering and Engineering Geology
Designing, Operation and Service
of Construction Site Engines

eISSN: 2500-0055
http://aej.spbgasu.ru/

Architecture and Engineering

Volume 10 Issue 1 (2025)

ISSN: 2500–0055

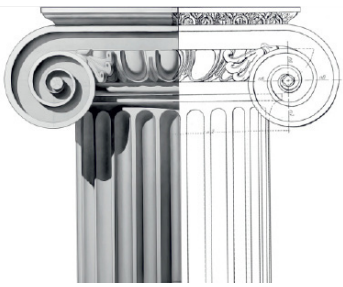

CONTENTS

Architecture and Engineering
peer-reviewed scientific journal
Start date: 2016/03
4 issues per year

Founder, Publisher:
Saint Petersburg State University of Architecture and Civil Engineering

Indexing:
Scopus, Russian Science Citation Index, Directory of Open Access Journals (DOAJ), Google Scholar, Index Copernicus, Ulrich’s Periodicals Directory, WorldCat, Bielefeld Academic Search Engine (BASE), Library of University of Cambridge and CyberLeninka

Corresponding address:
4 Vtoraya Krasnoarmejskaja Str.,
St. Petersburg, 190005, Russia

Website: http://aej.spbgasu.ru/
Phone: +7(812) 316 48 49
Email: aejeditorialoffice@gmail.com

Date of issue: March 28, 2025

The Journal was re-registered by the Federal Service for Supervision of Communications, Information Technologies and Mass Communications (Roskomnadzor) on May 31, 2017;
registration certificate of media organization El No. FS77–70026

DOI: 10.23968/2500-0055-2025-10-1-3-15

CRITICAL REVIEW OF MUSEUM ARCHITECTURE FROM A NEURO-ARCHITECTURE PERSPECTIVE

İlker Erkan

Faculty of Architecture, Suleyman Demirel University, 32260, Çünür, Isparta, Turkey

*Corresponding author's email: ilkererkan@sdu.edu.tr

Abstract

Introduction: This study focused on the behavior of people in museums. Museum visitors are known to explore the works of art through various presentation methods. People's behavior during the museum exhibit was analyzed. The **purpose of the study** was to obtain physiological responses to indoor and outdoor tours in terms of neuro-architecture. Therefore, the focus was on evaluating the cognitive responses people have to spaces during museum tours. Based on this evaluation, it aimed to make spatial arrangements more human-centered. **Methods**: The study was conducted in a virtual reality environment. A virtual museum was designed for the study, and experiments took place in this museum. Unlike other studies, this study used Electroencephalogram (EEG), Eye Tracking (ET), Heart Rate Variability (HRV), and Skin Conductance Response (SCR) techniques. The focus was on two presentation methods commonly used in museums: audio description (AD) and information board (IB). As a **result**, most striking findings came from the examination of the AD+IB presentation technique. EEG records and the data from other physiological measurement devices indicated that the AD+IB presentation technique induced stress in the visitors. That is, the participants could not focus enough on the works of art. Audio description alone was found very effective in museum visits. However, if it was used simultaneously with information board (IB), the effect of the artworks on the visitors was reduced to a minimum.

Keywords: interior design; neuro-architecture; museum architecture; cognitive design.

Introduction

Human perception often tries to recognize or identify objects when viewing them in everyday life. This perception is engaged when viewing and observing artworks in galleries and museums. It sometimes offers the opportunity to recognize the work of art and evoke proper cognitive responses. Cupchik et al. (2009) described this experiential perception as a particular psychological process, characterized by a focus on objects (works of art) and suppression of everyday concerns. If this particular psychological process is managed in the right way, it is possible to perceive the presented works correctly. Although the studies explain the cognitive processes involved in the perception and evaluation of works of art, the aesthetic experiences they provide and the related stimuli are still controversial. Some studies claim that such criteria as stimuli, colors, symmetry, and mathematical proportions in works of art play an essential role in promoting people's aesthetic experiences (Jacobsen and Höfel, 2003). Museums are entities presenting millennia-long history. Planning museum areas, especially museum architecture, covers protection, restoration, security, and display. The primary purpose here is for visitors to view the exhibits comfortably. Many researchers focused on visitors' behavior (Del Chiappa et al., 2014; Huber at al., 2019; Nurse Rainbolt et al., 2012; Ross et al., 2012; Skov et al., 2018; Trunfio et al., 2022) and highlighted the importance of museum architecture in shaping these behaviors.

On the other hand, Livio (2008) stated that titles, text, and other art structures could influence aesthetic assessments of visitors. This experience is intense in museums and art galleries. Therefore, there are many specific factors, from the presentation style of the works to the lighting method, the choice of architectural colors, the design of the space in museums and art galleries, to focus on the works of art. According to Becker (2008), the way objects or collections are presented and positioned can evoke various emotions in people. Thus, arranging or displaying the exhibited elements is crucial for creating spatial environments for people and enhancing cognitive recall mechanisms associated with space. Hence, researchers who emphasized the importance of designing museums and exhibition spaces correctly (MacLeod et al., 2015; Olesen et al., 2020; Wineman and Peponis, 2010) stated that this is not enough. They indicate that even the locations of objects are essential for museum design and human experience (Alberti, 2005; Antonelli et al., 2003).

Museums have to offer the necessary comfort values and establish a communication-interaction between the visitors and works of art when presenting their identity. In this respect, visiting a museum can be an exciting, aesthetically impressive, and multifaceted experience that involves learning and having fun (Pine and Gilmore, 1998). In addition to museums' functionality today, different methods have been developed for the correct presentation of the exhibited works. First, an information board is located next to the object exhibited. This method, called the Information Board (IB), involves placing boards at specific points. These information boards are placed at an angle and in size that users can see.

An audio description system gives detailed information/contents about the work exhibited if requested. Audio Description (AD) is a verbal description method that aims to make visual elements of objects exhibited in museums and/or galleries accessible by a voice guide. Within the context of both the research and practice, the AD is in a relatively early development stage compared to the information board. There were studies evaluating how Audio Description (AD) meets visitors' demands and assessing the effect of auditory narrative on visitors' understanding (Braun, 2008; Hutchinson and Eardley, 2019; Walczak and Fryer, 2017).

Neuro-architecture, especially in recent years, has been offering new analysis and examination methods by looking at architectural research from different perspectives. Combining neurosciences with architecture, neuro-architecture enhances the field of architecture, particularly in human-centered design aspects (Higuera Trujillo et al., 2016), from wayfinding to spatial analysis (Prandi et al., 2023), from urban design (Erkan, 2024b) to spatial sensations (Erkan, 2024a).

This study was designed to measure the neuro-cognitive effects created by the presentation methods on museum visitors, rather than making cognitive assessments of the works of art themselves. Thus, the study questions the cognitive effects of the two essential elements (information boards and the audio description system) that appear in today's museums and are used to present the works of art.

Methods

This study used a method involving neuro-architecture tools.

Participants

The study was conducted with 304 volunteers (mean age = 25.6, SD = 1.9, 144 males). Having healthy vision, good cardiac health, healthy psychological condition, and not receiving any stimulant medication were prerequisites for inclusion in the study. All participants were right-hand dominant.

Experimental Environment

The study was completed in about 11 months. The experimental environment was prepared and isolated from the outside for the study. The environment of appropriate temperature and humidity was provided for the study to allow a comfortable setting for the participants.

Apparatus

The experiment employed the following technical means: one electroencephalography (EEG) monitor, one virtual reality headset (VR), one eye-tracking device (ET), one galvanic skin conductance response device (SCR), one Wii controller (WII), and one heart rate variety (HRV) device. The participants were introduced to the devices and provided with the needed information before the experiment began. Participants who were not eligible for any of these devices were excluded from the experiment.

Experimental Procedure

All stages of the experiment were explained to the participants individually before starting the experiment. At this stage, participants who did not want to be involved in the experiment were excluded from the study. A museum was designed in a virtual reality environment for the experiment. The entire experiment was developed to analyze the current presentation methods that people encounter during museum visits. Two different areas were designed for the experimental stages:

The first space consisted of an "exhibition designed entirely in open space". The architectural space, called the outdoor exhibition area, contained architectural landscape elements and urban furniture. There were sculptures, archaeological remains, paintings, and objects in different artistic styles exhibited outdoors. Participants passed through this outdoor exhibition to the second stage of the experiment.

The second stage was an indoor exhibition space. This indoor space was designed with an open architectural style and presented artistic objects of different disciplines (paintings, sculptures, etc.). The action plan of the participants in the experimental environment is shown in Fig. 1.

The primary reason the experiment was designed to move from outdoors to indoors is that it closely mirrors real life. That is, people who want to visit the museum approach the building in a specific direction. In other words, when people approach the buildings (especially the buildings with an architectural identity, such as a museum), they exhibit specific emotional responses. Therefore, recording these responses was of importance for the study.

Both environments were designed with Cinema 4D and transferred to a virtual reality environment with the help of C++. Objects of different artistic styles (from sculptures to paintings, handwork, etc.) in both of the designed spaces (indoors and outdoors) cater to many different art disciplines (Appendix 1). All the participants visited the outdoor and indoor exhibition areas one by one. The participants were required to

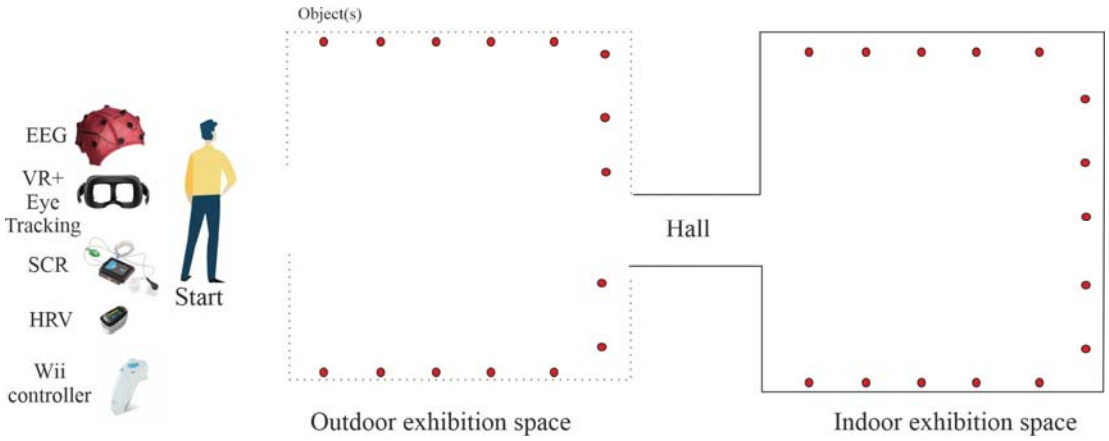

Fig. 1. Experimental architecture plan

see all the works. The participants were required to wait a maximum of 180 seconds when they arrive in front of the exhibited works of art. At the end of this period, the system automatically redirected them to the other object, and no participant exceeded this period. Fig. 2 shows an example of the indoor space and the display area in front of the exhibited object, as seen by the virtual reality goggles.

As shown in Fig. 2, a specific approach was set to each exhibited work. Visitors faced three different options in front of the exhibited works of art (paintings, sculptures, reliefs, etc.).

The first option was the information board (IB) in front of the displayed element. This board contained 300 words of information about the work of art. The participants were asked to read the IB texts on the works.

The second option provided just the audio description (AD) system, without an information board, when participants approached an object. Information about the exhibited work was narrated through the headset to the viewer. This voice guide narrated 300 words of information to the visitors.

The third option (IB+AD) was a combination of information board and audio description (IB+AD) in front of the exhibited work. While the participants were reading the information board, they were also informed via a headset. Besides the 300-word information board, different 300 words were provided by the voice guide. In other words, the information board and the voice guide system had different information. Fig. 3 shows a simple diagram of the visitors' navigation.

There was a total of 30 objects, with 15 of these objects exhibited outdoors, and 15 indoors. Each participant tested different presentation methods indoors and outdoors five times each. In other words, it was possible to test AD for 10 objects, IB for 10, and the AD+IB for another 10 objects indoors and outdoors. The participants traveled in a virtual reality environment using the Wii remote. With it, they were able to turn right, left, and move back and forth. The participants were also asked to rate the work displayed

Fig. 2. The larger picture – the indoor space visited by participants, and the smaller one depicts the virtual reality environment when they reach the artworks

on the screen from 1 to 10 (10 being the best) after examining all three stages. After the participants rated the objects, the experiment continued.

In the final stage of the experiment, participants were asked about the works they saw/remembered in the virtual reality environment after completing their indoor and outdoor museum tours. This process was performed with the "WHILE NAVIGATING" software developed for this study. The interface of the software developed is shown in Appendix 2. With the help of the software developed, 60 different works of art were shown to the participants at 5-second intervals. In other words, this stage also included 30 different exhibition elements that were not shown in the previous stages. This stage determined the objects the participants were able to recall.

Analysis

Statistical Analysis

To explore the relationships among skin conductance data, heart rate data, EEG data, and architectural liking scores, we employed a general linear model (ANOVA) for repeated measurements using R software. We established a significance

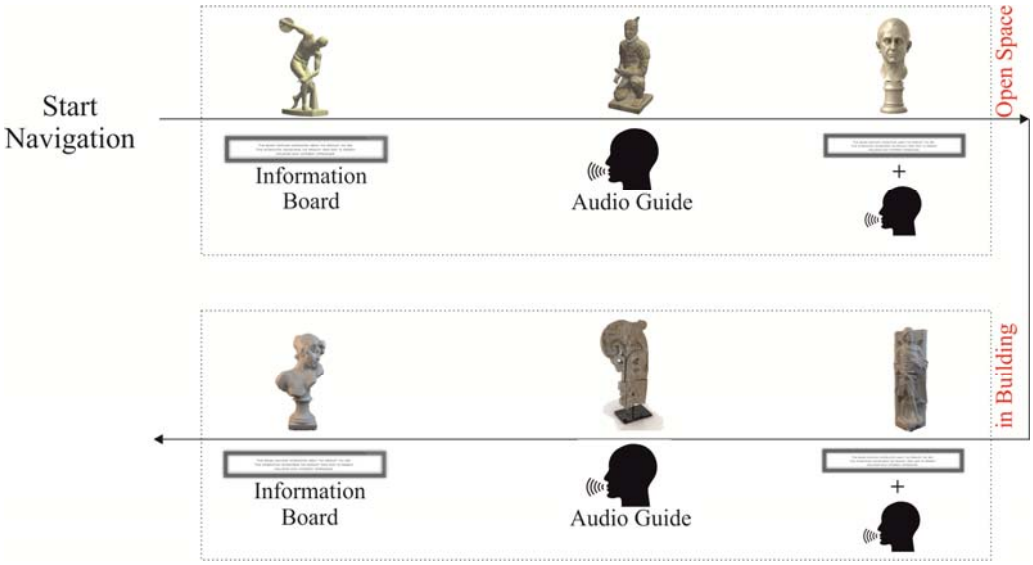

Fig. 3. Example of participants' navigation route

threshold of $p < 0.05$. To further investigate potential double significance across different conditions, we conducted t-tests on these variables, also with a significance level of $p < 0.05$. Additionally, we utilized bootstrap methods in EEGLAB for a comprehensive analysis of the EEG data, maintaining a significance level at $p < 0.05$. This multi-faceted approach enhances our understanding of the data and findings.

EEG Data

A 14-channel EEG device was used for this study. Data processing was carried out using the toolbox software developed for this study with MATLAB. This software uses Fast Fourier Transform (FFT) to analyze the spectral power of EEG rhythms, following the methods of Polat and Güneş (2007) and Murugappan et al. (2014). Eye blinks were corrected as described by Gratton et al. (1983), and the quality of all electrodes was assessed to minimize the impact of poor channels on the analysis.

Five different cases were taken into account when analyzing the EEG data:

• first case, brain images of the visitors recorded during the museum visits only in the information board (IB) setting;

• second case, brain images of the visitors recorded during the museum visits only in the audio description (AD) setting;

• third case, brain images of the participants recorded during the museum visits in both IB and AD (IB+AD) setting;

• fourth case, brain images of the participants recorded while rating the works of art;

• fifth case, the participants' responses during the "recall test" at the end of the experiment.

Skin Conductance Response (SCR)

SCR reflects excitement-related physiological reactions, and physiological or psychological stimuli. Fear, joy, or stress are the conditions that affect skin conductance (Dawson et al., 2011). Skin conductance is used to indicate ongoing emotional processes and emotional arousal. It is a reliable measurement technique. Skin conductance data were collected from the participants using SCR wristbands. The participants were fitted with wristbands prior to any equipment; the data were recorded continuously until completion of the entire experiment. The SCR signals were recorded from the left fingers.

Heart Rate Variability (HRV)

HRV analyses are regarded as an indicator of autonomic nervous system activity, which is responsible for the body's involuntary movements (Acharya et al., 2006). Heart rate variability (HRV) provides an insight into the cardiovascular autonomic function using RR intervals (interval variance).

A polar HR sensor was used in the study. The HR sensor was set on a strap attached to the participants' chests. HRV is used for determining power spectral density, sympathetic and parasympathetic autonomic nervous system activities. In the power spectrum, the low-frequency component (LF) ranges from 0.04 to 0.15 Hz, influenced by both sympathetic and parasympathetic activities. Meanwhile, the high-frequency component (HF), which is between 0.15 and 0.4 Hz, is primarily affected by parasympathetic activity. LF/HF ratio is regarded as an indicator of sympathovagal balance (Massaro and Pecchia, 2019). In studies conducted to measure and evaluate stress, the most commonly used parameters are the mean heart rate (HR), LF, HF, and LF/HF (Taelman et al., 2009).

Eye Tracking

The basic idea behind the eye-tracking technique is to make inferences about cognitive processes based on eye movements (Jacob and Karn, 2003). The eye-tracking device used in the study was

placed inside the virtual reality goggles. Thus, the participants' eye-tracking responses to the spaces were recorded while they navigated the museum in a virtual reality environment. In the eye-tracking study, a heat map and fixation count were examined. The heat maps show the points that participants are looking at and the duration of their gazes. It is a color-coded measurement data formed by combining points of view, fixation points, and dynamic (moving) points. It is a method to see the points of the objects that draw attention. Heat maps visualize the focus areas, from green to red, indicating less focus to more intense focus, respectively. Red areas show a high focus count and an increased level of interest, while yellow and green areas show a lower focus count, hence weaker visual interest.

The Fixation Count analysis shows how many times people focus on these areas in total. In the analysis, the view screen is divided into segments as desired. The focus count data of the participants were processed into these segments, together with the colorings determined by the focus intensity.

Liking Score

The participants were asked to give a score between 1 and 10 to each work of art on the screen after examining the objects in all three stages. This rating was mandatory, and the experiment could not continue unless the participant rated the object. Each participant rated both the indoor and outdoor works. The analysis of the liking scores was inspired by Erkan (2021). Statistical values were calculated for the scores given by each participant. The participants gave liking scores for both indoor and outdoor spaces.

Recall Test

A special software was developed for this study. This software tried to determine which works were recalled by the participants in the space they visited. The recall test was the final stage of the experiment. At this stage, the participants were asked, with the help of the software interface shown in Appendix 2, if they had seen the objects on the screen.

Results and Discussion

The study explored the cognitive and physiological impacts of various presentation techniques in museums by utilizing different physiological measurement devices and examining how these effects are reflected in museums. The study used such physiological measurement instruments as SCR and HRV. A cognitive analysis was performed using EEG. The eye-tracking device identified the participants' points of focus. The author developed a software for a recall test, "Remember-Again", to reveal recall statuses of the participants. In addition, architectural liking scores of the participants regarding the works were analyzed.

The study focused on the prefrontal cortex and orbitofrontal cortex, as they are specifically related to the understanding, decision-making, and selection processes in humans. During the IB stage, visitors tried to comprehend the objects by focusing solely on the text they had read. During the IB stage, the prefrontal cortex was the most active region of the participants' brains. If it is examined in more detail by taking the Talairach Stereotactic System into account with the approach by Koessler et al. (2009), intense interaction with the "dorsolateral prefrontal cortex" is observed. The prefrontal cortex has been associated with various cognitive processes, from identification to perception and viewing (Siddiqui et al., 2008). However, when an individual experiences a stressful situation, changes in the prefrontal cortex can occur, which can lead to lower decision-making abilities and error handling (Arnsten, 2009) and a decline in working memory (Qin et al., 2009). In this study, alpha activity in the frontal lobe was examined in detail. A decrease in alpha activity in the dorsolateral prefrontal cortex was detected, especially during the IB+AB stage, and this decrease is believed to be stress-induced. The decreasing tendency in alpha activity in EEG analysis may also result from a decline in people's perception or reasoning about the objects. This result is due to the stress caused by reading and listening simultaneously.

However, theta activity in the frontal region was studied in three different stages. As with alpha activity, frontal theta activity was significantly reduced during the AD+IB stage. Our findings confirm the theory by Mizuki et al. (1992) that frontal theta synchronization is associated with decreased anxiety; as supported by EEG records, the third stage is more stressful than two other stages (Fig. 4).

Changes in SCR and HRV data were also observed when there was a decrease in EEG alpha wave while the subjects were under acute stress (Fig. 5).

SCR records showed that the participants' SCR values increased during the AD+IB stage and decreased during the IB stage. The HRV data of the same participant was obtained. Both HRV and SCR analyses demonstrated that the 3rd (IB+AD) stage was the most stressful. Physical and mental burden significantly affects the cardiovascular response. Stressors cause decreased oscillations in heart rate variability (HRV) that reflect parasympathetic nervous system activity. Accordingly, the LF/HF ratio increases. In individuals experiencing stress, cardiovascular responses may persist even during the periods of rest. Studies report that short-acting stressors suppress the parasympathetic nervous system and increase sympathetic nervous system activity (Acharya et al., 2006). Low LF/HF ratio was evaluated as an indicator of increased vagal activation. The mean and standard deviations of HRV and related parameters obtained from all participants are shown in Table 1.

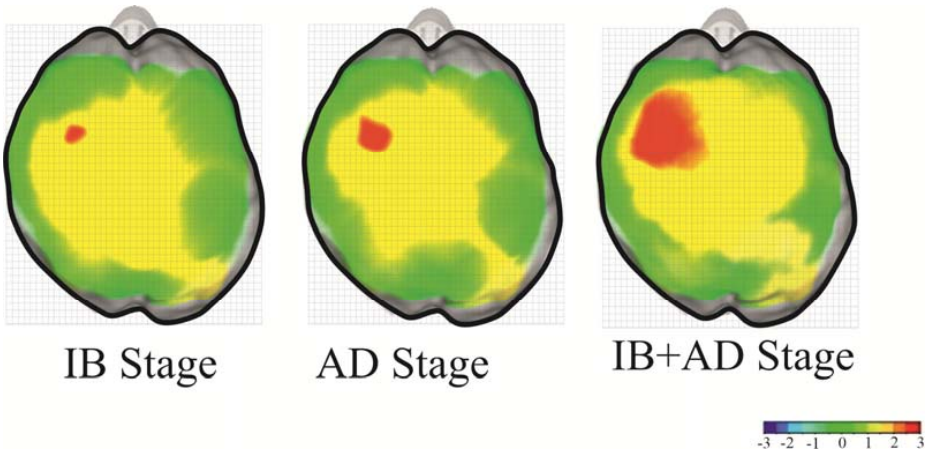

Fig. 4. Brain map showing the state of alpha and theta activity in the prefrontal cortex in the first three stages

Statistical HF values were found to decrease in all participants in the careful analysis of the experimental stages. The decreased parasympathetic activity was associated with people exposed to fatigue, stress, and anxiety (Kemp et al., 2017; Shaffer and Ginsberg, 2017).

Table 1 also showed that an increase in participants' LF/HF ratio was statistically significant during the same experimental stages. Therefore, when both HF and LF/HF ratios are examined, it can be stated that participants face the most intense stress during the AD+IB stage. Statistical values of

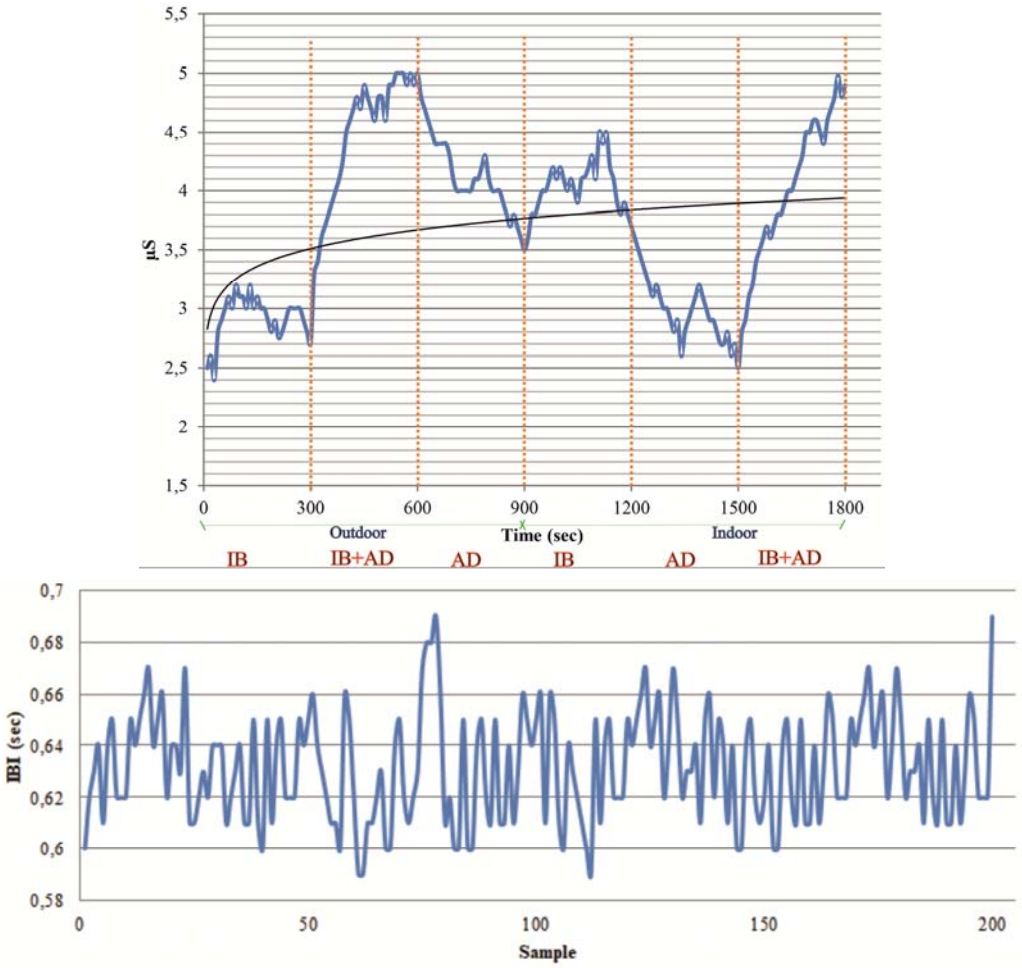

Fig. 5. SCR and HRV graph recorded when a participant was navigating both the indoor and outdoor spaces with different presentation methods

Table 1. **Comparison of the HRV feature results for different presentation types**

Presentation/HRV	IB		AD		IB+AD	
	Avg	SD	Avg	SD	Avg	SD
Inter-Beat Interval (IBI) (Avg)	700.45	134.45	700.14	124.47	700.15	121.14
HR (Avg)	84.14	16.45	84.11	14.11	83.77	12.47
Low frequency (LF), ms²	304.48	277.47	412.14	341.44	421.74	377.89
High frequency (HF), ms²	221.45	265.84	219.11	231.40	205.14	212.01
LF/HF	1.89	1.21	1.92	1.45	1.98	1.67

skin conductance were collected in all stages of the experiment. Average skin conductance attributes obtained by SCR devices for all participants are presented in Table 2. In this comprehensive study, an increase was observed in all statistical findings related to skin conductance.

Changes in SCR were found to reflect the stress levels of individuals. Analysis of the SCR data showed that SCR increased among users as their cognitive load increased. When different presentation techniques were analyzed, all statistical findings were observed in the data on skin conductance. SCR was at its highest in the AD+IB stage. Thus, SCR data can be correlated with the stresses the participants experienced in the AD+IB stage.

Table 2. **Comparison of SCR feature results for different presentation types**

Skin Conductance Attribute Types	IB		AD		IB+AD	
	Avg	SD	Avg	SD	Avg	SD
Min	2.12	0.95	2.21	0.98	2.31	1.02
Avg	2.42	0.96	2.84	0.97	2.96	1.01
Max	2.78	1.16	2.96	0.99	3.24	1.12
SD	0.12	0.04	0.14	0.06	0.21	0.08
Median	2.41	1.05	2.74	1.05	2.88	1.04
Skewness	–0.44	1.14	–0.21	0.78	–0.10	0.98
Kurtosis	3.44	1.42	3.88	1.49	3.99	1.24

In addition to SCR and HRV analyses, eye-tracking data showing the focus of the participants were collected. Fig. 6 shows a participant's eye-tracking analysis in the same artist's works in different presentation techniques.

As shown in Fig. 6, in the AD setting, the participant scrutinized the work of art in detail and even concentrated on many areas, as confirmed by total fixation count (fixation count in the AD setting Avg:439.46 SD:36.92, fixation count in the IB+AG setting Avg:354.43 SD:26.63). In the study, participants focused on specific areas in the IB+AD environment, as reflected in heat map analysis, and the cause for this might have been the participants' distraction.

Also, the eye-tracking heat map of almost all visitors (96.65 %) showed that the smallest areas were in the AD+IB stage. In other words, at the AD+IB stage, the areas that people look at and even examine carefully are smaller than those in other settings. Besides, each object was examined separately in the fixation count analysis. The fixation counts of a total of 30 objects grouped by presentation methods are shown in Fig. 7.

The fixation count analysis can be efficient for studies that deal with the focus on the desired area rather than the focus duration. It was found that the total focus count on the works was greater in the AD setting compared to others.

Finally, the liking status of the participants was evaluated. Given that they were obliged to rate the works from 1 to 10, it was possible to determine the

Fig. 6. Heat map in paintings that a participant examined in different presentation techniques

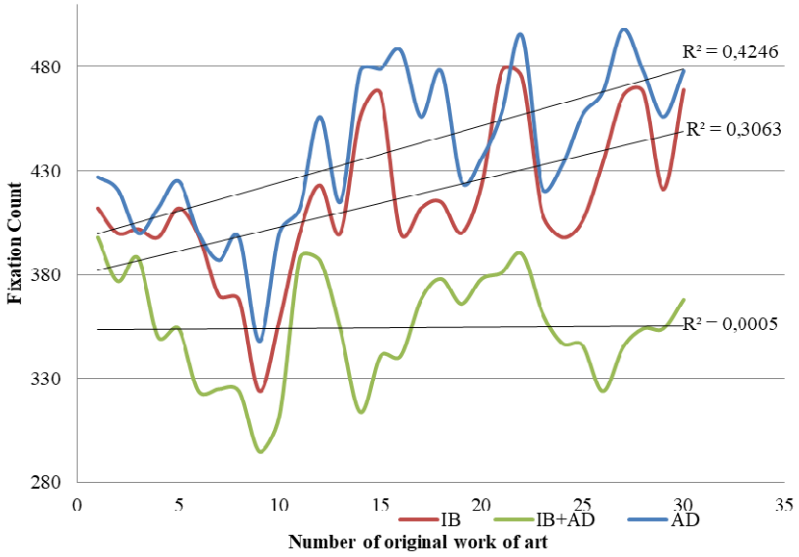

Fig. 7. Examination of the participants' fixation count analysis for each presentation technique

participants' architectural liking about the indoor and outdoor spaces. The results of repeated analyses for IB, AD, and IB+AD environments, which are independent variables in the study, are shown in Table 3.

The total liking scores for the indoor and outdoor were analyzed, and the binary differences between the three settings were statistically significant. Participants were asked which objects they remembered during their museum visits. The primary purpose here was to measure which space and which presentation setting was suitable for recalling the objects. The participants examined a total of 30 different works of art (15 were outdoors) during their museum trips. However, the participants were shown 60 works during the recall test. The goal here was to find the recall percentages of 30 different objects in total. In the recall test performed indoors and outdoors, the average for the indoor space (12.68, SD: 1.78) was higher than that for the outdoor space (11.59, SD: 1.67). Each participant's recall percentages, for both indoors and outdoors, are shown in Fig. 8.

Table 3. **Results of repeated analyses for IB, AD, and IB+AD settings**

Pairwise Comparisons						
Indoor						
(X)	(Y)	Mean Difference (X-Y)	Std. Error	Sig.[b]	95 % Confidence Interval for Difference[b] (Bonferroni)	
					Lower Bound	Upper Bound
IB	AD	0.964*	0.071	0.000	0.792	1.135
	IB+AD	2.306*	0.063	0.000	2.154	2.458
AD	IB	–0.964*	0.071	0.000	–1.135	–0.792
	IB+AD	1.342*	0.074	0.000	1.163	1.521
IB+AD	IB	–2.306*	0.063	0.000	–2.458	–2.154
	AD	–1.342*	0.074	0.000	–1.521	–1.163

* The mean difference is significant at the 0.05 level

Outdoor

(X)	(Y)	Mean Difference (X-Y)	Std. Error	Sig.[b]	95 % Confidence Interval for Difference[b] (Bonferroni)	
					Lower Bound	Upper Bound
IB	AD	1.643*	0.094	0.000	1.418	1.869
	IB+AD	2.949*	0.084	0.000	2.746	3.152
AD	IB	–1.643*	0.094	0.000	–1.869	–1.418
	IB+AD	1.306*	0.081	0.000	1.112	1.500
IB+AD	IB	–2.949*	0.084	0.000	–3.152	–2.746
	AD	–1.306*	0.081	0.000	–1.500	–1.112

* The mean difference is significant at the 0.05 level

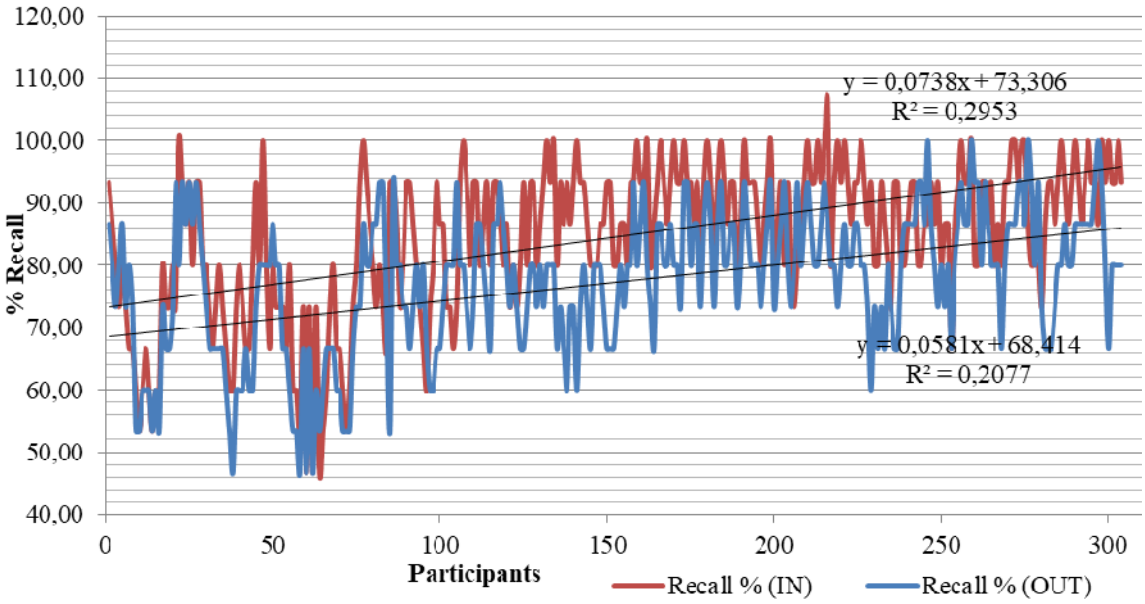

Fig. 8. Indoor and outdoor recall percentages of the participants

The participants usually had a better recollection of the indoor objects (t-value = 7.75003, $p < 0.00001$.). Another important finding was that participants in both the AD+IB setting and outdoors had the least recall percentage.

Conclusion

The study investigated presentation methods of exhibited objects in a virtual reality environment using different measurement techniques. Detailed analyses resulted in the following conclusions.

One of the most striking findings of the study was the examination of the AD+IB presentation technique. EEG records and the data from other physiological measurement devices indicated stress during this presentation technique; that is, the participants could not focus enough on the works of art. There follows a chain reaction. As a result of the stress experienced during this presentation technique, the visitor, who cannot concentrate on the work, cannot examine it adequately and gives it a lower score. Remarkably, the recall rate is at its lowest with this presentation technique.

While the IB setting is traditionally considered helpful in understanding art, eye-tracking analysis shows the AD setting is more beneficial.

In addition, we analyzed two different environments (indoors and outdoors) for three different presentation techniques. In these three settings, the average liking scores were found to be different. Moreover, the statistical analysis showed that this difference was statistically significant.

The recall rate of exhibited objects in the indoor space was much higher than that in outdoors. This recall rate may be due to the stimulating factors of the outdoors. Therefore, it is recommended to minimize outdoor stimulating factors and pay attention to this critical point when designing outdoor display units.

The study showed that the IB presentation method alone was not enough for people to understand the works of art. The AD method has significant importance for perceiving art, according to many physiological tests. In addition, it is clear that examining art in an IB+AD setting is not beneficial for visitors and hinders understanding in the museum.

Given that one of the primary goals of museum architecture is to offer genuine access to the museum experience, museums must acknowledge the visual information of visitors and consider the social, cognitive, and emotional aspects of their visits. From this perspective, it is believed that audio description systems (AD) will help museums of the future to evolve beyond the visual museum concept.

The study is expected to aid virtual tours and online presentations of artworks. During the pandemic, museums relied heavily on virtual presence to highlight their collections. This study could help the developers of virtual museum tours regarding the use of emerging technologies and user interfaces to improve presentation techniques. This paper also emphasizes the value of universal access to collections for those who cannot physically visit a museum due to medical risks or distance, which may help address the underrepresentation of certain groups in existing visitor populations. The study can also improve experts' experience prior to visits by assisting practitioners and museum managers in understanding visitors' desires and getting ready for an in-person meeting.

The paper can also be reframed to understand the importance of virtual examination of artworks in future studies. This paper helps practitioners understand the growing interest in virtual representation that

deepens interaction with works of art outside the museum. Different physiological and cognitive approaches can be experimented with, considering the better utilization of virtual infrastructures.

The study considered only indoor and outdoor space interactions as architectural influences. It can be improved in further studies to incorporate color, light, and even space geometry studies. This way, the effects of different stimuli on people's cognitive states can also be studied for the spaces in question. Besides, not all outdoor stimuli were taken into account in the study. In this regard, outdoor sounds are one of the most critical limitations of the study. Indeed, it is clear that outdoor sounds significantly stimulate and impact people's cognitive states.

Moreover, the interiors were predominantly designed in black and white colors in the study. Color is one of the limitations of this study; it is clear that many color and pattern factors influence cognitive perception. Therefore, further studies can experiment with different colors and architectural styles.

This study analyzed visitor behavior at a museum space using both physical and cognitive methods. In light of the visitors' behavioral and cognitive feedback, inferences about the different presentation techniques in museums were made. Since the study was conducted across multiple disciplines, it is multifaceted and provides both emotional/behavioral and sociological/psychological insights. The study was conducted in a museum space. Since it was an experimental setup in a simulation, using a wide range of analysis methods, the study could affect many behavioral mechanisms.

Acknowledgements

The author would like to thank the participants.

Funding

This work was supported by the SDU Scientific Research Unit.

Appendices

Appendix 1. **Objects Used in Virtual Reality Environments**

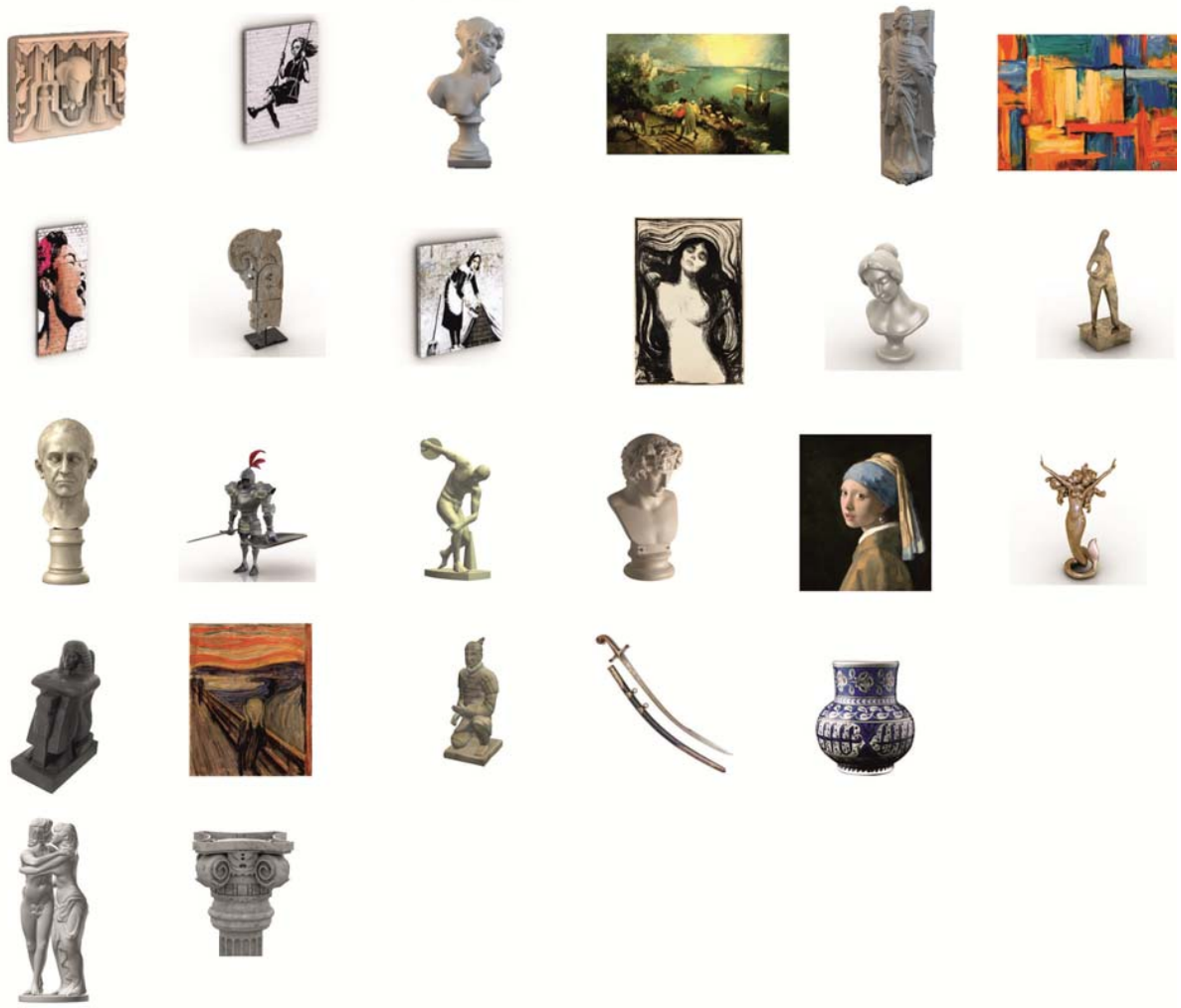

Appendix 2. **Software Interface**

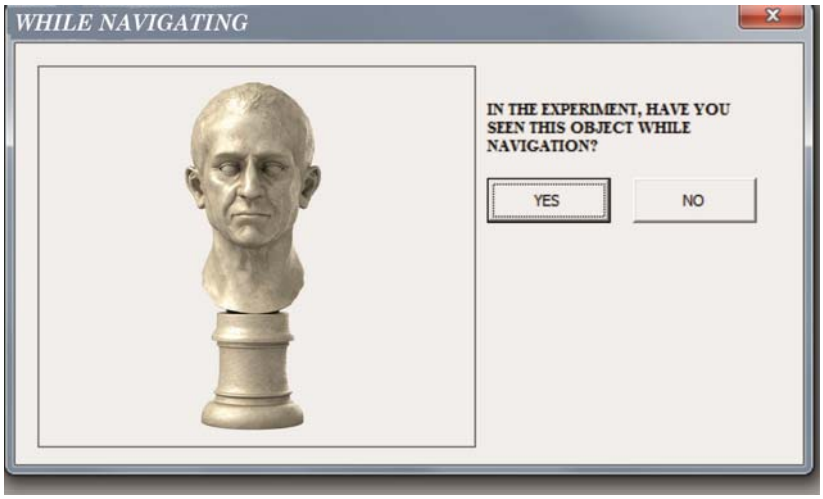

References

Acharya, U. R., Joseph, K. P., Kannathal, N., Lim, C. M., and Suri, J. S. (2006). Heart rate variability: a review. *Medical and Biological Engineering and Computing*, Vol. 44, Issue 12, pp. 1031–1051. DOI: 10.1007/s11517-006-0119-0.

Alberti, S. J. M. M. (2005). Objects and the museum. *Isis*, Vol. 96, No. 4, pp. 559–571. DOI: 10.1086/498593.

Antonelli, P., Riley, T., and McQuaid, M. (eds.) (2003). *Objects of design from the Museum of Modern Art*. New York: The Museum of Modern Art, 288 p.

Arnsten, A. F. T. (2009). Stress signalling pathways that impair prefrontal cortex structure and function. *Nature Reviews Neuroscience*, Vol. 10, Issue 6, pp. 410–422. DOI: 10.1038/nrn2648.

Becker, H. S. (2008). *Art worlds*. Berkeley: University of California Press, 440 p.

Braun, S. (2008). Audiodescription research: state of the art and beyond. *Translation Studies in the New Millennium*, Vol. 6, pp. 14–30.

Cupchik, G. C., Vartanian, O., Crawley, A., and Mikulis, D. J. (2009). Viewing artworks: contributions of cognitive control and perceptual facilitation to aesthetic experience. *Brain and Cognition*, Vol. 70, Issue 1, pp. 84–91. DOI: 10.1016/j.bandc.2009.01.003.

Cupchik, G. C. and Winston, A. S. (1996). Confluence and divergence in empirical aesthetics, philosophy, and mainstream psychology. In: Friedman, M. P. and Carterette, E. C. (eds.). *Cognitive Ecology. Handbook of Perception and Cognition*. 2nd edition. New York: Academic Press, pp. 61–85. DOI: 10.1016/B978-012161966-4/50005-0.

Dawson, M. E., Schell, A. M., and Courtney, C. G. (2011). The skin conductance response, anticipation, and decision-making. *Journal of Neuroscience, Psychology, and Economics*, Vol. 4, No. 2, pp. 111–116. DOI: 10.1037/a0022619.

Del Chiappa, G., Andreu, L., and Gallarza, M. G. (2014). Emotions and visitors' satisfaction at a museum. *International Journal of Culture, Tourism and Hospitality Research*, Vol. 8, No. 4, pp. 420–431. DOI: 10.1108/IJCTHR-03-2014-0024.

Erkan, İ. (2021). Cognitive response and how it is affected by changes in temperature. *Building Research & Information*, Vol. 49, Issue 4, pp. 399–416. DOI: 10.1080/09613218.2020.1800439.

Erkan, İ. (2024a). Sense of urban and architectural environment. *Architecture and Engineering*, Vol. 9, No. 2, pp. 33–46. DOI: 10.23968/2500-0055-2024-9-2-33-46.

Erkan, İ. (2024b). The neuro-cognitive approach to urban planning: wayfinding behavior analysis and its effect on urban planning. *Journal of Urban Technology*, Vol. 31, Issue 2, pp. 45–71. DOI: 10.1080/10630732.2023.2289144.

Gratton, G., Coles, M. G. H., and Donchin, E. (1983). A new method for off-line removal of ocular artifact. *Electroencephalography and Clinical Neurophysiology*, Vol. 55, Issue 4, pp. 468–484. DOI: 10.1016/0013-4694(83)90135-9.

Higuera Trujillo, J., Marín Morales, J., Rojas, J., and López Tarruella Maldonado, J. (2016). Emotional maps: neuro architecture and design applications. *Systems & Design: Beyond Processes and Thinking*, pp. 677–685. DOI: 10.4995/IFDP.2016.3170.

Huber, D., Milne, S., and Hyde, K. F. (2019). Conceptualizing senior tourism behaviour: a life events approach. *Tourist Studies*, Vol. 19, Issue 4, pp. 407–433. DOI: 10.1177/1468797619832318.

Hutchinson, R. S. and Eardley, A. F. (2019). Museum audio description: the problem of textual fidelity. *Perspectives*, Vol. 27, Issue 1, pp. 42–57. DOI: 10.1080/0907676X.2018.1473451.

Jacob, R. J. K. and Karn, K. S., (2003). Commentary on Section 4 - eye tracking in human-computer interaction and usability research: ready to deliver the promises. In: Hyönä, J., Radach, R., and Deubel, H. (eds.). *The Mind's Eye. Cognitive and Applied Aspects of Eye Movement Research*. Amsterdam, Boston: North Holland, pp. 573–605. DOI: 10.1016/B978-044451020-4/50031-1.

Jacobsen, T. and Höfel, L. (2003). Descriptive and evaluative judgment processes: Behavioral and electrophysiological indices of processing symmetry and aesthetics. *Cognitive, Affective, & Behavioral Neuroscience*, Vol. 3, Issue 4, pp. 289–299. DOI: 10.3758/CABN.3.4.289.

Kemp, A. H., Koenig, J., and Thayer, J. F. (2017). From psychological moments to mortality: a multidisciplinary synthesis on heart rate variability spanning the continuum of time. *Neuroscience & Biobehavioral Reviews*, Vol. 83, pp. 547–567. DOI: 10.1016/j.neubiorev.2017.09.006.

Koessler, L., Maillard, L., Benhadid, A., Vignal, J. P., Felblinger, J., Vespignani, H., and Braun, M. (2009). Automated cortical projection of EEG sensors: anatomical correlation via the international 10–10 system. *NeuroImage*, Vol. 46, Issue 1, pp. 64–72. DOI: 10.1016/j.neuroimage.2009.02.006.

Livio, M. (2008). *The golden ratio: the story of phi, the world's most astonishing number*. New York: Broadway Books, 294 p.

MacLeod, S., Dodd, J., & Duncan, T. (2015). New museum design cultures: harnessing the potential of design and 'design thinking' in museums. *Museum Management and Curatorship*, Vol. 30, Issue 4, pp. 314–341. DOI: 10.1080/09647775.2015.1042513.

Massaro, S. and Pecchia, L. (2019). Heart rate variability (HRV) analysis: A methodology for organizational neuroscience. *Organizational Research Methods*, Vol. 22, Issue 1, pp. 354–393. DOI: 10.1177/1094428116681072.

Mizuki, Y., Kajimura, N., Kai, S., Suetsugi, M., Ushijima, I., and Yamada, M. (1992). Differential responses to mental stress in high and low anxious normal humans assessed by frontal midline theta activity. *International Journal of Psychophysiology*, Vol. 12, Issue 2, pp. 169–178. DOI: 10.1016/0167-8760(92)90008-Y.

Murugappan, M., Murugappan, S., Balaganapathy, and Gerard, C. (2014). Wireless EEG signals based neuromarketing system using Fast Fourier Transform (FFT). In: *2014 IEEE 10th International Colloquium on Signal Processing and its Applications, Kuala Lumpur, Malaysia, March 7–9, 2014*, pp. 25–30. DOI: 10.1109/CSPA.2014.6805714.

Nurse Rainbolt, G., Benfield, J. A., and Loomis, R. J. (2012). Visitor self-report behavior mapping as a tool for recording exhibition circulation. *Visitor Studies*, Vol. 15, Issue 2, pp. 203–216. DOI: 10.1080/10645578.2012.715035.

Olesen, A. R., Holdgaard, N., and Laursen, D. (2020). Challenges of practicing digital imaginaires in collaborative museum design. *CoDesign*, Vol. 16, Issue 3, pp. 189–201. DOI: 10.1080/15710882.2018.1539109.

Pine, B. J. and Gilmore, J. H. (1998). Welcome to the experience economy. *Harvard Business Review*, Vol. 76, No. 4, pp. 97–105.

Polat, K. and Güneş, S. (2007). Classification of epileptiform EEG using a hybrid system based on decision tree classifier and fast Fourier transform. *Applied Mathematics and Computation*, Vol. 187, Issue 2, pp. 1017–1026. DOI: 10.1016/j.amc.2006.09.022.

Qin, S., Hermans, E. J., van Marle, H. J. F., Luo, J., and Fernández, G. (2009). Acute psychological stress reduces working memory-related activity in the dorsolateral prefrontal cortex. *Biological Psychiatry*, Vol. 66, Issue 1, pp. 25–32. DOI: 10.1016/j.biopsych.2009.03.006.

Ross, S. R., Melber, L. M., Gillespie, K. L., and Lukas, K. E. (2012). The impact of a modern, naturalistic exhibit design on visitor behavior: a cross-facility comparison. *Visitor Studies*, Vol. 15, Issue 1, pp. 3–15. DOI: 10.1080/10645578.2012.660838.

Shaffer, F. and Ginsberg, J. P. (2017). An overview of heart rate variability metrics and norms. *Frontiers in Public Health*, Vol. 5, 258. DOI: 10.3389/fpubh.2017.00258.

Siddiqui, S. V., Chatterjee, U., Kumar, D., Siddiqui, A., and Goyal, N. (2008). Neuropsychology of prefrontal cortex. *Indian Journal of Psychiatry*, Vol. 50, Issue 3, pp. 202–208. DOI: 10.4103/0019-5545.43634.

Skov, M., Lykke, M., and Jantzen, C. (2018). Introducing walk-alongs in Visitor Studies: a mobile method approach to studying user experience. *Visitor Studies*, Vol. 21, Issue 2, pp. 189–210. DOI: 10.1080/10645578.2018.1549396.

Taelman, J., Vandeput, S., Spaepen, A., and Van Huffel, S. (2009). Influence of mental stress on heart rate and heart rate variability. In: Vander Sloten, J., Verdonck, P., Nyssen, M., and Haueisen, J. (eds.). *4th European Conference of the International Federation for Medical and Biological Engineering. IFMBE Proceedings*, Vol. 22. Berlin, Heidelberg: Springer, pp. 1366–1369. DOI: 10.1007/978-3-540-89208-3_324.

Trunfio, M., Lucia, M. D., Campana, S., and Magnelli, A. (2022). Innovating the cultural heritage museum service model through virtual reality and augmented reality: the effects on the overall visitor experience and satisfaction. *Journal of Heritage Tourism*, Vol. 17, Issue 1, pp. 1–19. DOI: 10.1080/1743873X.2020.1850742.

Walczak, A. and Fryer, L. (2017). Creative description: the impact of audio description style on presence in visually impaired audiences. *British Journal of Visual Impairment*, Vol. 35, Issue 1, pp. 6–17. DOI: 10.1177/0264619616661603.

Wineman, J. D. and Peponis, J. (2010). Constructing spatial meaning: spatial affordances in museum design. *Environment and Behavior*, Vol. 42, No. 1, pp. 86–109. DOI: 10.1177/0013916509335534.

КРИТИЧЕСКИЙ ОБЗОР МУЗЕЙНОЙ АРХИТЕКТУРЫ С ТОЧКИ ЗРЕНИЯ НЕЙРОАРХИТЕКТУРЫ

Илкер Эркан

Факультет архитектуры, Университет Сулеймана Демиреля, Испарта, Турция

E-mail: ilkererkan@sdu.edu.tr

Аннотация

Введение. Данное исследование посвящено поведению людей в музеях. Известно, что люди, посещающие музей, изучают произведения искусства, представленные различными методами. В статье представлено когнитивное обсуждение поведения людей во время осмотра произведений искусства в музее. **Цель исследования**: проанализировать физиологические реакции посетителей на экскурсии снаружи и внутри музея с точки зрения нейроархитектуры. Таким образом, мы сосредоточились на оценке когнитивных реакций на архитектурные пространства во время экскурсий по музею. На основе этой оценки мы попытались сделать пространственные решения более «человекоцентричными». **Методы:** исследование было проведено в среде виртуальной реальности; для исследования был разработан виртуальный музей, в котором и проводились эксперименты. В отличие от других исследований, в нашем использовались такие методы, как электроэнцефалограмма (ЭЭГ), отслеживание движения глаз, вариабельность сердечного ритма и реакция кожной проводимости. Внимание было сосредоточено на двух методах представления информации, часто используемых в музеях: аудиоописании и информационной табличке. Одним из наиболее поразительных **результатов** исследования стало одновременное использование методов аудиоописания и инфотаблички. Согласно ЭЭГ и данным других приборов для измерения физиологических показателей, одновременное использование этих методов вызывало стресс у посетителей — участники не могли в достаточной степени сосредоточиться на произведениях искусства. Аудиоописание само по себе оказалось очень эффективным при посещении музея. Однако если оно использовалось одновременно с информационной табличкой, воздействие произведений искусства на посетителей сводилось к минимуму.

Ключевые слова: интерьерный дизайн; нейроархитектура; музейная архитектура; когнитивный дизайн.

DOI: 10.23968/2500-0055-2025-10-1-16-30

ARCHITECTONIC DEVELOPMENT STUDIES: FROM MAJAPAHIT TEMPLE TO DESIGN OF CONTEMPORARY HIGH-RISE BUILDING IN SURABAYA

Handy Nugraha Witama*, Rahadhian Prajudi Herwindo, Yuswadi Saliya

Department of Architecture, Parahyangan Catholic University, Bandung, 40141, West Java, Indonesia

*Corresponding author's email: handynugraha13@gmail.com

Abstract

Introduction: Urban areas in Indonesia are experiencing significant cultural and architectural shifts towards modernization. This trend is particularly noticeable in major cities where tall, contemporary buildings are becoming more prevalent, reducing the influence of local cultures. For instance, the profound historical legacy of Majapahit culture is gradually fading. The erosion of local cultural identity is exacerbated by fast-paced lifestyles and evolving societal norms, exemplified by the emergence of large, multi-functional buildings that consolidate various functions. Thus, it is deemed paramount to restore fading cultural values. **Purpose of the study:** We aimed to explore the optimal transformation of traditional Majapahit architecture in Indonesia within the context of modern times, as an example of preservation efforts. **Methods**: This qualitative research uses a descriptive-analytical approach to explore the cultural values of Majapahit architecture and modern high-rise buildings. It outlines the scope of their study concerning current developments, with transformation theory as a foundation. Through interpretation approach, it aims to generate potential for local-modern transformations. These transformation possibilities are then selected and visualized in 3D using modeling and rendering applications to clarify their visual outcomes. **Results and discussion:** The 3D visual render of the transformation potential reveals elements that should be preserved in their original form attributed to Majapahit culture and aspects that can be modernized to align with current trends. This serves as a model of modern design integrating local culture to safeguard indigenous heritage.

Keywords: traditional architecture; Majapahit architecture; high-rise building; mixed use; architecture transformation.

Introduction

The architecture in major Indonesian cities tends to reflect the change in its time periods. The architectural styles and shapes predominantly focus on a modern building of universal design which is applied worldwide, inducing a competition with other designs for complete dominance (Parker and Wood, 2013). This modern architectural style tends to impose rigidity on the identity of each region in Indonesia, failing to reflect the characteristics of local communities and culture. Ideally, they should be manifested in an urban landscape with highly distinctive design elements shaping the image of a city (Lynch, 1960).

Indonesia is a diverse nation with a broad spectrum of religions, races, and cultures, each closely embraced by their respective communities. This diversity is reflected in the archetypal patterns of cities, which symbolize the various community entities within them (Lobell, 2018). Particularly in architecture, this distinctiveness is embodied in traditional buildings such as temples (candi) and traditional houses, which represent the unique values of their regions and foster a strong emotional connection between users and their locations (Norberg-Schulz, 1980). The form of traditional Indonesian architecture is believed to be influenced by the kingdoms that previously existed in its territory, with their impact still noticeable in economic and social values of modern Indonesia (Wijaya, 2014).

The kingdoms in Indonesia emerged and developed alongside the arrival of foreign priests and traders. Majapahit was the largest Hindu-Buddhist kingdom in Indonesia that exerted strong influence on its culture. Its power nearly spanned across the entire Indonesian archipelago. It was established by Raden Wijaya in 1293 after repelling the Mongol forces led by Kublai Khan (Hidayat, 1975).

The buildings from the Majapahit era are typically preserved and maintained as historical cultural heritage, especially in the Trowulan district, the former capital of Majapahit. These structures are divided into residential buildings for habitation and temples as places of Hindu-Buddhist religious worship to honor the gods and goddesses as well as to pay homage to the kings' ancestors. Herwindo (2018) stated that the Hindu-Buddhist sacred buildings from the Majapahit era are divided into several types (Fig.1), including gate/gateways, tower-type temples, stepped-type temples, water sanctuary-type temples, and cave-type temples, each with their own specific features.

The Hindu-Buddhist sacred buildings were built using various types of materials, reflecting the development of technology and the local community, while still adhering to the original cultural values to

For citations: Witama, H. N. , Herwindo, R. P., Saliya, Y. (2025). Architectonic development studies: from Majapahit temple to design of contemporary high-rise building in Surabaya. Architecture and Engineering, No 1 (10), pp. 16–30. DOI: 10.23968/2500-0055-2025-10-1-16-30.

Fig. 1. Types of Majapahit Hindu-Buddhist sacred buildings. Source: authors, 2024

support their functions. The materials evolved from andesite stone to red brick due to cost and time considerations, as well as responding to Indonesia's geographical conditions. Eventually, it developed further in Eastern Indonesia, particularly on the island of Bali, where wood materials were used for tiered roofs known as Meru, according to Wijaya (2002).

The Majapahit architecture appears to have deteriorated and disappeared due to colonization and climatic influences. This underscores the importance of making architecture reflect local identity while combining modern achievements and the potential of the existing environment in a cultural preservation movement, according to Frampton (2020). Therefore, in response to present time trends, the cultural values of Majapahit architecture are suitable for application in modern design as symbols of identity and collective memory for the local community, which will influence its social and economic aspects. According to Ching (2007), its design also fits well with the typology of tall buildings today as a response to the identity crisis in modern high-rise design, while also depicting the form of the main temples of ancient times adapted to modern times in preserving cultural symbols, especially in architectural design that refers to the essential elements of its design standards. Alexander et al. (1977) emphasized that any built environment inherently comprises various interconnected patterns that adapt to cultural, environmental, and other contexts.

Traditional Majapahit architecture

Traditional Majapahit architecture embodies distinct characteristics that reflect local cultural values. It serves as a holistic representation of these values, sometimes presenting intricate and even contradictory impressions, as noted by Venturi (1977). Despite these complexities, it maintains a cultural coherence recognizable to its people. The architecture of the ancient Majapahit kingdom in the strategically located Trowulan district exemplifies this through structures like gateways and temples, capturing unique patterns in its design.

Stutterheim, referenced in Gomperts et al. (2008), elaborates on the order of the Majapahit kingdom, evident in the strategic canal network designed to adapt to seasonal changes and ecology, emphasizing water transportation. His mapping of the Trowulan area reveals three main components: the alun-alun (a large open field in front of the palace), the kraton/palace area (a center of royal governance) in north-south direction, and the temple buildings (in west-east direction). These elements are pivotal in comprehending the cultural manifestation of the kingdom, preserved albeit incompletely compared to ancient times (Fig. 2).

Despite the form and arrangement of the Majapahit kingdom area in Trowulan, Majapahit buildings tend to have their exterior divided into three parts: head (Swarloka), body (Bhuvarloka), and foot (Bhurloka). They manifest themselves through physical elements that are present in each of the Majapahit era buildings. The physical elements of Majapahit Hindu-Buddhist sacred buildings (Fig. 3) can be identified as follows:

1. Molding profile: continuous horizontal lines surrounding the temple buildings, created with a forward-backward expression.

2. Kala head: the statue of a guardian spirit as the protector of the temple building, located above the entrance.

3. Simbar/Jaladwara: statues depicting creatures spouting water around the temple's building, usually located at the lower levels of the structure (foot part).

4. Tiered roof and crown: the temple's roof narrows towards the top forming a triangle.

5. Entrance design: there are elements of doors and stairs as accents, often supported by carved niches or windows.

6. Stair design: located in the center, complemented by the Kala head element.

7. Decorations: carvings or ornaments emphasizing the sacred form of the building, depicting specific motif concepts.

The design of Hindu-Buddhist sacred buildings is not only limited to the physical elements present in their external appearance, but is also manifested

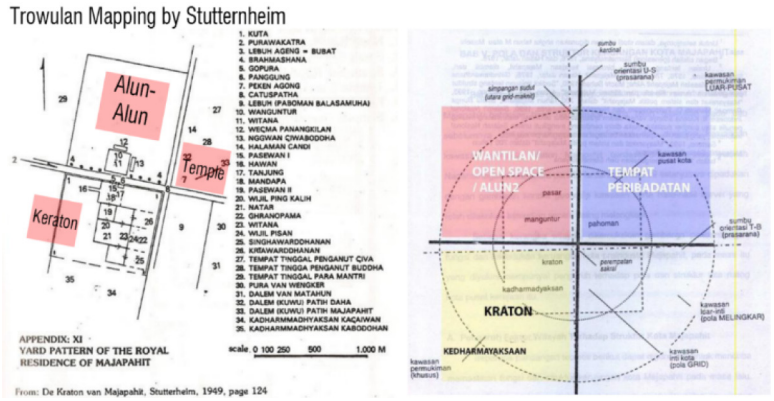

Fig. 2. Trowulan mapping by Stutternheim. Source: Stutterheim, 1948 (left), Hermanislamet, B., 1999 (right)

in a number of essential features, distinctive for this type of buildings. These features must be viewed comprehensively to ensure their integrity in the context of Hindu-Buddhist sacred buildings' design (Table 1).

The architectural values of Majapahit display consistent patterns and aspects applied throughout its building structures, providing a reference for transforming traditional designs. This consistency is also reflected in modern designs, which adhere to standards as outlined by Ching (2007). These standards encompass six ordering principles of architecture: axis, symmetry, hierarchy, datum, rhythm, and transformation. Consequently, traditional temple building designs and modern high-rise architecture share notable similarities, underscoring the relevance of these traditional patterns in contemporary architectural discussions.

Modern tall building architecture

According to Parker and Wood (2013), building design adapts to societal changes and advancements while maintaining cultural identity. In response to such current challenges as population growth and urban density, buildings increasingly take the form of high-rise structures. These designs must integrate local cultural values while meeting contemporary standards for high-rise architecture.

Ashihara (1970) emphasized that modern high-rise buildings adhere to standards encompassing design requirements, typology, structural types, and other criteria. He argued that the external appearance of a building is influenced by elements such as form, color, texture, space, and scale. A space intentionally designed by humans for specific purposes is termed positive space, whereas space that forms spontaneously is considered negative space.

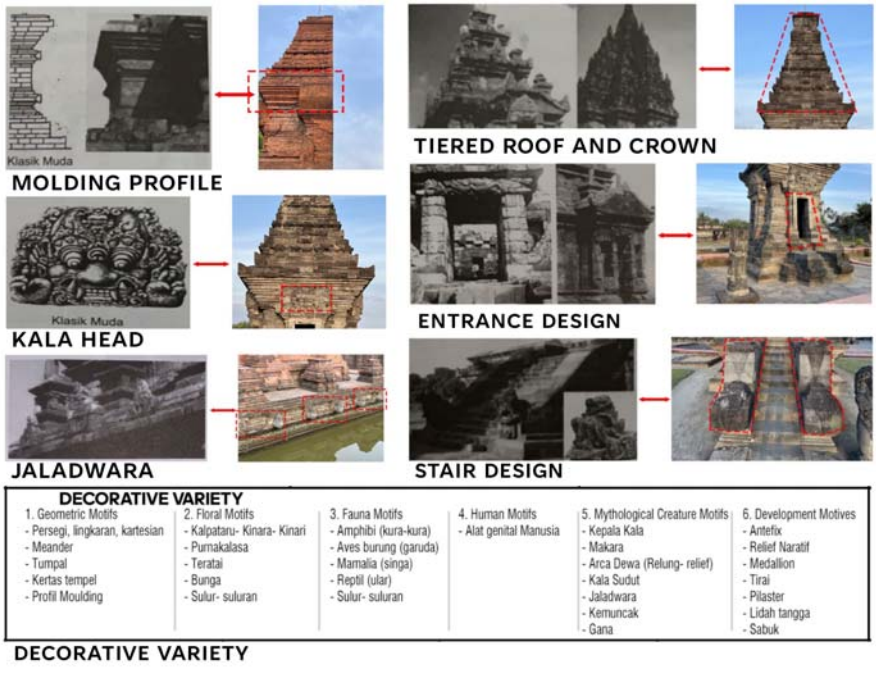

Fig. 3. Physical elements of Majapahit sacred buildings. Source: authors, 2024

Table 1. **Distinctive features of Majapahit sacred buildings**

No.	Distinctive features	Status	Meaning and philosophy in Majapahit architecture	Image
1	Majapahit Geometry	Transformation	The heavenly nature of the building is manifested in a cruciform with the use of squares, rectangles, and circles.	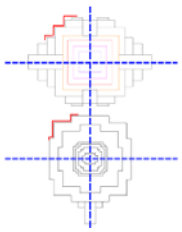
2	Majapahit Volumetric Composition	Preservation	Massive structural elements are combined in a way to emphasize the zoning.	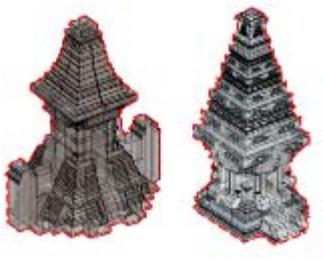
3	Majapahit Hierarchy – Triangle Shape – Effect of Perspective	Transformation	The shape of the building narrows towards the top to form a triangle as a depiction of the sacred Mount Meru.	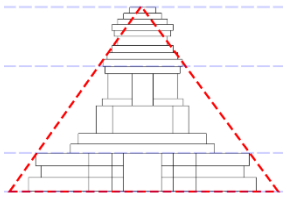
4	Majapahit Tripartition	Preservation	Both vertical and horizontal division into three sections.	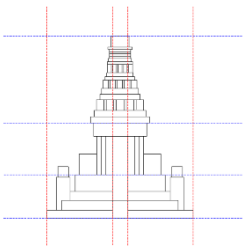
5	Majapahit Rhythm – Repetition	Transformation	Repetition of the head-body-leg elements as a unity in form, color, and material.	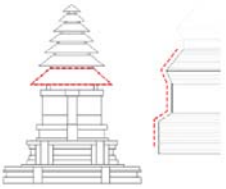
6	Majapahit Symmetry	Preservation	Balanced building form supported by the symmetry of the door element.	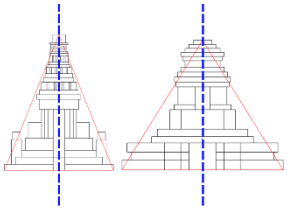
7	Majapahit Mimesis	Preservation	Building elements resemble real objects, for example, Mount Meru, and are usually adorned with carvings and ornaments.	

Table 1. Ending

No.	Distinctive features	Status	Meaning and philosophy in Majapahit architecture	Image
8	Majapahit Texture – Material	Preservation	The use of andesite stone and brick as distinctive materials of Majapahit era.	
9	Majapahit Line Elements – Light-Dark Effects	Transformation / Preservation	The continuous play of horizontal lines with the forward-backward movement forms' shadows within the interior space.	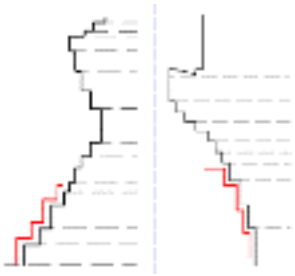
10	Majapahit Axis	Preservation	The building is oriented in a specific direction, for example, to face important areas during a king's reign.	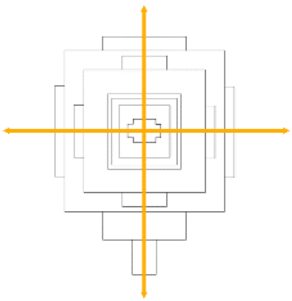
11	Majapahit Proportions and Scale	Transformation	The form of a large and cohesive building in terms of its length and width.	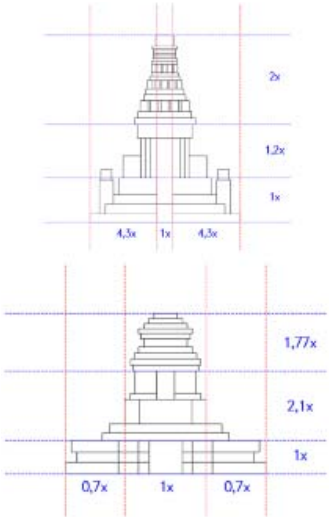
12	Majapahit Duality	Transformation	The combination of two aspects that make a building design complete and cohesive.	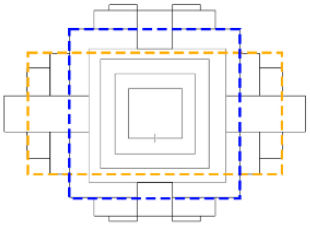

Source: authors, 2024

Modern high-rise building design adheres to various standards, including client needs, cost efficiency, choice between renovation and new construction, technological advancements, materials, and environmental sustainability. Mixed-use building design involves segmented stages with detailed site analysis, encompassing factors like accessibility, functional relationships, land costs, and site dimensions. This approach enables the strategic integration of diverse functions such as offices, hotels, residences, retail spaces, meeting areas, recreational zones, and other activities within mixed-use developments. While certain functions may dominate at times, they typically balance each other out, contributing to a harmonious whole. According to Schwanke (1987), the design of mixed-use areas should sequentially consider the following aspects:

- *The design process and design team:* stages of preliminary design, design development, and final design.
- *Physical and structural configuration:* the types of mixed-use building arrangements include mixed-use tower, multi-tower mega structures, free standing structures with pedestrian connection, and their combinations.
- *External design:* site area, cost, land use allocation, topography, climate adjusted to the appearance of each function's building.
- *Internal design:* the arrangement of spaces equipped with easily understandable signs for users according to the proximity of functions.
- *People-oriented spaces:* there is site processing aimed at gathering points or resting areas for the community within it connected by pedestrian pathways.
- *Parking design:* according to the functional needs based on the scenario as needed.
- *Adaptive use and historic preservation:* development by incorporating local cultural elements and values as inherent cultural identity.

The above aspects serve as guidelines for designing appropriate and effective types of high-rise building structures. According to Ching et al. (2014), common types of high-rise building structures include shear wall cores, rigid frame structures, braced-frame cores, and others. These aspects change over time in response to societal and environmental changes, making current standards a continually evolving benchmark, as noted by Schueller (1977). Therefore, the construction of high-rise buildings not only addresses present-day needs but also anticipates future possibilities.

Local-modern architectural transformation

In the Indonesian dictionary (KBBI), 'transformasi' means the process of changing form or appearance while retaining meaning. In architecture, local traditional cultural values require transformation to be integrated into contemporary designs, adapting to current trends. Specifically, transforming the traditional cultural values of Majapahit temples into modern high-rise buildings necessitates a strong theoretical basis. This transformation involves two critical elements: 'Penanda' (the physical form of the building) and 'Petanda' (the conceptual idea), shaped by the designer's vision and character. Jencks (1984) classified architectural development into six styles, including: *Historicism* (traditional culture manifested in modern form), *Straight Revivalism, Neo-Vernacular* (traditional culture combined with modern elements), *Ad Hoc Urbanism, Metaphor and Metaphysics, and Post-Modern Space.*

Jencks' architectural styles provide a guideline for understanding the fundamental process of transformation in architecture. Transforming Majapahit's local culture into modernity can be linked to the poetic transformation of architecture as described by Antoniades (1992) which encompasses both tangible and intangible aspects. This includes the Metaphor method, which naturally imitates an object in a way that is widely recognizable. Antoniades further categorizes architectural transformation into three types: Traditional, Borrowing, and Decomposition. This theoretical study of transformation is also supported by Laseau (2001), who categorized the process of architectural form transformation into four types (Fig. 4):

1. Geometry Transformation: geometric shapes that change within the same forming scope.

2. Ornamental Transformation: changing the existing position, location and composition without changing its form and meaning.

3. Reversal Transformation (Inversion): an object's image is changed to its opposite.

4. Distortion Transformation (Confusing): freedom of transformation according to creativity.

According to Rahadhian (2011), architectural transformation exhibits three characteristic types: *Adoption* (favoring modern influences), *Adaptation* (favoring local influences), and *Assimilation* (finding a balance between the two). Therefore, studying cultural theory alone is insufficient; it must be complemented by an examination of transformation types and their characteristics to ensure effective and appropriate transformations. Furthermore, this process can be informed by precedent buildings, allowing an understanding of past preservation efforts and facilitating further development.

Methods

This qualitative research employs a descriptive-analytical and interpretative approach to study the cultural values and architectural characteristics of Majapahit, focusing particularly on temples, gateways, modern high-rise architecture, and local-modern transformation theory. The study is supported by topics on architectural identity and forms based on literature reviews, field observations,

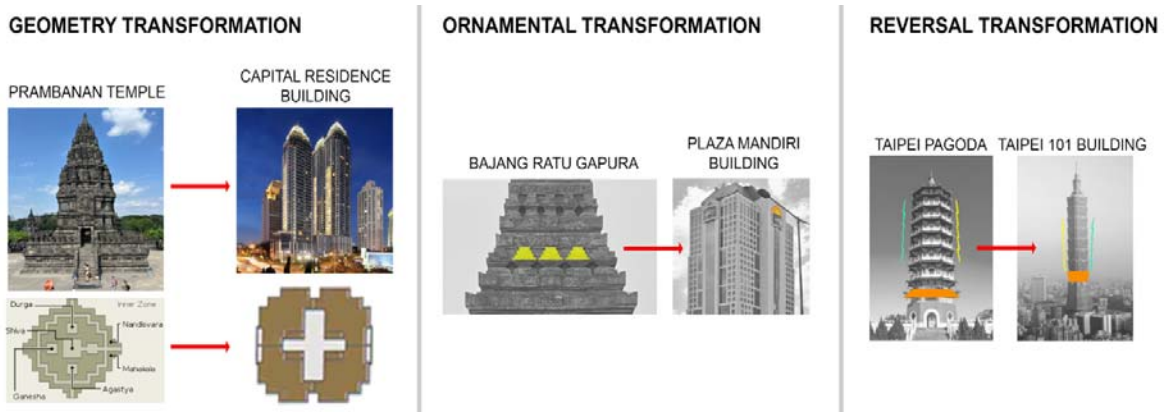

Fig. 4. Examples of local-modern transformation. Source: authors, 2024

and interviews in Trowulan for future development. Thus, this study can produce a good example of the transformation process in the preservation of culture, particularly traditional Majapahit architecture. The research process unfolds in the following stages:

1. Descriptive method: describing traditional Majapahit architecture and modern mixed-use high-rise buildings as foundational elements to establish the scope (physical elements and key aspects of Majapahit architecture concerning modern high-rise design standards).

2. Analytical method: assessing the boundaries established in the descriptive phase within the scope of architectural transformation, specifically focusing on local-modern elements, to generate potential for transformations.

3. Interpretative method: exploring transformation possibilities that are suitable for designing modern mixed-use high-rise buildings. Interpretation of transformation potential includes: studying architectural characteristics of Majapahit, dissecting and analyzing their basic forms, producing diverse potential transformation forms and ornamentation, conducting 3D model simulations of selected potential designs, and drawing conclusions on elements that are essential (immutable) and adaptable (transformable).

Results and discussion

The potential transformation focuses on five iconic buildings from the Majapahit era: Wringin Lawang Gate, Bajang Ratu Gate, Brahu Temple, Penataran Temple, and Jago Temple (Fig. 5). These structures, renowned for their height during their time, typify Majapahit architecture with their use of brick and stone materials. They are well-suited for transformation into modern mixed-use buildings, aligning with planned contextual changes. This transformation aims to highlight the geometric compositions inherent in each Majapahit building, serving as the foundation for creating contemporary architectural forms in mixed-use developments.

Bajang Ratu Gapura building

The Bajang Ratu Gate served as a double-layered entrance leading to the palace or the area of the junior king of Majapahit in ancient times. This grand and monumental structure narrows at the top, featuring a central opening as an entrance. It is adorned with intricate carvings of animals, plants, and other detailed motifs. Architectural studies of Bajang Ratu reveal nine form compositions, creating a triangular perspective effect, with the repeated head elements being the most dominant ornamental feature (Fig. 6).

The transformation of this form can be adapted to emphasize a futuristic appearance for a main

Fig. 5. Selection of Majapahit buildings. Source: authors, 2024

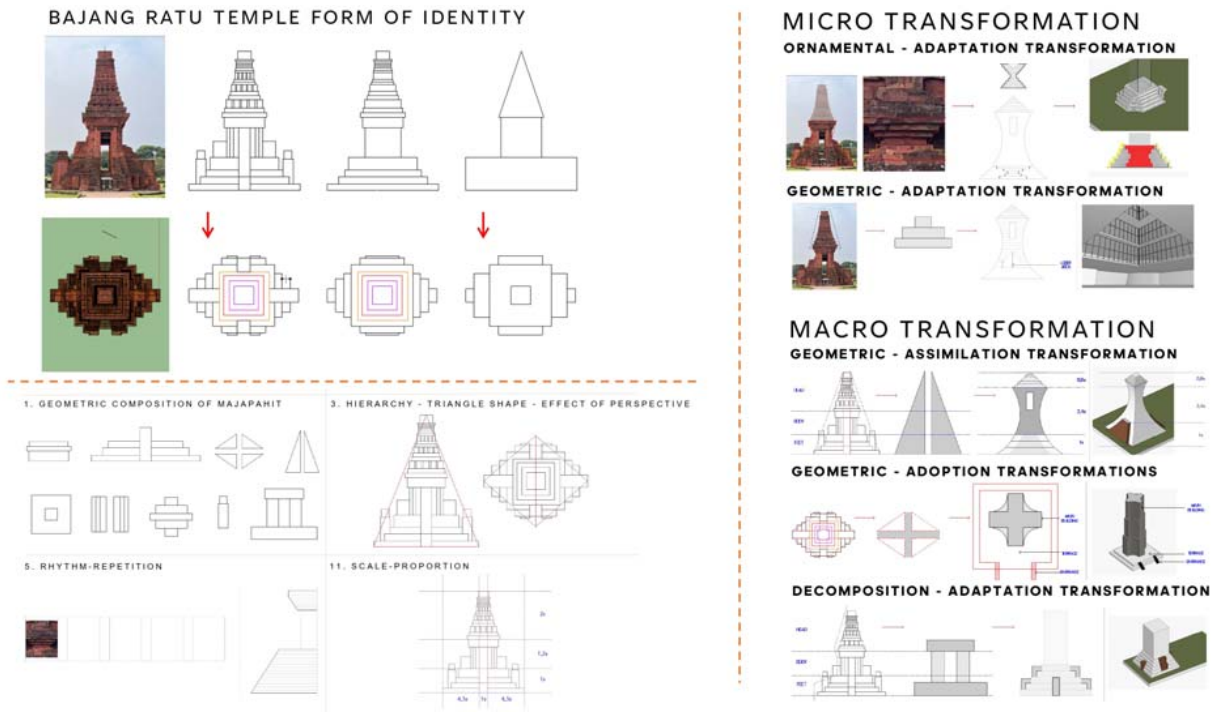

Fig. 6. Characteristics of Majapahit Bajang Ratu and transformation potential. Source: authors, 2024

mixed-use building. On a micro scale, this includes Ornamental-Adaptation, such as stepped patterns on the podium forming a rhombus shape, and Geometric-Adaptation, involving internal spatial manipulation with a void that narrows upwards. On a macro scale, transformations through Geometric-Assimilation, Geometric-Adaptation, and Decomposition-Adaptation reveal a building divided into symmetrical head-body-foot segments, with a prominent entrance design.

The transformation potential of the Bajang Ratu building can be chosen based on the conditions and design needs of the current mixed-use project (Fig. 7). The first photo depicts a macro transformation with a tiered podium as the initial stage and the main tower in the innermost courtyard, featuring a curved form and crowned top visible from all directions. The second photo illustrates a macro transformation of the podium's secondary entrance, responding to Majapahit architecture with a gawangan (gateway)

Fig. 7. Visual form of the local-modern transformation of Majapahit Bajang Ratu. Source: authors, 2024

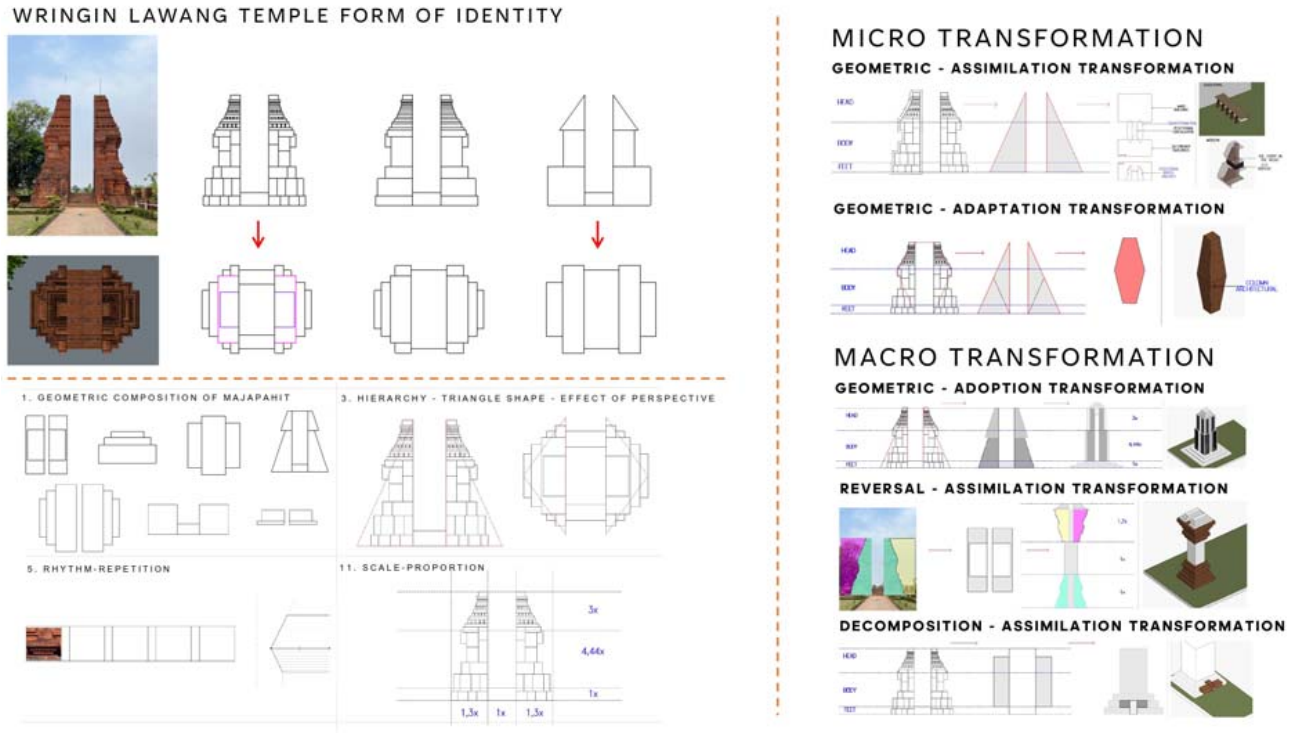

Fig. 8. Characteristics of Majapahit Wringin Lawang and transformation potential. Source: authors, 2024

and balconies oriented towards the east-west axis. The third photo shows a micro transformation of the interior space, forming a tiered void similar to Majapahit interiors, complemented by natural vegetation elements.

Wringin Lawang Gapura building

Wringin Lawang is the first-layer gate of the Majapahit royal complex, symbolized by its iconic large banyan tree. Constructed using red bricks, it appears grand and monumental with intricate carvings and ornaments depicting animal and plant motifs. The study on the characteristics of Wringin Lawang reveals seven form compositions, featuring symmetrical split forms and repeated head elements, as well as horizontal lines across all sides of the building (Fig. 8).

In the design manifestation of mixed-use buildings, on a micro scale, Geometric-Adaptation can be observed in the silhouette shapes of pedestrian bridges (architectural and structural). On a macro scale, we can see potential for enlarging the building at its peak, with consistent division into head-body-foot segments across all sides.

The transformation of the form and characteristics of Wringin Lawang can help create integrated designs in modern mixed-use buildings (Fig. 9). The first image depicts micro-scale transformation, where the modernized rendition of the Wringin Lawang Gate supports the multi-functional aspect of bridge-building. Meanwhile, the second image shows a distinct separation between the left and right sides of the entrance, serving as an inviting focal point for an upscale and sophisticated shopping center.

Brahu Temple building

Candi Brahu is a 15th-century religious building from the reign of King Hayam Wuruk, originating from the Javanese language meaning “blessing”, and symbolizing gods or ancestors. The structure appears simple with horizontal lines in the head-body-foot elements made of red brick. The study on the characteristics of Candi Brahu (Fig. 10) describes seven form compositions with perspective effects and triangular shapes (narrowing at the top).

Its form is suitable for the design of a monumental mixed-use tower (single building mass). Micro-scale transformation potential can be achieved through Geometric-Adaptation, such as playing with cruciform silhouette shapes in interior elements and tenant stands. Meanwhile, the macro scale shows stepped building forms with curved accents, depicting symmetrical arrangements in the head-body-foot structure.

The transformation potential of the Majapahit architecture in the Brahu Temple is apparent in the interior layout tailored for tenant spaces, marked by tiered platforms that vary in size to delineate commercial sections. Furthermore, the building’s structure incorporates a play of advancing and receding elements, echoing the architectural style of the Majapahit Brahu Temple (Fig. 11).

Penataran Temple building

Penataran Temple is the largest and most significant monument of the Majapahit era, featuring

Fig. 9. Visual form of the local-modern transformation of Majapahit Wringin Lawang. Source: authors, 2024

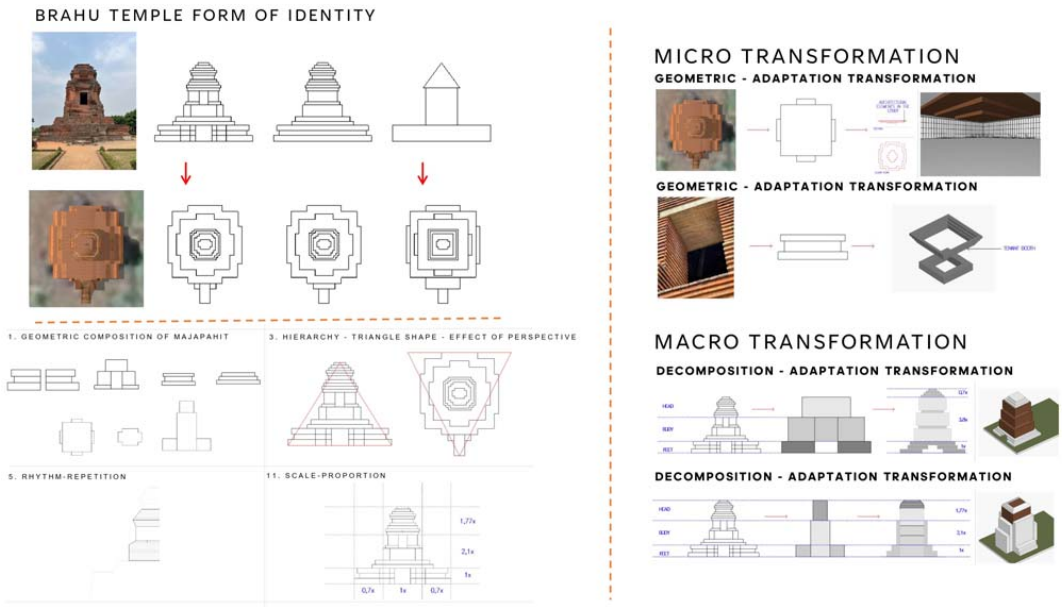

Fig. 10. Characteristics of Majapahit Brahu Temple and transformation potential. Source: authors, 2024

multiple temples within its complex with the main structure located in the innermost courtyard. It is built from andesite stone. The temple is renowned for its detailed carvings and decorations, including unique medallion motifs. Its architectural design incorporates six distinct forms that utilize perspective effects to create triangular shapes.

Fig. 11. Visual form of the local-modern transformation of Majapahit Brahu Temple. Source: authors, 2024

Its transformation potential inspires futuristic designs in contemporary architecture (Fig. 12). This includes Ornamental-Adaptation on a micro scale for interior elements and diamond/cruciform patterns reflecting Majapahit symbolism. On a macro scale, Decomposition-Adoption leads to modern buildings with symmetrical divisions and curved, tiered structures. Ornamental-Adaptation also includes base elements with tiered landscape ornaments, echoing Majapahit aesthetics, and reinterpretations of Majapahit motifs on modern facades.

As an aspect to strengthen the local-modern design, the transformation of Penataran Temple is very effective and robust (Fig. 13). One example is shown in the first image, depicting a macro transformation with a tiered canopy structure forming triangles and carvings depicting Majapahit stories; it is accompanied by tiered landscaping resembling a cruciform shape at the base of the curtain wall adorned with medallion ornamentation. The subsequent images illustrate micro-scale transformations: skylights in cruciform shapes

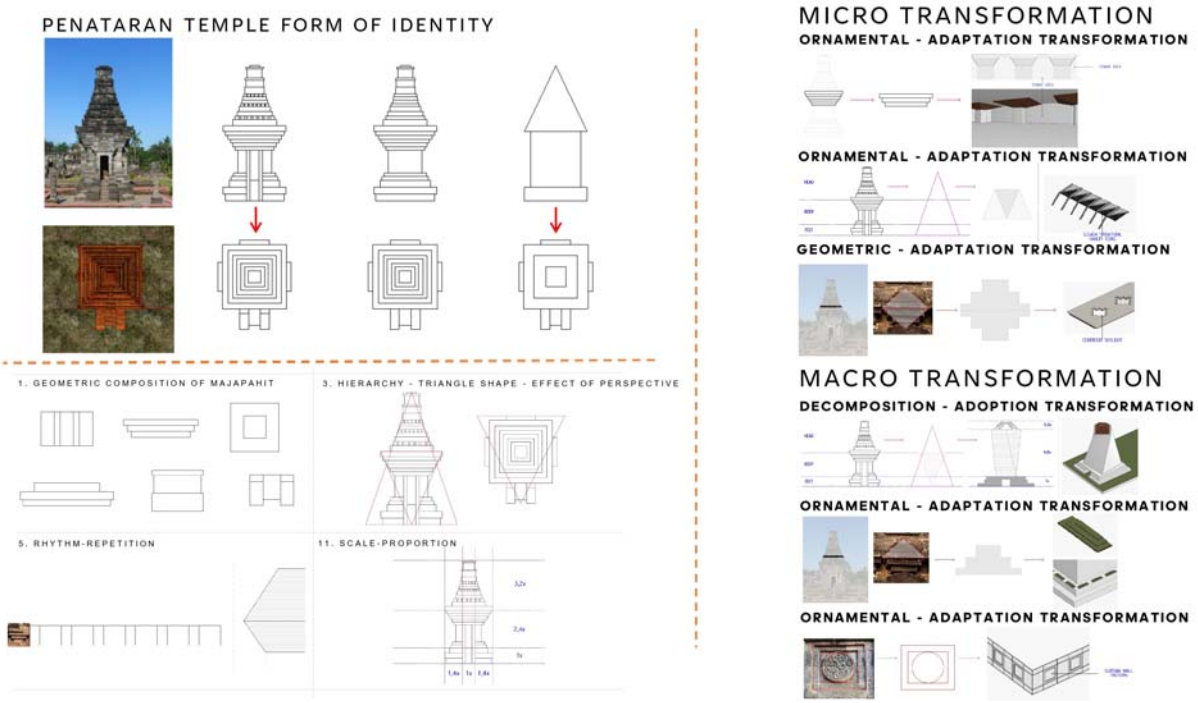

Fig. 12. Characteristics of Majapahit Penataran Temple and transformation potential. Source: authors, 2024

on bridge areas, and interior spaces showcase apartment room lights shaped similarly to Surya Majapahit motifs.

Jago Temple building

Jago Temple is a Meru style structure that evolved alongside the Majapahit kingdom, responding to cost, construction time, and Indonesian climate demands, while using the same system as its predecessors. Jago Temple's design is characterized by tiered roofs with an odd number of layers, symbolizing the sacred Mount Meru and associated with Hindu deities. Jago Temple itself features eight form compositions creating triangular perspective effects and symmetrical shapes.

The potential transformations, seen at a micro scale through Geometric-Adaptation, include building silhouette forms as architectural columns, as well as raising platforms and entrances. At a macro scale, Decomposition-Adaptation manifests in unique building forms with head-body-foot elements, featuring stepped terrace treatments as entry areas that enhance aesthetics. They are also crowned by tiered roofs in response to the traditional tiered roof design (Fig. 14).

Fig. 13. Visual form of the local-modern transformation of Majapahit Penataran Temple. Source: authors, 2024

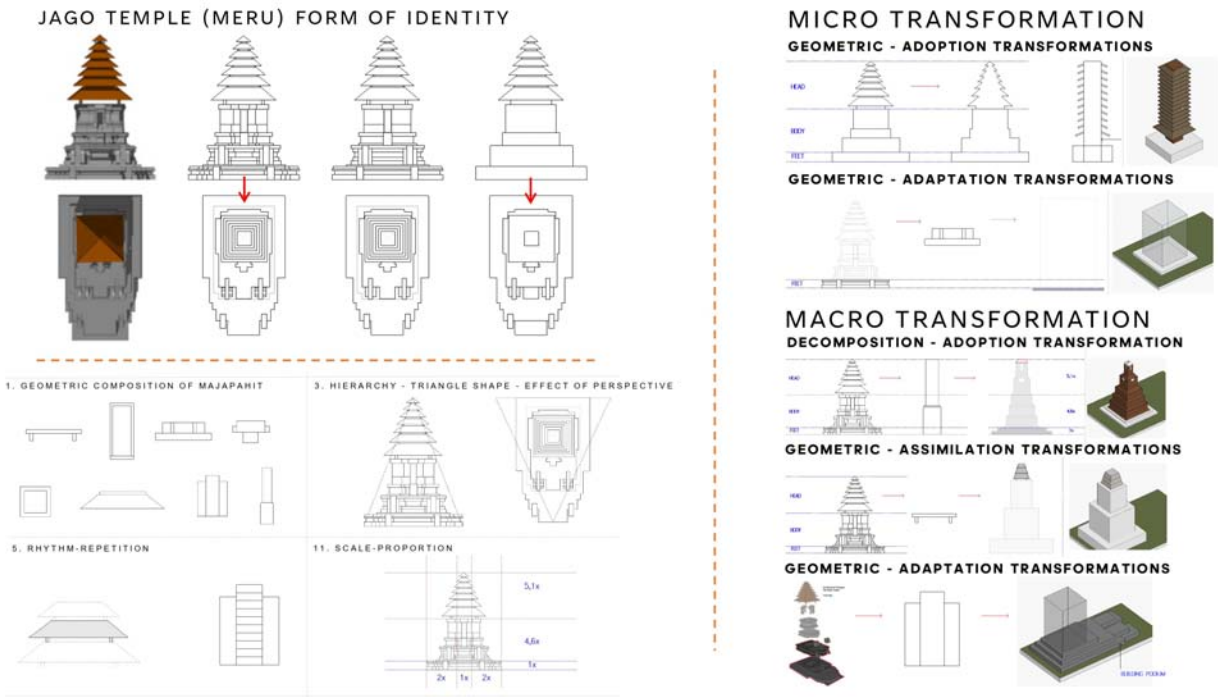

Fig. 14. Characteristics of Majapahit Jago Temple and transformation potential. Source: authors, 2024

Modern mixed-use building architecture takes cues from Jago Temple, an early precursor to the Meru style in Bali (Fig. 15). The first image illustrates a macro transformation with a stepped layout and terraces, forming the foundation for a mall area. Another macro transformation (seen in the second picture) is evident at the top of the building tower, housing a private restaurant and Mechanical Electrical Service Floor (Building Sustainability Utilities). This design incorporates tiered roof steps reminiscent of evolving tiered roof architecture of Majapahit, adapted over time to respond to environmental factors like climate.

Conclusion

Exploring potential transformations in mixed-use building design rooted in Majapahit architecture offers extensive opportunities for designers to innovate creatively in line with modern development trends. Emphasizing authentic cultural preservation over simplistic judgments of good or bad allows for nuanced evaluation of transformation potential. This approach spans both micro and macro scales, integrating complementary elements to enhance ambiance and atmosphere, thereby enriching spatial experiences with the essence of Majapahit culture.

The sought-after transformation is not confined to individual aspects of single buildings; rather, it can integrate diverse elements from various structures to form a unified whole. Traditional cultural architecture typically retains consistent and cohesive foundational values, despite variations in function and form. Therefore, transforming these cultural values through design involves more than just modernizing their appearance; it should infuse them with spirit to create a robust design arrangement that serves as the binding identity of the city. In the context of

Fig. 15. Visual form of the local-modern transformation of Majapahit Jago Temple. Source: authors, 2024

the aforementioned transformation of Majapahit architecture, this can be summarized as follows:

1. It is essential to preserve the manifestation of Majapahit cultural elements that cannot be transformed, such as Volumetric Composition – solid-void, Tripartition, Symmetry, Mimesis, Texture – Material, Line Elements – Light-Dark Effects, and Axis – Convergence.

2. Modern designs should still involve the head-body-feet division.

3. The scale and proportion of the building can be adjusted by referring to the original, considering the form of the mixed-use tower (single mass) or mixed-use buildings with pedestrian access (multiple masses).

4. It is important to maintain the triangular perspective effect with a form that gradually narrows at the top, as well as enlarge the floor area at the junction of the body and the top of the building.

5. A symmetrical or centralized form should be both in plan and elevation.

6. The main building is positioned at the innermost part and is equipped with circulation paths leading towards it.

7. Pedestrian and human circulation with landscape features such as ponds or canal flows should be prioritized over vehicle transportation.

8. Strict and comprehensive orientation in the east-west (values of the Majapahit temples) and north-south (Majapahit city planning) direction.

The identified aspects of transformation function as core design principles, embodying the essence of Majapahit culture in a definitive and essential way. These guidelines provide a foundation for developing impactful and suitable transformation designs that respond to evolving societal demands and changing times. Therefore, exploring the transformation of Majapahit culture alongside modern influences is not confined to current aspect but can be expanded. This includes exploring opportunities to transform other traditional cultures in Indonesia, highlighting their cultural richness, and reinforcing local socio-economic values to bolster regional identity.

Acknowledgements

- Ministry of Research, Technology and Higher Education Indonesia. - KEMENRISTEKDIKTI (DIREKTORAT RISET, TEKNOLOGI, DAN PENGABDIAN KEPADA MASYARAKAT);
- Balai Pelestarian Kebudayaan Wilayah XI-Jawa Timur;
- Department of Architecture, Parahyangan Catholic University, Indonesia;
- Institute for Research and Community Services, Parahyangan Catholic University-LPPM UNPAR.

References

Alexander, C., Ishikawa, S., and Silverstein, M. (1977). *A pattern language: towns, buildings, construction*. New York: Oxford University Press, 1171 p.

Antoniades, A. C. (1992). *Poetics of architecture: theory of design*. New York: John Wiley & Sons, 320 p.

Ashihara, Y. (1970). *Exterior design in architecture*. New York: Van Nostrand Reinhold, 143 p.

Ching, F. D. K. (2007). *Architecture: form, space, and order.* 3rd edition. Hoboken: John Wiley & Sons, 448 p.

Ching, F. D. K., Onouye, B., and Zuberbuhler, D. (2014). *Building structures illustrated*. 2nd edition. Hoboken: John Wiley & Sons, pp. 278–289.

Frampton, K. (2020). *Modern architecture: a critical history*. 5th edition. London: Thames and Hudson, 736 p.

Gomperts, A., Haag, A., and Carey, P. (2008). Stutterheim's enigma: The mystery of his mapping of the Majapahit kraton at Trowulan in 1941. *Bijdragen tot de Taal-, Land- en Volkenkunde*, Vol. *164* (4), pp. 411–430. DOI: 10.1163/22134379-90003649.

Herwindo, R. P. (2018). *Eksistensi Candi Sebagai Karya Agung Arsitektur Indonesia di Asia Tenggara*. PT Kanisius (IKAPI Member).

Hermanislamet, B. (1999) 'Tata Ruang Kota Majapahit, Analisis Keruangan Pusat Kerajaan Hindu Jawa Abad XIV di Trowulan Jawa Timur', *Universitas Gadjah Mada (Dissertation, Not Open Access)* [Preprint].

Hidayat, W. (1975). *Hari Jadi Kota Surabaya*. The Municipal Government of Surabaya, Level 2 Regional City.

Jencks, C. (1984). *The language of post-modern architecture*. 4th edition. New York: Rizzoli International Publications, 168 p.

Laseau, P. (2001) *Graphic thinking for architects and designers*. third. New York: John Wiley & Sons.

Lobell, M. (2018). *Spatial archetypes: the hidden patterns of psyche and civilization*. New York: JXJ Publications, 598 p.

Lynch, K. (1960). *The image of the city*. Cambridge, MA, and London: The M.I.T. Press, 194 p.

Norberg-Schulz, C. (1980). *Genius loci: towards a phenomenology of architecture*. New York: Rizzoli International Publications, 213 p.

Parker, D. and Wood. A. (eds.) (2013). *The tall buildings reference book*. London, New York: Routledge, 496 p.

Rahadhian, P. H. (2011). The persistence of 'Candi' representation in modern architecture in Indonesia. *International Journal of Engineering & Technology IJET-IJENS,* Vol. 11, No. 04, pp. 134–141.

Schueller, W. (1977). *High-rise building structures*. New York: John Wiley & Sons, 274 p.

Schwanke, D. (1987). *Mixed-use development handbook*. Washington, D.C. : ULI, 364 p.

Stutterheim, W. , F. (1948). *De Kraton Van Majapahit: Vol. VII*. Den Haag, pp. 119–126.

Venturi, R. (1977). *Complexity and contradiction in architecture*. 2nd edition. New York: The Museum Of Modern Art, 132 p.

Wijaya, M. (White, M.). (2002). *Architecture of Bali: a source book of traditional and modern forms*. Singapore: Archipelago Press, 224 p.

Wijaya, M. (White, M.). (2014). *Majapahit Style*. Vol. 1. Jakarta: Wijaya Words, 336 p.

ИССЛЕДОВАНИЕ РАЗВИТИЯ АРХИТЕКТОНИКИ: ОТ ХРАМА ЭПОХИ МАДЖАПАХИТА ДО ПРОЕКТИРОВАНИЯ СОВРЕМЕННОГО ВЫСОТНОГО ЗДАНИЯ В СУРАБАЕ

Ханди Нуграха Витама*, Рахадхиан Праджуди Хервиндо, Юсвади Салия

Институт архитектуры, Католический университет Парахьянган
Бандунг, 40141, Западная Ява, Индонезия

*E-mail: handynugraha13@gmail.com

Аннотация
Введение. Городские районы Индонезии переживают значительные культурные и архитектурные изменения на пути к модернизации. Эта тенденция особенно заметна в крупных городах, где высокие современные здания появляются все чаще, снижая влияние местных культур. Например, богатое историческое наследие культуры Маджапахита постепенно исчезает. Размывание местной культурной идентичности усугубляется быстрым темпом жизни и меняющимися общественными нормами, примером чего является появление больших многофункциональных зданий, объединяющих различные функции. Таким образом, восстановление угасающих культурных ценностей приобретает особую важность. **Цель исследования**. Целью данного исследования является изучение оптимальной трансформации традиционной архитектуры Маджапахита в Индонезии в контексте современности в качестве примера сохранения культурного наследия. **Методы**. Мы использовали описательно-аналитический подход метода качественного исследования для понимания культурных ценностей архитектуры эпохи Маджапахита и современных высотных зданий. Основываясь на теории трансформации, мы определили объем их исследования с учетом современных достижений в архитектуре. Посредством интерпретационного подхода мы стремились создать потенциальные варианты локально-современных трансформаций. Затем мы отобрали и визуализировали в 3D возможные варианты трансформации при помощи приложений для моделирования и рендеринга для понятной иллюстрации готовых проектов. **Результаты и обсуждение**. 3D-визуализация потенциальных трансформаций выявляет элементы, которые необходимо сохранить в первоначальной форме культуры Маджапахита, и аспекты, которые можно модернизировать для соответствия современным тенденциям. Они служат образцом современного дизайна, включающего элементы местной культуры для сохранения наследия коренного населения.

Ключевые слова: традиционная архитектура; архитектура Маджапахита; высотное здание; многофункциональное проектирование; архитектурная трансформация.

DOI: 10.23968/2500-0055-2025-10-1-31-48

DIGITIZING URBAN CODES TO SUSTAIN URBAN CHARACTER OF HISTORIC DISTRICTS: A CASE STUDY OF ROSETTA CITY, EGYPT

Mokhtar Hosni Akl*, Sherif A. Sheta, Lamis El Gizawi

Mansoura University, Elgomhouria St., Mansoura City, Egypt

*Corresponding author's email: mokhtarakl@mans.edu.eg

Abstract

Introduction: Effective urban planning relies on comprehensive knowledge of both physical and non-physical urban elements, which is vital for developing GIS models that support sustainable urban development by providing realistic representations of urban contexts. Accurate 3D models are critical for analyzing urban systems and processes. **Aim:** This study aimed to evaluate the impact of 3D GIS urban digitizing techniques and visualization methods on the feasibility of urban codes in preserving urban identity and character, with a focus on Rosetta City, Egypt. **Methods:** The research employed descriptive, analytical, and empirical approaches. Field visits, surveys, GIS simulations, and digital tools like ESRI CityEngine were used to create 3D GIS models. These models help digitize and analyze urban code parameters by using the form-based code approach. **Results:** The study demonstrates that 3D GIS models can enhance urban planning by improving the understanding of urban codes and their implications for preserving urban identity. The models provide insights into maintaining historical character while supporting development. **Discussion:** The findings highlight the potential of 3D urban models to improve decision-making in urban planning and underscore the value of such models in preserving the unique identity of historic districts like Rosetta City, offering a framework for similar regions.

Keywords: urban character; urban codes; historic districts; 3D GIS modeling.

Introduction

Urban knowledge, which includes data on both tangible and intangible elements, is crucial for the development of Geographic Information System (GIS) models that facilitate sustainable urban development. These models provide realistic description of urban environments, which are critical for analyzing urban systems and processes. Accurate 3D urban models have become essential tools for supporting urban knowledge and evaluating the performance of urban systems in the context of sustainable development (Billen et al., 2014). As highlighted by Batty (2013), understanding urban systems is a key requirement for achieving sustainable development goals in cities.

Spatial analytics, which involves understanding and managing space, is another crucial component of urban planning. The increasing availability of data from the web and sensors has significantly transformed the way we perceive and manage cities, particularly when dealing with urban transformations. Geography is crucial for understanding how the cities adapt and enhancing their resilience to developmental challenges (Kitchin, 2014). In the era of smart cities, 3D GIS models are indispensable tools for urban planners. These models enable enhanced visualization and analysis of urban systems, facilitating better decision-making processes that contribute to sustainable development. Additionally, these models improve the management of resources and infrastructure, fostering resilience and adaptability in cities (Townsend, 2013; Voghera and La Riccia, 2019).

Urban planning initiatives in Egypt, however, face several challenges. Current development strategies follow conventional planning processes that often overlook key factors such as location dynamics, target beneficiaries, and the economic foundations of new towns, as well as effective market incentives (Sims, 2015). Moreover, there is a notable gap in the understanding of the environmental and physical characteristics of selected development sites, compounded by the lack of sufficient studies and clarity (Kipper and Fischer, 2009). According to the Housing and Building Research Center, Egypt has around 50 building codes and design guides. Among these, the most relevant to urban form, identity, and building regulations (height, setbacks, cantilevers, etc.) are Unified Building Law No. 119 and the National Organization for Urban Harmony guides and periodicals (MHUC, 2008), (NOUH, 2008). While authorities have made efforts to introduce new codes for different regions, these codes still fall short of reflecting sustainable design approaches and preserving urban identity.

The research question is to what extent can 3D GIS urban digitization techniques and visualization

methods, aligned with a form-based code approach, assess the feasibility of urban codes in sustaining a neighborhood's identity and character? The hypothesis is that 3D urban models can effectively visualize the current physical urban context of a selected neighborhood and its relevant urban parameters, thereby supporting the digitization of urban codes to enhance smart urban management. The aim of this research is to analyze urban codes for a selected case study in Egypt using GIS analysis, digitize its urban parameters into 3D urban models, and visualize the impact of these urban codes on the city's character and identity. The structure of this research is divided into five sections. The first section offers a comprehensive literature review on urban character and the application of form-based codes, setting the theoretical foundation for the study. The second section outlines the research methodology, detailing the analysis of urban code parameters and the tools employed, including 3D GIS modeling techniques. The third section focuses on the case study of Rosetta City, Egypt, where the urban code parameters are critically analyzed to understand the local urban context. The fourth section explains the process of creating 3D GIS models, involving four key steps: upgrading GIS data, defining building use, developing building shape grammar, and visualizing urban code parameters. The final section presents the results of the study, discussing the findings and their implications for both urban planning and the preservation of historic districts.

Literature Review

Urban Character

The redefinition of urban land use classifications and zoning, along with the design of essential urban components such as nodes, special districts, and paths, plays a key role in enabling compatible mixed-use growth and promoting sustainable development. Kevin Lynch emphasized that identifying and reinforcing existing urban "nodes, paths, and districts" is crucial for sustainable urban development (Lynch, 1960). He defined special districts as areas of significant size associated with notable activities or characteristics (McGeough et al., 2014).

The growing loss of urban character in modern cities has led stakeholders and residents to place greater emphasis on areas where urban identity is linked to economic benefits. The preservation and development of urban character are vital for a city's vibrancy, as it reflects local culture. Urban character extends beyond visual appeal, fulfilling an emotional need for belonging. Identifying with the character of one's surroundings is essential for emotional well-being, and the loss of urban character can threaten cultural diversity as well as economic progress (Tiesdell et al., 1996; Yu, 2013).

This study is based on the regulations and standards established by the National Organization for Urban Harmony (NOUH), created by Decree No. 37 of 2001. NOUH's goal is to protect the aesthetic and cultural values of buildings, urban spaces, archaeological sites, and the architectural and urban character of Egypt while preserving the natural environment (NOUH, 2008). Relevant regulations, including urban design standards, heritage conservation, and architectural character preservation, are codified in Unified Building Law No. 119 and its procedural appendix No. 144 (MHUC, 2008).

Form-Based Codes

Form-based codes, a New Urbanism tool, aim to restore the form- and utility-based cityscapes of American cities' pre-zoning era. Form-based codes are used to maximize land use, benefit the general public, focus on producing a particular physical form, and design the development process and public spaces in alignment with the community's vision (MAP 2007), (Parolek et al., 2008). Form-based coding regulation of the built environment differs from traditional methods. This is because the use-based approach to zoning has proven ineffective in managing diverse, urban, mixed-use areas (Talen, 2012), (Zhang, Y. and Schnabel, M. A., 2017).

Form-based codes prioritize physical form over the separation of uses, fostering predictable built environments and a high-quality public realm. These codes are adopted into city law as regulations rather than guidelines. As regulatory tools, form-based codes provide an effective alternative to conventional zoning. They are specifically drafted to implement a community plan, resulting in neighborhoods that promote walkability, social interaction, and increased local investments (FBCI, 2023). Fig. 1 illustrates the main differences between conventional zoning and form-based codes.

Form-based codes are essential tools, particularly for historic districts, as they help maintain the identity of the district by considering all related urban elements. These standards include criteria for streetscapes, such as on-street parking, sidewalk width, and street trees, since the building form and streetscape are interconnected (Parolek et al., 2008). Many other rules found in traditional zoning ordinances, such as definitions, administrative processes, zoning board of appeals, nonconforming uses, and more, are also incorporated into form-based codes (Sitkowski and Ohm, 2006).

Research Methodology

The research methodology relies mainly on the descriptive, analytical and empirical approaches to reach reliable results. Different methods are used to monitor and analyze the current situation of the case study through data analysis, study visits, questionnaire, surveys and GIS urban simulations as shown in Table 1. We used digital tools and programs like Google My Maps, Google Earth, and

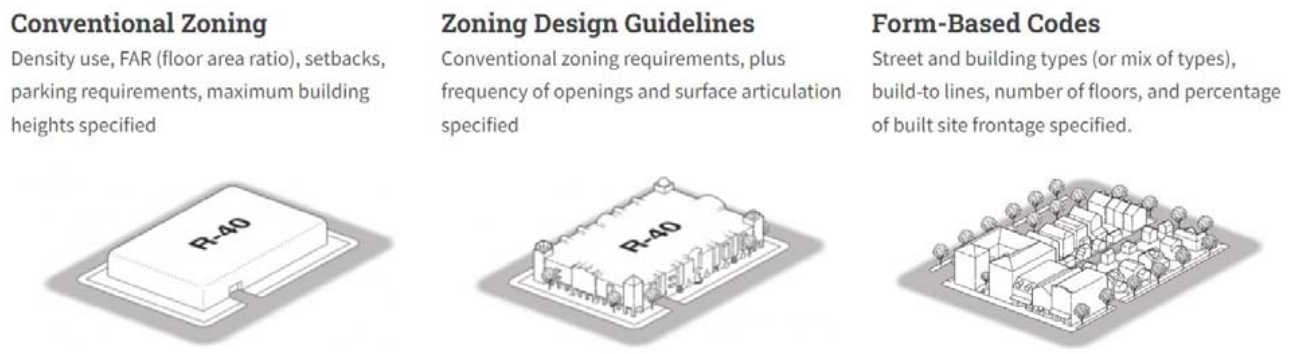

Fig. 1. Differences between conventional zoning and form-based codes, source: (FBCI, 2023; Zhang et al., 2018)

GIS platforms such as ArcMap, ArcScene, and Esri City Engine as a 3D city platform to aid in digital documentation and converting 2D spatial data into a 3D GIS model. Esri City Engine is widely used for rule-based modelling in the urban programming community (Souza, L. and Bueno, C., 2022).

Analyzed Urban Code Parameters

The application of digital tools using GIS will focus on specific urban parameters determined by the analysis of form-based codes and related Egyptian codes and guidelines, especially Urban Harmony guidelines and their executive regulations, as shown in Table 2. These urban parameters are analyzed using GIS analysis and processed with CityEngine into a 3D GIS model to create the identity of the selected neighborhood according to its regulations and design requirements.

Case Study Analysis

The city of Rosetta is located in the far north of Egypt on the west bank of the Rosetta branch of the Nile River and bordered to the north by the Mediterranean Sea, as shown in Fig. 2.

In terms of the number of its Islamic houses, Rosetta is the second-largest city after Cairo. The number of Ottoman-era heritage buildings has declined from 52 in 1963 to 37 at the present time (UNESCO, 2003; UN-HABITAT, 2006). The Rosetta stone, which enabled the discovery of hieroglyphs, is Rosetta City's most well-known historical monument. The Rosetta stone was found here during the French expedition in 1799, at the castle of Qaitbay at Burj Rasheed. Ancient ruins were discovered around the area, including those on Abu Mandur hill.

Table 1. **Assigned research methods and software, source: authors**

Methods/Tools	Software used
Field visits & survey	Google My Maps, printed maps
Case study analysis	ESRI ArcGIS Pro, Arc Scene
Experimental	ESRI ArcGIS Pro ESRI CityEngine

Digitizing the urban code using GIS is mainly based on the analysis of the Urban Harmony Guide for Rosetta historic district. There are two types of protection zones: (1) Zone A of max. protection that includes all historic buildings inside it, and (2) Zone B that surrounds Zone A and includes the waterfront of the historic district on Nile River (NOUH, 2022).

Urban Form Analysis

This section shows the analysis of legal requirements for building forms such as building ratio and heights. These parameters are defined in the "Specific to Transect Zones" section in the form-based code.

Building ratio

The urban fabric must be preserved in all areas. Land plots should not be subdivided. Buildings should be constructed right on the plot borders without setbacks or side spaces, creating solid and continuous blocks that result in a compact urban fabric similar to the historic urban layout in Rosetta (NOUH, 2022). Spaces left from building ratio regulations should be in the form of internal courtyards, skylights or back gardens, with the use of tree types similar to palm trees in the city. The reference for the boundaries of the buildings is the cadastral maps of 1936, as shown in the maps in Fig. 3, while Fig. 4 displays the regulated percentage of building ratio based on the land plot area.

Building heights

The height requirements mentioned in this guide should not contradict the Armed Forces Operations Authority or the Civil Aviation authorities, as well as Antiquities Protection Law No. 117 of 1983 and their executive regulations. Building heights are determined according to the street width in each zone. The study through survey and analysis of building heights in the historic district shows that approx. 30 % of the buildings do not comply with the requirements and regulations of building heights in the guide due to the weak control over construction from the concerned authorities, insufficient application of laws, administrative corruption and the landowners' demand for more profits (Fig. 5). These practices impact the urban form and character of

Table 2. **Urban parameters of Rosetta historic district for GIS analysis and CIM (city information modeling) development, source: authors**

Form-based codes	Related Egyptian codes and guidelines	Analyzed urban parameters
Specific to Transect Zones	Urban Harmony for Rosetta City Egyptian Classification of Urban Development Areas Guideline Egyptian Code for Housing and Residential Cluster Design	Building ratio Building heights
Specific to Building Types	Urban Harmony for Rosetta City	Architectural style Facade materials Balconies and cantilevers Openings Facade details
Specific to Frontage Types	Urban Harmony for Rosetta City	Storefronts
Supplemental to Transect Zones	Urban Harmony for Rosetta City Urban Harmony basics and criteria for heritage buildings and areas Urban Harmony basics and criteria for city centers Urban Harmony basics and criteria for advertisements and banners	Lighting Vegetation
Specific to Creating a Walkable Neighborhood	Egyptian Code for Housing and Residential Cluster Design	Building ratio
Specific to Thoroughfares	Road Elements Design Standards Guide Egyptian Code for Urban and Aerial Road Works — Part 3	Roads and Sidewalks

Fig. 2. Case study location, source: authors, processed by Google Earth Pro

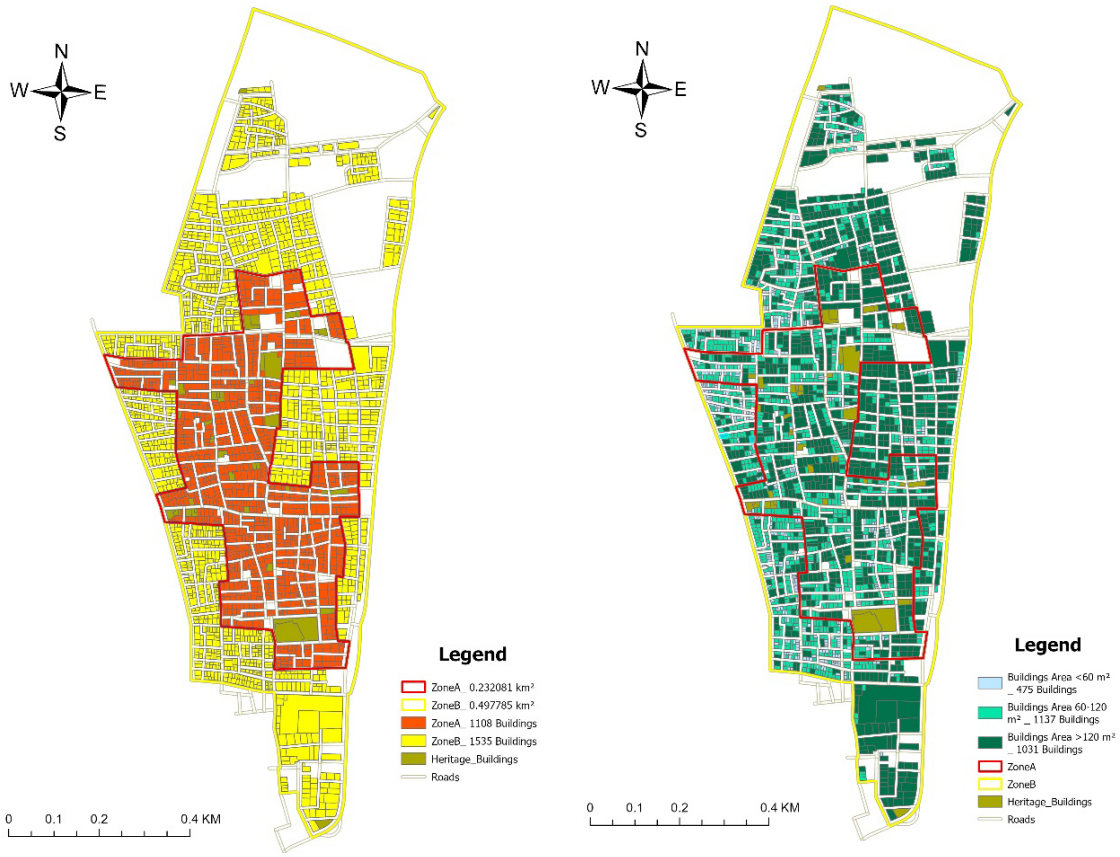

Fig. 3. Protection zones of Rosetta historic district, source: authors

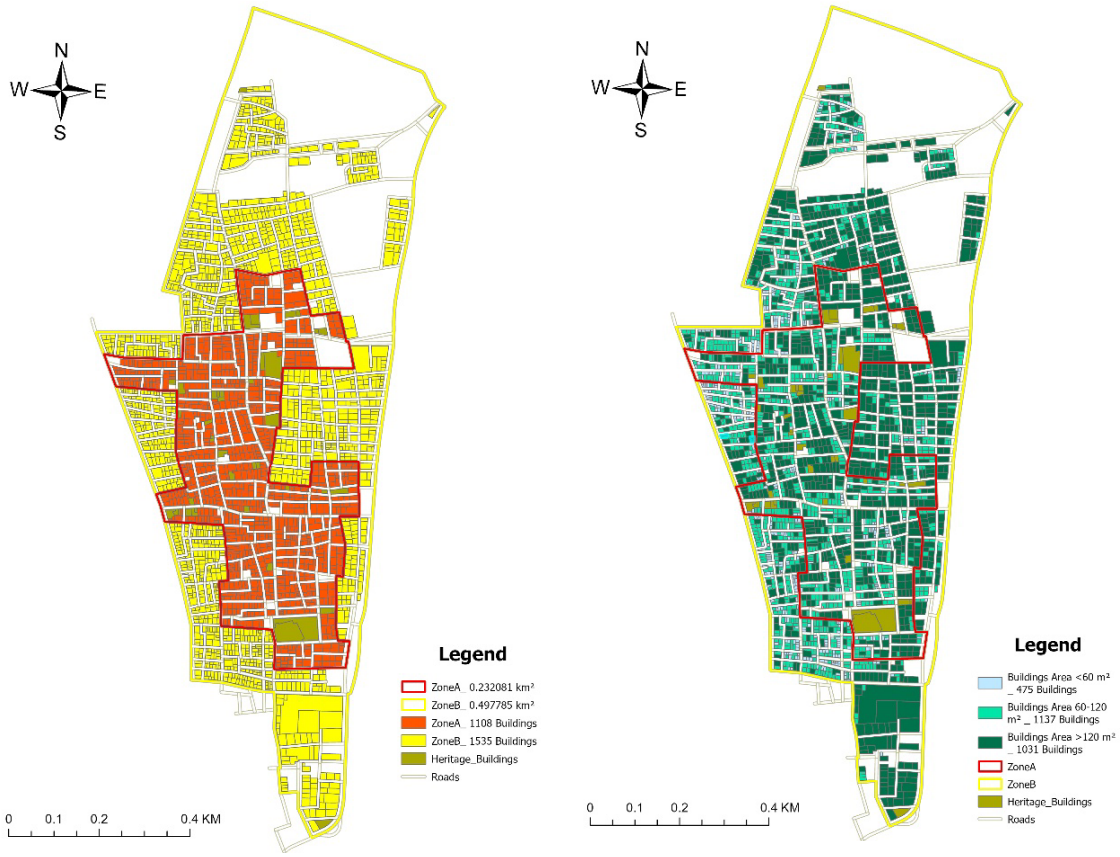

Fig. 4. Protection zones of Rosetta historic district, source: authors

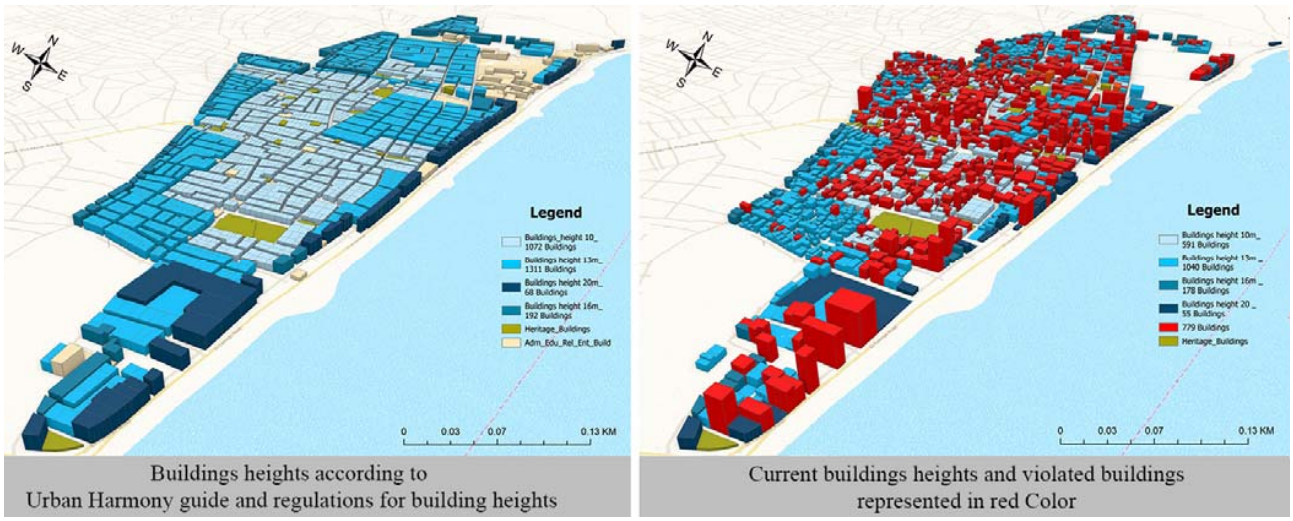

Buildings heights according to Urban Harmony guide and regulations for building heights

Current buildings heights and violated buildings represented in red Color

Fig. 5. Building heights compliance with the Urban Harmony Guide and regulations for Rosetta urban district, source: authors

the historic district, influencing its preservation and development to enhance tourism appeal and boost social and economic vitality.

Architectural Style of Building Types

This section outlines the building standards and architectural styles within the Rosetta historic district, analyzing them in accordance with the Urban Harmony Guide for building design standards, which aligns with the "Specific to Building Types" section in form-based codes. New architectural styles for buildings should be compatible with the existing character of the historic district, avoiding any distinctly different or unusual details. Figs. 6 and 7 highlight the original architectural character of the city, which reflects the Islamic style from the Mamluk and Ottoman periods. A blend of European and local architectural styles also emerged at the end of the 18th and early 19th centuries during the Khedivial period, though few buildings from this era remain in the historic district, as shown in Fig. 8.

Building facades should feature earth tones, such as shades of beige and gray. Brick cladding is required for ground floors, with a minimum height of 60 cm from the sidewalk, not exceeding the height of the first-floor slab, particularly in Zone A. In Zone B, bricks, stones, and natural materials are permitted. Wrought iron, in black, is used for vertical and horizontal grilles to protect the ground and mezzanine floors (NOUH, 2022).

In Zone A, openings are based on historic building features, with rectangular vertical shapes, brown-toned wooden doors and windows, transparent non-reflective glass, and the optional use of sunshades or mashrabiya as coverings. Balconies are only allowed in inner courtyards in Zone A. In Zone B, balconies are permitted on buildings facing streets wider than 10 meters, with restrictions on their width (not exceeding 10 % of the street width and a maximum of 120 cm). Cantilevered projections are allowed to a certain extent, with a maximum of 50 % of the facade surface. Limits on extrusion depend on the street width: up to 60 cm for streets under 12 meters wide and 100 cm for wider streets. In the historic district, only 10 % of buildings are allowed to have balconies, while 89 % may have cantilevers with a maximum protrusion of 60 cm (NOUH, 2022).

Storefronts

This section outlines the standards for the design of private frontages in the form-based code. The Urban Harmony Guide focuses only on storefront facade in terms of the original design of the building facade. Fig. 9 shows samples of storefronts inside the historic district, the photos show violations of some and their encroachment on the street. The Urban Harmony Guide for Rosetta City shows samples of the preferred architectural style from old storefronts and a sample for a new shop which adhered to this style as shown in the following Fig. 10.

GIS Analysis for Building Types Distribution

The development of each building type in Rosetta historic district is analyzed using GIS mapping to study their distribution according to the building standards and regulations discussed earlier, as shown in Tables 3 and 4. The GIS analysis focuses on three main parameters: building location (Zone A or Zone B), plot area, and street width. These parameters help determine the form of each building in terms of building ratio, heights, balcony and cantilever regulations. Based on data from GOPP GIS, street widths in the Rosetta historic district fall into two ranges: 5–10 meters and 12–20 meters.

The findings are categorized into 12 cases of varying urban regulations, which will be digitized using CityEngine to allow for easy control and visualization by different users. Each case is defined with specific details; for instance, Case 01 consists of 131 buildings and includes such information as area, building ratio, height, and

Fig. 6. Samples of historic residential buildings in Rosetta (Arab kulli, Al-Amasyali and Asfour houses), source: authors

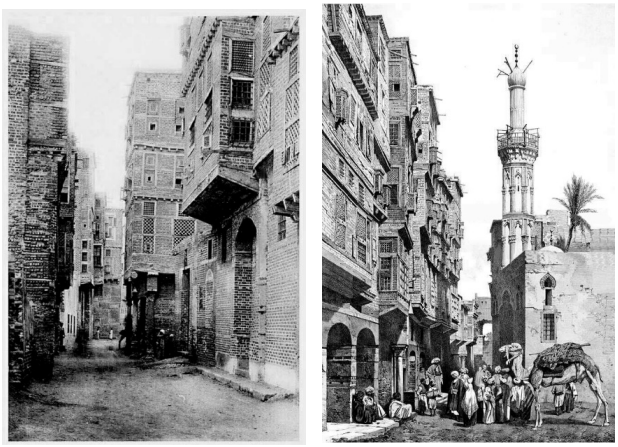

Fig. 7. Historic architectural style in Rosetta City, source: Rosetta online archive

Fig. 8. Mixed architectural style in Rosetta City, source: Rosetta online archive

Fig. 9. Samples of storefronts inside Rosetta historic district, source: authors

Fig. 10. Example of a new shop which adhered to the guide regulations, source: NOUH (2022)

the dimensions of balconies and cantilevers. This digitized approach enables local residents, urban planners, architects, local government authorities, developers, investors, and other stakeholders to identify and apply the relevant regulations for each building, ensuring compliance with design features

Table 3. **GIS analysis of Building Types Distribution for streets 5–10 m wide, source: authors**

Plot area	Zone A	Zone B
	Street width 5–10 m	
< 60 m²	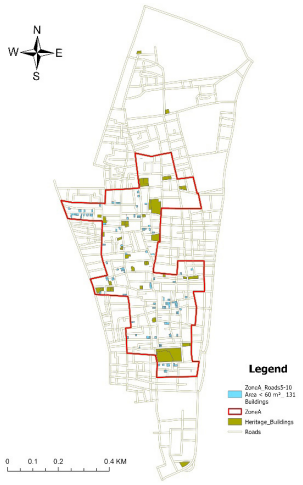	
	Case 01: 131 buildings < 60 m², building ratio 100 %, heights 10 m No balconies, 25–50 cm cantilevers	Case 02: 287 buildings < 60 m², building ratio 100 %, heights 13 m No balconies, 25–50 cm cantilevers
60–120 m²	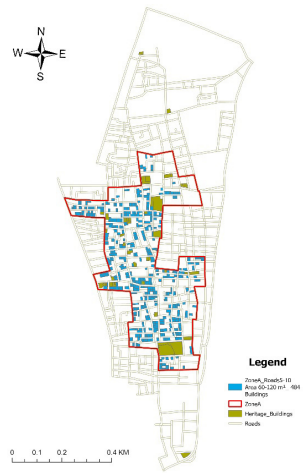	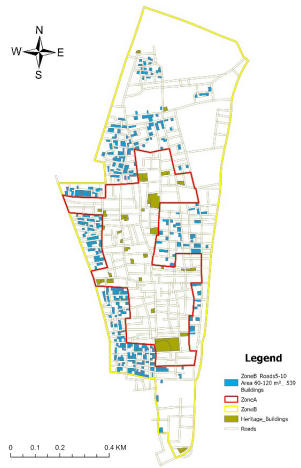
	Case 03: 483 buildings 60–120 m², building ratio 80 %, heights 10 m No balconies, 25–50 cm cantilevers	Case 04: 539 buildings 60–120 m², building ratio 80 %, heights 13 m No balconies, 25–50 cm cantilevers
> 120 m²	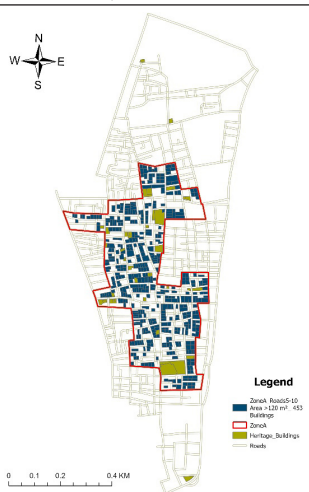	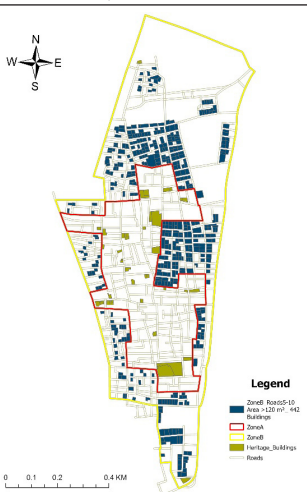
	Case 05: 453 buildings > 120 m², building ratio 70 %, heights 10 m No balconies, 25–50 cm cantilevers	Case 06: 442 buildings > 120 m², building ratio 70 %, heights 13 m No balconies, 25–50 cm cantilevers

Table 4. **GIS analysis of Buildings Types Distribution for streets 12–20 m wide, source: authors**

Building ratio	Zone A	Zone B
	Street width 12–20 m	
< 60 m²		
	Case 07: 4 buildings < 60 m², building ratio 100 %, heights 13 m No balconies, 60–100 cm cantilevers	Case 08: 54 buildings < 60 m², building ratio 100 %, heights 16 m 120 cm balconies, 60–100 cm cantilevers
60–120 m²		
	Case 09: 20 buildings 60–120 m², building ratio 80 %, heights 13 m No balconies, 60–100 cm cantilevers	Case 10: 96 buildings 60–120 m², building ratio 80 %, heights 16 m 120 cm balconies, 60–100 cm cantilevers
> 120 m²	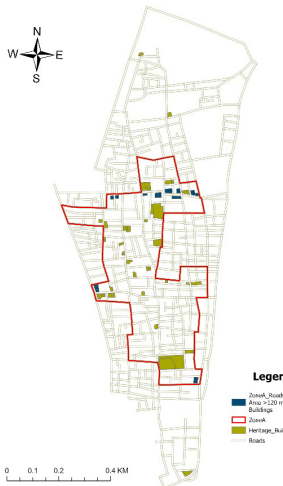	
	Case 11: 16 buildings > 120 m², building ratio 70 %, heights 13 m No balconies, 60–100 cm cantilevers	Case 12: 117 buildings > 120 m², building ratio 70 %, heights 16 m 120 cm balconies, 60–100 cm cantilevers

and facilitating the implementation of form-based codes. As a result, users will better understand and manage the urban landscape of the Rosetta historic district, enhancing both preservation and development efforts.

Roads and Sidewalks

The Thoroughfares section in form-based codes provides thoroughfare guidelines and components. The thoroughfares guidelines in the Urban Harmony Guide are classified into two types according to the location in Zones A and B. Based on the field survey, most streets need restoration and development, as many of them are deteriorated, with different finishing types, specifications and measurements. They do not comply with the requirements and regulations of the Urban Harmony Guide as shown in Fig. 11. Even the main waterfront street of Rosetta city has problems related to infrastructure and maintenance with no accessibility or crossing places for pedestrians and people with special needs as shown in Fig. 12.

Lighting

Lighting poles need to be installed every 30 meters on streets 12 meters wide or more. In the streets of less width, the lighting should be in the form of cables fixed to the building walls at a height of no less than 4 meters. Based on the field survey, lighting elements inside the historic district should be replaced and modified, as shown in Fig. 13. Lighting poles were found inside the historic district in the streets less than 12 m wide, while cables were seen hanging in the air between buildings, which distorts the visual image of the historic district. Fig. 14 shows lighting poles which located on the main waterfront street of Rosetta City.

Vegetation

It is allowed to plant plazas, squares and main streets more than 6 meters wide using appropriate techniques to protect the heritage buildings from the impact of irrigation water. These trees should not cover the facades of heritage buildings. Palm trees of the types found in the Rashid area should be used whenever possible as shown in Fig. 15.

Fig. 11. Example of narrow streets inside Rosetta historic district, source: authors

Fig. 12. Waterfront street of Rosetta City, source: authors

Fig. 13. Lighting elements in Rosetta historic district, source: authors

Fig. 14. Lighting elements on the waterfront street of Rosetta City, source: authors

Fig. 15. Palm trees as vegetation elements in Rosetta City, source: authors

Generating 3D GIS Models

Step 01: Upgrading the existing GIS data

The GIS database of Rosetta City from the General Organization for Physical Planning in Egypt is inaccurate, outdated, and different from the reality of the current situation. Field surveys were performed to update its GIS data for the current buildings' features of the historic district in June 2022. 3D GIS modeling for the historic district was developed using ArcGIS Pro to visualize the current urban context as shown in Fig. 16. The main aim was to check and update the GIS dataset for the historic urban district of Rosetta City and develop a 3D GIS urban model that could provide a clear visualization for the current urban data and form.

Step 02: Defining building use

Most buildings in Rosetta historic district are mixed-use residences as the ground floor is mainly used for commercial purposes while the rest of the floors are residential. A color coding for each building is scripted using Python as a CGA rule to define the use of each floor in CityEngine as shown in Fig. 17. The CGA rule file was mainly created by ESRI R&D Center and Devin Lavigne, Houseal Lavigne Associates, but it was edited by the researchers to be suitable for the urban context of the Rosetta case.

Step 03: Building shape grammar

Building regulations and forms were developed using Python-based CGA rule. The code defines the urban parameters that could be adapted according to the 12 previous cases for a better visualization of the whole urban district. The CGA rule was applied depending on the previously analyzed urban parameters such as building ratio, setbacks, heights, cantilevers, facade order and opening proportions as shown in Fig. 18. Facade design and order could be

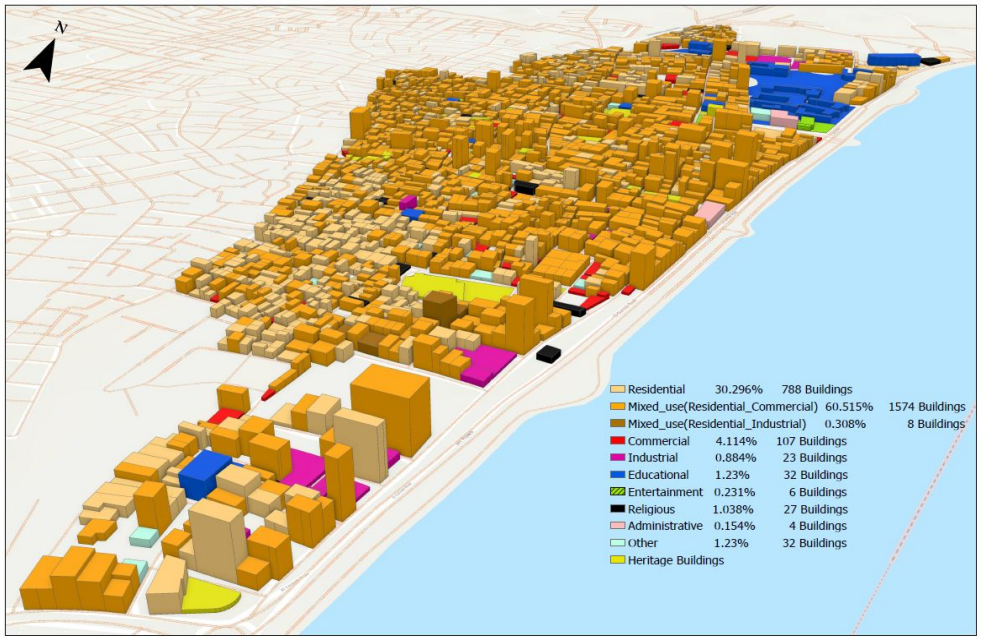

Fig. 16. 3D GIS land use map for Rosetta historic district, processed by ArcGIS Pro, source: authors

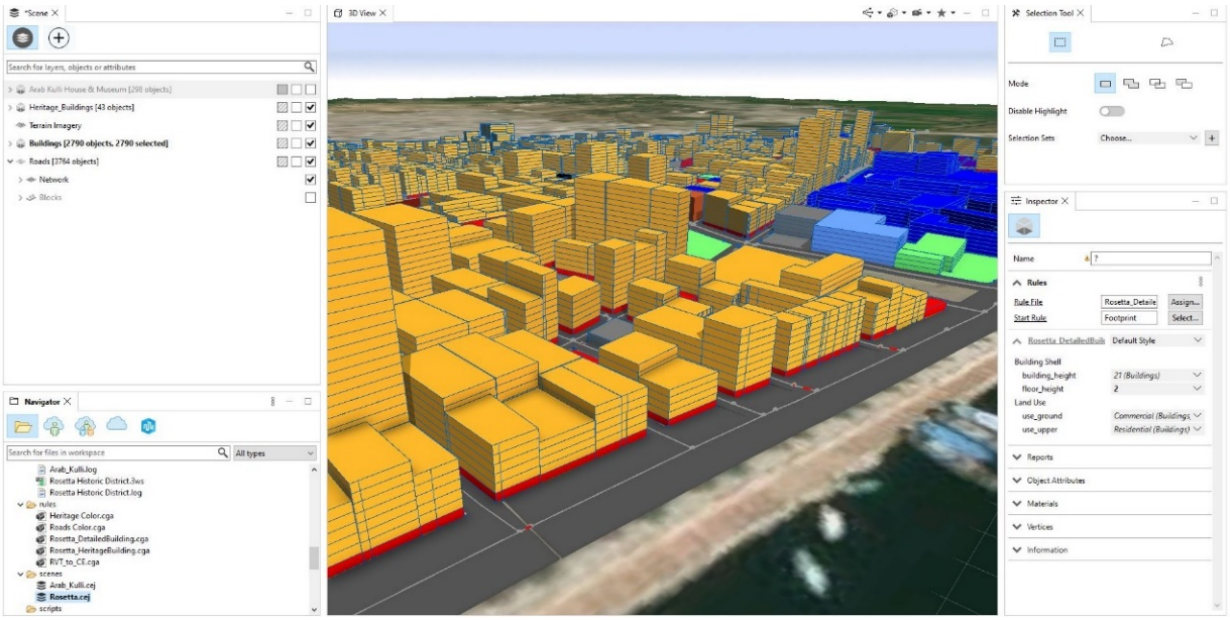

Fig. 17. Building floor uses in CityEngine viewport, source: authors

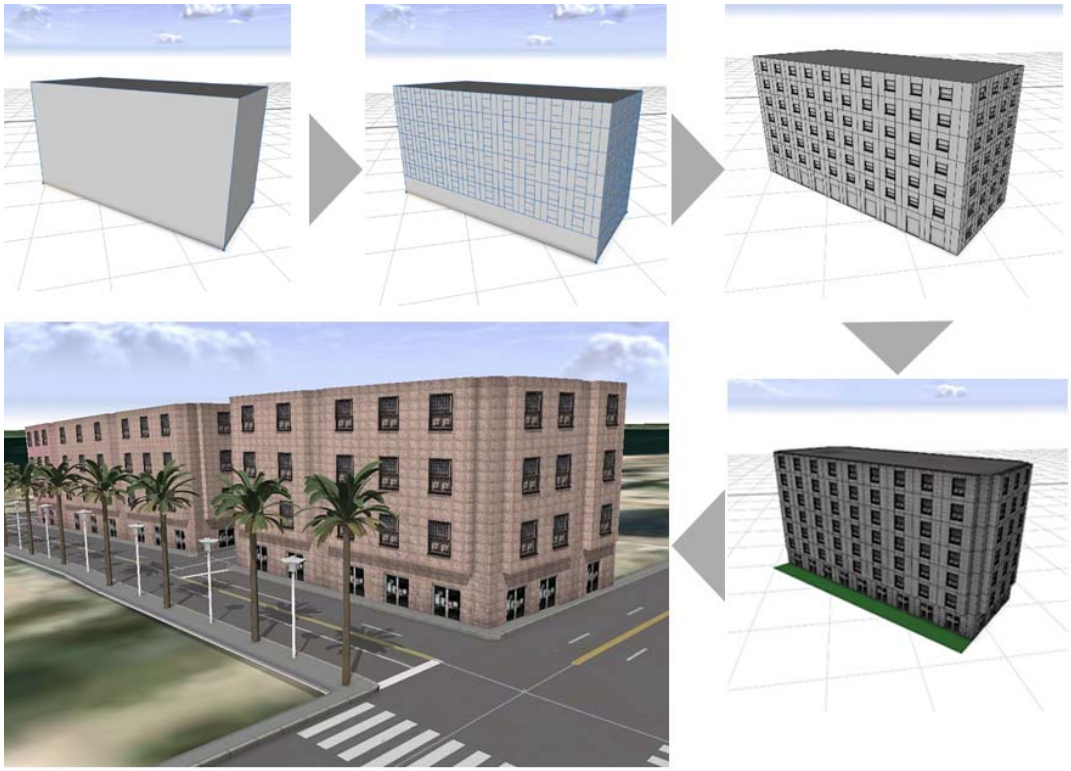

Fig. 18. CGA rule development for the controlled urban parameters, source: authors

Table 5. **Urban code procedural modeling: controlling different urban parameters affecting urban character, source: authors**

Urban parameters	Control parameters
Building parameters	Building ratio, setbacks, heights, cantilevers, facade order and openings proportions, storefronts, and texture mapping.
Street parameters	Street, lanes, right sidewalk and left sidewalk width, pedestrian crossing lines, street lines and texture mapping.
Tree parameters	Tree types, height, radius and visualization options.
Lights parameters	Lights height — depends on 3D model in .obj format.

developed by CGA rules to define the architectural style and order of buildings. All these parameters could be changed and modified easily through Python scripting and “inspector” tab in CityEngine which contains all the defined urban parameters.

Step 04: Urban code control parameters and visualization

Table 5 shows the application of different urban elements in CityEngine platform and the ability to control their parameters.

The 12 cases of different urban regulations in Tables 4 and 5 for Rosetta historic district were digitized using CityEngine to be controlled and visualized by different users as show in Fig. 19. Figs. 20 and 21 show the ESRI CityEngine web-based model. which could be shared with all users and stakeholders to check the regulations and building forms for each plot.

Results and Discussion

City information modeling platforms could support the decision makers to develop a comprehensive, integrated, upgrading methodology using a GIS-based spatial data management framework. This framework could efficiently assist the policies

Fig. 19. Twelve cases of different urban regulations, source: authors, processed by CityEngine

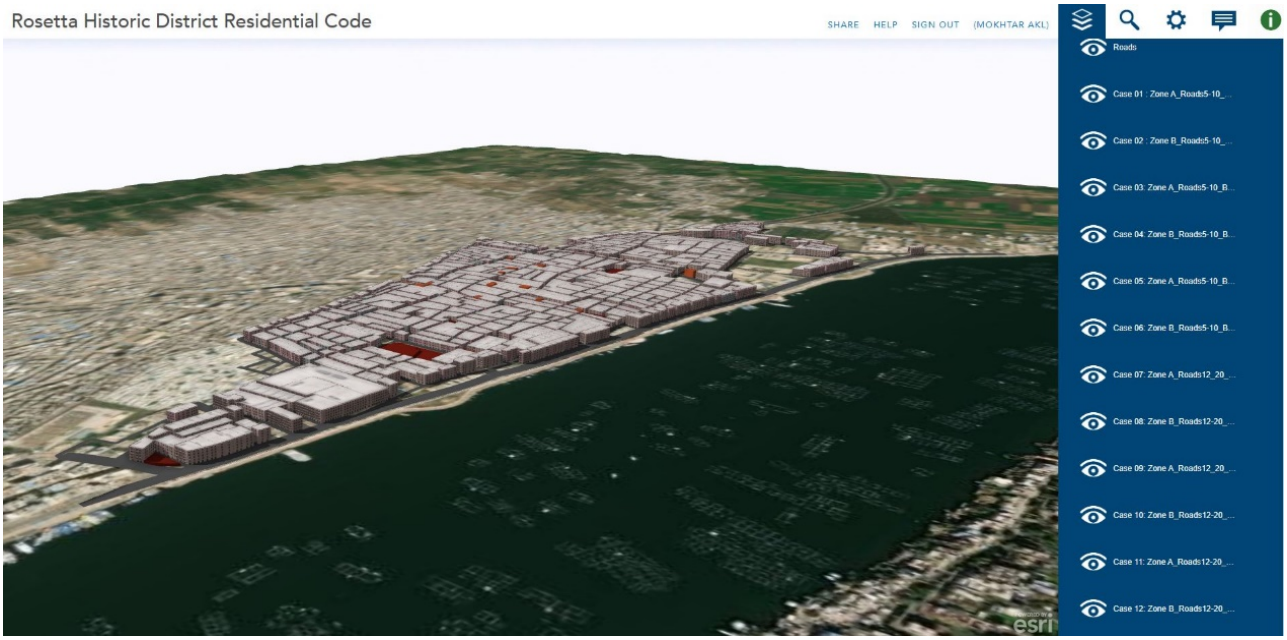

Fig. 20. Twelve cases of different urban regulations in the ESRI CityEngine web-based model, source: authors

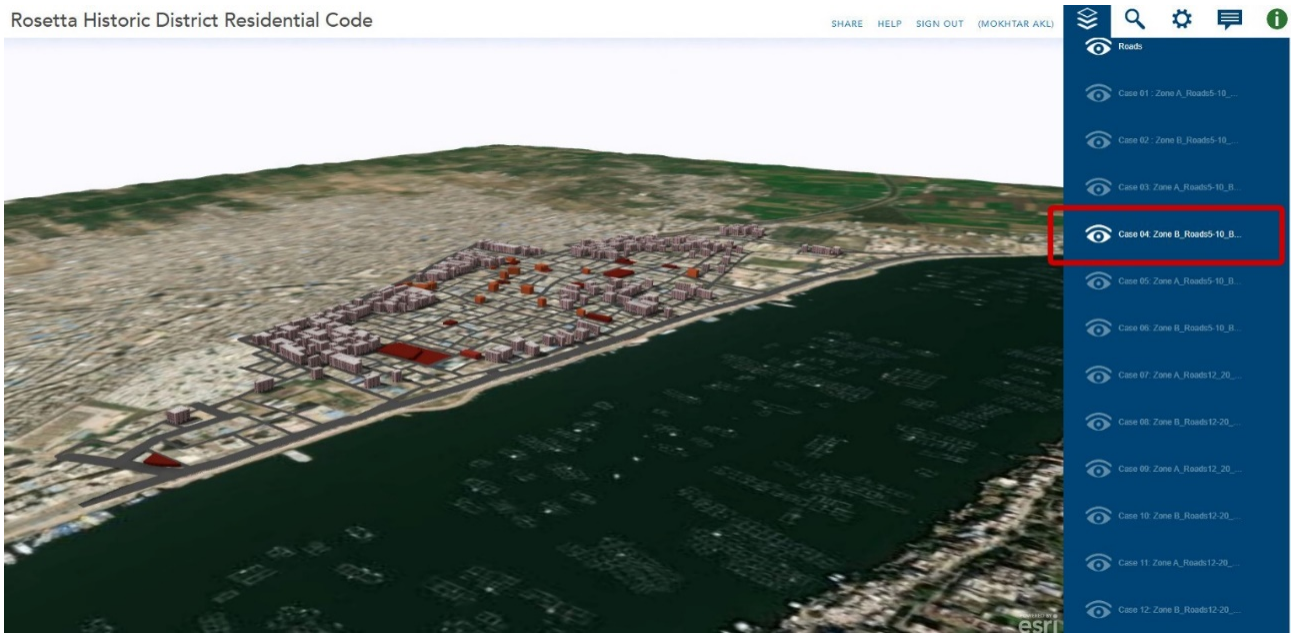

Fig. 21. Case 4 selected from different urban regulations in the ESRI CityEngine web-based model, source: authors

of urban development, urban regeneration, conservation, protection, and rehabilitation of urban neighborhoods. The development of urban codes using digital urban tools could preserve the urban elements manifesting urban identity.

The research results could be summarized as shown in Fig. 22.

We developed and updated the GIS dataset for the historic urban district of Rosetta city and a 3D GIS urban model that could provide a clear visualization for the current urban data and form.

We digitized urban code parameters representing the regulations of Rosetta historic district as a CGA rule (scripted using Python language) in CityEngine. The digitized urban code enables visualization of the district's urban character using 3D GIS models.

The developed 3D GIS model represents form-based code approach as it visualizes the criteria of urban form in which building form and streetscape are interconnected.

The study develops three 3D urban models with different level of detailing and visualization methods. The three developed models were compared to determine their extent in visualizing a realistic description of current physical urban context and all urban parameters that support the digitizing of urban code. The comparison criteria show the level of details achieved, ease of modeling and modifications, application of procedural modeling and the ability of online dissemination. In addition, we analyzed how much urban and building details could be visualized in each model.

The results indicate a progressive enhancement in the models' capacity to visualize urban contexts and support urban code digitization as shown in Table 6:

Fig. 22. Key results of the study, source: authors

Table 6. **The three developed 3D urban models with different level of details, source: authors**

	GIS System extruded by Arc Scene	Developing GIS System using City Engine	
	Model 01	**Model 02**	**Model 03**
	Updated GIS Data	Scripting Building Use	Scripting Building Details from Urban Codes
	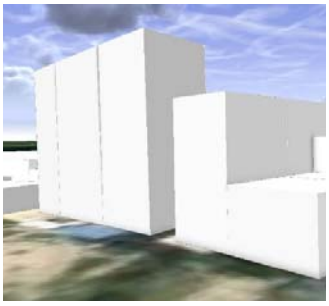	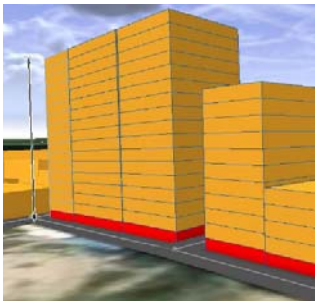	
Level of Details	LoD01	LoD02 - supports LoD04	LoD03 - supports LoD04
Ease of Modeling	*	*	*
Ease of modifications		*	*
Procedural Modeling		*	*
Online Dissemination	*	*	*
Open Source Software	*		
Urban Details			
Land Use	*	*	*
Building Footprint	*	*	*
Total Floor Areas		*	*
Roads and Side walks			*
Lightings			*
Vegetation			*
Building Details			
Building Use		*	*
Buildings Heights	*	*	*
Buildings Ratio		*	*
Architectural style			*
Balconies and Cantilevers			*
Openings			*
Façade details			*
Facades Materials			*
Storefronts design			*
Indoor Spaces			
	6/21 – 28 %	11/21 – 52 %	20/21 – 95 %

Model 01 achieves 28 % of the criteria. This model, using basic GIS data, offers minimal detail and lacks advanced urban information, making it more suitable for basic visualizations without complex urban forms or architectural styles.

Model 02 fulfills 52 % of the criteria. It enhances the basic model by adding key urban data like total floor areas, building use, and ratios. The inclusion of procedural modeling makes modifications easier and supports further urban data integration.

Model 03 performs the best, meeting 95 % of the criteria. This model integrates detailed urban information, including roads, sidewalks, lighting, vegetation, and specific architectural elements such as facade materials and storefront designs. It also supports online dissemination and procedural modeling, making it the most robust for visualizing and managing urban environments.

The progression from Model 01 to Model 03 reflects the increasing level of detail and complexity required to digitize urban codes and enhance urban planning. Model 01 provides a basic foundation, but it is insufficient for detailed urban analysis. Models 02 and 03, particularly with the application of CGA

rules and procedural modeling, offer significant improvements in the visualization of urban and building details, making them valuable for decision-making in urban management.

Model 03, with its higher level of detail, supports a more accurate and realistic portrayal of urban neighborhoods, crucial for implementing form-based codes and maintaining the architectural integrity of historic districts. This model's ability to display specific architectural elements is particularly useful for stakeholders aiming to preserve or replicate the character of historic cities like Rosetta. The importance of online dissemination in Model 03 also satisfies the need for real-time updates and collaboration between different government sectors and urban planners.

Building on the initial comparison and discussion, it is essential to emphasize the increasing significance of each model's level of detail (LoD) and its broader implications for urban planning, especially in historic districts such as Rosetta. The progressive enhancement of the models is not merely a technical achievement but a reflection of the need for advanced urban analysis tools that can bridge the gap between traditional urban fabric and modern urban management strategies.

Conclusion

Neglecting the built environment and urban sprawl, along with not enforcing regulation codes, heightens the vulnerability of urban structures to disaster risks. At the same time, a well-conserved natural and historic environment supported by urban regulations and design codes can play a significant role in the physical, social, and economic resilience of communities. The integration of digital urban tools and new technologies at different stages of planning and implementation should be improved to provide more options to sustain our cities. The collection of data on existing buildings or a certain urban area is quite challenging due to the lack of connections between databases of different governmental institutions as they create their own data for specific purposes independently. The research results could be discussed in four main aspects: the importance of GIS platforms in decision making, GIS data accuracy in Egypt, the importance of urban code simulations for city identity, and the suitability of form-based codes application and integration into local urban codes.

GIS Platforms and Decision-Making

Digital urban platforms could support the decision makers to develop a comprehensive, integrated, upgrading methodology using GIS-based spatial data management framework. This framework could efficiently assist the policies of urban development, urban regeneration, conservation, protection, and rehabilitation of urban neighborhoods. The development of urban codes using digital urban tools could preserve the urban elements that reflect urban identity.

GIS Data Accuracy

The accuracy of GIS data mapping for urban districts needs to be updated and expanded. The issues in Egypt stem from the GIS data at the General Organization for Physical Planning being inaccurate and lacking. The GIS databases for each organization are not the same and there is no unified governmental source to support spatial data for all organizations. Many of the Egyptian cities have missing data on the online GIS platforms such as "open street maps" compared to other developed cities. Also, the compacted urban fabric and narrow streets of old cities in Egypt complicate the digitizing of these cities and require mixed methods to collect, survey and digitize the current urban data.

Urban Code Modeling for City Identity

Inability to envision or picture the visual image of neighborhoods after implementing building requirements might result in an unsuitable view, visual boredom, or distortion. Thus, it is important to model building requirements and regulations to examine the visual identity of cities before implementing them in real life. The software offers a chance to change several urban parameters which could develop many alternatives of building regulations and analyze their effect on the visual identity of neighborhoods.

Form-Based Code Integration

The form-based code could be integrated after undergoing certain adaptations. There are different legislative, social, economic, environmental constraints which could affect the upgrading of current Egyptian codes. There is a need to develop and initiate special legislative system for urban neighborhoods, especially the historic and valued ones. In addition to introducing a set of planning regulations and guidelines which help in implementing the ideas of the form-based code, the study considers utilizing already-existing legislation that is not mandatory or currently in use.

References

Batty, M. (2013). *The new science of cities*. Cambridge, MA: The MIT Press, 520 p.

Billen, R., Cutting-Decelle, A.-F., Marina, O., de Almeida, J.-P., Caglioni, M., Falquet, G., Leduc, T., Métral, C., Moreau, G., Perret, J., Rabino, G., San Jose, R., Yatskiv, I., and Zlatanova, S. (2014). *3D city models and urban information: current issues and perspectives. European COST Action TU0801*. Les Ulis: EDP Sciences, 115 p.

MHUC, Egyptian Ministry of Housing, Utilities, and Urban Communities (2008). *Unified Building Law No. 119/2008 and its executive appendix Ministerial Decree no. 144/2009*. Cairo: Egyptian Ministry of Housing, Utilities, and Urban Communities. Published in The Egyptian Al-Waqa'i' newspaper, Issue No. 82 (Supplement 1), 8 April 2009.

FBCI (2023). *Form-based codes*. [online] Available at: https://formbasedcodes.org/ [Date accessed October 05, 2023].

Kipper, R. and Fischer, M. (eds.) (2009). *Cairo's informal areas: between urban challenges and hidden potentials*. Cairo: German Technical Cooperation, 224 p.

Kitchin, R. (2014). *The data revolution: big data, open data, data infrastructures and their consequences*. Thousand Oaks, CA: Sage Publications*, 240 p.*

Souza, L. and Bueno, C. (2022). City Information Modelling as a support decision tool for planning and management of cities: A systematic literature review and bibliometric analysis. *Building and Environment*, Vol. 207, Part A, 108403. DOI: 10.1016/j.buildenv.2021.108403.

Lynch, K. (1960). *The image of the city*. Cambridge, MA, and London: The M.I.T. Press, 194 p.

MAP, Michigan Association of Planning (2007). *Form-based codes; Smart growth tactics*. Issue 28., USA. [online] Available at: https://www.mml.org/pdf/map_article_issue28.pdf [Date accessed April 10 2023].

NOUH, The National Organization for Urban Harmony, 2008. *Urban Harmony Periodicals.* [Online] Available at: http://urbanharmony.org/Periodicals/1, [Date accessed: March 12 2023].

NOUH, National Organization for Urban Harmony (2022). *Urban Harmony guide for Rosetta city*. [Online] Available at: http://www.urbanharmony.org/nouh/Upload/Instructions/AttachmentFile/35/rashid2022.pdf, [Date accessed: March 12 2023].

Parolek, D. G., Parolek, K. and Crawford, P. C. (2008). *Form-based codes: a guide for planners, urban designers, municipalities, and developers*. Hoboken: John Wiley & Sons*, 368 p.*

Sims, D. (2015). *Egypt's desert dreams: development or disaster?* Cairo: American University in Cairo Press, 401 p.

Sitkowski, R. J. and Ohm, B. W. (2006). Form-based land development regulations. *Urban Lawyer*, Vol. 38, No. 1, pp. 163–172.

Talen, E. (2012). *City rules: how regulations affect urban form*. Washington, DC: Island Press*, 200 p.*

Tiesdell, S., Oc, T., and Heath, T. (1996). *Revitalizing historic urban quarters*. Oxford: Architectural Press, 234 p.

Townsend, A. M. (2013). *Smart cities: big data, civic hackers, and the quest for a new utopia*. New York: W. W. Norton & Company*, 400 p.*

McGeough, U., Newman, D., and Wrobel, J. (2014). *Model for sustainable urban design*. [online] Available at: https://www.energy.gov/sites/prod/files/2013/11/f4/model_for_sustainable_urban_design.pdf [Date accessed March 21 2023].

UNESCO (2003). *World Heritage Convention. Tentative Lists. Historic quarters and monuments of Rosetta/Rachid*. [online] Available at: https://whc.unesco.org/en/tentativelists/1831/ [Date accessed December 20, 2023].

UN-HABITAT (2006). *Rosetta*. Kenya: United Nations Human Settlements Programme, 8 p.

Voghera, A. and La Riccia, L. (2019). *Spatial planning in the big data revolution*. Hershey PA, USA: IGI Global, 359 p.

Zhang, Y., Azzali, S., Janssen, P., and Stouffs, R. (2018). Design for walkable neighborhoods in Singapore using form-based codes. In: *11th International Forum on Urbanism (IFoU) Congress 2018, December 10–12, 2018*, Barcelona, Spain.

Zhang, Y. and Schnabel, M. A. (2017). Parametric modeling in form-based urban design code for high-dense cities. in Turrin, M., Peters, B., O'Brien, W., Stouffs, R., and Dogan, T. (eds.) *Proceedings of the Symposium on Simulation for Architecture and Urban Design 2017: SimAUD 2017,* May 22-24 Toronto, Canada, pp. 265–272.

Yu, Z. (2013). *Regulation of urban character: style, colour and historic character in a modern Chinese city – the case of Harbin*. PhD Thesis in Humanities.

ЦИФРОВИЗАЦИЯ ГРАДОСТРОИТЕЛЬНЫХ КОДЕКСОВ ДЛЯ СОХРАНЕНИЯ ГОРОДСКОГО ХАРАКТЕРА ИСТОРИЧЕСКИХ РАЙОНОВ: НА ПРИМЕРЕ ГОРОДА РОЗЕТТА, ЕГИПЕТ

Мохтар Хосни Акль*, Шериф А. Шета, Ламис Эль Гизави

Университет Мансура, улица Эльгомхурия, город Мансура, Египет

*E-mail: mokhtarakl@mans.edu.eg

Аннотация

Введение: эффективное городское планирование опирается на всестороннее знание как физических, так и нефизических городских элементов. Они имеют решающее значение для разработки моделей ГИС, которые поддерживают устойчивое городское развитие, обеспечивая реалистичные представления об урбанистическом контексте. Точные 3D-модели играют главную роль в анализе городских систем и процессов. **Цель:** оценка влияния методов городской оцифровки и визуализации 3D ГИС на целесообразность градостроительных кодексов для сохранения городской идентичности и характера на примере города Розетта (Рашид), Египет. **Методы:** мы использовали описательный, аналитический и эмпирический подходы. Полевые исследования, опросы, моделирование ГИС и цифровые инструменты, такие как ESRI CityEngine, использовались для создания 3D-моделей ГИС. Эти модели помогают оцифровывать и анализировать параметры градостроительных кодексов на основе объемно-пространственного регламента. **Результаты:** исследование показало, что 3D-модели ГИС могут улучшить городское планирование благодаря лучшему пониманию градостроительных кодексов и их последствий для сохранения городской идентичности. Модели дают представление о сохранении исторического характера при поддержке развития. **Обсуждение:** результаты подчеркивают потенциал городских 3D-моделей для улучшения принятия решений в городском планировании и ценность таких моделей для сохранения уникальной идентичности исторических районов, таких как город Розетта, предлагая основу для подобных регионов.

Ключевые слова: городской характер; градостроительные кодексы; исторические районы; 3D-моделирование ГИС.

DOI: 10.23968/2500-0055-2025-10-1-49-58

PRIVACY AND SEGREGATION IN TRADITIONAL DOMESTIC SPACES: SPACE SYNTAX ANALYSIS OF THE "QUALITY OF LIFE" IN ISLAMIC TRADITIONAL HOUSES

Nelly Shafik Ramzy[1]*, Razan Ebrahim Arafa[1], Ebrahim Sedki Ebrahim[2], Ali Kamal Altawansy[1]

[1]Damanhour University, 27 Galal Qoreitem Sq, Damanhour, Egypt
[2]Menoufia University, Gamal Abdel Nasser, Qism Shebin El-Kom, Menoufia, Egypt

*Corresponding author's e-mail: tawswzwm@yahoo.com

Abstract

Introduction: The concept of home goes far beyond physical aspects, and its essence is interwoven with the spiritual nature of humankind. **Purpose of the study**: This paper aims at examining the spatial formations of five contemporaneous historical Islamic residences in three cities: Cairo, Damascus, and Aleppo. We intend to show that their layouts, which were mainly governed by certain traditions of privacy and visibility, were negatively affected by those factors in terms of functional and psychological efficiency. **Methods**: The paper utilizes Space Syntax formulas and the UCL Depthmap software to investigate and analyze the spatial configurations of these residences to provide a new comprehension of the life experience and the functional performance in these abodes, which were always regarded as ideal. **Results** show that the layouts in the five residences offer satisfactory qualities in terms of the privacy level, which is certainly a fundamental human need. However, the hierarchy of access to spaces has negative consequences for psychological requirements and functional efficiency. **Conclusions:** In order to meet certain social considerations, the spatial configurations in these residences failed to meet other functional and psychological needs of the inhabitants.

Keywords: domestic architecture; traditional houses; spatial configuration; functional efficiency; Space Syntax.

Introduction

Space Syntax theory of architecture and urban design originated in the 1970s. The Space Syntax term reflects its early analogies to linguistic theories. It was believed that, just as there are certain combinations of words that can be assembled into a meaningful sentence, only certain configurations of spaces would actually make sense. Here, spatial and social forms are in such a close relationship that a certain spatial configuration may define different social patterns. A set of thematic graphs, algorithms and software was developed for the representation, quantification, analysis and interpretation of spatial configuration (Ramzy, 2016).

Quality of life is dynamic, people and the environment change over time. However the historical domains of durability, convenience and beauty continue to be essential needs. Giving priority to one of these qualities over the others may lead to low functional efficiency and performance levels of the layouts. In this paper, we consider the functional qualities of five residences that date back to the Mamluk and Ottoman eras. The architecture of traditional Islamic houses, which have been always considered as perfect places for life (Hwaish, 2015), with their spacious sunlit courtyards and private sheltered spaces, correlate with the concept of quality of life, covering psychological, utilitarian, and interpersonal issues.

For Franz et al. (2005), the property of segregation is an indicator of the degree of social-functional efficiency of space**.** In traditional Islamic houses, the concept of privacy refers principally to the segregation between males and females. Achieving privacy in a house requires the interior space to be invisible to strangers and the spatial configuration to provide the least amount of communication between the spaces dedicated to males (*Salamlik*) and to females (*Haramlik*) in the house. The paper's hypothesis is that this kind of segregation may have affected the functional performance of the residences. Therefore, the aims of the analysis performed in this paper are to investigate, first, whether space-segregation indeed helped attaining high levels of privacy; and secondly, its influence on the functional performance and the quality of life within residential environments.

The question that arose here was: how to evaluate the impact of spatial configuration on the functional efficiency of these layouts. The paper here suggested Space Syntax analysis as a quantifiable syntactic approach and a complementary tool for illuminating new dimensions of life in historical communities. It is used to detect and measure the functional performance and assess the life quality across the five dwellings subjected to the study.

With this in mind, a Space Syntax analysis of the five residences was performed in four phases. The initial phase has two steps which show: a) the sampling logic behind the choice of the five

For citations: Ramzy, N. S., Arafa, R. E., Ebrahim, E. S., Altawansy, A. K. (2025). Privacy and segregation in traditional domestic spaces: space syntax analysis of the "quality of life" in islamic traditional houses. Architecture and Engineering, No 1 (10), pp. 49–58. DOI: 10.23968/2500-0055-2025-10-1-49-58.

residences as representatives of traditional Islamic residences; and b) the formulas and tools of Space Syntax analysis adopted for the research. In the second phase, we discuss the special qualities chosen to evaluate the residences and the syntactical and mathematical formulas to quantify these qualities. The next phase overviews the results of the syntactic study, showing the numerical results obtained by the UCL Depthmap software for the chosen measures. The final phase presents the conclusions of the study.

Methods

The methodology of Space Syntax was selected here as an approach for analyzing the spatial models on a scientific basis by interpreting them in numerical graphical forms. This method gives the research a good level of credibility and realism in understanding configured space, especially its formative process and cultural significance (Bafna, 2003).

Samples and sampling strategy

To choose suitable samples and representatives of residential architecture from the Mamluk/Ottoman Era, we selected five distinct traditional residences from various cities (Cairo, Damascus, and Aleppo), featuring different sizes (small houses, large houses, and a palace) and different designs (one court, two courts, a court and a large backyard) for analysis. The only common factor among the selected residences is that they all belong to the same cultural background of Islam, where segregation between male and female areas of activities in the house was a must. The samples also cover a wide span of time during both Mamluk and Ottoman eras (1600s–1900s) in Egypt and Syria.

Residences from Cairo

Two residences from Cairo were selected for the study:

(a) *The House of Al-Sohaymi* (or *Abdel Wahab El-Tablawy* house): it was originally built in 1648 (Ottoman Era) in Al-Darb Al-Asfar, Cairo. The house is built around a *Sahn* (court with a fountain). Like all traditional Islamic houses, the house has strictly separated public *Salamlik* and private *Haramlik*.

(b) *The House of Zaynab Khatun*: located in the old town, near Al-Azhar Mosque, it was originally built in 1486 (Mamluk Era), with later additions in 1713 (Ottoman Era).

Such an entrance[1] allows not a glimpse inside for the outsiders. It leads to a large *Sahn*. The ground floor includes a *Mandara* (guest room for men), a kitchen, a mill, and a grain storage room. The terrace overlooking the courtyard in the *Salamlik* is connected to a small corridor that leads to the *Haramlik*.

Residences in Syria

Three residences were selected for the study; two houses from Damascus and one from Aleppo:

(a) *The House of Sheikh Badr El-Din Al-Hasani, Damascus*: it dates back to the late 17th and the beginning of the 18th century with some parts of it being of the 20th century (all belong to the Ottoman era in Syria). It is located inside the wall of the Ancient City of Damascus.

The house has one open courtyard with an *Iwan* (formal lobby leading to the main hall) on the southern side and the main hall on the northern side. Ten rooms on the first floor surround the perimeter of the house, except for the western side (Keenan, 2000).

(b) *Al-Azem Palace, Damascus*: the palace was built during the Ottoman era in 1749, north of the market of Al-Buzuriyah in the Ancient City of Damascus. This residence is actually a palace, with an area of 6400 m², consisting of the two usual wings, *Haramlik* and *Salamlik*, with an addition of a wing for the servants, the *Khadamlik*.

(c) *Ajaq Bash House, Aleppo*: the house dates back to the Ottoman era (1758). It is located at the first Jasmine Gate in Al-Saliba northwest of Aleppo outside the walls of the Ancient City.

The house is currently below the street level. The entrance leads to a large courtyard with a pond in the middle. An *Iwan* is located directly in front of the northern main hall. Bedrooms are located on the upper floor (*Haramlik*).

Formulas and tools

UCL Depthmap software, which was developed by Alasdair Turner and his colleagues, offers a variety of techniques and tools. Based on the data sets needed for the analysis as will be discussed in section 3, we chose the following tools for the study.[2]

(a) *Visibility Graph Analysis* (VGA) with two levels of measurements: local properties, such as Connectivity, Clustering Coefficient (CC) and Visual Control (VC) values; and global properties such as Integration and Relativized Entropy (RE) values (Bada and Farhi, 2009).

(b) *Isovists*, which are sets of all points visible from given vantage points in space and with respect to the environment. The geometrical properties of Isovists are used to measure visibility (eye level isovists) or accessibility (floor level isovists) from each of these locations (Benedikt and Burnham, 1985).

(c) *Agent-based analysis* is a computational model for simulating the actions and interactions of autonomous agents (both individual or collective entities). This tool is particularly useful in archaeological/historical research since it allows insights into the relationship between the built environment and human behavior. It simulates natural human movements, providing researcher with an important measurement called Gate Counts,

[1] An entrance that is not directly connected to the house court is an intermediate space fencing it from the street.

[2] For more details about formulas and tools of Space Syntax analysis see the work by Ramzy (2016).

to predict how a certain space was (or would be) navigated (Bada and Farhi, 2009).

Privacy versus functional efficiency in traditional Islamic houses

A building achieves its function not through its built form, but mainly through the qualities of its spaces (Franz et al., 2005). The discussion in this section seeks to define the life qualities and the spatial properties that have to be measured in the five residences under examination. The criteria for privacy, functional and psychological performance of the five abodes were based on studies by Alitajer and Nojoumi (2016), Franz and Wiener (2005), Mustafa and Hassan (2010), and others, who identified these qualities as fundamental to spatial performance and preference patterns.

Spatial measurements to quantify the level of privacy in a spatial layout

A much discussed notion in the field of environmental psychology is the notion of privacy. To obtain a desirable state of privacy, each individual resorts to certain means, depending on their sociocultural milieu that reflects the ideas of a particular society at a given time (Forgas, 1994). In their study of 2016, Alitajer and Nojoumi suggested the following measurements of Space Syntax theory as indicators of privacy level in spatial layouts.

(1) *Connectivity*: the number of points, at which a space is directly connected to other spaces. For instance, the connectivity of a room with two entrance doors to adjacent spaces equals two.

(2) *Step Depth*: it is basically illustrated as the number of steps (spaces) one must take to pass from one point to the other points. A point is considered deep when a large number of steps lie between this point and the other points.

(3) *Integration*: the integration of a point indicates the degree of connection or separation between one point and the general system or the subordinate system. A space exhibits a high degree of integration when it is assimilated with other spaces.

(4) *Agent analysis*: in agent-based analysis, virtual "people" (agents) are released into the environment, and they make decisions on where to move within such an environment. This indicator is reflected by the so-called Gate Counts (Alitajer and Nojoumi, 2016).

Spatial measurements to quantify the level of functional Efficiency in a spatial layout

Functional efficiency of a building may be defined as the degree to which the activities are supported by its spatial configuration. This is associated with the spatial relationship between rooms (functional zoning) and the routing through the building for the distribution of people, goods and services, etc. (van der Voordt et al., 1997). Functional factors such as the relationship between spaces and activities, appropriate axes of movement, flexibility, suitability, safety, and so forth are key aspects in this respect, with two principal matters to be considered (Mustafa and Hassan, 2010):

a. Physical efficiency, or the ease with which users and visitors can reach, enter and move through a building, thus being able to use its various spaces. A focal point in particular is the integral accessibility, which means that people with physical disabilities can also enter and move through the building independently. Relevant spatial aspects include: a recognizable entrance, clear transitions, and circulation from public to private.

*b. Psychological efficiency***,** or to what extent a building "invites" the potential users to enter, utilize the facility, and engage in the activities taking place within**.** These are syntactical characteristics which facilitate spatial-functional orientation, clear outline of a building layout, visual axes, points of recognition, differentiation in the use of spaces, etc.

Physical efficiency

Mustafa and Hassan (2010) proposed specific quantifiers as indicators of physical efficiency within residential environments. However, they employed A-Graph analysis techniques, while this study uses the tools of the UCL Depthmap software to acquire the results for the same indicators.

(1) *Symmetry/Asymmetry*. Mustafa and Hassan (2010) suggested the kinetic-visual depth as an indicator. According to their interpretation, a space is more symmetrical when it has less depth than other spaces in the system, and vice versa. As the number of visual-kinetic steps between areas in a residential layout increases, spatial segregation increases correspondingly, leading to a weaker functional link (less efficiency). In the same vein, Hillier (2006) suggested that layouts with maximized depth are functionally rigid and unsuitable for most functional patterns. Conversely, minimizing depth seems to offer greater adaptability and is better suited for a broader array of functions, leading to a more efficient house function.

From Space Syntax indicators, Mustafa and Hassan (2010) suggested Mean Depth and Real Relative Asymmetry (RRA) as indicators related to this property.

(2) *Distributedness/Non-distributedness*. Distributedness, which is sometimes also called "permeability" (Beck and Turkienicz, 2009; Hillier, 2006), refers to the available ways to access all spaces in a house layout (Mustafa and Hassan, 2010). It demonstrates the resident's movement through the spatial system in a smooth, efficient, and flexible manner, highlighting the presence of multiple non-intersecting routes from one point in the system to another. If there is only one route for any two points in the system, then the system is said to be non-distributed. By increasing the number of ways of accessing a particular space, its distributedness

increases, which means high level of permeability of the space.

Although Mustafa and Hassan (2010) only proposed integration values as a measurement for this property, Beck and Turkienicz (2009) suggested that Intelligibility[3] (connectivity/integration) is a more accurate indicator of this attribute.

Moreover, in his study of 2006 "Studying cities to learn about minds", Hillier brings about the concept of Natural Movement, suggesting Control Value (CV)[4] as a measurement to quantify easy navigation or permeability of a certain space. Control Value quantifies the degree to which a space controls access to its immediate neighbors, considering the number of alternative connections that each of these neighbors has (Klarqvist, 1993).

(3) *Difference Factor of Space*. Measuring how strong or weak social relations correlate with spatial ordering, e.g., the degree to which a space may be shared with others (Arslan and Köken, 2016). The degree of variance in integration values is considered as an indication of this property, where integration values of spaces should be in a consistent order across a layout. In most spatial complexes, different functions and activities are assigned to spaces, which integrate the complexes to different degrees (numerical values). If the integration values of these spaces are in a consistent order across a layout, consequently, a cultural pattern might be said to be spatially expressing itself (Mustafa and Hassan, 2010).

(4) *Degree of Spaceness (space-link ratio)*. In Space Syntax terminology, there are four types of space: a-type space, which has one link; b- and c-type spaces, which have more than one connection but with differences in positions; and d-type space with more than two connections (Mustafa and Hassan, 2010). It is assumed that a-type spaces are more suitable for occupation since there is no "through" circulation. Movement is better in b- and c-type spaces, while d-type spaces offer the greatest variety of movement options. In Space Syntax tools, Choice is a general value for this property that can be best understood as "water flow in space" (Jiang et al., 2000).

(5) *Airflow*. In addition to the previous measurements suggested by Mustafa and Hassan (2010), another factor of efficiency is suggested by Du **(**2019**)**, which is airflow. For him, the VGA analysis method seems the best choice of the Space Syntax method for the airflow analysis. He suggests the levels of connectivity and integration as the quantifiers for this quality.

Psychological efficiency

Privacy, as previously discussed, is one of the crucial factors in psychological efficiency. But, according to Franz and Wiener (2005), there are other factors that are equally important to psychological comfort. Franz and Wiener (2008) pointed out four spatial qualities of architectural space that make the space preferable by people; these are spaciousness, enclosure, complexity, and order. They suggested some calculations and values to quantify these four qualities in relation to isovist properties as follows:

(1) *Spaciousness:* (Isovist area / Number of vertices).

(2) *Enclosure:* Jaggedness (Isovist perimeter^2 / area), Revelation ((Σ area adjacent isovists – isovist area) / isovist area) and Openness (the length of open edge / the length of closed edge) as opposed to it.

(3) *Complexity:* Vertices (number of vertices), Density (number of vertices / area) and Roundness (Isovist area / perimeter^2).

(4) *Order:* Symmetry (number of symmetry axes) and Redundancy/Regularity (number of unique polygon sections / number of symmetry axes + 1).

Results and discussions

A syntactic analysis was performed on the five residences using the UCL Depthmap software to acquire graphs and numerical measures for the aforementioned spatial qualities. Two sets of analytical processes were performed on the five chosen examples. The first set deals with the residences as a whole to obtain both global and local indicators, such as integration, control value, and connectivity values; the second set is concerned with the properties of the isovists in certain spaces within each residence: the court and the largest adjacent space. The points with the highest integration value in each area were selected as observation points to generate the most representative isovist in the space.

Table 1 illustrates the graphs and attributes of the five residences produced by the UCL Depthmap software, while Table 2 shows the numerical results obtained from the analysis of the attributes in Table 1 after respective calculations. It should be noted that deviant results sometimes appear for the exceptionally large Al-Azem palace and the backyard of Al-Sohaymi. Same is true for Badr El-Din Al-Hasani, which is a very small residence (compared to the others).

The results of the analyses, as shown in Tables 1 and 2, demonstrate the following:

A) ***In terms of privacy***

The values of connectivity are very low in most of the spaces in the five residences and very high only in certain points of the courts (Sahn). Minimal connectivity values are observed in kitchens,

[3] It was measured by Hillier (2006) as the correlation between connectivity and integration. It is notable here that this property contradicts the aforementioned indicators of privacy, as suggested by Alitajer and Nojoumi (2016), by default.

[4] To calculate this value, each space is assigned a score of 1, which is then divided by the number of the neighboring spaces (1/n) to which it is connected. The scores received by each space from its surrounding spaces are totaled. The higher the CV, the more controlling the space is. If a space ends up with a CV exceeding 1, it can be considered controlling; if control values approach 0, it is deemed controlled.

Table 1. **UCL Depthmap graphs and attributes for the five residences**

Residence	Floor Plan	VGA	Isovists	Agent A.	Attributes
Al-Sohaymi		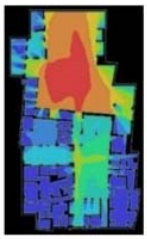	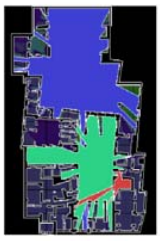	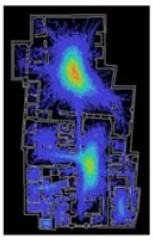	Attribute / Minimum / Average / Maximum Choice 0 583.64 224186 Connectivity 3 470.539 1695 Control 0.0501773 1 3.0541 Controllability 0.0132743 0.237298 0.597156 Entropy 1.29069 1.72243 2.16113 Harmonic Mean Depth 17.6723 47.1129 121.295 Integration [HH] 2.29048 6.63778 14.9548 Mean Depth 1.61837 2.52523 5.03739 Mean Depth [Connectivity Wgt] 1.33658 2.25643 4.83712 Node Count 3638 3638 3638 RA 0.000340136 0.000844462 0.00222079 RA [Penn] 0.494701 0.728214 0.845302 RRA 0.066368 0.166014 0.436589 Total Depth 5886 9220.64 18321 Step Depth 0 1.29076 4 Gate Counts 1 8.84388 171
Zaynab Khatun		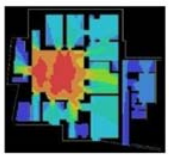		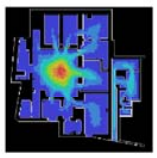	Attribute / Minimum / Average / Maximum Choice 0 1132.88 2264 Connectivity 29 329.5 630 Control 0.041993 0.959968 1.68067 Controllability 0.042328 0.24756 0.512245 Entropy 1.03136 1.99677 3.72534 Harmonic Mean Depth 3.90226 108.801 201.365 Integration [HH] 2.68702 7.33292 17.5866 Mean Depth 1.27157 2.10201 4.41829 Mean Depth [Connectivity Wgt] 1.00828 1.92973 3.37745 Node Count 1867 1867 1867 RA 0.00144771 0.00212963 0.00467157 RA [Penn] 0.664812 0.722595 0.822394 RRA 0.0514756 0.148332 0.524353 Total Depth 1997 4174.49 6482 Step Depth 0 1.8255 4 Gate Counts 1 88.5933 695
Badr El-Din Al-Hasani	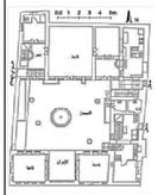	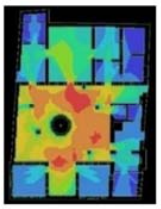	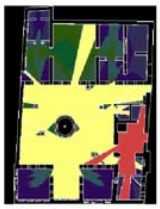	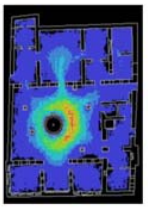	Attribute / Minimum / Average / Maximum Choice 0 500.618 3391 Connectivity 3 188.988 372 Control 0.0588666 1 1.82946 Controllability 0.046083 0.35361 0.634812 Entropy 0.99297 1.29879 1.77965 Harmonic Mean Depth 8.48871 24.2439 145.81 Integration [HH] 2.18704 8.89606 17.025 Mean Depth 1.39057 1.84279 4.0404 Mean Depth [Connectivity Wgt] 1.2297 1.59702 3.96933 Node Count 595 595 595 RA 0.00131729 0.00284247 0.0102543 RA [Penn] 0.493262 0.799182 0.901944 RRA 0.0587373 0.126746 0.457239 Total Depth 826 1094.62 2400 Step Depth 0 2.16975 4 Gate Counts 1 46.6122 509
Al- Azem Palace		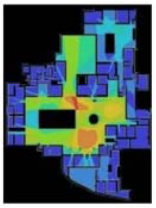	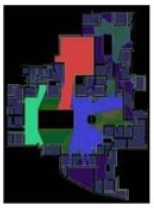	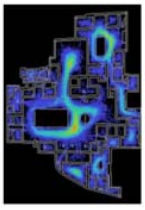	Attribute / Minimum / Average / Maximum Choice 0 3775.73 496286 Connectivity 4 144.244 409 Control 0.0389332 0.993869 2.08025 Controllability 0.0259179 0.326664 0.622642 Entropy 2.02975 2.42847 2.74479 Harmonic Mean Depth 18.1726 48.3167 147.094 Integration [HH] 1.30857 3.27803 5.79431 Mean Depth 2.35501 3.73207 7.00434 Mean Depth [Connectivity Wgt] 1.54188 3.01248 6.43782 Node Count 1383 1383 1383 RA 0.0019638 0.00396686 0.00869564 RA [Penn] 0.451771 0.650876 0.772425 RRA 0.172583 0.34772 0.764192 Total Depth 3256 5157.73 9680 Step Depth 0 2.56182 6 Gate Counts 1 5.8053 85
Ajaq Bash	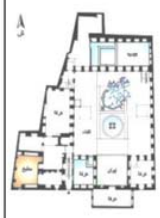	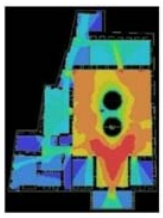		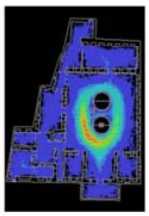	Attribute / Minimum / Average / Maximum Choice 0 1141.68 15698 Connectivity 15 198.624 502 Control 0.161916 0.999968 2.63067 Controllability 0.042328 0.24756 0.512245 Entropy 1.04936 1.39687 1.72534 Harmonic Mean Depth 5.91426 164.891 429.365 Integration [HH] 3.07747 7.33292 13.9966 Mean Depth 1.53185 2.10201 3.41892 Mean Depth [Connectivity Wgt] 1.40828 1.93873 3.37985 Node Count 1037 1037 1037 RA 0.00102774 0.00212943 0.00467424 RA [Penn] 0.514811 0.707591 0.822373 RRA 0.0714457 0.148037 0.324942 Total Depth 1587 2177.68 3542 Step Depth 0 1.8216 4 Gate Counts 1 27.9593 325

storage, dining rooms, toilets, backyards, and stairs.

Step-depth values are generally high, with values up to six steps, which means that most of the spaces are not easily accessible. The lowest step-depth values are in the yards and the corridors between them, and the highest are in some parts of the stairs, the toilets, and the rooms of housekeeping activities.

As for integration, the highest values are recorded in the courtyards and the corridors connected to them. The lowest values are found in the storerooms, kitchens, bathrooms, stairs, and backyards. Al-Sohaymi house in Cairo is a special case in this regard, as the highest levels of integration and connectivity are found in the backyard. The average values of both indicators were found in the middle court (Sahn). This is undoubtedly due to the unusually large area of the backyard in this house, which is 7 times larger than the backyard at Zaynab Khatun's and about 2.5 times larger than the middle court. However, values of integration and connectivity in the middle court of Al-Sohaymi house are almost in the same range as recorded in other houses' courts; it is the backyard where the integration values are exceptionally high.

As for the Gate Count, the highest values are also observed in the courts and the corridors between them. It is the lowest in the backyards, storerooms,

Table 2. **Numerical results and calculations for the five residences**

	Al-Sohaymi	Z. Khatun	Al-Hasani	Al- Azem	Ajaq Bash
Privacy					
Connectivity	3-1695	29-630	3-372	4 - 409	15 - 502
Step Depth	2.19 - 5	1.83 - 4	2.17- 4	2.56 - 6	1.82 - 4
Integration	2.29- 14.96	2.69- 17.59	2.19 - 17.03	1.30- 5.79	3.08 - 13.99
Gate counts	8.8-171	88.6 – 695	46.6-509	5.8-85	28-325
F. Efficiency					
(A) Symmetry/Asymmetry					
Mean depth	1.62 - 5.08	1.92- 4.41	1.39 - 4.04	2.36 - 7.00	1.53 – 3.14
RRA	0.07- 0.45	0.051 - 0.52	0.06 - 0.46	0.17 - 0.76	0.071-0.32
(B) Distributedness/Non-distributedness					
Intelligibility (Connectivity: Integration)	113.3	35.8	21.8	70.6	35.9
Control (CV)	0.05 - 3.05	0.04 - 1.68	0.06 - 1.83	0.04 - 2.08	0.16 - 2.63
(C) Difference Factor of Space					
Variance in integration values	2.29-14.96 (12.67)	2.69- 17.59 (14.9)	2.19- 17.03(14.84)	1.30- 5.79 (4.49)	3.08 - 13.99 (10.91)
(D) Degree of Spaceness:					
Choice	5583.64-226613	1132.89 - 2264	500.62-3391	3775. 73 - 496286	1141.68 – 15689
(E) Airflow					
Connectivity	3-1695	29-630	3-372	4-409	15-502
Integration	2.29 -14.96	2.69- 17.59	2.19 - 17.03	1.30- 5.79	3.08 - 13.99
P. Efficiency					
Isovists Attributes					
Iso. Area (the court)	427	166.05	126.8 + 95.4	525.4	294.73
Iso. Area (adjacent isovist)	35.7	49.41	63.8	72.2	86.1
Perimeter	301.8	155.5	144.6	294.4	133.8
Vertices (the court)	47	39	27	31	33
Vertices(Adjacent space)	20	21	29	12	33
Adjacent isovists	831.35 + 64.1+ 35.7 + 67.8 + 343 + 232.2 + 25.8 + 8	49.41+43.85 + 96.75 + 40.68 + 43.35 + 20.4 + 10.7	86.3 + 30.7 + 63.8 + 46.7 + 28.8 + 32.21 + 22	252.2 + 26.5 +72.2 + 62.6+ 12 + 78	105.2 + 40.4 + 86.1 + 84 + 47.6 + 27.5
	1697.95	705.14	310.51	503.5	390.8
S. Axes	6	9	11	9	6
Measures and Calculations					
(A) Spaciousness					
Isovist area / Number of vertices					
In the Court	427 / 47 = 9.09	166.05 / 39 = 4.26	222.2 / 27 = 8.23	525.4 / 31- 16.9	284.73 / 33=8.6
Adjacent Isovist	35.7 / 20 = 1.8	49.41 / 21= 2.35	63.8 / 29 = 2.2	72.2 / 12 = 6	86.1 / 33= 2.6
(B) Enclosure					
Openness $\frac{\text{length}_{\text{open edge}}}{\text{length}_{\text{closed edge}}}$	0.18	0.26	0.32	0.42	0.16
Jaggedness Isovist perimeter^2/area	91083.24/427= 213.3	24180.25/166 .05=145.6	20909.16/222 .2 = 94.1	86671.36/525 .4=165	17902.44/284 .73= 62.9
Revelation (Σ area adjacent isovists – isovist area)/ isovist area	(1697.95-427)/427=3	(705.14-166.05)/ 166.05 = 3.25	(310.51-222.2)/ 222.2 = 0.4	(503.5-525.4)/ 525.4= (-0.04)	(390.8-284.73)/ 284.73=0.37
(C) Complexity					
Vertices Number of vertices	47	39	27	31	33
Vertex Density Number of vertices/area	47/427= 0.11	39/166.05= 0.23	27/222.2= 0.12	31/525.4= 0.06	33/284.73= 0.11
Roundness Isovist area/perimeter^2	427/301.8 = 1.4	166.05/155.5 = 1.07	222.2/144.6 = 1.5	525.4/294.4 = 1.8	284.73/133.8 = 2.12
(D) Order					
Symmetry: ^{n} symmetry axes	6	9	11	11	6
Redundancy/ regularity ^{n} unique polygon sections / ^{n} symmetry axes + 1	8/6+1= 1.14	10/9+1=1	8/11+1= 0.6	6/9+1= 0.6	6/6+1 = 0.86

kitchens, toilets, stairs, and surrounding spaces. Notably, high levels of movement of the virtual agents are observed in none of the five residences, but in the house of Badr El-Din Al-Hasani. This can be explained by the limited number of spaces (gates) in this house compared to the number of agents used in the analysis (50 agents), causing each agent to pass through the same gate multiple times during the process. A smaller number of agents is usually employed for such a small house, but for the sake of

consistency of the experiment, the same number of agents was used for both small and big residences.

B) ***In terms of physical efficiency***

As for the measures of Symmetry/Asymmetry, the average values of Mean Depth are almost always around 2, with some values reaching up to 5.08. This indicates that the houses appear to be symmetric, which implies the spaces connect to the original space (root space, i.e., the court) almost directly and are not connected to each other. As previously explained, increasing the so called "symmetry of space" decreases its segregation, which in turn leads to less functional efficiency. This is supported by the low values of RRA, which implies the tendency of the system to be more segregated (less accessible / more controlled). RRA values of 0.6 or lower are considered strongly segregating (Lau**,** 2010). Thus, with the values consistently below 0.6, this shows the tendency of the system to be more segregated / less accessible.

For Distributedness/Non-distributedness, depending on results obtained for Intelligibility (Connectivity/Integration ratio), it can be said that three of the five layouts have low distributedness, and thus give an impression of low efficiency at the spatial-functional level (Mustafa and Hassan, 2010). The high values of intelligibility in the two other residences, Al-Sohaymi house and Al-Azem palace, are justified by the above-mentioned exceptionally large area of the backyard in the former (with oddly high values of connectivity, raising the average value as a whole) and the unusually low value of integration in the latter due to its distinct layout as a palace in contrast with usual residences. The values in these two residences, although low in comparison with the other three, are actually still high in general. The confined "flow" in the residences is further accentuated by high values of Control (CV), which are all around 2, indicating less accessible spaces and complicated navigation throughout the layout.

Regarding the Difference Factor of Space, the results show very high variance in integration values in all the residences between the courts and the corridors around them, and those in the areas of housekeeping activities, reaching up to 14.9. Note the consistency of the integration values for inner layout areas like kitchens, storage, dining rooms, toilets, and backyards, with differences within 2–3, indicating that these spaces are fairly interchangeable.

As for Spaceness (space-link ratio), the study shows very high values of Choice in the middle areas of the five residences, with average and low values in the other spaces. It is assumed that occupation is more appropriate in areas without "through" circulation, whereas movement is more effective in spaces providing the greatest movement options. The efficiency of the space depends on the balance between the two types of spaces (Mustafa and Hassan, 2010). Except for the house of Badr El-Din Al-Hasani, and due to a small number of spaces included, significant differences are observed between the average values and the maximum values of choice in the other layouts, which indicates that there is a considerable lack of balance. Nevertheless, by taking into account the layouts as a whole, there are all types of spaces present. Although b-and c-types are rather rare, they are not absent.

As for the Airflow, although the court-house plan was always considered an ideal climate solution, the low connectivity and integration values in some areas of the five residences suggest inadequate airflow in those spaces.

C) ***In terms of psychological efficiency***

In general, in places where isovists tend to be larger and spread in different directions, the observer is permitted a better evaluation of the space and thus more convenience (Benedikt and Burnham, 1985). Examining the isovists in Table 1, we notice a significant difference between the isovists in the courts, which are large but do not extend in various directions, and those in the adjacent spaces (adjacent isovists), which are skewed with deep dilation in certain directions.

The numerical results and the calculations in Table 2 show moderate values of Spaciousness in most courts, except for Al-Azem palace, where the values are high. In adjacent spaces (adjacent isovists), again except for Al-Azem palace, the values are really low, which characterizes unpleasantly secluded paces.

As for Enclosure, the results show low values of openness and revelation, even in the courts, reaching an extreme of –0.04 in Al-Azem palace, as the area of the isovist in the court exceeds the total of the areas of all adjacent isovists. A result that Franz and Wiener themselves probably could not foresee. High values of jaggedness of the isovists also reflect an intermittent sight-line in the spaces, including ones around the central court.

High Complexity is considered a positive feature of space in Franz and Wiener's opinion. The results show that all spaces are rather complicated or very complicated with big number of vertices and vertex-density for each isovist. For Franz and Wiener, values of roundness over 0:9 are considered high and the spaces are considered complex. Looking at the results in Table 2, it is remarkable that all the values of roundness are over 0:9 reaching 2.12 in Ajaq Bash.

Concerning Order, a large number of symmetry axes (reflecting numerous polygons in every isovist) is a factor of disorder. Rather low values of the redundancy/regularity ratio (below 1) further support this fact.

Conclusion

Confirming the outcomes of many other studies, this paper verifies Space Syntax analysis as a powerful tool that creates a valid alternative to interpret and comprehend spaces by making intangible aspects of space-experience more tangible, or in other words, measurable. Moreover, it is another step towards demonstrating the link between sociocultural background of historical styles and their spatial configuration as captured by Space Syntax methodologies. Space Syntax tools played a role in comprehending these relations, first, by presenting a new language of space that is more statistical and, thereby, more solid, secondly, by constituting a quantitative approach for "evidence-based" analysis of historical architecture, and thirdly, they gave a unique chance to evaluate historical buildings not only in terms of geometric measurements and artistic style, but rather as a social organism with explicit characteristics experienced by the inhabitants.

The analysis of the residences under study, as shown in Tables 1 and 2, reveals that in order to pursue privacy, the inner (activity) spaces of the residences became highly segregated and less functional. The five residences enjoyed good privacy, interchangeability, spaceness and complexity. The visual fields in some inner spaces allow deep vision and fair observation for some of the adjacent and outer spaces, although through very narrow spans.

Nonetheless, in terms of functional efficiency, out of five indicators of physical efficiency, three were found to be lacking, while only two were satisfactory. In terms of psychological efficiency, out of four indicators, only one was found to be satisfactory and three were not. High values of intelligibility in two residences show that, in such segregated layouts, the only chance to produce attractive spaces for life is to make a residence very large. However, in general and for medium spaces, an architectural arrangement with weak connections and great depths of spaces would inevitably exacerbate accessibility and obstruct movement.

The lack of spatial integration and connectivity in activity spaces is also indicative of the layouts with low efficiency at the spatial-functional level. High values of Control also imply complicated navigation throughout the layout and insufficient airflow in most of the spaces.

The results and the configurations of the isovists show that visual fields are either jagged or disrupted, making spaces unpleasantly isolated. They also lack order and uniformity, making the spaces (especially activity spaces in this case) less desirable, as well as less welcoming.

The results of the analysis show that traditional Islamic houses, which have been always considered exemplary for modern generations, are not really pleasant all over the layout of the house, especially in activity areas, or suitable for modern life styles. As the "sacred" interior is safe from being seen by strangers, the overall spatial performance is mild and comfortable only in the courts and the area around them. The daily life activities in these houses are more taxing and are done in unpleasantly secluded spaces.

Acknowledgements. The researchers wish to acknowledge the effort undertaken by Salwa Magdy, Engy Atef, Salma Ahmed, and Taghreed Saied in preparing the GRAPH file. They also wish to thank Mr. Emad Ramsey for proofreading the paper.

References

Alitajer, S. and Nojoumi, G. M. (2016). Privacy at home: analysis of behavioral patterns in the spatial configuration of traditional and modern houses in the city of Hamedan based on the notion of space syntax. *Frontiers of Architectural Research*, Vol. 5, Issue 3. pp. 341–352. DOI: 10.1016/j.foar.2016.02.003.

Arslan, H. D. and Köken, B. (2016). Evaluation of the space syntax analysis in post-strengthening hospital buildings. *Architecture Research*, Vol. 6, No. 4, pp. 88–97. DOI: 10.5923/j.arch.20160604.02.

Bada, Y. and Farhi, A. (2009). Experiencing urban spaces: isovists properties and spatial use of plazas. *Courrier du Savoir*, No. 9, pp. 101–112.

Bafna, S. (2003). Space syntax: a brief introduction to its logic and analytic techniques. *Environment and Behaviour*, Vol. 35, Issue 1, pp. 17–29. DOI: 10.1177/0013916502238863.

Beck, M. P. and Turkienicz, B. (2009). Visibility and permeability: complementary syntactical attributes of wayfinding. In: Koch, D., Marcus, L., and Steen, J. (eds.). *Proceedings of the 7th International Space Syntax Symposium*. Stockholm: KTH, pp. 9-1–9-7.

Benedikt, M. and Burnham, C. A. (1985). Perceiving architectural space: from optical arrays to isovists. In: Warren Jr., W. H. and Shaw, R. E. (eds.). *Persistence and change: Proceedings of the First International Conference on Event Perception*. Hillsdale, NJ: Lawrence Erlbaum Associates, pp. 103–114.

Du, X. (2019). Methods of spatial analysis for natural ventilation potential. *Architecture and the Built Environment*, No. 9 (10), pp. 239–248. DOI: 10.7480/abe.19.10.4112.

Forgas, J. P. (1994). Sad and guilty? Affective influences on the explanation of conflict in close relationships. *Journal of Personality and Social Psychology*, Vol. 66, No. 1, pp. 56–68. DOI: 10.1037/0022-3514.66.1.56

Franz, G., von der Heyde, M., and Bülthoff, H. H. (2005). Predicting experiential qualities of architecture by its spatial properties. In: Martens, A. and Keul, B. (eds.). *Designing Social Innovation: Planning, Building, Evaluating*. Cambridge, MA: Hogrefe, pp. 157–166.

Franz, G. and Wiener, J. M. (2008). From space syntax to space semantics: A behaviorally and perceptually oriented methodology for the efficient description of the geometry and topology of environment. *Environment and Planning B: Planning and Design*, vol. 35, pp. 574 – 592.

Hillier, B. (2006). Studying cities to learn about minds: how geometric intuitions shape urban space and make it work. In: Hölscher, C., Conroy Dalton, R., and Turner, A. (eds.). Space Syntax and Spatial Cognition: proceedings of the workshop held in Bremen. Bremen: Universität Bremen, pp. 11–31.

Hwaish, A. N. A. (2015). Concept of the "Islamic house": a case study of the early Muslims house. In: Proceedings of 4th IASTEM International Conference, Amsterdam, Netherlands, November 12, 2015. [online] Available at: https://www.worldresearchlibrary.org/up_proc/pdf/103-144851360386-93.pdf [Date accessed June 8, 2024].

Jiang, B., Claramunt, C., and Klarqvist, B. (2000). Integration of space syntax into GIS for modeling urban spaces. *International Journal of Applied Earth Observation and Geoinformation*, Vol. 2, Issues 3–4, pp. 161–171. DOI: 10.1016/S0303-2434(00)85010-2.

Keenan, B. (2000). Damascus: hidden treasures of the old city. London: Thames & Hudson, 224 p.

Klarqvist, B. (1993). A space syntax glossary. Nordisk Arkitekturforskning, No. 2, pp. 11–12.

Lau, W. (2010). *Spatial configuration analysis: revealing the underlying spatial structure of single-family homes on Oahu. PhD Thesis in Architecture*.

Mustafa, F. A. and Hassan, A. S. (2010). Using space syntax analysis in determining level of functional efficiency: a comparative study of traditional and modern house layouts in Erbil city, Iraq. In: Wibowo, A. (ed.). *Proceedings of the 2nd International Seminar on Tropical ECO-Settlements: Green Infrastructure: A Strategy to Sustain Urban Settlements*, November 3–5, 2010, Sanur Denpasar, Bali, Indonesia, pp. 131–144.

Ramzy, N. S. (2016). Morphological logic in historical settlements: Space syntax analyses of residential districts at Mohenjo-Daro, Kahun and Ur. *Urban Design International*, Vol. 21, Issue 1, pp. 41–54. DOI: 10.1057/udi.2015.11.

van der Voordt, T. J. M., Vrielink, D., and van Wegen, H. B. R. (1997). Comparative floorplan-analysis in programming and architectural design. *Design Studies*, Vol. 18, Issue 1, pp. 67–88. DOI: 10.1016/S0142-694X(96)00016-6.

ПРИВАТНОСТЬ И СЕГРЕГАЦИЯ В ПРОСТРАНСТВЕ ТРАДИЦИОННОГО ДОМА: АНАЛИЗ «КАЧЕСТВА ЖИЗНИ» В ИСЛАМСКИХ ТРАДИЦИОННЫХ ДОМАХ МЕТОДОМ ПРОСТРАНСТВЕННОГО СИНТАКСИСА

Нелли Шафик Рамзи[1]*, Разан Ибрагим Арафа[1], Ибрагим Седки Ибрагим[2], Али Камаль Альтаванси[1]

[1]Университет Даманхур, площадь Галал Корейтем, 27, Даманхур, Египет
[2]Университет Менуфия, Гамаль Абдель Насер, кафедра Шебин Эль-Ком, Менуфия, Египет

*E-mail: tawswzwm@yahoo.com

Аннотация
Введение. Понятие дома выходит далеко за рамки физических аспектов, его сущность неразрывно связана с духовной природой человечества. **Цель исследования**. Данная статья направлена на изучение пространственных формирований пяти исторических исламских резиденций, построенных примерно в одно время в трех городах: Каире, Дамаске и Алеппо. Авторы намерены показать, что на их планировки, в основе которых лежали традиции приватности и видимости, те же традиции оказали негативное влияние с точки зрения функциональной и психологической эффективности. **Методы**. В статье используются формулы пространственного синтаксиса и ПО UCL Depthmap для исследования и анализа пространственных конфигураций этих жилых помещений, с тем чтобы обеспечить новое понимание жизненного опыта и функциональных характеристик, которые всегда считались идеальными. **Результаты** показывают, что планировки в пяти резиденциях предлагают удовлетворительные качества с точки зрения уровня приватности, что, безусловно, является фундаментальной человеческой потребностью. Однако иерархия доступа к пространствам имеет негативные последствия для психологических потребностей и функциональной эффективности. **Результаты**. Это приводит к выводу, что из-за определенных социальных соображений пространственные конфигурации в этих резиденциях, возможно, не могли удовлетворить другие функциональные и психологические потребности пользователей.

Ключевые слова: жилая архитектура; традиционные дома; пространственная конфигурация; функциональная эффективность; синтаксис пространства.

Civil Engineering

DOI: 10.23968/2500-0055-2025-10-1-59-69

EFFECTS OF ENVIRONMENTS CONTAMINATED WITH CHLORIDES AND SULFATES ON RC COLUMNS

Dinh-Quoc Phan, Van-Phuc Phan*, Ngoc-Long Tran

Vinh University, 182-Le Duan Street, Vinh, Vietnam

*Corresponding author's email: vanphuckxd@vinhuni.edu.vn

Abstract

Introduction: Corrosion of steel reinforcement is a very complex process with clear differences in each geographical location. Many research models predicting the quality deterioration of reinforced concrete structures in areas contaminated with chlorides and sulfates are being developed around the world. However, these models still have a fairly wide application range and fail to accurately and fully reflect the reduction in structure quality in each specific condition. The **purpose of the study** was to survey the current status of reinforced concrete (RC) structures located in chloride- and sulfate-contaminated environments in coastal areas of Vietnam, analyze the result and compare it with previously researched proposals to clarify the impact of corroded steel reinforcement on the quality of RC columns. The following **methods** were used: Experimental Survey, Non-Destructive Testing, and Empirical Formula for determination of the deterioration of parameters including compressive strength of concrete, thickness of protective layer, diameter of reinforcement, and cross-sectional area of RC columns. In addition, this study was combined with the available recommendations on reinforcement corrosion to determine the residual physical and mechanical characteristics of concrete and reinforcement steel. As a **result**, the quality deterioration of RC columns with corroded reinforcement depends on the reinforcement location in the same longitudinal member. This indicates remarkable deterioration in the quality of structural sections that are regularly and directly affected by seawater.

Keywords: concrete; steel; reinforced concrete; corrosion; seawater; chloride.

Introduction

Reinforced concrete (RC) structures are common in civil construction, often used in saline areas with high concentrations of chloride and sulfate. These structures are often affected by the corrosion of steel reinforcement due to chlorides and sulfates in the environment.

Corrosion is a chemical or electrochemical process through which metals or other materials are destroyed by environmental influences (Nguyen et al., 2022). In the case of RC structures in coastal areas, corrosion is mainly caused by seawater components and salt-containing air (Viet Duc, 2021). Seawater contains a lot of salt, especially sodium chloride (NaCl). Chloride from the seawater environment can penetrate into concrete through voids and hollow structures, causing metal corrosion in reinforced concrete (Kumar, 1998).

During the process of corroding steel reinforcement, elemental Iron (Fe) converts to $Fe(OH)_2$ or hydroxide ions, known as common rust, which reacts with dissolved oxygen and produces hydrated iron oxide ($Fe_2O_3 \cdot H_2O$) in reddish brown color, Fe_3O_4 in black color and then hydrates into ($Fe_3O_4 \cdot H_2O$) in green color (Liu, 1996). Because the volume of rust is higher than that of iron, the process of rusting increases the volume of reinforcing steel, which leads to cracking and peeling of the protective layer (Liu, 1996).

To study the loss of RC strength with corroded reinforcement, Shayanfar et al. (2016) conducted experiments on various types of reinforcement, keeping all effective parameters on compressive strength constant except for the water-cement ratio (0.4, 0.45, and 0.5). Compressive strength tests were performed on corroded and non-corroded samples. The degree of reduction in compressive strength was measured at different corrosion levels. Other studies (Diamond, 1986; Enevoldsen et al., 1994; Ghods et al., 2009; Hussain et al., 1995; Moreno et al., 2004; Page and Vennesland, 1983) showed that the agents causing corrosion in steel reinforcement mainly come from chemical components containing sodium and potassium. This highlights the importance of considering cement composition and environmental exposure conditions when specifying allowable chloride limits to prevent reinforcement corrosion in concrete structures. The corrosion process is difficult to fully and accurately determine. However, some recent studies (Andrade and Alonso, 2001; Assouli et al., 2008; Schiegg et al., 2009; Suryavanshi et al., 1991) managed to

For citations: Phan, D.-Q., Phan, V.-P., Tran, N.-L. (2025). Effects of environments contaminated with chlorides and sulfates on RC columns. Architecture and Engineering, No 1 (10), pp. 59–69. DOI: 10.23968/2500-0055-2025-10-1-59-69.

partially quantify the reinforcement corrosion over the time. Corrosion behavior of steel reinforcement due to sulfates and chlorides was also investigated (Pradhan, 2014), the performance of corroded steel reinforcement in RC structures was evaluated through a comprehensive experiment in which the structures were exposed to mixed solutions of chloride and sulfate ions.

Chloride is the main agent that causes corrosion of steel reinforcement in concrete. It penetrates into the structure mainly in the process of mixing and pouring fresh concrete mixture into the structure from the outside environment (Arya and Xu, 1995; Dehwah et al., 2002; Saricimen et al., 2002). These studies highlight the complex interplay between chloride binding, pore solution chemistry, and transport properties in influencing reinforcement corrosion in chloride-contaminated concretes made with different cementitious materials. Especially in case of RC structures located in an environment with chloride content, chloride ions directly penetrate into the structure itself through voids and hollows, causing corrosion of the steel reinforcement (Shaheen and Pradhan, 2017; Vu and Stewart, 2000).

The effects of chloride, sulfate and chloride-sulfate solutions on the corrosion of steel embedded in cement paste were studied. Reinforcement corrosion was evaluated by measuring the corrosion potential and corrosion current density using the linear polarization resistor technique. The results indicated that the corrosion of specimens immersed in pure sulfate solution is minimal (Al-Amoudi and Maslehuddin, 1993). However, Pradhan's study show that in the later stages of corrosion process, the formation of sulfate compounds increases the reacted product volume and breaks down the protective layer of the reinforcement. Then, the corrosion process of the reinforcement is increased due to chloride intrusion (Pradhan, 2014).

Corrosion of RC is the cause of a decrease in the bearing capacity and longevity of the structure (Rodriguez et al., 1997), reducing the cross-section and physical and mechanical properties of the reinforcement (Ballim and Reid, 2003). It causes the expansion of the protective concrete layer and cracking of the structure. Thereby, it keeps increasing the possibility of corrosion of the reinforcement (Cabrera, 1996), and the deterioration of the bond between the reinforcing steel and the concrete (Ahmad, 2003).

The main research method for RC corrosion involves surveying, evaluating current conditions, and using the corrosive acceleration method in experimental models. Osuji et al. (2020) assessed the level of deterioration of an existing 45-year-old concrete harbor structure in the Niger Delta zone of Nigeria. The applied methodology included a visual inspection of the structure to determine the current condition and the testing required. The results show that the corrosion rate and durability loss depend on the characteristics and exposure time. Structural elements exposed to tidal conditions have a higher degree of damage than the continuously submerged ones. The experimental survey method has proven to be reliable because it covers unique characteristics. The number of experimental studies on RC corrosion, as in these studies, has highly reliable conclusions (Ma et al., 2021; Medeiros et al., 2013; Nasser et al., 2021; Okada et al., 1988).

In experimental studies, the reduction in diameter and mechanical properties of reinforcement is quantified using a proposed formula (Du et al., 2005). As steel reinforcement corrodes, it creates oxides and increases the size of voids and cracks on the surface of the protective concrete layer. The expansion of steel reinforcement can cause concrete to crack and reduce its bearing capacity. This proves that the decrease in concrete strength depends on the level of reinforcement corrosion. This problem was raised by Shayanfar et al. (2016). An electrochemical corrosion experiment was conducted, and a formula to calculate the loss of concrete strength when reinforced steel is corroded was proposed. According to Tapan and Aboutaha (2011), the ratio between the protective concrete layer thickness and the longitudinal reinforcement diameter (c/d) is an important parameter that affects the remaining bearing capacity of the column structure after steel reinforcement is corroded. The destruction of the protective concrete layer occurs when the levels of longitudinal reinforcement corrosion are $Q_{corr} = 2.25\ \%$ and 5.25 %, corresponding to the cases of c/d = 1 and c/d = 2.5. Gonzalez et al. (1995) as well as Andrade and Alonso (2001) proposed a formula to determine the reduction in reinforcement diameter as corrosion occurs. The rate of corrosion of steel reinforcement over time depends on many factors. However, according to Yokozeki et al. (1997), a formula to determine the rate of corrosion of steel reinforcement depends on the ratio of water/cement and protective layer thickness. Liu and Weyers (1998) developed a formula based on Yokozeki's research (Yokozeki et al., 1997) to determine the corrosion rate of steel reinforcement over time.

Corrosion of steel reinforcement is a very complex process with clear differences in each geographical location. Many research models predicting the quality deterioration of reinforced concrete structures in areas contaminated with chlorides and sulfates are being developed around the world. However, these models still have a fairly wide application range and fail to accurately and fully reflect the reduction in structure quality in each specific condition.

A survey was conducted on RC bridges in coastal areas of Vietnam. The visual and experimental results were combined to clarify the effects of chloride- and

sulfate-contaminated environments on the decline in quality of RC bridges.

Methods

1. Experimental method

A survey of RC structures in chloride- and sulfate-contaminated areas was conducted by the research team. Visual inspection results show that damage commonly occurs in structures that are in close contact with seawater, such as bridge columns (Fig. 1).

Fig. 1a shows cracks along the concrete cover / protective layer of what appears to be a reinforced concrete column or a structural member. The cracks seem to be running parallel to the reinforcing bars within the concrete, suggesting that the cracking may be related to reinforcement corrosion and expansion.

In Fig. 1b, the cross-section reveals a decrease in the effective area of the concrete due to cracking, spalling, and potential loss of concrete cover. This reduction in the cross-sectional area can lead to a loss of structural capacity and compromise the strength and durability of the member.

Fig. 1c shows the revealed and corroded reinforcing bars within the concrete member. The reinforcement appears to be heavily rusted and corroded, indicating advanced deterioration due to factors such as chloride ingress or carbonation. The loss of concrete cover has exposed the reinforcement, making it vulnerable to further corrosion and potentially leading to a loss of the bond between the steel and concrete.

In addition to the visual assessment, the research team conducted a numerical survey of 10 RC bridge columns with design data. Column cross section — 300×300mm. Concrete w/c ratio = 0.45. Compressive strength of concrete f_c' = 35 MPa. Reinforcement is arranged with eight φ20 main steel bars, each having a tensile strength of f_y = 300 MPa (Fig. 2).

This structure is located in the chloride- and sulfate-contaminated coastal region of Central Vietnam, with the indicators shown in Table 1 (Sample 2). The indicators of other samples from different coastal regions in Vietnam are also summarized in Table 1 for comparison purposes. It can be seen that the concentrations of chlorides and sulfates in samples from different coastal areas are not significantly different. Therefore, Sample 2 can be considered representative of the coastal region of Central Vietnam.

The survey was carried out on the basis of determining the thickness of the protective concrete layer, diameter of reinforcement, and compressive strength of concrete on RC bridge column components at different sections. The equipment used included a rebound hammer (Fig. 3a), a rebar detector PROCEQ PM-650 (Fig. 3b), and a concrete ultrasonic machine (Fig. 3c). The field investigation results are presented in Table 2.

Here, Ai is the survey cross-section condition; f_c' (MPa) is the compressive strength of concrete; c (mm) is the thickness of the protective layer; d (mm) is the diameter of the reinforcement; A_c (mm^2) is the survey cross-section area. Zone I was at the bottom of the column which is frequently submerged, Zone II was the middle of the column, and the top of the column was Zone III.

2. Basis for determining the reduction in the bearing capacity of RC columns as the reinforcement corrodes

a. Reduction in the cross-section area and tensile strength of longitudinal bars

Corrosion damage can reduce the stiffness and ductility of steel reinforcement. Cracks and rusts caused by corrosion on the reinforcement surface can reduce the load-bearing and bending capacity of the column. Corrosion of steel reinforcement can lead to loss of elastic properties, causing the structure to become less flexible and more susceptible to damage when subjected to force. The empirical formula proposed by Du et al. (2005) is used to determine the reduction of the tensile strength and cross-sectional area of reinforcement.

$$f_{y,corr} = (1 - 0.005Q_{corr}) f_{y,0}; \quad (1)$$

$$A_{y,corr} = (1 - 0.01Q_{corr}) A_{s,0}; \quad (2)$$

a) Cracks along the protective layer

b) Decreased cross-section area

c) Rusty reinforcement revealed

Fig. 1. Types of damage to RC structures caused by corroded reinforcement

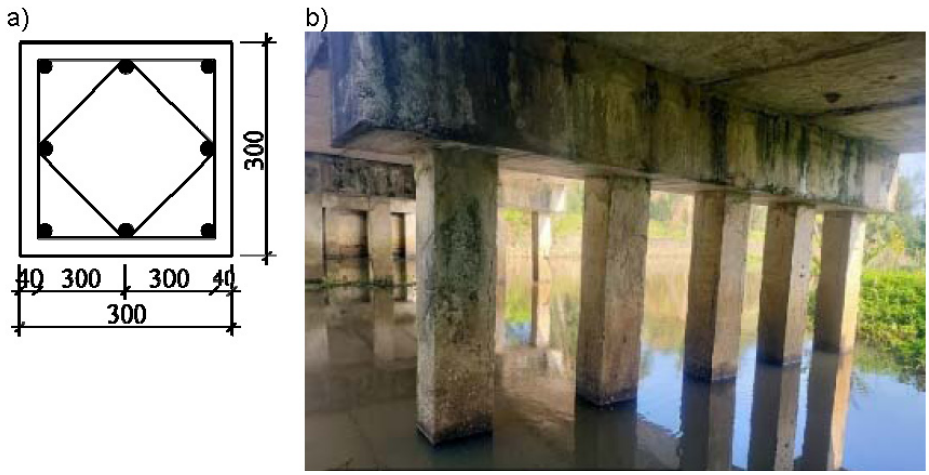

Fig. 2. a — column cross-section without corrosion; b — current status

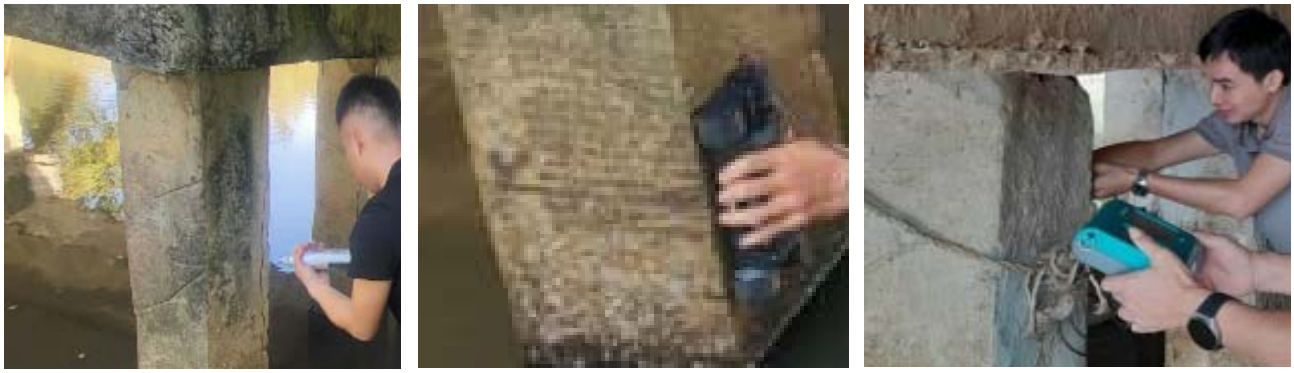

a) using a rebound hammer b) using a rebar detector c) using an ultrasound machine

Fig. 3. Equipment used in actual surveys

Table 1. **Results of water sample analysis from the coastal region of Central Vietnam**

No.	Indicator	Method	Unit	Sample 1	Sample 2	Sample 3	Sample 4	Sample 5	Sample 6
1	Chloride (Cl^-)	TCVN 6194:1996	mg/l	16.724	16.868	15.559	14.897	17.708	17.989
2	Sulfate (SO_4^{2-})	TCVN 6200:1996	mg/l	2.369	1.997	2.257	1.996	2.044	2.066

Table 2. **Results obtained from surveying the current status of RC columns**

No.	Design	Column 1			Column 2			Column 3			Column 4			Column 5		
A_i	–	Zone III	Zone II	Zone I	Zone III	Zone II	Zone I	Zone III	Zone II	Zone I	Zone III	Zone II	Zone I	Zone III	Zone II	Zone I
f_c'	35	32.0	28.8	26.4	30.1	27.8	25.0	30.0	27.1	24.3	31.7	28.8	24.9	31.8	27.5	25.8
c	30	28	24	20	28	27	24	28	27	23	28	26	22	27	27	22
d	20	20	19	18	19.8	19.7	18.6	20	19.2	18.3	19.9	19.5	18.6	19.6	19.7	18.4
A_b	300	296	288	280	296	294	288	296	294	286	296	292	284	294	294	284
No.	Design	Column 6			Column 7			Column 8			Column 9			Column 10		
A_i	–	Zone III	Zone II	Zone I	Zone III	Zone II	Zone I	Zone III	Zone II	Zone I	Zone III	Zone II	Zone I	Zone III	Zone II	Zone I
f_c'	35	30.2	27.9	25.8	30.2	28.5	25.7	29.7	28.0	24.8	30.9	28.6	25.0	31.7	27.4	24.8
c	30	28	26	22	28	26	23	27	27	23	29	26	24	28	25	24
d	20	19.6	18.7	18.3	19.8	18.8	18.3	19.7	19	18.4	19.7	19.4	18.2	19.7	19.4	18.4
A_c	300	296	292	284	296	292	286	294	294	286	298	292	288	296	290	288

$$Q_{corr} = 1 - \left(\frac{d_{corr}}{d_0} \right)^2. \quad (3)$$

Here, $f_{y,corr}$, $f_{y,0}$ are the post-corrosion and initial tensile strength of the reinforcement, respectively. $A_{s,0}$, $A_{y,corr}$ are the initial and post-corrosion reinforcement area. Q_{corr} is the degree of steel reinforcement being corroded. d_0, d_{corr} are the initial reinforcement diameter and the remaining reinforcement diameter after corrosion, respectively.

b. Decrease in the compressive strength of concrete

As steel reinforcement corrodes, it creates oxides, which expand in volume, leading to cracks on the surface of the protective concrete layer. The expansion of steel reinforcement can cause cracks in concrete and reduce its bearing capacity. This proves that the decrease in concrete strength depends on the level of reinforcement corrosion. Shayanfar et al. (2016) proposed a formula to calculate the loss of concrete strength by conducting electrochemical corrosion experiments on corroded RC as follows:

$$f'_{c,corr} = (1-\lambda) f'_{c,0}; \quad (4)$$

$$\begin{aligned} N/X = 0.40 \quad & \lambda = 2.72 Q_{corr} - 1.98 \\ N/X = 0.45 \quad & \lambda = 2.288 Q_{corr} - 1.733 \\ N/X = 0.50 \quad & \lambda = 2.576 Q_{corr} - 1.876. \end{aligned} \quad (5)$$

Here, $f'_{c,corr}$, $f'_{c,0}$ are the post-corrosion and initial compressive strength of the concrete, respectively. λ is the percentage reduction in the compressive strength of concrete depending on the level of reinforcement corrosion and the water/cement ratio.

c. Reduction in rebar diameter over time

According to Gonzalez et al. (1995) as well as Andrade and Alonso (2001), when corrosion of reinforcement occurs, the reduction in reinforcement diameter can be determined according to the following formula:

$$D_{corr} = d_0 - 0.0232 I_{corr}(t) \cdot t_p. \quad (6)$$

Here, I_{corr} is the corrosion rate of reinforcement (μA/cm²), t_p is the interval between the onset of reinforcement corrosion and the calculation time. According to Vu and Stewart (2000), the magnitude of I_{corr} depends on two parameters: water/cement ratio (N/X) and protective concrete layer thickness (c), determined by the following formula:

$$I_{corr}(t) = 32{,}1 \frac{(1-\frac{N}{X})^{-1{,}64}}{C} t_p^{-0{,}29}. \quad (7)$$

Results

1. Results of the field survey

Fig. 4 shows the results of the field survey of 10 RC bridge columns on the compressive strength of concrete and the thickness of the protective concrete layer.

The chart in Fig. 4 shows that the compressive strength of concrete in Zone I reduced significantly compared to the design (26–31 %). The compressive strength reduction of concrete in Zone III compared to the design (8.5–15 %) is less than that in Zone I. In addition, the thickness of the protective concrete layer in Zone I decreased significantly compared to the design (20–33 %). The reduction in the thickness of the protective concrete layer in Zone III compared to the design (3–10 %) is less than that in Zone I. Thus, it is evident that the impact of frequent exposure to the water environment is significant.

2. Results based on the survey-theory combination

Based on the survey data and experimental formulas, the tensile strength of the reinforcement was determined. Data on the steel reinforcement strength of 10 RC columns at different zones are shown in Fig. 5. The X-axis represents the order of columns, and the Y-axis represents the tensile strength of the reinforcement in MPa. The data points show the measured tensile strength values for each column zone after the onset of corrosion. The graph allows for visualizing and comparing the remaining tensile strength values of the reinforcement in different column sections subject to corrosion.

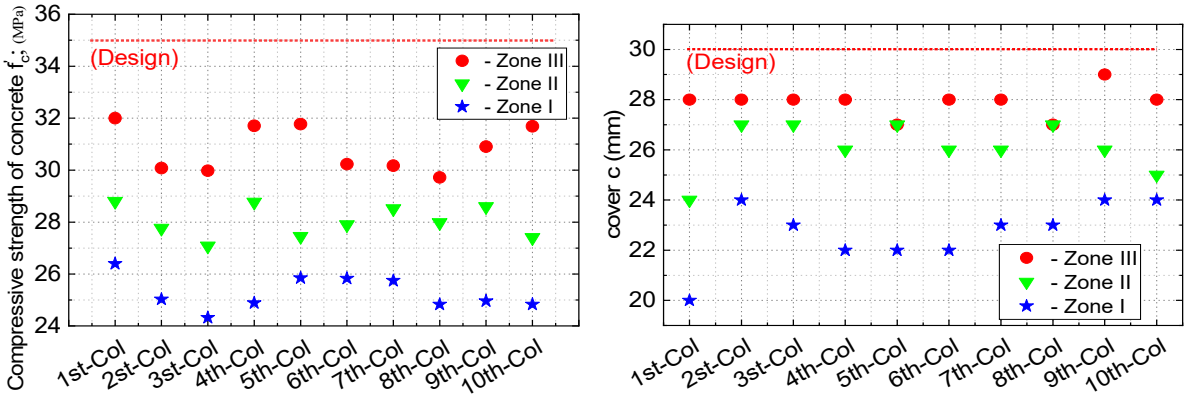

a) Compressive strength of concrete

b) Cover

Fig. 4. Results of the survey on the compressive strength of concrete and the thickness of the protective layer

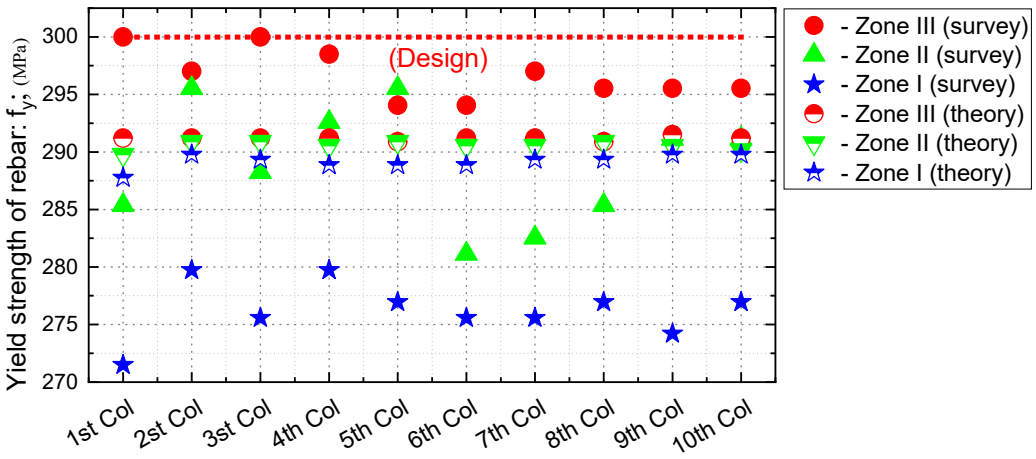

Fig. 5. Decrease in the reinforcement tensile strength after corrosion

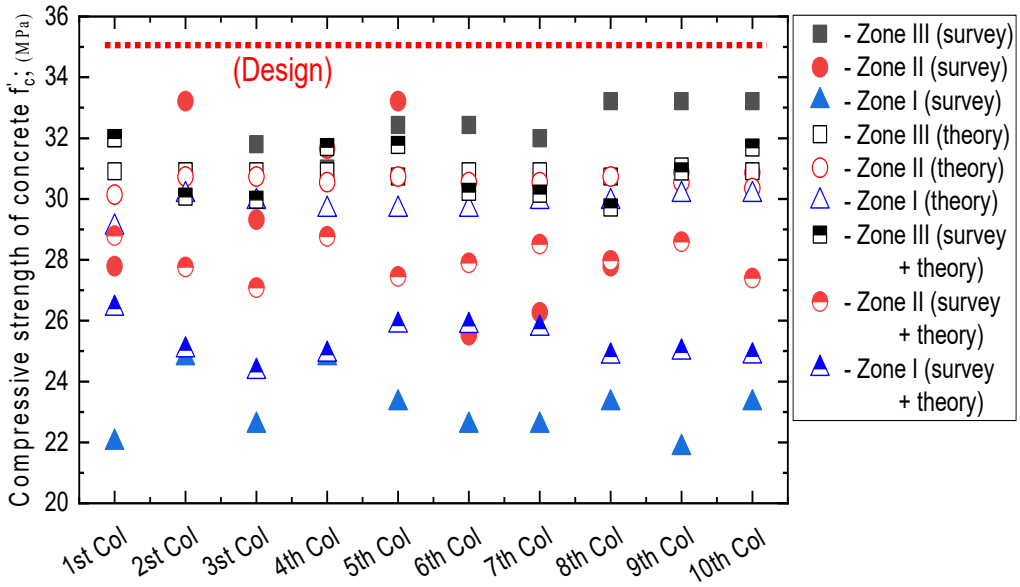

Fig. 6. Decrease in concrete strength after corrosion

The chart shows that the tensile strength of the reinforcement was greatly reduced after corrosion compared to the design specifications. According to the field survey, the tensile strength reduction in Zone I (6.5–8.6 %) is higher than that in Zone III (0–2 %). According to the proposed empirical formula, the tensile strength reduction in Zone I (3.4–4.1 %) is slightly higher than that in Zone III (2.9–3.1 %). The results show a clear difference in the reduction of reinforcement tensile strength at different zones of the same structure. The bottom zone of the column frequently exposed to seawater (Zone I) has a significant reduction compared to the column top area (Zone III). In addition, the results also show that calculations based entirely on the proposed theoretical formulas only approximate a specific cross-section in Zone II.

Fig. 6 shows the compressive strength of concrete after reinforcement corrosion. The results were obtained based on calculating survey data and combining it with the empirical formulas.

It can be seen that the decrease in the compressive strength of the protective concrete layer was actually significant (8.5–30 %). The decrease in the compressive strength of concrete columns, according to the survey combined with the experimental formulas (5–37 %) is higher than that of the theoretical calculation (11.7–15 %). Besides, the reduction of the compressive strength of concrete in different zones of the same structure has a remarkable difference in case of the survey alone (23 %), in case of the theory only (4.5 %), and in case of the theory combined with experimental data (37.2 %).

3. Predicting the loss of material strength over time after corrosion

In addition, by applying the theory of Gonzalez et al. (1995), Andrade and Alonso (2001), and Vu

and Stewart (2000), along with the field survey data, a predictive curve is presented, showing the reduction in steel tensile strength (Fig. 7), concrete compressive strength (Fig. 8), and the remaining diameter of steel rebars over 80 years from the onset of corrosion.

Figs. 7, 8, and 9 collectively illustrate the detrimental effects of the steel reinforcement corrosion on the material properties and structural performance of reinforced concrete components over time.

In Fig. 7, the curve represents the reduction in the strength of reinforcement steel over time. This curve was determined using empirical formulas proposed by Du et al. (2005), Gonzalez et al. (1995), and Vu and Stewart (2000). The points shown in Fig. 7 at the 20-year mark represent the strength of the reinforcement steel as experimentally determined by the authors. It should be noted that the surveyed structures have different ages. However, data on the bridge columns of a specific structure were collected to obtain a sufficient dataset for analysis and evaluation. According to local investigations, this structure was 20 years old at the time of the survey.

In Fig. 8, the curve represents the reduction in concrete strength over time. This curve was determined using empirical formulas proposed by Du et al. (2005), Shayanfar et al. (2016), Gonzalez et al. (1995), and Vu and Stewart (2000). The points shown in Fig. 8 at the 20-year mark represent the concrete strength as experimentally determined by the authors. The reduction in steel tensile strength, concrete compressive strength, and steel rebar diameter can significantly affect the durability, serviceability, and safety of the affected structures. When comparing the predicted degradation results

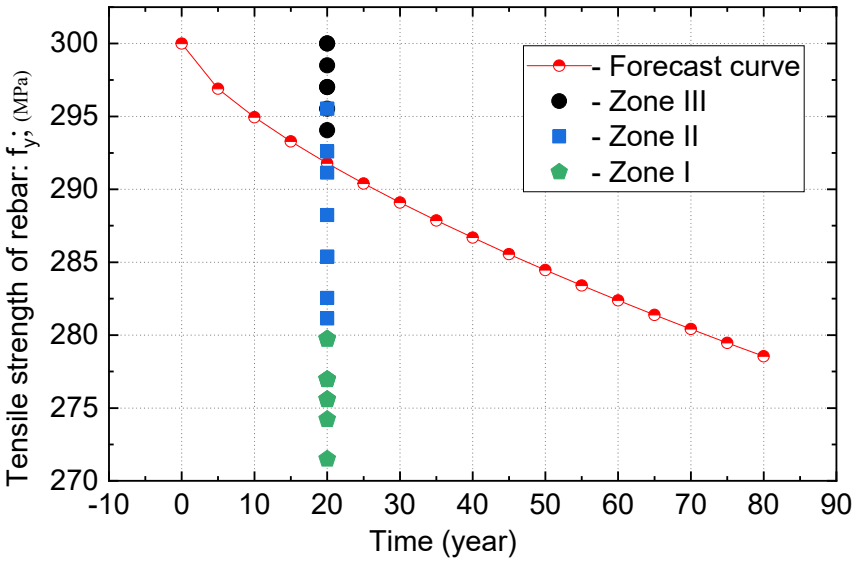

Fig. 7. Decrease of reinforcement tensile strength over time

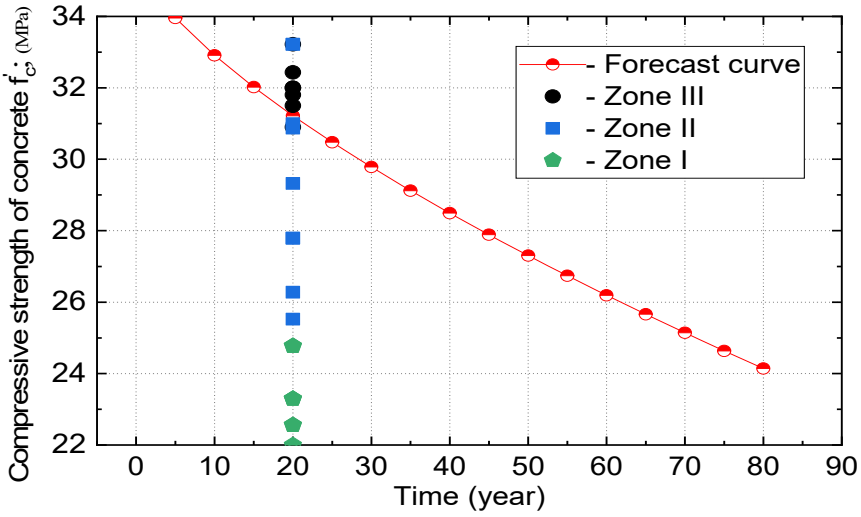

Fig. 8. Decrease of concrete compressive strength over time

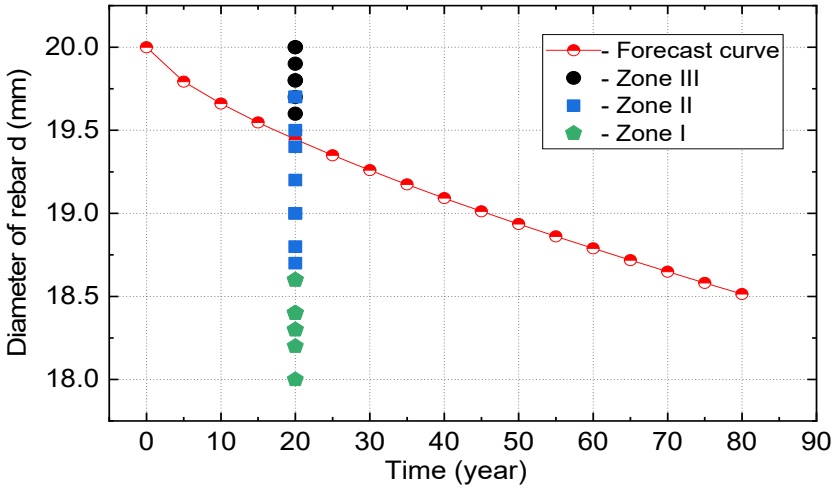

Fig. 9. Decrease of reinforcement diameter over time

with the current survey data (for the 20-year-old structure), the reduction rates of material strength and remaining rebar diameter over time closely approximate the empirical formula predictions only in Zone II (approximately –2 % to 4 %). However, significant discrepancies were observed between the measured values and the predicted results based on proposed empirical formulas in both Zone I and Zone III. This suggests that the existing empirical models have limited applicability across different structural zones and may require zone-specific calibration for accurate long-term performance assessment. The reduction in mechanical properties in Zone I is greater (4 % to 7 %) than that in Zone II, while the reduction in Zone III (–1 % to –3 %) is less than in Zone II.

In Fig. 9, the curve represents the reduction in the diameter of reinforcement steel over time. This curve was determined using empirical formulas proposed by Gonzalez et al. (1995) and Vu and Stewart (2000). The points shown in Fig. 9 at the 20-year mark represent the diameter of the reinforcement steel as experimentally determined by the authors.

This again reflects that the corrosion rate of the structure, or the reduction in the bearing capacity of the column components when corroded, depends not only on the general environmental conditions but also on the specific cross-sections within the structure. This should be taken into serious consideration when calculating the residual bearing capacity of the components after steel reinforcement corrosion.

Discussion

A survey was carried out on RC bridges in the coastal regions of Vietnam. We compared the survey results with the estimates obtained using a formula to calculate the loss of concrete strength, the reduction of tensile strength and cross-sectional area of reinforcement. We managed to draw the following conclusions:

1. Corrosion of reinforced concrete columns in zones contaminated with chlorides and sulfates in coastal areas of Vietnam occurs unevenly depending on the height of the structure.

2. The most corroded is the area at the column foot frequently submerged by flooding (Zone I). This can be attributed to the water level rising and falling regularly in this region, leading to the highest rate of corrosion.

3. Analysis of the survey results indicated that the bearing capacity of reinforced concrete columns affected by steel reinforcement corrosion in the study area must be assessed in Zone I.

4. These conclusions are based on the structural and environmental conditions of the study area (coastal regions of Vietnam). However, they offer a different perspective compared to some of the conclusions from previous studies.

5. While this study included some field survey experiments, the authors propose expanding the research to a larger scale, involving more structures and additional corrosive agents, to obtain more reliable results.

Acknowledgements

We would like to express our deep gratitude to those who provided comments, support and encouragement during this research. In particular, we would like to thank Professor **Valery Ivanovich Morozov**, Saint Petersburg State University of Architecture and Civil Engineering, for taking the time and effort to provide constructive suggestions, thereby helping us improve the article.

References

Ahmad, S. (2003). Reinforcement corrosion in concrete structures, its monitoring and service life prediction — a review. *Cement and Concrete Composites*, Vol. 25**,** Issues 4–5, pp. 459–471. DOI: 10.1016/S0958-9465(02)00086-0.

Al-Amoudi, O. S. B. and Maslehuddin, M. (1993). The effect of chloride and sulfate ions on reinforcement corrosion. *Cement and Concrete Research*, Vol. 23**,** Issue 1, pp. 139–146. DOI: 10.1016/0008-8846(93)90144-X.

Andrade, C. and Alonso, C. (2001). On-site measurements of corrosion rate of reinforcements. *Construction and Building Materials*, Vol. 15**,** Issues 2–3, pp. 141–145. DOI: 10.1016/S0950-0618(00)00063-5.

Arya, C. and Xu, Y. (1995). Effect of cement type on chloride binding and corrosion of steel in concrete. *Cement and Concrete Research*, Vol. 25**,** Issue 4, pp. 893–902. DOI: 10.1016/0008-8846(95)00080-V.

Assouli, B., Ballivy, G., and Rivard, P. (2008). Influence of environmental parameters on application of standard ASTM C876-91: half cell potential measurements. *Corrosion Engineering, Science and Technology*, Vol. 43**,** Issue 1, pp. 93–96. DOI: 10.1179/174327807X214572.

Ballim, Y. and Reid, J. C. (2003). Reinforcement corrosion and the deflection of RC beams — an experimental critique of current test methods. *Cement and Concrete Composites*, Vol. 25**,** Issue 6, pp. 625–632. DOI: 10.1016/S0958-9465(02)00076-8.

Cabrera, J. G. (1996). Deterioration of concrete due to reinforcement steel corrosion. *Cement and Concrete Composites*, Vol. 18**,** Issue 1, pp. 47–59. DOI: 10.1016/0958-9465(95)00043-7.

Dehwah, H. A. F., Maslehuddin, M., and Austin, S. A. (2002). Long-term effect of sulfate ions and associated cation type on chloride-induced reinforcement corrosion in Portland cement concretes. *Cement and Concrete Composites*, Vol. 24**,** Issue 1, pp. 17–25. DOI: 10.1016/S0958-9465(01)00023-3.

Diamond, S. (1986). Chloride concentrations in concrete pore solutions resulting from calcium and sodium chloride admixtures. *Cement, Concrete, and Aggregates*, Vol. 8**,** Issue 2, pp. 97–102. DOI: 10.1520/CCA10062J.

Du, Y. G., Clark, L. A., and Chan, A. H. C. (2005). Residual capacity of corroded reinforcing bars. *Magazine of Concrete Research*, Vol. 57**,** Issue 3, pp. 135–147. DOI: 10.1680/macr.2005.57.3.135.

Enevoldsen, J. N., Hansson, C. M., and Hope, B. B. (1994). The influence of internal relative humidity on the rate of corrosion of steel embedded in concrete and mortar. *Cement and Concrete Research*, Vol. 24**,** Issue 7, pp. 1373–1382. DOI: 10.1016/0008-8846(94)90122-8.

Ghods, P., Isgor, O. B., McRae, G., and Miller, T. (2009). The effect of concrete pore solution composition on the quality of passive oxide films on black steel reinforcement. *Cement and Concrete Composites*, Vol. 31**,** Issue 1, pp. 2–11. DOI: 10.1016/j.cemconcomp.2008.10.003.

Gonzalez, J. A., Andrade, C., Alonso, C., and Feliu, S. (1995). Comparison of rates of general corrosion and maximum pitting penetration on concrete embedded steel reinforcement. *Cement and Concrete Research*, Vol. 25**,** Issue 2, pp. 257–264. DOI: 10.1016/0008-8846(95)00006-2.

Hussain, S. E., Rasheeduzzafar, Al-Musallam, A., and Al-Gahtani, A. S. (1995). Factors affecting threshold chloride for reinforcement corrosion in concrete. *Cement and Concrete Research*, Vol. 25**,** Issue 7, pp. 1543–1555. DOI: 10.1016/0008-8846(95)00148-6.

Kumar, V. (1998). Protection of steel reinforcement for concrete – a review. *Corrosion Reviews*, Vol. 16**,** No. 4, pp. 317–358. DOI: 10.1515/CORRREV.1998.16.4.317.

Liu, Y. (1996). *Modeling the time-to corrosion cracking of the cover concrete in chloride contaminated reinforced concrete structures.* PhD Thesis in Civil Engineering.

Liu, T. and Weyers, R. W. (1998). Modeling the dynamic corrosion process in chloride contaminated concrete structures. *Cement and Concrete Research*, Vol. 28**,** Issue 3, pp. 365–379. DOI: 10.1016/S0008-8846(98)00259-2.

Ma, Y., Peng, A., Su, X., Wang, L., and Zhang, J. (2021). Modeling constitutive relationship of steel bar removed from corroded PC beams after fatigue considering spatial location effect. *Journal of Materials in Civil Engineering*, Vol. 33**,** No. 4, 04021019. DOI: 10.1061/(ASCE)MT.1943-5533.0003644.

Medeiros, M. H. F., Gobbi, A., Réus, G. C., and Helene, P. (2013). Reinforced concrete in marine environment: Effect of wetting and drying cycles, height and positioning in relation to the sea shore. *Construction and Building Materials*, Vol. 44**,** pp. 452–457. DOI: 10.1016/j.conbuildmat.2013.02.078.

Moreno, M., Morris, W., Alvarez, M. G., and Duffó, G. S. (2004). Corrosion of reinforcing steel in simulated concrete pore solutions: Effect of carbonation and chloride content. *Corrosion Science*, Vol. 46**,** Issue 11, pp. 2681–2699. DOI: 10.1016/j.corsci.2004.03.013.

Nasser, H., Van Steen, C., Vandewalle, L., and Verstrynge, E. (2021). An experimental assessment of corrosion damage and bending capacity reduction of singly reinforced concrete beams subjected to accelerated corrosion. *Construction and Building Materials*, Vol. 286**,** 122773. DOI: 10.1016/j.conbuildmat.2021.122773.

Nguyen, S.-M., Phan, V.-L., Tran, N.-L., Nguyen, X.-H., and Nguyen, T.-H. (2022). Time-dependent reliability assessment of a continuous I-shaped steel beam considering corrosion effects. *Engineering, Technology & Applied Science Research*, Vol. 12**,** No. 6, pp. 9523–9526. DOI: 10.48084/etasr.5273.

Okada, K., Kobayashii, K., and Miyagawa, T. (1988). Influence of longitudinal cracking due to reinforcement corrosion on characteristics of reinforced concrete members. *Structural Journal*, Vol. 85**,** Issue 2, pp. 134–140. DOI: 10.14359/2687.

Osuji, S. O., Ogirigbo, O. R., and Atakere, F. U.-O. (2020). Assessment of the condition of an existing marine concrete structure in the Niger Delta Region of Nigeria. *Journal of Civil Engineering Research*, Vol. 10**,** No. 3, pp. 63–71. DOI: 10.5923/j.jce.20201003.02.

Page, C. L. and Vennesland, Ø. (1983). Pore solution composition and chloride binding capacity of silica-fume cement pastes. *Matériaux et Construction*, Vol. 16**,** Issue 1, pp. 19–25. DOI: 10.1007/BF02474863.

Pradhan, B. (2014). Corrosion behavior of steel reinforcement in concrete exposed to composite chloride–sulfate environment. *Construction and Building Materials,* Vol. 72**,** pp. 398–410. DOI: 10.1016/j.conbuildmat.2014.09.026.

Rodriguez, J., Ortega, L. M., and Casal, J. (1997). Load carrying capacity of concrete structures with corroded reinforcement. *Construction and Building Materials,* Vol. 11**,** Issue 4, pp. 239–248. DOI: 10.1016/S0950-0618(97)00043-3.

Saricimen, H., Mohammad, M., Quddus, A., Shameem, M., and Barry, M. S. (2002). Effectiveness of concrete inhibitors in retarding rebar corrosion. *Cement and Concrete Composites*, Vol. 24**,** Issue 1, pp. 89–100. DOI: 10.1016/S0958-9465(01)00030-0.

Schiegg, Y., Büchler, M., and Brem, M. (2009). Potential mapping technique for the detection of corrosion in reinforced concrete structures: investigation of parameters influencing the measurement and determination of the reliability of the method. *Materials and Corrosion*, Vol. 60**,** Issue 2, pp. 79–86. DOI: 10.1002/maco.200805042.

Shaheen, F. and Pradhan, B. (2017). Influence of sulfate ion and associated cation type on steel reinforcement corrosion in concrete powder aqueous solution in the presence of chloride ions. *Cement and Concrete Research*, Vol. 91**,** pp. 73–86. DOI: 10.1016/j.cemconres.2016.10.008.

Shayanfar, M. A., Barkhordari, M. A., and Ghanooni-Bagha, M. (2016). Effect of longitudinal rebar corrosion on the compressive strength reduction of concrete in reinforced concrete structure. *Advances in Structural Engineering*, Vol. 19**,** Issue 6, pp. 897–907. DOI: 10.1177/1369433216630367.

Suryavanshi, A. K., Syam Sunder, S., and Nayak, B. U. (1991). Comparison of surface potentials of r. c. structures using reference electrodes - Part 2. *Corrosion Prevention and Control*, No. 38**,** pp. 128–31.

Tapan, M. and Aboutaha, R. S. (2011). Effect of steel corrosion and loss of concrete cover on strength of deteriorated RC columns. *Construction and Building Materials*, Vol. 25**,** Issue 5, pp. 2596–2603. DOI: 10.1016/j.conbuildmat.2010.12.003.

Viet Duc, N. (2021). Improving the mechanical performance of shell precast concrete blocks for coastal protection structures of hydraulic works. *Engineering, Technology & Applied Science Research*, Vol. 11**,** No. 1, pp. 6787–6791. DOI: 10.48084/etasr.4009.

Vu, K. A. T. and Stewart, M. G. (2000). Structural reliability of concrete bridges including improved chloride-induced corrosion models. *Structural Safety*, Vol. 22**,** Issue 4, pp. 313–333. DOI: 10.1016/S0167-4730(00)00018-7.

Yokozeki, K., Motohash, K., and Okada, T. T. I. (1997). A rational model to predict the service life of RC structures in marine environment n marine. *American Concrete Institute (ACI)*, Special Publication, Vol. 170**,** pp. 777–796. DOI: 10.14359/6853.

ВЛИЯНИЕ ЗАГРЯЗНЕННЫХ ХЛОРИДАМИ И СУЛЬФАТАМИ СРЕД НА ЖЕЛЕЗОБЕТОННЫЕ КОЛОННЫ

Динь Куок Фан, Ван Фук Фан*, Нгок Лонг Чан

Университет Винь, улица Ле Зуана, 182, Винь, Вьетнам

*E-mail: vanphuckxd@vinhuni.edu.vn

Аннотация
Введение. Коррозия стальной арматуры — сложный процесс, имеющий явные различия в разных географических регионах. Во всем мире разрабатываются многочисленные модели для прогнозирования ухудшения качества железобетонных конструкций в районах, загрязненных хлоридами и сульфатами. Тем не менее из-за слишком широкой сферы применения эти модели не способны полно и точно отразить снижение качества структуры в каждом конкретном случае. **Целью исследования** было изучение текущего состояния железобетонных (ЖБ) конструкций, расположенных в средах, загрязненных хлоридами и сульфатами, в прибрежных районах Вьетнама. Мы также проанализировали результаты и сравнили их с ранее исследованными предложениями, чтобы уточнить влияние коррозии стальной арматуры на качество ЖБ колонн. Были использованы следующие **методы**: экспериментальное исследования, неразрушающий контроль для определения снижения таких характеристик, как прочность бетона на сжатие, толщина защитного слоя, диаметр арматуры и площадь поперечного сечения ЖБ колонн. Кроме того, данное исследование было объединено с имеющимися рекомендациями по коррозии арматуры для определения остаточных физико-механических характеристик бетона и арматурной стали. В **результате** ухудшение качества ЖБ колонны с подвергшейся коррозии арматурой зависит от местоположения арматуры в одном и том же продольном элементе. Это указывает на значительное ухудшение качества конструктивных элементов, регулярно подвергающихся непосредственному воздействию морской воды.

Ключевые слова: бетон; сталь; железобетон; коррозия; морская вода; хлорид.

DOI: 10.23968/2500-0055-2025-10-1-70-80

NATURAL VIBRATIONS OF A STEEL-CONCRETE CYLINDRICAL SHELL IN A SOIL MEDIUM

Andrei Dmitriev*, Vladimir Sokolov, Tatyana Maltseva

Industrial University of Tyumen, 38 Volodarskogo St., Tyumen, Russia

*Corresponding author's email: dmitrievav@tyuiu.ru

Abstract

Introduction. Cylindrical shells embedded in the soil medium are generally used in pipeline transportation. To prevent damage to pipelines by concrete weights when the structure surfaces in a waterlogged environment, it is proposed to use concrete pipe products, with the inner part made of steel and the outer part formed by a concrete layer 30–50 mm thick. In this case, the designer faces the question of which calculation method to use for determining the natural vibration frequencies. **Purpose of the study:** To compare the values of natural vibration frequencies of a large-diameter steel-concrete gas pipeline in the ground, obtained using an analytical dependency, with the values determined in the Lira software package. **Methods:** The first method of determining frequency is based on an analytical expression obtained using the semi-momentless theory of cylindrical shells. The second method is based on the finite element method with the construction of a computational model in the Lira-SAPR software. Modeling of steel and concrete layers of the composite shell in the software package was carried out using 4-node plates, which are combined into a common structure with the help of perfectly rigid bodies (PRB). In the first case, the calculation for the soil medium surrounding the shell was carried out by creating a mass (measuring 5.3×5.3 meters) using volumetric bodies, while in the second case, it was done by setting a coefficient of subgrade reaction for the concrete layer. **Results:** We established that the second method of setting soil conditions allows a 5–6 times reduction in data entry time while achieving the same results. The discrepancy in the natural vibration frequencies for the research object, determined by the analytical method and the finite element method (FEM), does not exceed 10 %, and for the first three frequencies of the spectrum, it is no more than 6 %. Therefore, all methods are applicable. However, the use of an analytical expression allows calculations to be performed 10 times faster and does not require specialized software, making it more advantageous in the design based on frequency characteristics.

Keywords: natural vibrations; finite element method; semi-momentless theory of cylindrical shells; frequency.

Introduction

Cylindrical shells laid in a soil medium are generally used in the oil and gas industry for the transportation of hydrocarbons. The main pipeline is a multi-kilometer structure that is laid in various soil conditions, including areas with anticipated waterlogging and in waterlogged soils. Balancing of such sections is carried out using encircling concrete weights, which can damage the original geometry of the pipe section during maintenance or operation, thereby negatively affecting the reliability of the structure. One of the options to prevent such scenarios is the use of concrete pipe products, where the inner part is made of large-diameter steel pipes (d<1000 mm) with a parameter of $0.015 \leq h/R \leq 0.05$, and the outer part is formed by a concrete layer 30–50 mm thick. The reliability of such structures must be ensured by proper calculations during the design phase, one of the tasks of which is to ensure vibration resistance. In this case, the designer faces the question of which calculation method to use to determine the frequencies and modes of natural vibrations when constructing the pipeline based on frequency characteristics.

In the analyzed open sources published over the last 10 years, an approach using analytical expressions is proposed, as well as the application of the semi-analytical finite element method (FEM) in various software packages. For example, in the works of Shao et al. (2022), Shui et al. (2023), and Tan and Tang (2023), it is proposed to use analytical dependencies, which were obtained for a calculation scheme in the form of a rod, to determine the natural vibration frequencies of single-layer pipelines, taking into account the flow velocity of the fluid. This approach does not account for the deformation of the section and can be used for thick-walled cylindrical shells with parameters $0.07 < h/R < 0.125$. Vibrational processes for cylindrical shells partially supported on the ground, based on the rod theory, were investigated by Xü et al. (2018). Leontiev and Travush (2020) studied the vibrations of an underwater pipeline for the pipe-fluid-soil system; however, the paper does not cover the issue of internal working pressure, which prevents the deformation of the cylindrical shell in the radial direction and is undoubtedly present during the transportation of oil or gas products. Shakiryanov and Akhmedyanov (2020) as well as

For citations: Dmitriev, A., Sokolov, V., Maltseva, T. (2025). Natural vibrations of a steel-concrete cylindrical shell in a soil medium. Architecture and Engineering, No 1 (10), pp. 70–80. DOI: 10.23968/2500-0055-2025-10-1-70-80.

Yulmukhametov et al. (2020) studied the influence of internal non-stationary pressure on bending vibrations for computational models of closed cylindrical shells, but did not address the issue of the external environment surrounding the shell. Farshidianfar and Oliazadeh (2012), Lee and Kwak (2015), Oliazadeh et al. (2013) used various shell theories to determine the natural frequencies of pipeline vibrations: Soedel, Flügge, Morley-Koiter, and Donnell. The result of the solution using these theories is a determinant, which, when extended, calculates the frequency of natural vibrations. The work by Piacsek and Harris (2019) is analogous, but with the focus on aluminum structures. In (Kumar et al., 2015) and (Kumar et al., 2017), radial oscillations are studied without considering soil conditions, and the solution is obtained using the semi-momentless theory of cylindrical shells by Vlasov–Novozhilov. In (Sokolov and Razov, 2020), analytical dependencies were obtained for determining the natural vibration frequencies of semi-underground large-diameter pipelines. In (Bochkarev, 2022), a similar approach was implemented for a two-parameter foundation, but without considering the effect of longitudinal compressive force and internal pressure. Shahbaztabar et al. (2019) examined the natural frequencies of a metal-ceramic cylindrical shell embedded in a Pasternak elastic foundation, but did not consider internal pressure. The works by Alshabatat and Zannon (2021), Baghlani et al. (2020), and Ebrahimi (2022) were dedicated to three-layer shells. However, the functionality of the solutions obtained is extremely limited, as they do not take into account the internal pressure on the shell wall, the longitudinal compressive force, or the resistance of the medium that prevents wall deformation. Jain et al. (2016) used a software based on the finite element method and developed a methodology for modeling and determining the natural vibration frequencies for a cylindrical shell in ANSYS with various types of constraints, but without considering the external environment, and compared the values with the previously obtained results. Kumar et al. (2015) used ABAQUS to model and determine the frequency spectrum, while Dyachenko et al. (2019) used the ANSYS software; subsequently, the authors compared the obtained results with the results of calculations using analytical formulas. Dashevskij et al. (2021) obtained the natural frequencies for a metro tunnel using MSC Patran/Nastran software, but without using analytical dependencies. The literature review shows that numerous works are dedicated to this topic, and the approaches to solving the problem are diverse.

The aim of this work is to analyze the influence of soil conditions on the values of the natural vibration frequencies for a steel-concrete pipeline, as well as to compare the obtained results for the two proposed methods for determining frequencies to identify the optimal approach to solving the problem.

Subject, objectives, and methods

The object of the study is a section of a cylindrical two-layer shell designed for the transportation of natural gas, with a radius of the main steel layer R = 0.71 m and a thickness of h_2 = 18 mm. The thickness of the second concrete layer is h_1 = 40 mm. The length of the considered section of the cylindrical shell is taken as 7, 8, and 9 m. The moduli of elasticity for concrete and steel, as well as the density of the layers, are respectively equal to $E_1 = 3.24711 \cdot 10^{10}$ (N/m^2), $E_2 = 2.06 \cdot 10^{11}$ (N/m^2), γ_1 = 24,516.6 (N/m^3), γ_2 = 76,982.2 (N/m^3). The Poisson's ratio for steel and concrete of class B30 is assumed to be v = 0.3. The internal pressure is assumed to be p_0 = 0 MPa, and the longitudinal compressive force is also not considered.

The problem considers four types of soil conditions:

- In the first case, the structure is placed in a peat mass with the following parameters: soil density γ_{gr} = 11,770 N/m^3; soil modulus of elasticity E_{gr} = 500,000 N/m^2; soil Poisson's ratio v_{gr} = 0.49.
- In the second case, the soil medium is represented by uncompacted fill soil with the following parameters: soil density γ_{gr} = 16,660 N/m^3; soil modulus of elasticity E_{gr} = 3,000,000 N/m^2; soil Poisson's ratio v_{gr} = 0.35.
- The third case considers compacted fill soil with the following parameters: soil density γ_{gr} = 17,660 N/m^3; soil modulus of elasticity E_{gr} = 5,000,000 N/m^2; soil Poisson's ratio v_{gr} = 0.35.
- The fourth case is clay: soil density γ_{gr} = = 19,620 N/m^3; soil elasticity modulus E_{gr} = 20,000,000 N/m^2; soil Poisson's ratio v_{gr} = 0.42.

The *first method* for determining the natural frequency is based on the use of an analytical expression derived for the calculation scheme shown in Fig. 1.

We consider a section of a steel gas pipeline in a concrete casing, with the ends of the section assumed to be hinged. The pipeline is buried in the ground no more than half its diameter from the top generatrix to the ground level. In the governing equation for this situation, in addition to the internal pressure p_0 in the cylindrical shell, the elastic resistance of the soil medium q_{gr} is taken into account, while the active soil pressure on the wall of the cylindrical shell is not considered, as it is minimal. The added mass of the soil, which may be involved in the vibration, and the longitudinal compressive force that appears during thermal deformations or uneven settlement of the structure, are also not taken into account.

The resistance of the soil medium is assumed to be radial and is described by expression (1), which corresponds to the distribution pattern along the circumference of the shell as shown in Fig. 1:

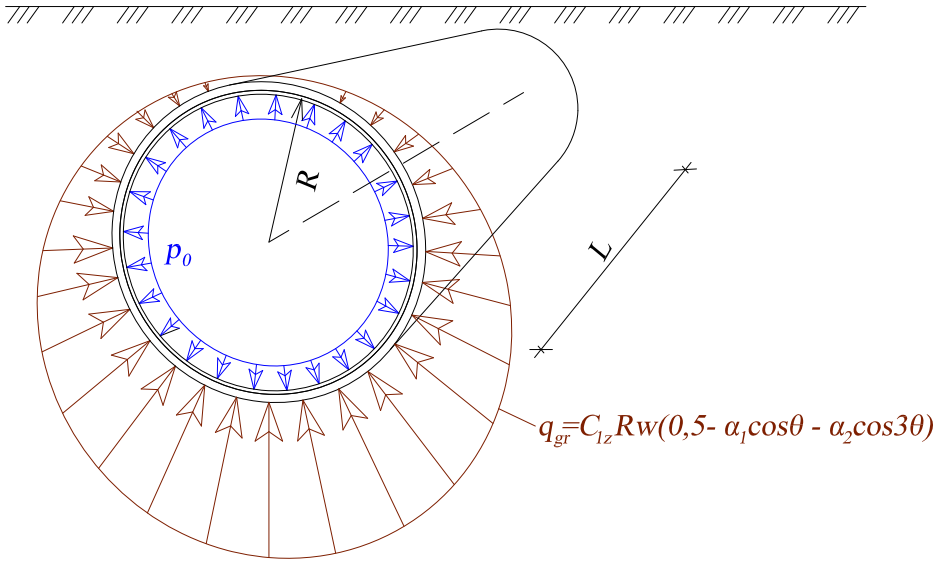

Fig. 1. Calculation scheme

$$q_{gr} = C_{1z} R w\left(0,5 - \alpha_1 \cos\theta - \alpha_2 \cos 3\theta\right), \quad (1)$$

here: q_{gr} — elastic resistance of the soil medium, preventing deformation of the cross-section; C_{1z} — coefficient of subgrade reaction; R — radius of the shell; w — displacement in the radial direction; α_1 and α_2 — coefficients ranging from 0.25 to 0.75, which are determined by selection depending on the radius of the cylindrical shell.

In solving the given problem, we applied the semi-momentless theory of cylindrical shells by Vlasov–Novozhilov, based on which the equilibrium equations for the cylindrical shell are written as follows:

$$\frac{\partial T_1}{\partial \xi} + \frac{\partial S}{\partial \theta} + R Q_2 \tau = -R X_1,$$

$$\frac{\partial T_2}{\partial \theta} + \frac{\partial S}{\partial \xi} + \frac{R}{R_2^*} Q_2 = -R X_2,$$

$$\frac{\partial Q_2}{\partial \theta} - \frac{R}{R_2^*} T_2 - \frac{R}{R_1^*} T_1 = -R X_3,$$

$$\frac{\partial M_1}{\partial \xi} + \frac{\partial H}{\partial \theta} - R Q_1 = 0, \quad \frac{\partial M_2}{\partial \theta} - \frac{\partial H}{\partial \xi} - R Q_2 = 0. \quad (2)$$

Transforming expressions (2) taking into account the relations of the semi-momentless theory (3):

$$\left(\frac{\partial \nu}{\partial \theta} + w = 0 ; \frac{\partial \nu}{\partial \xi} + \frac{\partial u}{\partial \theta} = 0 ; \vartheta_2 = \frac{\partial w}{\partial \theta} - \nu \right), \quad (3)$$

we obtain the equation in forces (4):

$$\frac{\partial^2 T_1}{\partial \xi^2} + \frac{\partial}{\partial \xi}\left(\tau \frac{\partial M_2}{\partial \theta} \right) - \frac{1}{R^2} \cdot \frac{\partial^3}{\partial \theta^3}\left(R_2^* \frac{\partial M_2}{\partial \theta} \right) -$$

$$- \frac{\partial}{\partial \theta}\left(\frac{1}{R_2^*} \frac{\partial M_2}{\partial \theta} \right) + \frac{\partial^2}{\partial \theta^2}\left(\frac{R_2^*}{R_1^*} T_1 \right) +$$

$$+ R \frac{\partial X_1}{\partial \xi} - R \frac{\partial X_2}{\partial \theta} - \frac{\partial^2}{\partial \theta^2}\left(R_2^* X_3 \right) = 0. \quad (4)$$

Inertial components $X_1 = -R h \rho_0 \frac{\partial^2 u}{\partial t^2}$ in the longitudinal direction, $X_2 = -R h \rho_0 \frac{\partial^2 v}{\partial t^2}$ in the circumferential direction, as well as

$$X_3 = -R\ h\ \rho_0 \frac{\partial^2 w}{\partial t^2} + p_0 -$$

$$-C_{1z} R\ w\left(0,5 - \alpha_1 \cos\theta - \alpha_2 \cos 3\theta\right),$$

in the radial direction are substituted into (4) and considering the dependencies between forces and deformations, displacements and deformations, without taking into account the nonlinear components (due to their insignificance compared to the linear ones), we obtain the linearized differential equation of motion in displacements:

$$\frac{\partial^3 u}{\partial \xi^3} + \eta h_v^2 \frac{\partial^3}{\partial \theta^3}\left(\frac{\partial^2 \vartheta_2}{\partial \theta^2} + \vartheta_2 \right) +$$

$$+2 \frac{\partial^2}{\partial \theta^2}\left(\frac{\partial^2 w}{\partial \xi^2} \varepsilon_0 \right) - \frac{R}{E_0 h} p_0 \frac{\partial^3 \vartheta_2}{\partial \theta^3} + \frac{1}{2} \frac{R^2 C_{1z}}{E_0 h} \frac{\partial^2 w}{\partial \theta^2} -$$

$$- \frac{R^2 \rho_0}{E h}\left(\frac{\partial^3 u}{\partial \xi \partial t^2} - \frac{\partial^3 v}{\partial \xi\, \partial t^2} - \frac{\partial^3 w}{\partial \theta^2 \partial t} \right) -$$

$$- \frac{R^2\, \alpha_1 C_{1z}}{E_0 h}\left(\frac{\partial^2 w}{\partial \theta^2} \cos\theta - 2 \frac{\partial w}{\partial \theta} \sin\theta - w \cos\theta \right) -$$

$$- \frac{R^2\, \alpha_2 C_{1z}}{E_0 h}\left(\frac{\partial^2 w}{\partial \theta^2} \cos 3\theta - \frac{\partial w}{\partial \theta} 6 \sin 3\theta - 9 w \cos 3\theta \right) = 0. \quad (5)$$

This expression contains unknown displacements in the longitudinal u, circumferential v, and radial w directions, as well as the angle of rotation of the initial and deformed states ϑ_2. By incorporating the semi-momentless theory relations (3), we obtain a complete system of differential equations.

The hinged support of the shell ends is described by expressions (6):

$$v\left\{\xi=0,\xi=\frac{L}{R}=0\right\},\ \theta_2\left\{\xi=0,\xi=\frac{L}{R}=0\right\};$$

$$w\left\{\xi=0,\xi=\frac{L}{R}=0\right\};\ \frac{\partial^2 w}{\partial\xi^2}\left\{\xi=0,\xi=\frac{L}{R}=0\right\}. \quad (6)$$

The solution is then carried out using the method of separation of variables. The double row for relative radial displacement *w* is written as (7):

$$w=\sum_m\cdot\sum_n b_{mn}\ \varphi(t)\sin(\lambda_n\xi)\cos(m\theta). \quad (7)$$

We determine displacements *u*, *v*, as well as ϑ_2 from (7) taking into account (3); they are described by expressions (8):

$$u=\sum_m\cdot\sum_n b_{mn}\frac{\lambda_n}{m^2}\varphi(t)\cos(\lambda_n\xi)\cos(m\theta);$$

$$v=\sum_m\cdot\sum_n b_{mn}\frac{1}{m}\varphi(t)\sin(\lambda_n\xi)\sin(m\theta);$$

$$\vartheta_2=-\sum_m\cdot\sum_n b_{mn}\frac{m^2-1}{m}\varphi(t)\sin(\lambda_n\xi)\sin(m\theta). \quad (8)$$

The vibration process for a cylindrical shell, occurring according to the harmonic law, is represented by the function φ(t) in the form:

$$\varphi(t)=\sin\omega_{mn}t;\ \varphi''(t)=-\omega^2\sin\omega_{mn}t, \quad (9)$$

where ω_{mn} is the natural frequency of vibrations.

By substituting expressions (7) and (8) into (5) taking into account (9), performing transformation, and denoting the coefficients of the unknowns as a_{ij}, we obtain system (10):

$$\begin{aligned}
&m=1 \quad a_{1,1}b_1+a_{1,2}b_2+a_{1,3}b_3=0;\\
&m=2 \quad a_{2,1}b_1+a_{2,2}b_2+a_{2,3}b_3+a_{2,4}b_4=0;\\
&m=3 \quad a_{3,1}b_1+a_{3,2}b_2+a_{3,3}b_3+a_{3,4}b_4+a_{5,5}b_5=0;\\
&\ldots\ldots\ldots\ldots\ldots\ldots\ldots\ldots\ldots\ldots\ldots\ldots;\\
&m=i \quad a_{i,1}b_1+a_{i,2}b_2+a_{i,3}b_3+a_{i,4}b_4+\\
&\qquad +a_{i,5}b_5+\ldots+a_{i,j}b_j=0.
\end{aligned} \quad (10)$$

Let us represent system (10) in the form of expression (11):

$$a_{m,m-3}b_{m-3,n}+a_{m,m-1}b_{m-1,n}+a_{m,m}b_{m,n}+$$
$$+a_{m,m+1}b_{m+1,n}+a_{m,m+3}b_{m+3,n}=0, \quad (11)$$

for which the a_{ij} coefficients are determined by expressions (12):

$$a_{m,m}=A_{n,m}-B_{n,m}\omega_{nm}^2;\ a_{m,m\pm1}=-\frac{m^2(m\pm1)^2}{2}q_{gr}^*\alpha_1;$$

$$a_{m,m\pm3}=-\frac{m^2[(m\pm3)^2-1]}{2}q_{gr}^*\alpha_2;$$

$$A_{n,m}=\lambda_n^4+\eta m^4(m^2-1)(m^2-1+\frac{p^*}{\eta})+$$
$$+C^*m^4-\lambda_n^4m^4P/n^2;$$

$$B_{n,m}=\rho^*Rh(\lambda^2h_\nu+m^2+m^4). \quad (12)$$

Expression (11) is solved using the matrix method, the result of which is presented in the form of (13):

$$\begin{vmatrix}
d_{11}-\lambda & d_{12} & d_{13} & d_{14} & \ldots\ldots & d_{1n}\\
d_{21} & d_{22}-\lambda & d_{23} & d_{24} & \ldots\ldots & d_{2n}\\
d_{31} & d_{32} & d_{33}-\lambda & d_{34} & \ldots\ldots & d_{3n}\\
d_{41} & d_{42} & d_{43} & d_{44}-\lambda & \ldots\ldots & d_{4n}\\
\ldots\ldots & \ldots\ldots & \ldots\ldots & \ldots\ldots & \ldots\ldots & \ldots\ldots\\
d_{p-41} & d_{p-31} & d_{p-21} & d_{p-11} & \ldots\ldots & d_{pn}-\lambda
\end{vmatrix}=0, \quad (13)$$

where:

$$d_{m,m}=\frac{0_{m,m}}{B_{n,m}};\ d_{m,m\pm1}=\frac{a_{m,m\pm1}}{B_{n,m}};\ d_{m,m\pm2}=\frac{a_{m,m\pm3}}{B_{n,m}},$$

and the coefficients $A_{n,m}, B_{n,m}, a_{m,m+1}, a_{m,m+3}$ are found using (12).

Subsequently, by expanding the determinant, we find the eigenvalues λ, where $\lambda=\omega_{n,m}^2$ is the square of the circular frequency of natural vibrations (1/s²) for the cylindrical shell.

Having analyzed the actions of the side coefficients of determinant (13), we established that their influence on the final result is no more than 2 %. Therefore, we will consider them equal to zero in the future, and determinant (13) takes the form:

$$\begin{vmatrix}
d_{11}-\lambda & 0 & 0 & 0 & \ldots\ldots & 0\\
0 & d_{22}-\lambda & 0 & 0 & \ldots\ldots & 0\\
0 & 0 & d_{33}-\lambda & 0 & \ldots\ldots & 0\\
0 & 0 & 0 & d_{44}-\lambda & \ldots\ldots & 0\\
\ldots\ldots & \ldots\ldots & \ldots\ldots & \ldots\ldots & \ldots\ldots & \ldots\ldots\\
0 & 0 & 0 & 0 & \ldots\ldots & d_{pn}-\lambda
\end{vmatrix}=0. \quad (14)$$

By solving the determinant (14), we obtain expressions for determining the frequencies of natural vibrations for pipelines:

$$\omega_{nm}=\frac{1}{2\pi}\sqrt{\frac{\lambda_n^4+\eta\cdot m^4\left(m^2-1\right)\left(m^2-1+\frac{p^*}{\eta}\right)+C_{1z}^*\cdot m^4}{\rho_{sh}^*\cdot R_0\cdot h\left(\lambda_n^4h_\nu+m^4+m^2\right)}}, \quad (15)$$

here:

n is the number of half-waves in the longitudinal direction;

m is the number of half-waves in the circumferential direction;

$\lambda_n=n\pi R_0/L\sqrt{h_\nu}$ is the length parameter of a two-layer cylindrical shell;

L is the length of the section (m);

$R_0=R-Z_0$ is the reduced shell radius (m);

R is the radius of the steel layer of the shell (m);

$Z_0=\frac{E_1h_1^2-E_2h_2^2}{2\left(E_1h_1+E_2h_2\right)}$ is the distance from the connection layer to the original surface (m) (Fig. 2);

h_1 is the thickness of the concrete layer of the shell (m);

h_2 is the thickness of the steel layer of the shell (m);

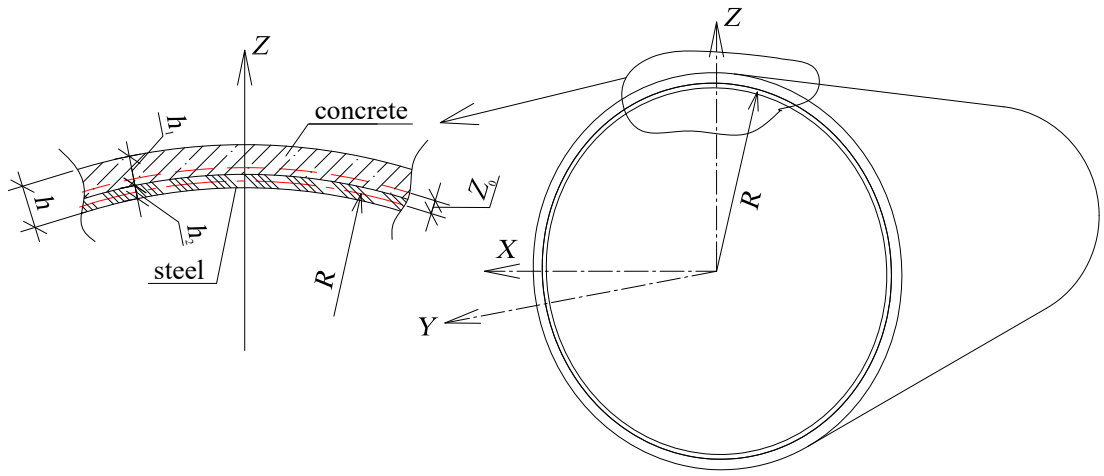

Fig. 2. Geometric dimensions of a two-layer shell

$h = h_1 + h_2$ is the wall thickness of the two-layer shell (m);

E_1 is the modulus of elasticity of the concrete layer (N/m^2);

E_2 is the modulus of elasticity of the steel layer (N/m^2);

$h_\nu = h / R_0 \sqrt{12\left(1-\nu^2\right)}$ is the parameter of the relative thickness of the shell;

ν is Poisson's ratio;

$\eta = E_\nu / E_0$ is inhomogeneity coefficient;

$E_\nu = \left(1-\nu^2\right)\cdot 12D / h^3$ is reduced modulus of elasticity (bending);

$$D = \frac{1}{3\left(1-\nu^2\right)}\times$$

$$\times\left[E_1\left\{\left(h_1 - Z_0\right)^3 + Z_0^3\right\} + E_2\left\{\left(h_2 + Z_0\right)^3 - Z_0^3\right\}\right]$$

is reduced bending stiffness;

$E_0 = \left[E_1 h_1 + E_2 h_2\right] / h$ is reduced modulus of elasticity (tension/compression);

$p^* = p_0\left(R_0 / E_0 h \cdot h_\nu^2\right)$ is internal working pressure parameter;

p_0 is internal pressure in a two-layer shell (N/m^2);

$\rho_{sh}^* = \rho_0\left(R_0 / E_0 \cdot h \cdot h_\nu^2\right)$ is the parameter of the material density of the shell (s^2/m^2);

$\rho_0 = \frac{1}{g}\left[\left(\gamma_1 h_1 + \gamma_2 h_2\right) / h\right]$ is the reduced specific weight of the shell material (N·s^2/m^3);

γ_1 is density of concrete (N/m^3);

γ_2 is density of steel (N/m^3);

$C_{1z}^* = R_0^2 C_{1z} / E_{gr} h \cdot h_\nu^2$ is the reduced coefficient of subgrade reaction;

$C_{1z} = E_{gr} / R_0\left(1+\nu_{gr}\right)$ is the coefficient of subgrade reaction for a cylindrical shell (N/m^3);

E_{gr} is modulus of elasticity for soil (N/m^2).

To calculate the natural frequencies of vibrations using the *second method*, we used the Lira-SAPR software. The modeling of each layer of the two-layer shell (Fig. 3) was carried out using four-node plate elements (Type 41) with dimensions of 0.1×0.1 m. Their geometric position corresponded to the position of the element of the midsurface for each layer. The stiffness characteristics of the layers are shown in Fig. 4. To ensure the synergy of the layers, we used displacement combinations for each corresponding node by setting perfectly rigid bodies (PRB). To fasten the shell ends according to the hinged-fixed scheme, we introduced a restriction on the linear displacements of the boundary nodes along the *Z* and *Y* axes.

Modeling of the medium (soil) in which the shell is placed was carried out in two ways:

- In the first method, we created a mass of universal spatial eight-node isoparametric finite elements (Type 36) with dimensions of 0.1×0.1×0.1 m. The overall size of the created medium mass in cross-section is 5.3×5.3 m. The stiffness characteristics of the volumetric elements of the soil mass are shown in Fig. 5.
- There was no soil mass created in the second method, and the elastic resistance of the soil was accounted for by assigning a coefficient of subgrade reaction (Fig. 6) for the plate concrete elements C_{1z} = 473,620 (N/m^3) for the first case of soil conditions, C_{1z} = 3,136,416 (N/m^3) for the second, C_{1z} = 5,227,360 (N/m^3) for the third, and C_{1z} = = 19,878,694 (N/m^3) for the fourth.

Only the self-weight of the shell layers was considered as external loads (excluding the weight of the soil medium).

We determined natural vibration frequencies using "Modal Analysis", which forms the mass matrix of the structure, and the number of natural vibration modes, which in this case was set to ten. The mass matrix is formed based on the density of the elements (Fig. 7).

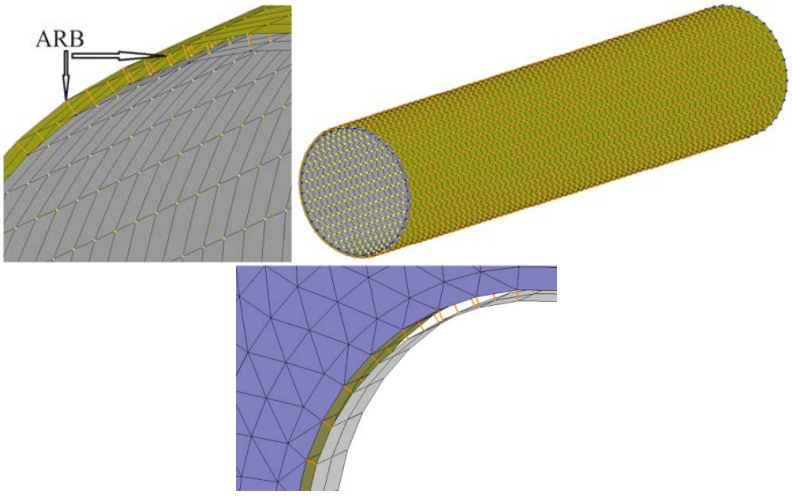

Fig. 3. Modeling of a composite cylindrical shell

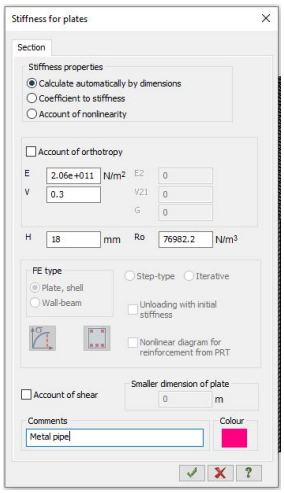

a) stiffness of the steel layer

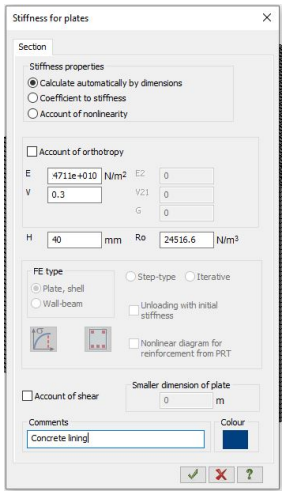

b) stiffness of the concrete layer

Fig. 4. Stiffness of plate elements of a composite shell

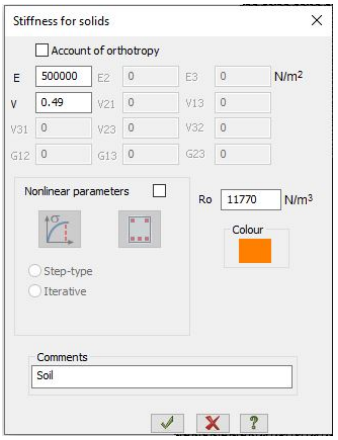

Fig. 5. Soil stiffness

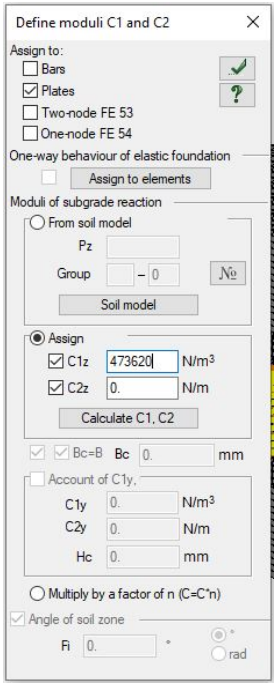

Fig. 6. Coefficient of subgrade reaction of the concrete layer

Results and discussion

All calculated natural vibration frequencies for different section lengths, as well as in various soil conditions, are compiled in Table for the ease of analysis. The first column presents the results of the calculation using expression (15); the second column contains the results of the calculation in the Lira software package with the set soil medium mass; the third one shows the results for the FEM with the set coefficient of subgrade reaction C_{1z}. The results correspond to seven vibration modes, images of which are shown in Fig. 8. For clarity, Fig. 9 shows the first three modes of vibration in the soil mass.

Analysis of the data in Table shows:

- For the considered section with a length of 7 m, the minimum frequencies are realized for ω_{12}, that is, with the flattening of the cross-section, and correspond to shell vibration modes, while for sections with lengths of 8 and 9 m, the minimum frequencies correspond to the ω_{11} mode (rod, without

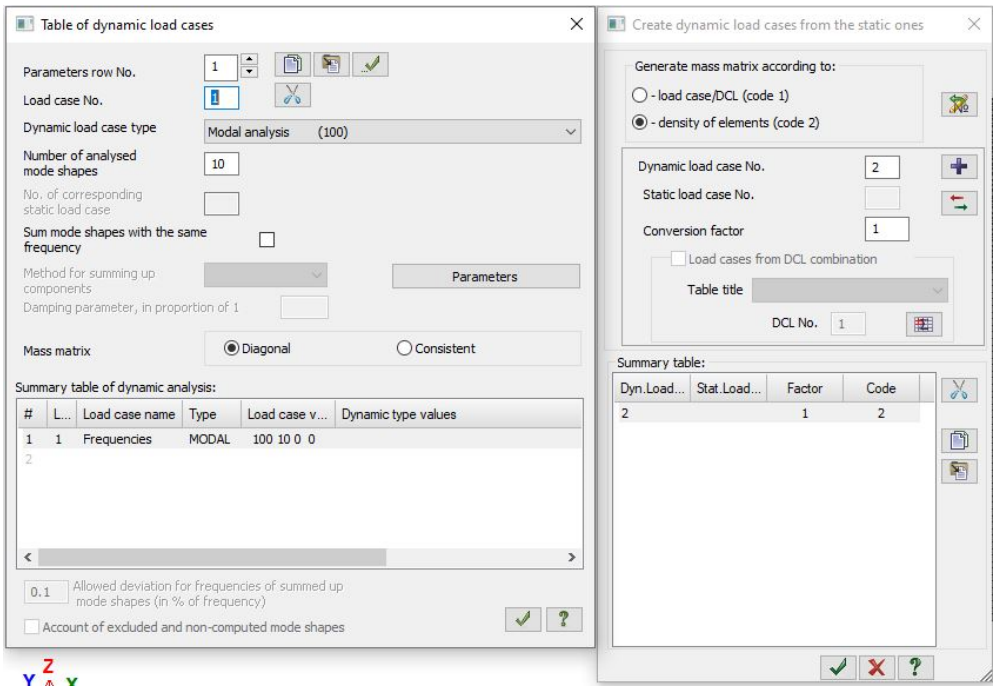

Fig. 7. Specification for dynamic impact calculation

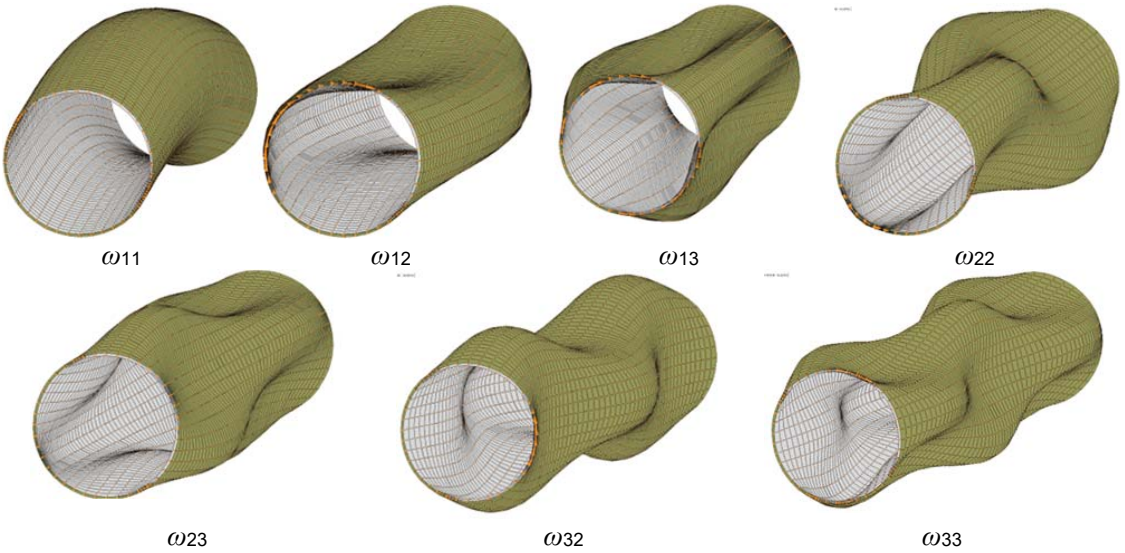

Fig. 8. Vibration modes for the considered section of the pipeline

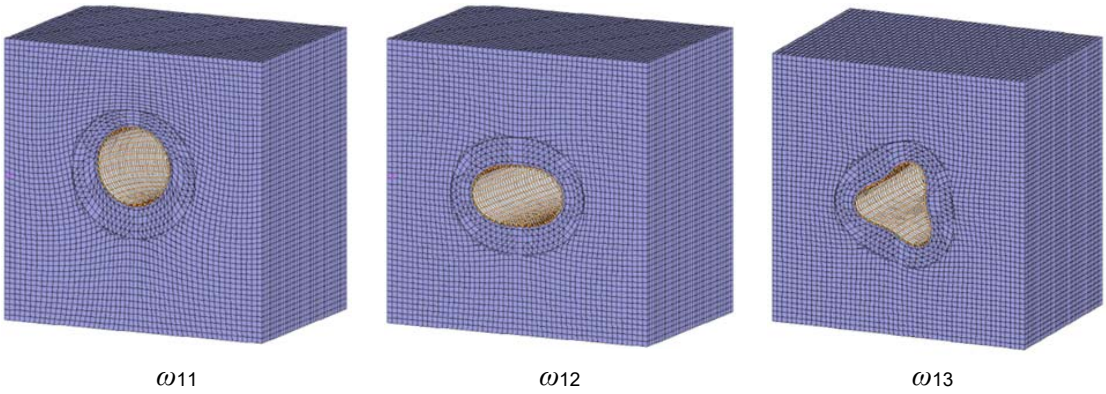

Fig. 9. Vibration modes for the considered section of the pipeline at n = 1 in the soil mass (the mass size is 5.3×5.3 m in cross-section)

Results of determining the natural vibration frequencies by various methods for different soil conditions

Analytical formula (Hz)	Lira-SAPR mass (Hz)	Lira-SAPR coefficient of subgrade reaction C_{1z} (Hz)	Analytical formula (Hz)	Lira-SAPR mass (Hz)	Lira-SAPR coefficient of subgrade reaction C_{1z} (Hz)	Analytical formula (Hz)	Lira-SAPR mass (Hz)	Lira-SAPR coefficient of subgrade reaction C_{1z} (Hz)
1	2	3	1	2	3	1	2	3
L=7 m (R/L=1/10)			L=8 m (R/L=1/11)			L=9 m (R/L=1/13)		
Peat C_{1z} = 473,620 (N/m^3), γ_{gr} = 11,770 N/m^3; E_{gr} = 5·10^5 N/m^2; v_{gr} = 0.49.								
ω_{11}=71.52	ω_{11}=69.80	ω_{11}=68.99	ω_{11}=55.16	ω_{11}=57.08	ω_{11}=56.04	ω_{11}=43.86	ω_{11}=48.4	ω_{11}=47.14
ω_{12}=64.23	ω_{12}=69.90	ω_{12}=63.13	ω_{12}=62.53	ω_{12}=68.21	ω_{12}=67.58	ω_{12}=61.61	ω_{12}=67.2	ω_{12}=66.54
ω_{13}=169.4	ω_{13}=164.7	ω_{13}=164.4	ω_{13}=169.3	ω_{13}=164.10	ω_{13}=163.8	ω_{13}=169.2	ω_{13}=163.8	ω_{13}=163.5
ω_{22}=109.2	ω_{22}=109.6	ω_{22}=109.3	ω_{22}=92.18	ω_{22}=95.40	ω_{22}=95.01	ω_{22}=81.62	ω_{22}=86.2	ω_{22}=79.20
ω_{23}=174.3	ω_{23}=174.6	ω_{23}=174.3	ω_{23}=172.1	ω_{23}=170.9	ω_{23}=170.6	ω_{23}=170.9	ω_{23}=168.7	ω_{23}= 168.4
ω_{32}=211.9	ω_{32}=186.5	ω_{32}=186.3	ω_{32}=167.4	ω_{32}=154.8	ω_{32}=154.6	ω_{32}=137.6	ω_{32}=132.3	ω_{32}=132.0
ω_{33}=194.6	ω_{33}=199.7	ω_{33}=199.5	ω_{33}=184.4	ω_{33}=188.2	ω_{33}= 187.9	ω_{33}=178.7	ω_{33}= 181.3	ω_{33}= 180.7
Uncompacted fill soil C_{1z} = 3,136,416 (N/m^3), γ_{gr} = 16,660 N/m^3; E_{gr} = 3·10^6 N/m^2; v_{gr} = 0.35.								
ω_{11}=72.45	ω_{11}=70.57	ω_{11}=69.97	ω_{11}=56.37	ω_{11}=58.89	ω_{11}=57.25	ω_{11}=45.38	ω_{11}=50.49	ω_{11}=48.57
ω_{12}=65.94	ω_{12}=71.61	ω_{12}=70.91	ω_{12}=64.29	ω_{12}=70.39	ω_{12}=69.26	ω_{12}=63.39	ω_{12}=69.39	ω_{12}=68.20
ω_{13}=170.17	ω_{13}=166.13	ω_{13}=165.15	ω_{13}=170.05	ω_{13}=165.70	ω_{13}=164.62	ω_{13}=169.98	ω_{13}=165.36	ω_{13}=167.28
ω_{22}=110.22	ω_{22}=110.79	ω_{22}=110.34	ω_{22}=93.37	ω_{22}=97.06	ω_{22}=96.17	ω_{22}=82.97	ω_{22}=88.03	ω_{22}=79.96
ω_{23}=175.03	ω_{23}=175.98	ω_{23}=175.02	ω_{23}=172.87	ω_{23}=172.46	ω_{23}=171.16	ω_{23}=171.72	ω_{23}=170.25	ω_{23}=169.18
ω_{32}=212.39	ω_{32}=187.30	ω_{32}=187.01	ω_{32}=168.07	ω_{32}=155.92	ω_{32}=155.31	ω_{32}=138.43	ω_{32}=133.54	ω_{32}=132.87
ω_{33}=195.23	ω_{33}=200.98	ω_{33}=200.09	ω_{33}=185.07	ω_{33}=189.60	ω_{33}=188.58	ω_{33}=179.44	ω_{33}=182.46	ω_{33}=180.12
Uncompacted fill soil C_{1z} = 5,227,360 (N/m^3), γ_{gr} = 17,660 N/m^3; E_{gr} = 5·10^6 N/m^2; v_{gr} = 0.35.								
ω_{11}=73.17	ω_{11}=71.72	ω_{11}=70.72	ω_{11}=57.30	ω_{11}=60.85	ω_{11}=58.18	ω_{11}=46.53	ω_{11}=51.76	ω_{11}=49.68
ω_{12}=67.26	ω_{12}=73.23	ω_{12}=72.12	ω_{12}=65.64	ω_{12}=72.38	ω_{12}=70.55	ω_{12}=64.76	ω_{12}=71.41	ω_{12}=69.56
ω_{13}=170.75	ω_{13}=167.38	ω_{13}=165.77	ω_{13}=170.63	ω_{13}=167.02	ω_{13}=165.24	ω_{13}=170.57	ω_{13}=166.68	ω_{13}=164.89
ω_{22}=110.99	ω_{22}=111.89	ω_{22}=110.13	ω_{22}=94.29	ω_{22}=98.54	ω_{22}=97.11	ω_{22}=84.01	ω_{22}=89.65	ω_{22}=88.12
ω_{23}=175.59	ω_{23}=177.19	ω_{23}=175.61	ω_{23}=173.43	ω_{23}=173.76	ω_{23}=171.72	ω_{23}=172.29	ω_{23}=171.55	ω_{23}=170.17
ω_{32}=212.79	ω_{32}=188.03	ω_{32}=187.38	ω_{32}=168.58	ω_{32}=156.88	ω_{32}=155.87	ω_{32}=139.05	ω_{32}=134.65	ω_{32}=133.53
ω_{33}=195.73	ω_{33}=202.09	ω_{33}=200.59	ω_{33}=185.59	ω_{33}=190.81	ω_{33}=189.12	ω_{33}=179.98	ω_{33}=183.69	ω_{33}=181.97
Clay C_{1z} = 19,878,694 (N/m^3), γ_{gr} = 19,620 N/m^3; E_{gr} = 2·10^7 N/m^2; v_{gr} = 0.42.								
ω_{11}=78.01	ω_{11}=80.92	ω_{11}=75.81	ω_{11}=64.44	ω_{11}=77.37	ω_{11}=64.32	ω_{11}=53.97	ω_{11}=71.29	ω_{11}=56.79
ω_{12}=75.82	ω_{12}=85.87	ω_{12}=80.09	ω_{12}=74.40	ω_{12}=88.80	ω_{12}=78.98	ω_{12}=73.64	ω_{12}=88.04	ω_{12}=78.11
ω_{13}=174.76	ω_{13}=177.17	ω_{13}=170.14	ω_{13}=174.64	ω_{13}=177.59	ω_{13}=169.49	ω_{13}=174.58	ω_{13}=177.27	ω_{13}=169.16
ω_{22}=116.31	ω_{22}=120.41	ω_{22}=116.59	ω_{22}=100.52	ω_{22}=110.79	ω_{22}=103.32	ω_{22}=90.96	ω_{22}=103.76	ω_{22}=94.94
ω_{23}=179.48	ω_{23}=186.56	ω_{23}=179.59	ω_{23}=177.37	ω_{23}=183.98	ω_{23}=176.02	ω_{23}=176.26	ω_{23}=181.88	ω_{23}=174.27
ω_{32}=215.54	ω_{32}=193.62	ω_{32}=190.64	ω_{32}=172.07	ω_{32}=164.79	ω_{32}=159.78	ω_{32}=143.30	ω_{32}=143.72	ω_{32}=138.08
ω_{33}=199.20	ω_{33}=209.42	ω_{33}=204.08	ω_{33}=189.27	ω_{33}=190.33	ω_{33}=192.81	ω_{33}=183.77	ω_{33}=193.46	ω_{33}=185.81
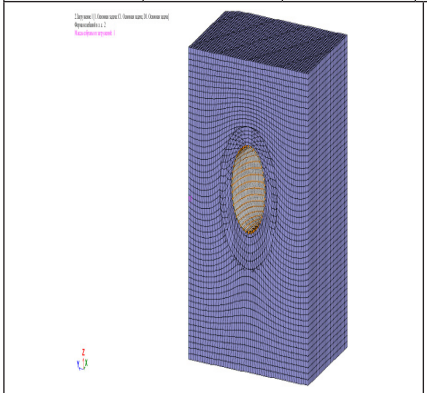						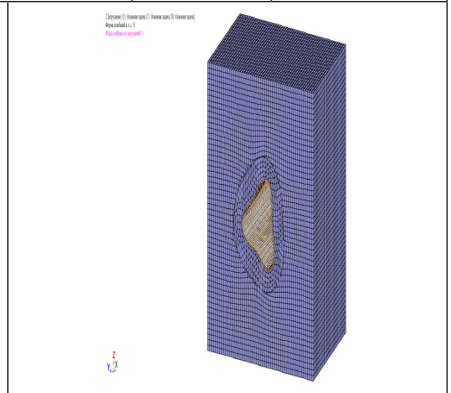		
ω_{11}			ω_{12}			ω_{13}		

cross-sectional deformation). All other vibration modes are shell-like.

- An increase in the length of the considered section by 1 m leads to a decrease in the value of the natural vibration frequencies by an average of 1.5–3.0 %, regardless of the method used to determine these values.
- An increase in the stiffness characteristics of the soil medium leads to higher values of the natural frequency of the steel-concrete-soil system. This is explained by the fact that the soil medium enhances the system's stiffness by preventing deformation of the cross-section.
- A comparison of the results for determining the natural vibration frequencies using expression (15) and software calculation shows that the difference for the first three frequencies does not exceed 6 %, and for the remaining results — 10 %.
- The difference in the values of natural vibration frequencies determined using the finite element method with the specification of the soil mass (column 2) and by assigning the coefficient of subgrade reaction (column 3) does not exceed 2 %. Therefore, to reduce labor costs when creating the model, it is recommended to use the second method of modeling soil conditions. This method allows reducing the model loading time by five times and the data processing speed by the processor by at least ten times.

The results of the work done allow us to draw the following conclusions:

- The analytical method for determining frequencies using expression (15) has clear advantages over the finite element method, as it required 40 times less time to compute the data while yielding practically identical results.
- In the analytical method, the influence of internal working pressure can be accounted for using parameter p^*. However, this factor is impossible to apply in the finite element method. When modeling this loading, the internal pressure is considered not as a force preventing the deformation of the cross-section, but as an additional mass that acts as a kind of damper, resulting in a sharp decrease in frequency values. Therefore, all the data in Table 1 were obtained at zero internal pressure.

Conclusions

1. The discrepancy in the natural vibration frequencies for the research object, determined by the analytical method and the finite element method (FEM), does not exceed 10 %, and for the first three frequencies of the spectrum, it is no more than 6 %. Therefore, all methods are applicable. However, the use of an analytical expression allows calculations to be performed 40 times faster and does not require specialized software, making it more advantageous in frequency characteristics based design.
2. When calculating the natural frequencies using the finite element method, the second method of setting soil conditions allows a 5–6 times reduction in data entry time while yielding practically identical results.
3. Based on the analysis conducted for maximum productivity, it is recommended to use analytical expression (15) presented in this work when designing large-diameter pipeline transport structures.

Financing

This research was funded as part of a government assignment for the project: "Computer modeling of mechanical, thermal, and dynamic processes in weak and permafrost soils to ensure the reliability of ground foundations for engineering structures" (No. FEWN-2024-0006).

References

Alshabatat, N. and Zannon, M. (2021). Natural frequencies analysis of functionally graded circular cylindrical shells. *Applied and Computational Mechanics*, Vol. 15, No. 2, pp. 105–122. DOI: 10.24132/acm.2021.654.

Baghlani, A., Khayat, M., and Dehghan, S. M. (2020). Free vibration analysis of FGM cylindrical shells surrounded by Pasternak elastic foundation in thermal environment considering fluid-structure interaction. *Applied Mathematical Modelling*, Vol. 78, pp. 550–575. DOI: 10.1016/j.apm.2019.10.023.

Bochkarev, S. A. (2022). Natural vibrations of a cylindrical shell with fluid partly resting on a two-parameter elastic foundation. *International Journal of Structural Stability and Dynamics*, Vol. 22, No. 06, 2250071. DOI: 10.1142/S0219455422500717.

Dashevskij, M. A., Mitroshin, V. A., Mondrus, V. L., and Sizov, D. K. (2021). Impact of metro induced ground-borne vibration on urban development. *Magazine of Civil Engineering*, Issue 6 (106), 10602. DOI: 10.34910/MCE.106.2.

Dyachenko, I. A. Mironov, A. A., and Sverdlik, Yu. M. (2019). Comparative analysis of theories and finite element models for calculating free vibrations of cylindrical shells. *Transport Systems*, Issue 3 (13), pp. 55–63. DOI: 10.46960/62045_2019_3_55.

Ebrahimi, Z. (2022). Free vibration and stability analysis of a functionally graded cylindrical shell embedded in piezoelectric layers conveying fluid flow. *Journal of Vibration and Control*, Vol. 29, Issue 11–12, pp. 2515–2527. DOI: 10.1177/10775463221081184.

Farshidianfar, A. and Oliazadeh, P. (2012). Free vibration analysis of circular cylindrical shells: comparison of different shell theories. *International Journal of Mechanics and Applications*, No. 2 (5), pp. 74–80. DOI: 10.5923/j.mechanics.20120205.04.

Jain, A. K., Rawat, A., and Kushwah, S. S. (2016). Free vibration analysis of circular cylindrical shells. *American Journal of Engineering Research (AJER)*, Vol. 5, Issue 10, pp. 373–380.

Kumar, A., Das, S. L., and Wahi, P. (2015). Instabilities of thin circular cylindrical shells under radial loading. *International Journal of Mechanical Sciences*, Vol. 104, pp. 174–189. DOI: 10.1016/j.ijmecsci.2015.10.003.

Kumar, A., Das, S. L., and Wahi, P. (2017). Effect of radial loads on the natural frequencies of thin-walled circular cylindrical shells. *International Journal of Mechanical Sciences*, Vol. 122, pp. 37–52. DOI: 10.1016/j.ijmecsci.2016.12.024.

Lee, H. and Kwak, M. K. (2015). Free vibration analysis of a circular cylindrical shell using the Rayleigh–Ritz method and comparison of different shell theories. *Journal of Sound and Vibration*, Vol. 353, pp. 344–377. DOI: 10.1016/j.jsv.2015.05.028.

Leontiev, Y. V. and Travush, V. I. (2022). Fluctuations of pipelines of gas-containing liquids under changing bearing conditions. *Structural Mechanics of Engineering Constructions and Buildings*, Vol. 18, No. 6, pp. 544–551. DOI: 10.22363/1815-5235-2022-18-6-544-551.

Oliazadeh, P., Farshidianfar, M. H., and Farshidianfar, A. (2013). Exact analysis of resonance frequency and mode shapes of isotropic and laminated composite cylindrical shells. Part I: Analytical studies. *Journal of Mechanical Science and Technology*, Vol. 27, Issue 12, pp. 3635–3643. DOI: 10.1007/s12206-013-0905-1.

Piacsek, A. A. and Harris, N. (2019). Resonance frequencies of a spherical aluminum shell subject to prestress from internal fluid pressure. *The Journal of the Acoustical Society of America*, Vol. 145, Issue 3 (Suppl.), 1881. DOI: 10.1121/1.5101813.

Shahbaztabar, A., Izadi, A., Sadeghian, M., and Kazemi M. (2019). Free vibration analysis of FGM circular cylindrical shells resting on the Pasternak foundation and partially in contact with stationary fluid. *Applied Acoustics*, Vol. 153, pp. 87–101. DOI: 10.1016/j.apacoust.2019.04.012.

Shakiryanov, M. M. and Akhmedyanov, A. V. (2020). Nonlinear oscillations of a pipeline under the action of variable internal pressure and moving supports. *Journal of Machinery Manufacture and Reliability*, Vol. 49, Issue 7, pp. 555–561. DOI: 10.3103/S1052618820070134.

Shao, Y.-F., Fan, X., Shu, S., Ding, H., and Chen, L.-Q. (2022). Natural frequencies, critical velocity and equilibriums of fixed–fixed Timoshenko pipes conveying fluid. *Journal of Vibration Engineering & Technologies*, Vol. 10, Issue 5, pp. 1623–1635. DOI: 10.1007/s42417-022-00469-0.

Shui, B., Li, Y.-D., Luo, Y.-M., and Luo, F. (2023). Free vibration analysis of Timoshenko pipes conveying fluid with gravity and different boundary conditions. *Journal of Mechanics*, Vol. 39, pp. 367–384. DOI: 10.1093/jom/ufad031.

Sokolov, V. and Razov, I. (2020). Free oscillations of semi-underground trunk thin-wall oil pipelines of big diameter. In: Murgul, V. and Pasetti, M. (eds.). *International Scientific Conference. Energy Management of Municipal Facilities and Sustainable Energy Technologies. EMMFT-2018. Advances in Intelligent Systems and Computing*, Vol. 982. Cham: Springer, pp. 615–627. DOI: 10.1007/978-3-030-19756-8_58.

Tan, X. and Tang, Y.-Q. (2023). Free vibration analysis of Timoshenko pipes with fixed boundary conditions conveying high velocity fluid. *Heliyon*, Vol. 9, Issue 4, e14716. DOI: 10.1016/j.heliyon.2023.e14716.

Xü, W.-H., Xie, W.-D., Gao, X.-F., and Ma, Y.-X. (2018). Study on vortex-induced vibrations (VIV) of free spanning pipeline considering pipe-soil interaction boundary conditions. *Journal of Ship Mechanics*, Vol. 22, Issue 4, pp. 446–453. DOI: 10.3969/j.issn.1007-7294.2018.04.007.

Yulmukhametov, A. A., Shakiryanov, M. M., and Utyashev, I. M. (2020). Bending vibrations of the pipeline under the influence of the internal added mass. In: *AIP Conference Proceedings. Proceedings of the XXVII Conference on High-Energy Processes in Condensed Matter, dedicated to the 90th anniversary of the birth of RI Soloukhin, 29 June – 3 July 2020, Novosibirsk, Russia,* Vol. 2288, Issue 1, 030093. DOI: 10.1063/5.0028885.

СОБСТВЕННЫЕ КОЛЕБАНИЯ СТАЛЕБЕТОННОЙ ЦИЛИНДРИЧЕСКОЙ ОБОЛОЧКИ В ГРУНТОВОЙ СРЕДЕ

Андрей Викторович Дмитриев* (Andrei Dmitriev), Владимир Григорьевич Соколов (Vladimir Sokolov), Татьяна Владимировна Мальцева (Tatyana Maltseva)

Тюменский индустриальный университет, ул. Володарского, 38, Тюмень, Россия

*Email: dmitrievav@tyuiu.ru

Аннотация

Введение. Цилиндрические оболочки, уложенные в грунтовую среду, как правило, используются в трубопроводном транспорте. Для исключения повреждения трубопроводов бетонными утяжелителями при всплытии конструкции в обводнённой среде, предлагается использовать трубобетонные изделия, внутренняя часть которых выполняется из стали, а внешняя часть образована бетонным слоем толщиной 30-50 мм. Перед проектировщиком в таком случае становится вопрос, какой из методов расчёта использовать для нахождения частот собственных колебаний. **Цель исследования:** Сравнить значения частот собственных колебаний сталебетонного газопровода большого диаметра в грунте, полученные при помощи аналитической зависимости со значениями, определёнными в программном комплексе ПК Lira. **Методы:** Первый метод определения частоты основывается на использовании аналитического выражения, которое было получено с использованием полубезмоментной теории цилиндрических оболочек. Второй базируется на методе конечных элементов с построением расчётной модели в среде Lira Sapr. Моделирование в программном комплексе слоёв стали и бетона композитной оболочки осуществлялось 4-х узловыми пластинами, которые объединены в общую структуру при помощи абсолютно жёстких тел (АЖТ). Учёт грунтовой среды, окружающей оболочку, в первом случае выполнялся путём создания массива (размером 5,3×5,3 метров) объемными телами, во втором случае путём задания коэффициента пастели для бетонного слоя. **Результаты:** Установлено, что второй способ задания грунтовых условий позволяет сократить время ввода данных в 5-6 раз при одинаковых результатах. Расхождение частот собственных колебаний для объекта исследования, определённых аналитическим методом и МКЭ не превышает 10 %, а для первых 3-х частот спектра не более 6 %, следовательно, все методы применимы. Однако использование аналитического выражения позволяет вычислять результаты в 10 раз быстрее и не требует специализированного программного обеспечения, поэтому является более выгодным при отстройке конструкции по частотным характеристикам.

Ключевые слова: собственные колебания; метод конечных элементов; полубезмоментная теория цилиндрических оболочек; частота.

DOI: 10.23968/2500-0055-2025-10-1-81-88

ASSESSMENT OF LONG-TERM WATER RESISTANCE OF MODIFIED PRESSED GYPSUM COMPOSITES

Aleksandr Viktorovich Kaklyugin[1]*, Luybov Ivanovna Kastornykh[1], Nonna Stepanovna Stupen[2], Viktor Viktorovich Kovalenko[2]

[1]Don State Technical University, 1 Gagarin Sq., Rostov-on-Don, Russia
[2]Brest State A.S. Pushkin University, 21 Kosmonavtov Boul., Brest, Belarus

*Corresponding author's email: kaklugin@gmail.com

Abstract

Introduction. The most important indicator of the durability of gypsum materials is their water resistance, which is most often assessed by the degree of strength reduction after short-term water saturation. In our view, the durability of composite building materials based on gypsum and other air binders can be more accurately predicted based on the results of longer laboratory tests, which include prolonged immersion of control samples in water, as well as an assessment of their ability to restore their original strength after re-drying. The **aim of this study** is to assess the effect of a complex modifier, consisting of a monosubstituted salt of orthophosphoric acid and a fine carbonate filler, on the water resistance properties of pressed gypsum composites after prolonged immersion in water. **Methods.** The technical characteristics of the studied composites were determined using standard methods with control samples manufactured by pressing. The long-term water resistance of the material was assessed based on the change in the values of the softening and water resistance coefficients, calculated based on the results of testing control samples stored for 1, 7, 28 and 90 days in water. **Results.** We show that the high-strength fine-crystalline structure of pressed gypsum binder without modifying additives is characterized by extremely low strength, both during short-term and long-term immersion of control samples in water, as well as reduced ability to restore its original strength after drying. This is revealed in the comparison of the water resistance indicators of the material, even with similar characteristics of cast samples made from pure gypsum binder, and especially with pressed samples from composite binders containing the proposed complex modifier. We established that gypsum-modified pressed composites are characterized by fairly high durability during prolonged immersion in water. After 90 days of testing, the softening coefficient of the studied compositions of composite binders ranged from 0.62 to 0.64, and the water resistance coefficient ranged from 0.90 to 0.95. This indicates the possibility of using products based on them in building enclosures, as well as in rooms with humidity above 75 %, provided that the water resistance of the studied pressed composites is maintained for a long time only if complete hydration of the gypsum binder is ensured.

Keywords*:* gypsum binders; chemical water treatment sludge from thermal power plants; monoammonium phosphate; pressed composites; water resistance.

Introduction

Various types of building products and structures are subject to temperature and humidity effects during operation, which involve prolonged and alternating moisture exposure, as well as repeated freezing and thawing. The ability of the material from which the products are made to resist these impacts primarily determines their durability (Ferronskaya, 1984, 2004). According to many authors, an important feature of the influence of various operational factors on gypsum materials is that the impact of alternating stresses is also accompanied by the dissolution of crystallization contacts of hardened calcium sulfate dihydrate, leading to an irreversible decrease in strength (Khalil et al., 2018; Petropavlovskaya et al., 2019; Safonova et al., 2018). Many researchers in Russia and other countries around the world are currently engaged in the search for methods and the development of technologies to enhance the durability of construction products based on gypsum binders (Domanskaya et al., 2018; Pervyshin et al., 2017; Petropavlovskaya et al., 2021; Zhukov et al., 2021). The research results allow a significant expansion of their application area, in particular making it possible to use them in building enclosures, as well as in rooms with indoor air humidity exceeding 75 %. The most well-known works in this field are related to the joint introduction of 15–25 % Portland cement and 10–25 % pozzolans of natural or technogenic origin into the composition of gypsum molding mixtures. The durability of products based on such mixed binders is ensured by the formation of sparingly soluble calcium hydrosilicates and hydroaluminates during hardening, as well as calcium hydrosulfoaluminate, which crystallizes in the monosulfate form (Barkovskaya and Terehova, 2023; Koroviakov and Bur'yanov, 2015; Lesovik et al., 2019).

Another method for increasing the strength and durability of construction materials and products based on low-fired gypsum binders is to reduce their porosity, primarily open porosity, by using intensive methods of compacting molding mixtures (Ferronskaya, 1984;

For citations: Kaklyugin, A. V., Kastornykh, L. I., Stupen, N. S., Kovalenko, V. V. (2025). Assessment of long-term water resistance of modified pressed gypsum composites. Architecture and Engineering, No 1 (10), pp. 81–88. DOI: 10.23968/2500-0055-2025-10-1-81-88.

Pervyshin et al., 2017; Petropavlovskaya et al., 2019). In this case, the highest strength is achieved when the water content in the gypsum mixture is close to the amount theoretically required to ensure the hydration of the binder (water-to-gypsum ratio of 18.6 %). This creates the conditions for the formation of a fine-crystalline structure of the resulting calcium sulfate dihydrate with maximum strength (up to 60 MPa and above) (Kaklyugin et al., 2020c). However, obtaining gypsum products from such semi-dry mixtures becomes possible only when using the method of high-pressure compaction. The possibility of using this method for the production of gypsum facing slabs, wall and partition stones, hollow-core interlocking blocks, and other small gypsum products has been attracting domestic and foreign researchers since the mid-20th century. Nonetheless, the production of pressed gypsum materials has not gained wide practical application, which, in our opinion, is due to the increased consumption of gypsum binder compared to products made using casting technology, as well as their insufficient water resistance for the intended use (Kaklyugin et al., 2020c).

In order to eliminate the above-mentioned shortcomings, we developed a complex modifier of gypsum binder and the structure of the resulting pressed composites, consisting of a carbonate-containing filler, sludge from chemical water treatment of thermal power plants, and a salt of orthophosphoric acid, monoammonium phosphate ($NH_4H_2PO_4$). The chemical interaction of the chemical additive with calcium sulfate of the gypsum binder and calcium carbonate of the modifying filler begins during the preparation of the molding mixture. At the same time, the chemical interaction between $NH_4H_2PO_4$ and $CaCO_3$ is accompanied by a short-term release of CO_2, which must be completed before the start of product molding. We described the mechanism of the proposed complex modifier in detail, with chemical reaction equations provided, in (Kaklyugin et al., 2020a, 2020b). The same studies show that the interaction of the chemical additive with the calcium sulfate of the binder and the calcium carbonate of the filler results in formation of screening phase films of sparingly soluble dicalcium phosphate dihydrate ($CaHPO_4 \cdot 2H_2O$) on the surface of the particles of the hydrated neoplasms and sludge grains. This compound is isomorphic with dihydrate gypsum, has 10 times lower solubility compared to it, and alters the crystallization structure of the pressed material. Films made of sparingly soluble calcium phosphate on the elements of the crystallization structure of the pressed material add to the cementing effect and contribute to an increase in its strength and water resistance (Kaklyugin et al., 2020a, 2020b).

One of the main technical characteristics determining the durability of gypsum products is considered to be their water resistance, which is assessed using the softening coefficient. The conditions for determining this coefficient for gypsum building products are currently not standardized. As a rule, it is calculated as the ratio of the compressive strength of the material after short-term (24–48 hours) water saturation to its strength in a dry state (Drebezgova et al., 2018; Cao et al., 2019). In our view, the durability of composite building materials based on gypsum and other air binders can be more accurately predicted based on the results of longer laboratory tests, which include prolonged immersion of control samples in water, as well as an assessment of their ability to restore their original strength after re-drying. The *aim of this study* is to assess the effect of a complex modifier, consisting of monoammonium phosphate and carbonate sludge from the chemical water treatment of a thermal power plant, on the water resistance indicators of pressed gypsum composites after prolonged immersion in water.

Methods

In experimental studies, we used G-5 grade gypsum binder according to GOST 125-2018 “Gypsum binders. Specifications”. With respect to the setting time, the binder is of normal setting type, and based on the degree of grinding, it is of medium grind. The water resistance of pressed gypsum composites was enhanced by introducing a complex modifier into the molding mixtures, consisting of a fine carbonate filler, chemical water treatment sludge from a thermal power plant, and a chemical additive, monoammonium phosphate. For these purposes, part of the gypsum binder in the studied compositions was replaced with powdered sludge. Monoammonium phosphate was dissolved in mixing water and introduced into the composition of the semi-dry molding mixture by sprinkling during its mixing in a laboratory slider mixer. The assessment of the long-term water resistance of gypsum-modified composites was carried out using control cylinder samples with a height and diameter of 50.5 mm, manufactured by pressing under 40 MPa. The choice of this pressing pressure is due to the fact that, as our previous studies have shown, lower values fail to provide the best combination of physical and mechanical properties of pressed gypsum composites, and in cases of higher values, we often observed water separation during the compaction of samples (Kaklyugin et al., 2022a, 2022b). Along with these tests, we also tested control samples made from gypsum mixtures without additives and molded under the same pressure, as well as the ones manufactured by casting from a paste of normal consistency (water-to-gypsum ratio of 0.52). The compositions of the studied molding mixtures, adopted based on the results of preliminary tests, as well as the physical and mechanical characteristics of the samples molded from them, are presented in the table.

After molding, all control samples were setting for three days in air-dry conditions. Five samples from each series were dried at a temperature of (50±2) °C until constant mass; then we determined their compressive strength. The remaining samples were immersed in containers with water, where they were kept for 1, 7, 28, and 90 days at a temperature of (25±3) °C. At the specified times, 10 control samples were removed from the water, 5 of which were immediately tested for compression, while the others were tested after being re-dried at the aforementioned temperature. Based on the calculated average strength values of the control samples, the softening (k_s) and water resistance (k_{wr}) coefficients of the material were determined, and water absorption by mass was calculated from the change in the mass of the samples before and after immersion in water. The softening coefficient was calculated as the ratio of the compressive strength of the material in a water-saturated state to that in a dried-to-constant-mass state, while the water resistance coefficient was determined as the quotient of the strength of dried-to-constant-mass samples, stored in water for a corresponding time, to the strength of dry samples not subjected to water saturation.

Results

Our laboratory studies revealed the effectiveness of the proposed method for modifying the composition and structure of pressed gypsum composites to ensure their long-term water resistance. The change in compressive strength of dried and water-saturated samples as the duration of their immersion in water increases is shown in Fig. 1. The analysis of research results shows that the strength of dried and water-saturated samples, molded from all studied compositions, decreases with an increase in the duration of their exposure to water. However, this trend is observed to varying degrees for the compositions under consideration. Thus, the greatest decrease in strength is observed in cast and pressed samples made from pure gypsum binder without a complex modifier (compositions 1 and 2). The strength of samples molded from gypsum paste of standard consistency after 90 days of storage in water in a dried state was 8.2 MPa, which is 24 % less than their strength before immersion in water, and in a water-saturated state, it was 4.0 MPa, which is almost 30 % less than the similar indicator after 1 day of water saturation. Composition No. 2 (pressed gypsum binder without additives) can be called the least water-resistant. It is characterized by the lowest softening coefficient: after just one day of water saturation, the samples had k_s of only 0.15, and with increased duration of sample storage in water, there is a further decrease in strength. After 90 days, the strength decreased by 40 % in a water-saturated state, and by 22.3 % in a dried state. This is explained by the excessive vulnerability of the crystallization structure of pressed gypsum binder to the wedging action of water films and indicates the extremely low durability of such material in humid conditions. As seen in Fig. 1, the reduction in the strength of hardened composite binders (compositions 3, 4, 5, 6) in a water-saturated state occurs to a lesser extent compared to compositions 1 and 2, and after drying, the material, within the accepted testing periods, mostly restores its initial strength. For example, after 24 hours of water saturation, the strength of the control samples molded from mixture composition No. 4 was 61.7 MPa in a dry state and 44.0 MPa in a water-saturated state. After 90 days of storing the samples in water, the strength of the pressed material decreased by 13.2 % and amounted to 38.2 MPa, while the strength of the samples after drying was 60.0 MPa, which is only 2.8 % less than the same indicator before the samples were immersed in water. This is explained by the change in the structure of the pressed stone and the appearance of newly formed sparingly soluble calcium phosphates among the products, which hinder the dissolution of the crystallization contacts of calcium sulfate dihydrate.

Compositions of molding mixtures and physical and mechanical characteristics of control samples

Number of composition	Content of components, % by mass		Monoammonium phosphate, over 100 %	Water-solid ratio	Compressive strength of samples, MPa		Average density, kg/m³	Water absorption by mass, %	Open porosity, %
	gypsum binder	sludge from chemical water treatment of thermal power plants			dry	water-saturated			
1	100	0	0	0.520	10.8	5.7	1200	28.4	34.0
2	100	0	0	0.190	32.0	5.3	1800	11.0	19.80
3	80	20	2	0.170	59.5	38.2	1930	7.3	14.00
4	80	20	2	0.185	61.7	44.0	1950	5.8	11.30
5	80	20	2	0.200	54.5	36.5	1940	8.0	15.50
6	60	40	2	0.170	46.8	29.5	1860	8.5	15.80

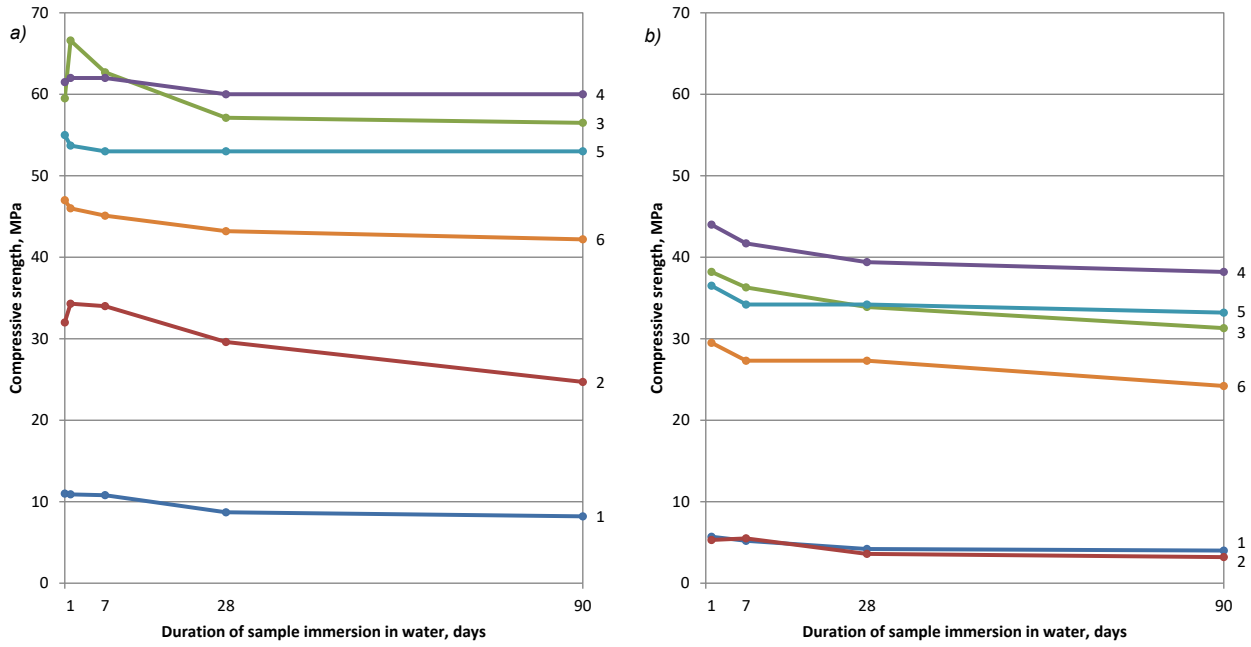

Fig. 1. The effect of the duration of keeping control samples in water on their strength in a dried (a) and water-saturated (b) state: 1–6 — composition numbers

The analysis of the change in the strength of samples made from compositions with the same content of a complex modifier, but with different water-solid ratios, shows that in humid conditions, the physical and mechanical characteristics of composition No. 3 deteriorate most noticeably, i.e., at a water-solid ratio of 0.17. Although samples of this composition, tested after 1 and 7 days of storage in water, exhibit strength in a dry state that is even slightly greater than before immersion in water, ultimately, after 28 and 90 days of water exposure, they show a decrease in strength, which is more noticeable than in samples made from compositions 4 and 5. Samples of composition No. 3, after 90 days of water immersion, exhibit a compressive strength of 31.1 MPa in a water-saturated state, which is 18.5 % less than the same indicator after 1 day of water saturation. Meanwhile, the strength of the samples of compositions 4 and 5 in a water-saturated state decreases by only 13 % and 9 %, respectively, and amounts to 38.2 and 33.2 MPa. A more noticeable decrease in the physical and mechanical properties of samples molded from mixture composition No. 3 after prolonged storage in water is explained by the fact that at a water-solid ratio of 0.17, complete hydration of the gypsum binder is not achieved during the hardening stage. When the samples are immersed in water, the unreacted calcium sulfate hemihydrate hydrates causing volumetric expansion of the stone and, consequently, weakening its crystalline structure. It should be noted that the decrease in the strength of samples made from all the studied compositions, when subjected to prolonged immersion in water, was accompanied by a slight increase in their water absorption by mass, as shown in Fig. 2.

This is due to the fact that with prolonged water saturation, water penetrates into increasingly smaller pores of the material, resulting in an intensified wedging effect on the crystallization structure of the gypsum stone. Fig. 3 shows how the softening and water resistance coefficients of the studied compositions change with the increase in time of the control samples immersion in water. As can be seen from the graphs presented in Fig. 3, the softening coefficient of gypsum-modified pressed composites of compositions 4, 5, and 6 exceeds 0.6 in all the tests. These compositions are also characterized by the highest water resistance coefficient k_{wr}, which was 0.90–0.97 after 90 days. This once again indicates a slight decrease in their strength when moistened and the ability to restore it upon drying. Fig. 3 also shows that with an increase in the duration of storage in water, the softening coefficient of samples of composition No. 3 decreases and after 90 days of testing is only 0.55, while its water resistance coefficient remains quite high (k_{wr} = 0.95).

As previously noted, control samples made from unmodified gypsum binder using casting (composition No. 1) and pressing (composition No. 2) methods are characterized by the greatest reduction in strength when saturated with water. After just one day of being in water, the softening coefficient of these compositions was 0.53 and 0.17, respectively, and with longer storage in water, it decreases even further, reaching 0.49 and 0.13 after 90 days. The extremely low water resistance

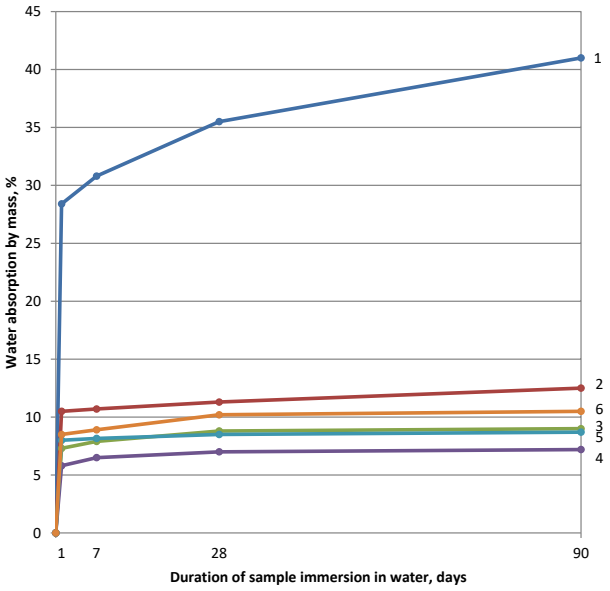

Fig. 2. Change in water absorption by mass of control samples with increasing duration of their immersion in water: 1–6 — composition numbers

of these compositions is further indicated by the obtained values of the water resistance coefficient. After 90 days of water storage, it decreased to 0.76 for samples made from paste of normal consistency and to 0.77 for pressed samples.

Discussion

The results of the conducted studies indicate that the high-strength fine-crystalline structure of pressed gypsum binder without modifying additives is characterized by extremely low durability, both during short-term and long-term immersion of control samples in water, as well as a reduced ability to restore its original strength after drying. This is revealed in the comparison of water resistance indicators of pressed samples even with similar characteristics of cast samples made from pure gypsum binder and, moreover, pressed samples from composite binders containing the proposed complex modifier. We established that gypsum-modified pressed composites are characterized by fairly high durability during prolonged immersion in water. After 90 days of testing, the softening coefficient of the studied compositions of composite binders ranged from 0.62 to 0.64, and the water resistance coefficient ranged from 0.90 to 0.95.

The increase in the long-term water resistance of the studied pressed gypsum composites is due to the synergistic effect of modifying additives: chemical water treatment sludge from a thermal power plant and monoammonium phosphate. Complex modification of gypsum binder ensures the formation of a monolithic fine-crystalline structure of artificial pressed stone-like material. The formation of an additional sparingly soluble framework of dicalcium phosphate dihydrate (brushite), which crystallizes isomorphously with dihydrate gypsum, enhances the resistance of the structure of modified composites to the wedging action of water films even during prolonged exposure to humid conditions. The presented kinetic dependencies of changes in the compressive strength of the material, as well as the softening and water resistance coefficients on the duration of storing control samples in water indicate the high water resistance of pressed modified gypsum composites and suggest the possibility

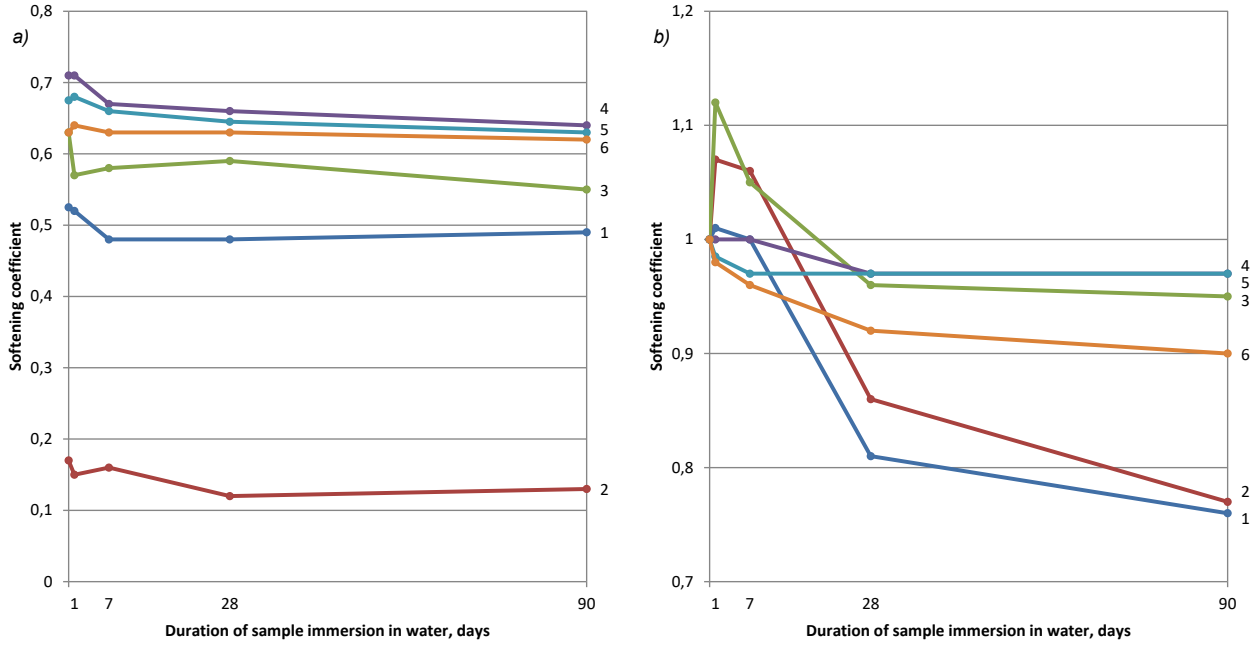

Fig. 3. Change in softening (a) and water resistance (b) coefficients with increasing duration of control samples immersion in water: 1–6 — composition numbers

of using products based on them in building enclosures, as well as in rooms with humidity above 75 %. At the same time, it is necessary to consider that the water resistance of the studied pressed composites is maintained for a long time only if the complete hydration of the gypsum binder is ensured.

The proposed method for increasing the water resistance of gypsum binders can only be used in the technology of manufacturing pressed products from semi-dry mixtures. This is due to the fact that during the mixing process of plastic consistency mixtures, as well as after they are poured into the mold, they will be significantly porous due to carbon dioxide released as a result of the chemical reaction between the calcium carbonate filler and the chemical additive. In the technology of pressed products, the formation of CO_2 occurs during the preparation of the molding mixture and does not negatively affect the structure formation of pressed composites.

In conclusion, it should be noted once again that prolonged laboratory observation of the changes in the physical and mechanical characteristics of artificial composites based on air binders, in our opinion, allows a more accurate and comprehensive prediction of their behavior in humid conditions. This is in contrast to the usual assessment of the water resistance of similar building materials, which is typically conducted by determining the softening coefficient after briefly soaking control samples in water. Therefore, the proposed method for assessing long-term water resistance is recommended for use in assessing the effectiveness of other methods of modifying gypsum binders and products based on them to enhance their durability.

References

Barkovskaya, S. V. and Terehova, L. O. (2023). Development features composite gypsum binder. *Chemistry, Physics and Mechanics of Materials*, No. 1 (36), pp. 55–66.

Cao, J.-Y., Li, J.-P., Jiang, Y.-M., Wang, S.-L., Ding, Y, and Oh, W.-C. (2019). Improvement in water resistance of desulfurized gypsum by novel modification of silicone oil paraffin composite emulsion-based waterproofing agent. *Journal of the Korean Ceramic Society*, Vol. 56, No. 6, pp. 558–565. DOI: 10.4191/kcers.2019.56.6.10.

Domanskaya, I., Bednyagin, S., and Fisher, H.-B. (2018). Water-resistant gypsum binding agents and concretes based thereof as promising materials for building green. *IOP Conference Series: Earth and Environmental Science*, Vol. 177, 012029. DOI: 10.1088/1755-1315/177/1/012029.

Drebezgova, M. Yu., Chernysheva, N. V., and Korbut, E. E. (2018). A study of the concrete weatherability of the composite gypsum binder. *Bulletin of Belgorod State Technological University named after V. G. Shukhov*, No. 7, pp. 6–11. DOI: 10.12737/article_5b4f02ae7b9974.05993554.

Ferronskaya, A. V. (1984). *Durability of gypsum materials, products and structures*. Moscow: Stroyizdat, 286 p.

Ferronskaya, A. V. (ed.). (2004). *Gypsum materials and products (manufacture and use). Reference book*. Moscow: ASV Publishing House, 488 p.

Kaklyugin, A. V., Stupen, N. S., Kastornykh, L. I., and Kovalenko, V. V. (2020a). Dependence of water resistance of moulded materials containing air-setting binders on effective porosity. *Proceedings of Universities. Investment. Construction. Real Estate*, Vol. 10, No. 1, pp. 68–75. DOI: 10.21285/2227-2917-2020-1-68-75.

Kaklyugin, A., Stupen, N., Kastornykh, L., and Kovalenko, V. (2020b). Pressed composites based on gypsum and magnesia binders modified with secondary resources. *Materials Science Forum*, Vol. 1011, pp. 52–58. DOI: 10.4028/www.scientific.net/MSF.1011.52

Kaklyugin, A. V., Kastornykh, L. I., Stupen, N. S., and Kovalenko, V. V. (2020c). Press-formed composites with alternate wetting and drying resistance based on modified gypsum binder. *Construction Materials*, No. 12, pp. 40–46. DOI: 10.31659/0585-430X-2020-787-12-40-46.

Kaklyugin, A., Stupen, N., Kastornykh, L., and Kovalenko, V. (2022a). A comparative assessment of gypsum and magnesite composites' air resistance modified by secondary resources. In: Guda, A. (ed.). *Networked Control Systems for Connected*

and Automated Vehicles. NN 2022. Lecture Notes in Networks and Systems, Vol. 509. Cham: Springer, pp. 1561–1570. DOI: 10.1007/978-3-031-11058-0_158.

Kaklyugin, A. V., Stupen, N. S., Kastornykh, L. I., and Kovalenko, V. V. (2022b). Gypsum and magnesite pressed composites with increased resistance to alternate moistening and drying. *News of Higher Educational Institutions. Construction*, No. 1 (757), pp. 31–43. DOI: 10.32683/0536-1052-2022-757-1-31-43.

Khalil, A. A., Tawfik, A., and Hegazy A. A. (2018). Plaster composites modified morphology with enhanced compressive strength and water resistance characteristics. *Construction and Building Materials*, Vol. 167, pp. 55–64. DOI: 10.1016/j.conbuildmat.2018.01.165.

Koroviakov, V. F. and Bur'yanov, A. F. (2015). Scientific and technical backgrounds of efficient application of gypsum materials in construction. *Housing Construction*, No. 12, pp. 38–40.

Lesovik, V. S., Chernysheva N. V., and Drebezgova M. Yu. (2019). Properties of composite gypsum binders depending on multicomponent mineral additives. *Materials Science Forum*, Vol. 945, pp. 238–243. DOI: 10.4028/www.scientific.net/MSF.945.238.

Pervyshin, G. N., Yakovlev, G. I., Gordina, A. F., Keriene, J., Polyanskikh, I. S., Fischer, H.-B., Rachimova, N. R., and Buryanov, A. F. (2017). Water-resistant gypsum compositions with man-made modifiers. *Procedia Engineering*, Vol. 172, pp. 867–874. DOI: 10.1016/j.proeng.2017.02.087.

Petropavlovskaya, V. B., Novichenkova, T. B., Belov, D. V., and Barkaya, A. T. (2019). Deformations of the creep of plaster composites. In: *Knowledge-Intensive Technologies and Innovations: Electronic Proceedings of the International Research-to-Practice Conference Dedicated to the 65th Anniversary of Belgorod State Technological University named after V. G. Shukhov*. Belgorod: Belgorod State Technological University named after V. G. Shukhov, pp. 330–334. DOI: 10.12737/conferencearticle_5cecedc3bc1066.56536029.

Petropavlovskaya, V., Zavadko, M., Novichenkova, T., Sulman, M. and Buryanov, A. (2021). Effective building mixtures based on hemihydrate plaster and highly dispersed mineral fillers. *Journal of Physics: Conference Series*, Vol. 1926, 012056. DOI: 10.1088/1742-6596/1926/1/012056.

Safonova, M., Syromyatnikova, A., Ammosova, N., and Filippova, K. (2018). Wall and partition products for low-rise buildings on the basis of gypsum with environmentally friendly natural filler. *MATEC Web of Conferences*, Vol. 245, 03010. DOI: 10.1051/matecconf/201824503010.

Zhukov, A. D., Bessonov, I. V., Bobrova, E. Yu., Gorbunova, E. A., and Demissie, B. A. (2021). Materials based on modified gypsum for facade systems. *Nanotechnologies in Construction*, Vol. 13, No. 3, pp. 144–149. DOI: 10.15828/2075-8545-2021-13-3-144-149.

ОЦЕНКА ДЛИТЕЛЬНОЙ ВОДОСТОЙКОСТИ ГИПСОВЫХ МОДИФИЦИРОВАННЫХ ПРЕССОВАННЫХ КОМПОЗИТОВ

Александр Викторович Каклюгин[1]*, Любовь Ивановна Касторных[1], Нонна Степановна Ступень[2], Виктор Викторович Коваленко[2]

[1]Донской государственный технический университет, площадь Гагарина, 1, Ростов-на-Дону, Россия
[2]Брестский государственный университет имени А.С. Пушкина, бул. Космонавтов, 21, Брест, Беларусь

*E-mail: kaklugin@gmail.com

Аннотация

Введение. Важнейшим показателем долговечности гипсовых материалов является их водостойкость, которую чаще всего оценивают по величине снижения прочности после кратковременного насыщения водой. На наш взгляд, более точно прогнозировать долговечность композиционных строительных материалов на основе гипсовых и других воздушных вяжущих, можно на основании результатов более длительных лабораторных испытаний, предусматривающих продолжительное выдерживание контрольных образцов в воде, а также оценку их способности восстанавливать первоначальную прочность в результате повторного высыхания. **Целью настоящей работы** является оценка влияния комплексного модификатора, состоящего из однозамещенной соли ортофосфорной кислоты и тонкодисперсного карбонатного наполнителя, на показатели водостойкости прессованных гипсовых композитов после их длительного выдерживания в воде. **Методы.** Технические характеристики исследуемых композитов определяли по стандартным методикам с использованием контрольных образцов, изготовленных методом прессования. Длительную водостойкость материала оценивали по изменению значений коэффициентов размягчения и водостойкости, рассчитываемых по результатам испытаний контрольных образцов хранившихся в течение 1, 7, 28 и 90 сут в воде. **Результаты.** Показано, что высокопрочная мелкокристаллическая структура прессованного гипсового вяжущего без модифицирующих добавок характеризуется крайне низкой стойкостью, как при кратковременном, так и при длительном выдерживании контрольных образцов в воде, а также пониженной способностью восстанавливать первоначальную прочность после высыхания. Это выявлено в сравнении показателей водостойкости материала даже с аналогичными характеристиками литых образцов из чистого гипсового вяжущего и, тем более, прессованных образцов из композиционных вяжущих, содержащих предлагаемый комплексный модификатор. При этом установлено, что гипсовые модифицированные прессованные композиты характеризуются достаточно высокой стойкостью при длительном хранении в воде. Через 90 сут испытаний коэффициент размягчения исследованных составов композиционных вяжущих составил от 0,62 до 0,64, а коэффициент водостойкости от 0,90 до 0,95. Это указывает на возможность использования изделий на их основе в ограждающих конструкциях зданий, а также в помещениях с влажностью более 75 %, учитывая, что водостойкость исследованных прессованных композитов сохраняется длительное время, только если обеспечивается полная гидратация гипсового вяжущего вещества.

Ключевые слова*:* гипсовые вяжущие вещества; шлам химводоподготовки теплоэлектростанций; однозамещенный фосфат аммония; прессованные композиты; водостойкость.

DOI: 10.23968/2500-0055-2025-10-1-89-102

ASSESSMENT OF THE TRANSPORT AND OPERATIONAL CONDITION OF ROADS BASED ON MOBILE LABORATORY DATA USING MACHINE LEARNING METHODS

Victoria Shamraeva

Financial University under the Government of the Russian Federation
49 Leningradsky Avenue, Moscow, 125993, Russia

*Corresponding author's email: VVShamraeva@fa.ru

Abstract
The subject of the study is the prediction of traffic intensity and pavement condition at a linear road section. The paper addresses a model of a neural network used to assess the usability of a road section and its transport and operational performance. The object of the study is a section of the M-1 Belarus road, 86th km, for the period from 2014 to 2023. The **purpose of the study** was to describe possible future scenarios of the road condition based on predicted traffic intensity and road quality condition metrics as part of the assessment of its usability with account for the International Roughness Index (IRI). In the course of the study, the following **methods** were used: Data Science (analysis of data collected from mobile laboratories) and machine learning algorithms (linear regression, gradient boosting, random forest, and neural networks based on long short-term memory (LSTM)). The output is a trained neural network capable of predicting the traffic intensity on the 86th km of the M-1 Belarus road. These methods reveal hidden patterns in the data and provide high-accuracy predictions. **Results**: The implementation of the deep learning model using the assessment of the condition of a linear road section will make it possible to address the main issues of road maintenance — to optimize time and reduce expenditures when planning and introducing measures at the stage of operation of transport infrastructure facilities, to take into account possible risks of road condition quality loss during re-pavement and design of new elements.

Keywords: transportation infrastructure; road diagnostics; defects; machine learning; Data Science; road information model.

Introduction

Road transport plays a paramount role in the transport infrastructure of the country. To ensure its development, the characteristics of roads must meet the traffic conditions since roads are subject to wear and tear as well as pavement deterioration due to heavy use and exposure to natural factors.

Nowadays, the role of digital technologies in business process management in almost all branches of technological industries has increased significantly. In this context, the road sector deserves special mention, where the growth rates of construction and reconstruction of linear road sections are quite high. For instance, the updated five-year road construction plan for 2024–2028 calls for 380 projects (see Resolution No. 3907-r dated 25.12.2023, http://government.ru/docs/50593/). These processes provide for an increase in the level of road maintenance, based on the diagnostics of linear road sections (Federal Law No. 257-FZ dated 08.11.2007 (amended on 04.08.2023) "On Motor Roads and Road Activities in the Russian Federation and Amendment of Certain Legislative Acts of the Russian Federation" (as amended and supplemented, effective from 01.03.2024), see https://legalacts.ru/doc/federalnyi-zakon-ot-08112007-n-257-fz-ob/, Article 14, Chapter 3).

Besides, switching to road construction financing with private investment (bonds and bank loans) has made it possible to increase the road network. Considering the lack of public resources, attraction of private investment requires the development of financial models that can guarantee payback at a required rate of return, which primarily depends on the correct prediction of traffic intensity on toll roads upon provision of comfort for road users. Thus, the compliance of pavement quality with the strict requirements for toll roads will increase the period between repairs and, therefore, optimize the repair budget, part of which can remain at the disposal of investors.

This paper is aimed to adapt machine learning methods to the prediction of the transport and operational condition of roads. For this purpose, approaches to pavement condition diagnostics are considered, the issues of predicting traffic intensity along a linear section and the influence of traffic on the transport and operational condition are addressed to determine the need for repair. Machine learning technologies open new horizons for road diagnostics goals and objectives. By applying these technologies, the expenses of companies can be significantly reduced due to timely diagnostics of road sections.

For citations: Shamraeva, V. (2025). Assessment of the transport and operational condition of roads based on mobile laboratory data using machine learning methods. Architecture and Engineering, No 1 (10), pp. 89–102. DOI: 10.23968/2500-0055-2025-10-1-89-102.

Methods

Both domestic (Apestin, 2011; Iliopolov et al., 2002; Vasilyev, 2013; and others) and foreign researchers (Panthi, 2009; Robinson et al., 1998; and others) have been studying the processes of road structure condition degradation. In the listed works, these processes are based on two levels (project level and network level (Fig. 1)) and two main indicators of pavement condition (operational and structural indicators (Fig. 2)). The project level is limited to the pavement design stage, while the network level considers pavement conditions throughout the entire life of the pavement. All stages of the life cycle of a road facility in the context of BIM modeling of linear road sections are described in (Shamraeva and Savinov, 2021).

The Russian Highways State Company adheres to a different methodology when assessing the actual level of the transport and operational condition of roads, which is based on the assessment of the residual life (Shamraeva, 2020) of road structures and division of operated road sections into three levels (standard-compliant, satisfactory and unsatisfactory) of pavement preservation (Fig. 3).

According to the regulatory requirements of Industrial Road Standards ODN 218.6.039–2018 "Recommendations on diagnostics and assessment of the technical condition of motor roads" (see https://files.stroyinf.ru/Data2/1/4294845/4294845825.pdf), the main transport and operational indicators of a road are as follows: speed provided by a road, traffic capacity, capacity for traffic of vehicles and road trains with axial and total weight established for the relevant categories of roads, etc. (Pugachev et al., 2024). All these indicators are fully reflected in such integrated indicator as traffic speed, expressed through the coefficient of design speed provision. As it is known, the transport and operational indicators of linear road sections are ensured by the parameters of longitudinal and transverse profiles, pavement strength, pavement evenness and adhesion characteristics, etc. (Figs. 1–3). Therefore, according to the methodology of ODM 218.4.039–2018 (Rosavtodor, 2018), the preservation of a road section depends on the average visual assessment score for pavement condition and the actual strength factor — the International Roughness Index (IRI) of non-rigid pavement.

Intensive road operation increases the risk of traffic accidents, reduces traffic safety, results in longer travel time and higher costs of transport repair and maintenance, etc. In this regard, it is important to

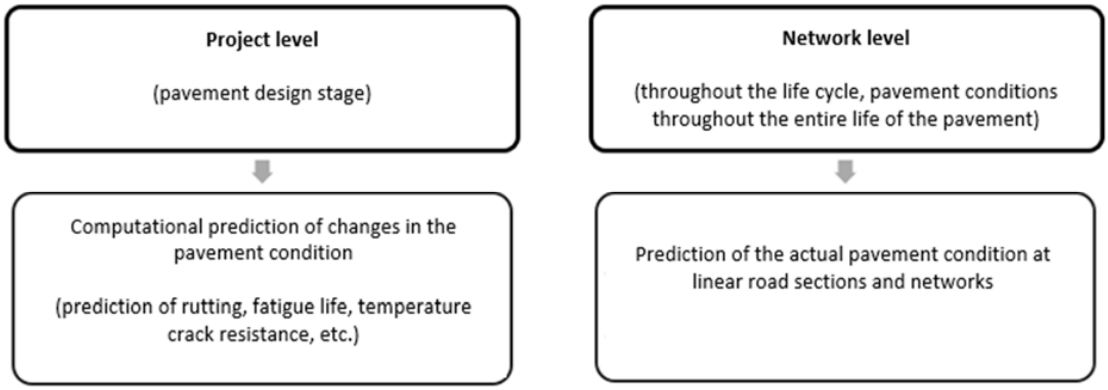

Fig. 1. Levels of road structure condition degradation processes

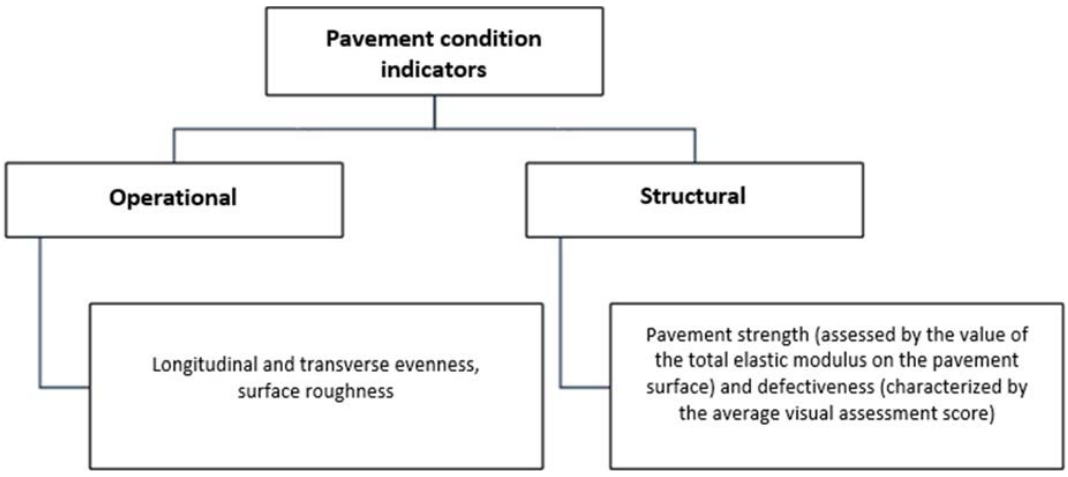

Fig. 2. Main groups of pavement condition indicators

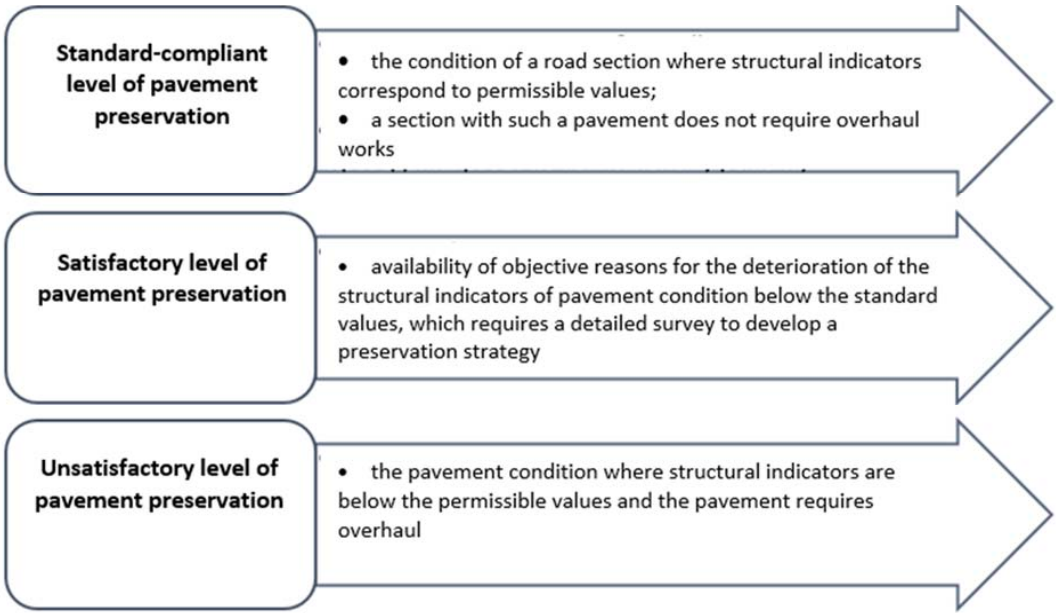

Fig. 3. Levels of pavement preservation

have in place effective methods for the diagnostics and assessment of the technical condition of roads. Transport and operational condition is assessed by specialized engineering organizations using mobile diagnostic laboratories, certified devices and equipment. Mobile units are equipped with modern devices and equipment (Znobishchev and Shamraeva, 2019) and may include panoramic video cameras of the latest generation (Stolbov et al., 2017) and even artificial intelligence technologies. Machine learning methods can be an alternative tool for monitoring the condition of road facilities (Marcelino et al., 2019).

The object of the study is a section of the M-1 Belarus road, 86th km, and its transport and operational condition. The aim was to develop a model for the diagnostics and assessment of the technical condition of roads using machine learning algorithms and medium-term prediction in accordance with the requirements of Organization Standard AVTODOR 2.28-2016 “Predicting the condition of operated roads of the Avtodor State Company” (Order No. 67 dated 06.05.2016) (Avtodor, 2016).

Input data processing

Two datasets are used as input data:

1 — data on traffic intensity with division into six categories of vehicles in the period from 2014 to 2023 inclusive in tabular format (Microsoft Excel), obtained from automated traffic counting points of the Avtodor State Company. The data are presented for each category of transport (cars, vans, light-duty trucks, single-unit vehicles, buses, road trains up to 13 m, from 13 to 18 m, and over 18 m) in forward and backward directions, including the total for two directions. In addition to the total intensity at a section for a certain period, the table uses the following structure: first the intensity is plotted by hours within one day, then the information for a day is summarized, and thus the data for a year are combined within one table sheet. As a result, information on traffic intensity for the past 10 years of observations for one section of the M-1 road is obtained.

2 — values of longitudinal evenness IRI by year for each road section from the 84th to 95th km of the M-1 Belarus road, obtained during measurements performed by a mobile diagnostic laboratory.

Following the basic idea of machine learning, it is necessary to provide a large number of proper examples based on which the program will “learn”. Therefore, it is important to check the input data for completeness so that they include all possible cases. Errors are critical since they will cause the model to give incorrect answers. The balance of the original dataset is also essential. If some cases are predominant, the model will favor the majority when making predictions. Therefore, when enough data are collected, it is necessary to pre-process them. The logic of the pre-processing of the intensity data from the first dataset is as follows: 1) the file is loaded and the names of all the table sheets in the sheet_ names (‘2014–2023’) list are read; 2) an empty combined_df dataframe is initialized to store the combined data from all the sheets, while the dataset is cleared of unnecessary data attributes. At the beginning of the cleanup function running, all sheets of the dataset table are visited, and the list of intensity data objects for the year of type pd.DataFrame is finally formed from the Microsoft Excel data source (Pandas library method — pd.read_excel()) into the combined_df variable, as well as unnecessary upper informative rows are deleted and a column with the date of the traffic intensity observation within the

accuracy of one day is added; 3) all elements of the list are combined into a large single dataframe with the logical deletion of the index column where the observation date was stored. This combined_df dataframe is the result of the pre-processing of the input dataset with data on traffic intensity for the past 10 years of expert observations; 4) the processed dataframe is saved to a new Excel file.

The intensity trend can vary from year to year for various global reasons: social, economic, or political. For example, the COVID virus affected the life of the country for several years and reduced the mobility of its inhabitants, thus affecting the intensity indicator. Month is also an important attribute that affects intensity. In some months, commercial traffic is increasing: for instance, many people travel by car to neighboring countries during summer. Intensity will also vary depending on the day of the week. For example, on weekdays/weekends, people may have different reasons for using the M-1 road. Thus, the model requires attributes from the date and values of total traffic intensity in forward and backward directions. Before moving on to this task, it is also important to understand the amount of the output data and whether there is a way to effectively reduce it in terms of dimensions without loss of quality. One of such ways described in this paper is to group all traffic intensity indicators (regardless of vehicle type) by date column, which is already represented and ready to be grouped within the accuracy of one day using the Pandas library capabilities, indicating the summation of intensity indicators for all hours within a day, which is very convenient in computation and informative in presentation. The final step in the dataset pre-processing is the selection of new temporal attributes of the dataset, necessary for further training of the neural network. Particularly in this case, the following attributes are selected: month number, day number, day number of the week, and year of traffic intensity observation. When predicting the road evenness, the number of vehicles that have traveled along the road over a year is used. Therefore, the date and intensity for that date will be used to develop the model. For each road that goes forward and backward, corresponding values shall be saved. Then the total count will be excessive and should not be kept.

The correlation matrix presented in Fig. 4 shows the relationships between different attributes, including forward and backward movement as well as time parameters (year, month, day of the week, day of the month). There is a correlation of 0.18 between forward and backward movement, indicating a weak positive relationship. This means that some tendency for an increase in forward movement is accompanied by an increase in backward movement. The correlation between year/month and traffic intensity is not significant (0.18 for year and month with forward movement; –0.14 and 0.14 for backward movement). This may indicate that there are no clear trends by year or month in the data, or that any trends are non-linear and are not captured by linear correlation. The correlations with

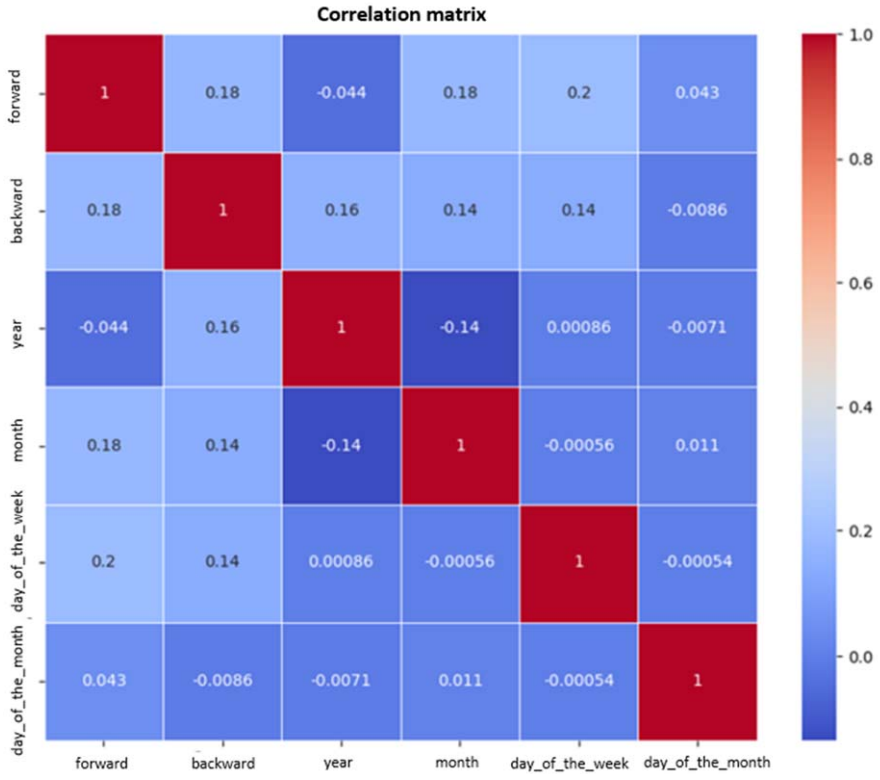

Fig. 4. Matrix of correlations between forward and backward traffic intensity and time

such attributes as the day of the week and the day of the month are also extremely low, indicating that there is no direct relationship of the day of the week or the day of the month with traffic intensity. When forming the output for a machine learning model, it is important to take into account that temporal attributes can significantly non-linearly affect the results. Despite the weak correlation between the forward and backward directions, these attributes can be useful when considered in conjunction with other variables that may strengthen their relationship or provide additional context.

Using machine learning methods that can capture such dependencies may yield more useful results. Such models as ensemble decision trees (e.g., random forest, gradient boosting) and neural networks (Goodfellow et al., 2018) can better handle such data as they are capable of detecting complex patterns and interactions between variables (Lasisi and Attoh-Okine, 2018).

In the second dataset with the IRI evenness values, a violation of the requirements of GOST 33388–2015 (Automobile roads of the general use. Requirements to conducting diagnostics and certification) (Interstate Council for Standardization, Metrology and Certification (ISC), 2016) can be observed, where the IRI value should not exceed 3.1 (https://nevacert.ru/dokumenty/normadoc/standartsbase-gost/gost-33388-2015). For instance, for 2023, such data are shaded in red in Fig. 5. In this file, the column with the GOST 33388-2015 standard values is redundant, not suitable for model training, and can be deleted during data pre-processing. Visualization of changes

	A	B	C	D	E	F	G
1	2023						
2	Beginning of the section, km	End of the section, km	Forward direction		Backward direction		GOST 33388-2015 standard value
3			Lane 1	Lane 2	Lane 3	Lane 4	
4	84,000	84,100	2,7	2,5	1,7	2,0	3,1
5	84,100	84,200	2,4	1,9	1,6	2,3	3,1
6	84,200	84,300	2,0	1,8	1,8	1,8	3,1
7	84,300	84,400	2,4	2,0	1,6	1,8	3,1
8	84,400	84,500	1,7	1,8	1,4	1,9	3,1
9	84,500	84,600	1,9	1,7	1,2	1,8	3,1
10	84,600	84,700	2,1	1,9	1,4	1,5	3,1
11	84,700	84,800	1,9	1,6	1,2	1,5	3,1
12	84,800	84,900	1,9	1,9	1,1	1,4	3,1
13	84,900	85,000	2,0	1,6	1,2	2,0	3,1
14	85,000	85,100	2,5	1,7	1,2	1,3	3,1
15	85,100	85,200	2,4	1,8	1,1	1,2	3,1
16	85,200	85,300	2,0	2,2	1,1	1,4	3,1
17	85,300	85,400	2,8	3,3	1,0	1,7	3,1
18	85,400	85,500	3,9	2,6	1,1	1,7	3,1
19	85,500	85,600	2,4	2,2	1,3	2,6	3,1
20	85,600	85,700	2,8	3,5	1,3	2,2	3,1
21	85,700	85,800	3,0	3,1	2,4	2,3	3,1
22	85,800	85,900	2,0	1,7	2,3	2,1	3,1
23	85,900	86,000	2,7	1,8	2,1	2,3	3,1
24	86,000	86,100	2,6	1,8	2,0	1,8	3,1
25	86,100	86,200	2,1	1,9	2,0	2,2	3,1
26	86,200	86,300	3,4	2,1	1,8	2,5	3,1
27	86,300	86,400	3,6	2,6	2,4	2,3	3,1

Sheet1 Sheet2

Fig. 5. IRI values at different sections of M-1 for 2023

in the mean IRI values for each lane (Fig. 6) shows that the road condition deteriorated over time.

For example, for lane 3 (Fig. 6), a slight asymmetry to the right is observed, where the bulk of the data is between 1 and 4. It can also be seen that the values did not change in the two years from 2019 to 2020

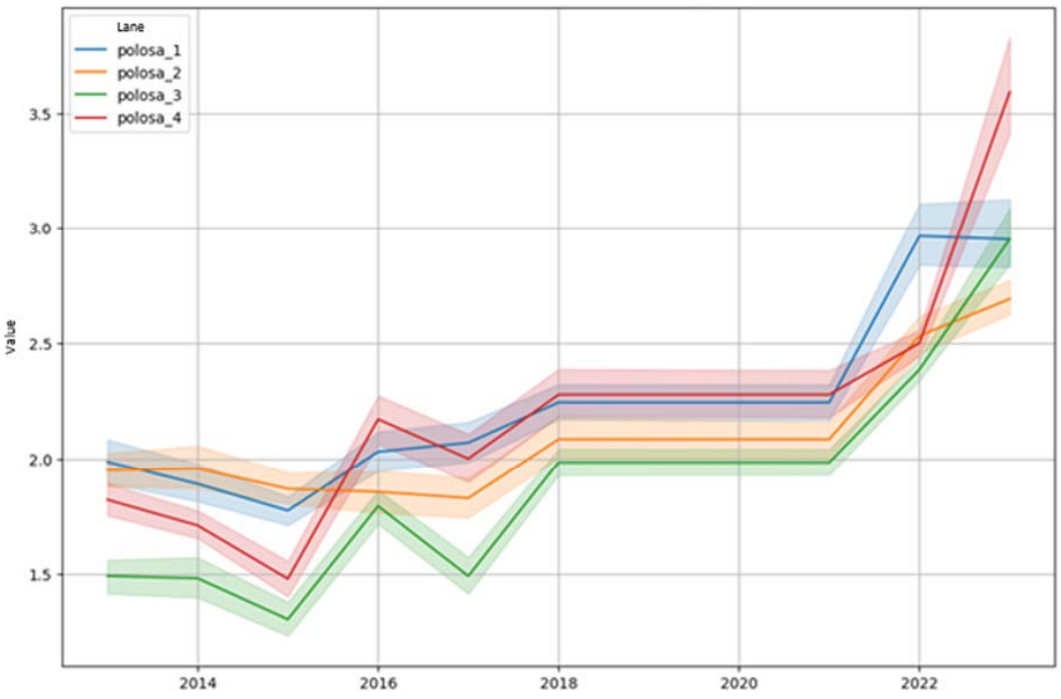

Fig. 6. Diagram of changes in the mean IRI values for each lane

(data for 2019–2020 were not available in the dataset provided). To determine the law of traffic intensity distribution for each lane, the SciPy library and the stats module of the dynamic Python programming language were used, which provides functions and statistical methods for work with probability distributions and statistical tests. For example, for lane 3 (Fig. 7), comparison of the values of the statistics of various tests (Kolmogorov–Smirnov, Pearson, Shapiro–Wilk, etc.) with the smallest p-value of the significance test equal to 0.05, resulted in a conclusion that the observed data are consistent with the Gumbel distribution on the right. As for other lanes, based on checks by statistical tests, it was concluded that the annual distributions of the IRI values are suitable for approximation modeling with subsequent transfer to machine learning models. The final IRI dataframe is shown in Fig. 8.

Training model selection and tuning

The preparatory stages of model building and training, with their further evaluation for the purposes of predicting values based on the second dataset with pre-processed data are as follows:

1. Break down the data sample into attributes and target values.
2. Select the attributes and variables based on which the target values will be predicted.
3. Divide the sample into training and test samples (it should be noted that for correct operation, the test sample should not be used for training).

This will result in an optimal prediction model for different target columns based on historical data and its application for further prediction for the period 2024–2034.

Let us briefly highlight the main points of the process of creating a suitable prediction model for different target columns.

Predicting changes in the IRI indicator

Creating model training functions: Here the data are split into test and training samples. Dataframe Y contains the values based on which the model will make predictions. These are the “start” values (Fig. 8) for the beginning of the road segment. Since all segments are of the same length, this value is sufficient. Year values are also used to track changes in pavement quality over the course of a year. Dataframe Y contains the IRI values themselves. Then, according to the principle of machine learning, the data are split into test and training samples in the proportion of 4 to 1. This is the optimal value since it allows for splitting so that there are more data left for training, but there are also data left for validation.

Model selection, training, tuning and evaluation of results: Model selection is carried out depending on the task (Cano-Ortiz et al., 2022), e.g.: classification, regression, clustering. Examples of models are decision tree, neural networks, linear regressions, support vector methods, etc. (Hosmer et al., 2013). Once the model is defined, it is trained, tuned, and the results are evaluated. If necessary, if the results are unsatisfactory, the model is reconfigured. Besides, when model training is too long or imprecise, it is possible to simplify or complicate it. When the resulting model shows good results, it can be used for practical tasks, and then it is implemented into the original system for which it was created (Gazarov, 2020).

A loss function is used to evaluate the model. With its help, the model “understands” how far it is from the ideal state. The difference between the answers or the resulting values is calculated. Once the loss function has been determined, it is necessary to understand how to fix the model, how to change the weights properly to improve further results. Optimization algorithms are used for this purpose. The main method to minimize the loss function is gradient descent, which, by gradually changing the parameters in the direction, reduces the error. XGBoost is a powerful machine learning model based on the gradient boosting method. It operates by starting from creating a simple model, such as a decision tree, for initial predictions. Next, prediction errors are obtained and new trees trained on the error

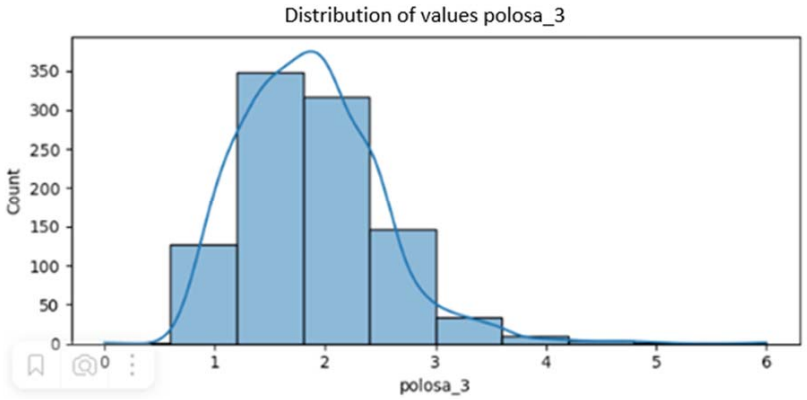

Fig. 7. Distribution of values polosa_3

	start	end	polosa_1	polosa_2	polosa_3	polosa_4	year
0	84.0	84.1	2.7	2.5	1.7	2.0	2013
1	84.1	84.2	2.4	1.9	1.6	2.3	2013
2	84.2	84.3	2.0	1.8	1.8	1.8	2013
3	84.3	84.4	2.4	2.0	1.6	1.8	2013
4	84.4	84.5	1.7	1.8	1.4	1.9	2013
...	...	...	...	...	...	...	...
985	94.5	94.6	2.5	2.3	3.2	2.8	2023
986	94.6	94.7	3.3	2.5	5.0	2.9	2023
987	94.7	94.8	2.8	2.4	4.7	3.1	2023
988	94.8	94.9	2.7	2.4	3.0	2.9	2023
989	94.9	95.0	2.7	2.5	2.9	2.5	2023

Fig. 8. IRI dataframe

are added based on them. These iterations continue until a given number of cycles have been executed or the error is small. When regulation and other optimization methods are used, the model shows good results. Random forest is an ensemble-based machine learning model that differs from the previous one in that it operates by creating multiple decision trees and combining their predictions. Each tree is trained on a random subsample of the input data, which promotes model diversity. Besides, each node partitioning step in the tree uses a random subset of attributes, which adds additional randomness and reduces the correlation between the trees. Once all trees are trained, the model predicts the result for a new observation by aggregating the predictions of all trees: in the case of the classification task, voting is applied, where the final class is determined by a majority vote, and in the regression task — the predictions are averaged. This algorithm is more robust and can show good results too.

The above models are trained on training data and their performance is evaluated on a test sample using the mean_squared_error and r2_score metrics (Shamraeva, 2024). The results are stored in the "results" dictionary. The attribute matrix X includes start and year columns, and the target variables are represented in data columns polosa_1, polosa_2, polosa_3 and polosa_4 (Fig. 8). For each target variable, models are trained and evaluated separately. The results are then displayed on the screen.

Creating a prediction model: New future_years data were created to predict values for the period 2024–2034. New future_years years were generated using the "range" function, and the structure of the new Dataframe was created so that each year is repeated for all unique values of the "start" column from the original data (Fig. 8). This preserves the consistency between the "start" values and the new years. Predictions were made using trained models. The results of the predictions are stored in the "predictions" dictionary.

To further visualize the predictions, graphs were constructed where the years are plotted on the X axis and the predicted values for each target variable are plotted on the Y axis. The mean prediction values for each year were calculated using the "groupby" method and plotted in the graphs. Thus, this process involves data loading, model training and evaluation, and prediction of future values followed by visualization of the results.

The above models showed unsatisfactory results and are not suitable for this task. Another method — linear regression — was tried.

Linear regression is a machine learning method that models linear relationships between a dependent (target) variable and one or more independent variables (attributes) (Hosmer et al., 2013). The model tries to find the best straight line that minimizes the sum of squares of errors among the predicted and actual values of the target variable. This can be achieved by estimating the coefficients of a linear equation, where each coefficient indicates how much the target variable will change if the corresponding attribute is changed by one unit. The training process involves finding coefficients that minimize the MSE using optimization techniques such as the least squares method. As a result, the MSE value amounts to 0.2667. This means that the mean square deviation of the predicted values from the actual ones is 0.2667. The values of the target variable vary within a small range, such as 2 to 6, therefore, the error of 0.2667 may be significant. This shows that this model did quite well in terms of results. However, this is not the best way to predict the IRI evenness — the traffic intensity prediction according to Organization Standard AVTODOR 2.28-2016 should be taken into account.

Predicting changes in traffic intensity

In this study, simple machine learning models, such as linear regression, random forest, gradient boosting, were used for each road direction. After training, visualization of the prediction for each movement was made (Fig. 9). Fig. 9 shows the results of the predictions of different traffic intensity models for the period from 2024 to 2034 covering forward movement. By examining each graph in Fig. 9, we can draw the following conclusions:

1. Linear regression (the model is represented by the blue line) shows the lowest accuracy of predictions; large deviations at the beginning and end of the period are especially noticeable.

2. Random forest (the model is represented by the orange line) shows more accurate predictions compared to linear regression but still has some deviations from the actual values, especially at peak times.

3. Gradient boosting (the model is represented by the green line) most accurately reproduces seasonal variations in traffic intensity and deviates least from the actual values.

It can be seen from the graph (Fig. 9) that traffic intensity has a pronounced seasonal nature with peaks and declines that are most accurately predicted by the gradient boosting model. A neural network was used to refine the results. For its setting, the values are balanced so that no attribute would dominate by its increased mean value.

In the course of this study, a long short-term memory (LSTM) model was created and trained. The LSTM model is a recurrent neural network (RNN) designed to efficiently train and predict time series and sequential data. It is capable of memorizing important information in long sequences and forgetting unnecessary information due to its special architecture consisting of memory cells controlling input, output and forget gates. The input gates decide which information from the current input to keep, the forget gates determine which information to delete from the memory cell, and the output gates regulate which information from the cell will be used to compute the output. This structure allows the LSTM to capture and preserve long-term dependencies. For the prediction task, the LSTM model includes two LSTM layers. The first LSTM layer contains 50 neurons and returns sequences, the second LSTM layer also contains 50 neurons. The LSTM layers are followed by a dense layer with 50 neurons and an activation function (rectifier linear unit (ReLU)), followed by a dense output layer with two neurons to predict two target variables. The results of the neural network training showed that the model was trained for 100 epochs, where 72 steps were performed at each epoch at a rate of about 3 milliseconds per step. In the last few epochs, the loss values in the training sample ranged between 0.0094 and 0.0098, while the loss values in the validation sample remained stable, fluctuating between 0.0106 and 0.0121. The final loss in the test sample was 0.0091, indicating that the model performed well with the training, validation and test samples with minimal variation in loss values.

Next, prediction was made for ten years. The graph (Fig. 10) shows complex relationships with peaks in summer months and declines in winter months. Traffic intensity in both forward and backward directions maintains an overall upward trend. This indicates a projected increase in traffic flow in the future.

Analysis of the results

Prediction of pavement technical condition assessment was made using two approaches:

- based on past years' IRI measurements using a linear regression model,

- based on equation 6.1 of Organization Standard AVTODOR 2.28-2016, using the traffic intensity of future years that was predicted by a neural network model.

Using Python code, predictions of the IRI values for the given years (Fig. 11a) and traffic intensity values (Fig. 11b) were generated using a machine learning model. The results of intensity value predictions are displayed on the screen, showing the date, intensity in forward and backward direction (Fig. 11b).

In this form, the data are ready to plot graphs of monthly forward and backward traffic (Fig. 12) and

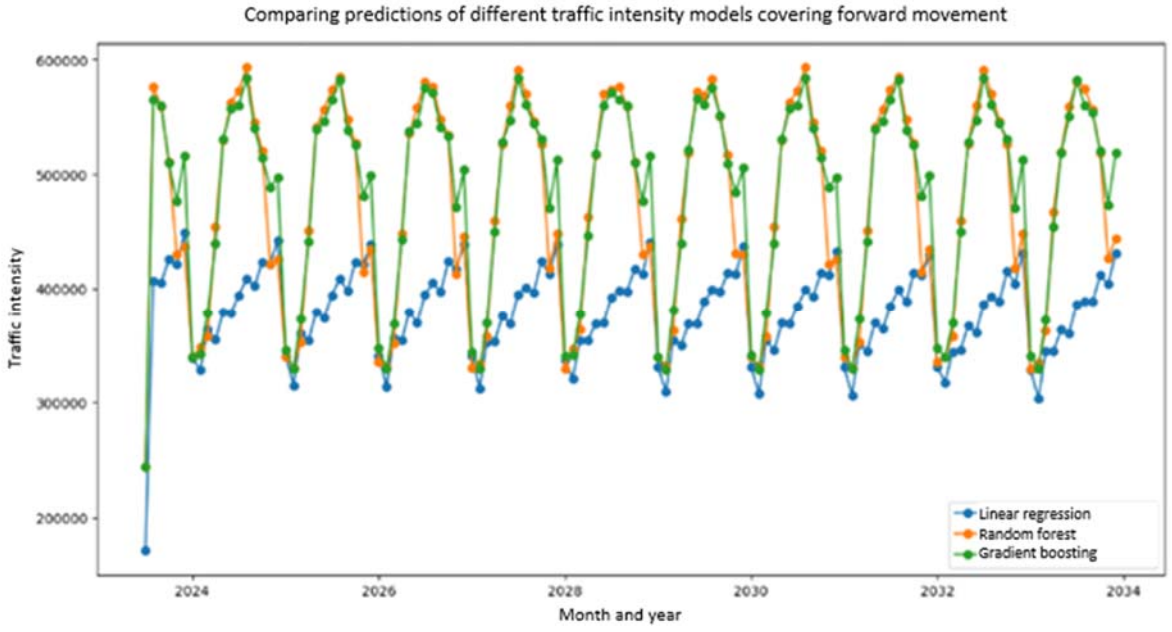

Fig. 9. Comparing predictions of different traffic intensity models covering forward movement

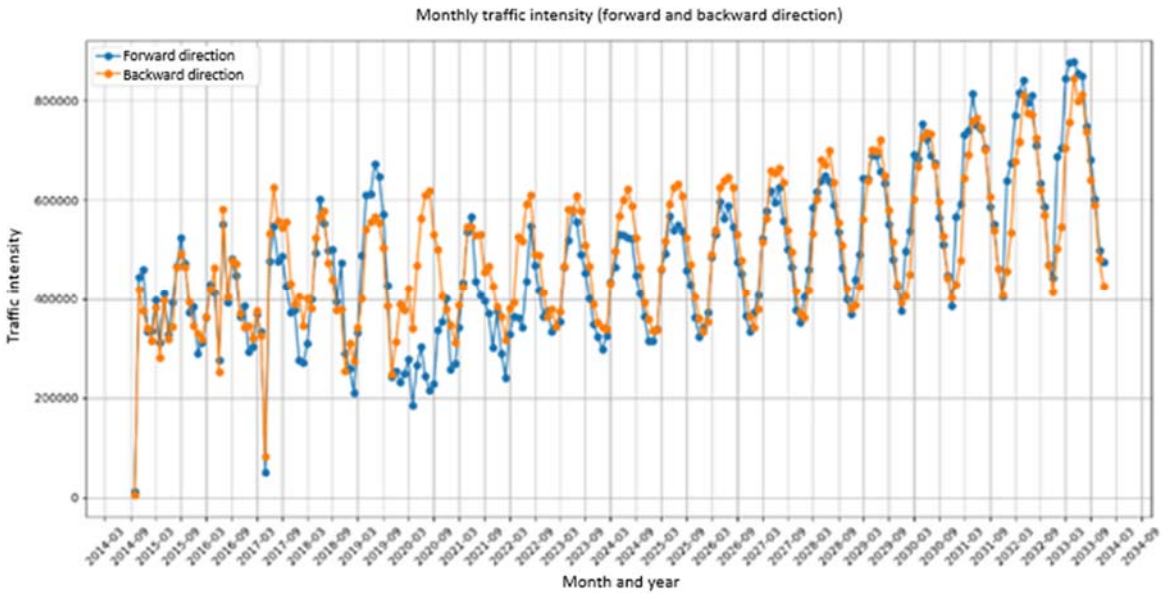

Fig. 10. Intensity prediction

	start	year	polosa_1	polosa_2	polosa_3	polosa_4
0	84.0	2024	3.170604	2.876721	2.659333	3.280827
1	84.1	2024	3.166205	2.871084	2.660291	3.278382
2	84.2	2024	3.161805	2.865447	2.661250	3.275937
3	84.3	2024	3.157406	2.859810	2.662209	3.273491
4	84.4	2024	3.153006	2.854174	2.663168	3.271046
...	...	...	...	...	...	...
1095	94.5	2033	3.688758	2.950728	3.955234	4.344944
1096	94.6	2033	3.684359	2.945091	3.956193	4.342499
1097	94.7	2033	3.679959	2.939454	3.957152	4.340054
1098	94.8	2033	3.675560	2.933817	3.958111	4.337608
1099	94.9	2033	3.671160	2.928181	3.959070	4.335163

a) Prediction results: IRI

```
131/131 [==============================] - 0s 1ms/step
```

	дата	прямое	обратное
0	2023-07-19	13300.680664	16415.083984
1	2023-07-20	16052.410156	15689.279297
2	2023-07-21	21617.058594	15172.226562
3	2023-07-22	19045.304688	17619.160156
4	2023-07-23	8680.833008	25879.925781
...	...	...	...
4179	2034-12-27	17137.482422	12002.160156
4180	2034-12-28	20424.916016	12052.699219
4181	2034-12-29	17821.062500	13173.458984
4182	2034-12-30	12690.513672	16863.751953
4183	2034-12-31	2375.298828	26900.529297

b) Predicting traffic intensity

Fig. 11. Prediction results

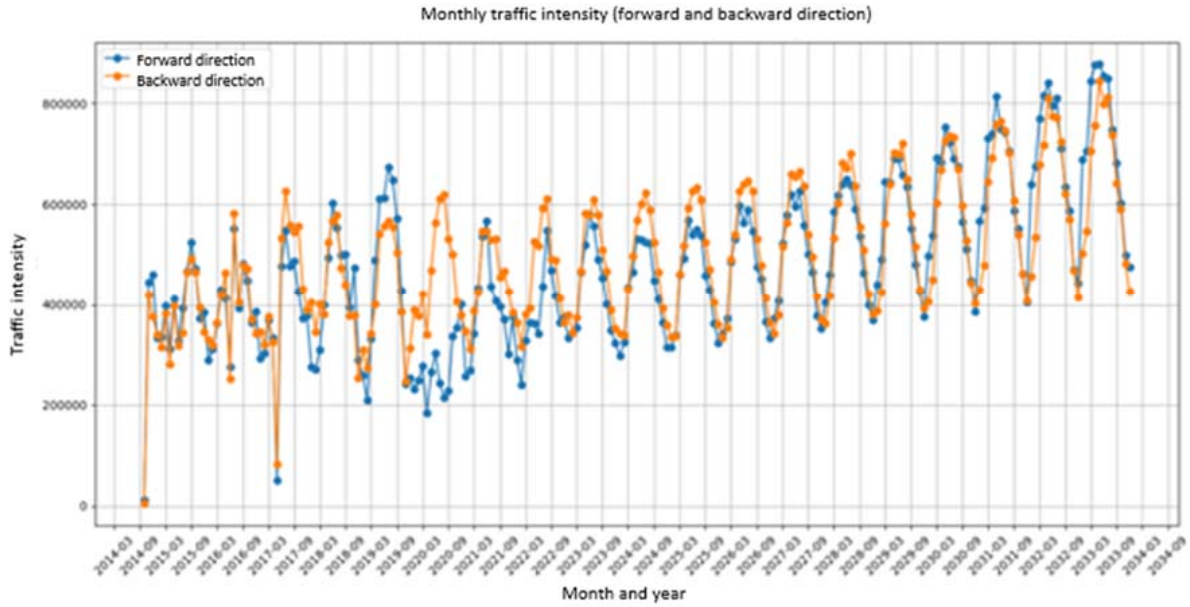

Fig. 12. Predictions of monthly traffic intensity in forward and backward directions through March 2034

draw conclusions with subsequent findings to make recommendations.

The prediction section (Fig. 12) shows that seasonal fluctuations continue, with peaks in summer months and declines in winter months. Traffic intensity in both forward and backward directions maintains an overall upward trend. This indicates a projected increase in traffic flow in the future. The forward (blue line) and backward movement (orange line) continue to show parallel trends with similar seasonal amplitudes. Despite year-to-year fluctuations, the overall trend is upward, which could indicate an expected increase in population or economic activity, or improved infrastructure. In 2033 and 2034, traffic intensity reaches values of approx. 800,000, which is significantly higher than the values in previous years. In general, the forecast indicates a steady increase in transportation intensity despite annual seasonal fluctuations, suggesting the need for further development of transport infrastructure.

To ensure a high level of M-1 Belarus road maintenance, it is necessary to implement measures for the development of transport infrastructure: road reconstruction, including increasing the number of lanes and constructing new interchanges (which will help distribute traffic flows and reduce the load on the existing infrastructure sections), preventive pavement repair to maintain the standard IRI value and ensure high average traffic speed. The analysis also revealed that the composition of traffic would not change. This route is characterized by an equal proportion of various means of transport. Fig. 13 shows a 10-year forecast for the IRI indicator using machine learning for four lanes of the road. Each of the four bar graphs shows the average IRI coefficient for the corresponding lane for the period from 2024 through 2033. Fig. 13a shows that IRI for the first lane gradually increases from 2024 to 2033, starting at about level 3 and reaching a value just above 4. This indicates a gradual deterioration of the pavement condition on the first lane. Fig. 13b shows a similar trend for the second lane, where IRI also gradually increases from just below 3 in 2024 to around 3.5 in 2033, also indicating an increase in pavement roughness. In Fig. 13c, the forecast for the third lane shows an increase in the IRI values from 2024 to 2033, starting at about 2.5 and reaching a value of about 3.5, indicating a deterioration of pavement quality on this lane. Fig. 13d shows an increase in IRI for the fourth lane, starting at just above 2.5 in 2024 and reaching critical values of 4 in 2033, which also indicates significant pavement deterioration.

Fig. 14 shows the 10-year IRI coefficient prediction for the four road lanes on the 86 km of the M-1 highway. Each line on the graph corresponds to one of the lanes: the blue line represents the first lane, the orange — the second, the green — the third, and the red — the fourth. The graph covers the period from 2024 to 2034, indicating a gradual deterioration of the pavement condition.

On the first lane (blue line), IRI increases from approx. 3.0 to 4.5. On the second lane (orange line), IRI starts around 2.8 and reaches approx. 4.2. The third lane (green line) shows an increase in IRI from 3.2 to 4.7. On the fourth lane (red line), IRI values start around 3.5 and increase to 5.5 by 2034. The red dashed line at level 4 on the Y axis indicates the maximum permissible IRI value. All four lanes show an uptrend. Fig. 14 shows that the IRI coefficients for all lanes tend to increase over time. Lane 4 (red line) already exceeded the maximum permissible value and continues to grow faster than the others. Lanes 1, 2, and 3 (blue, orange, and green lines, respectively) also show growth but currently remain below acceptable levels. All lanes show a linear increase in the IRI coefficient, indicating continuous pavement deterioration over the next ten years. The highest rate of deterioration is observed in the fourth lane, while the lowest start and end points are characteristic of the second lane. This highlights the importance of planning financial expenditures for pavement improvement and rehabilitation to slow down the development of bumps and preserve road quality.

In addition to assessing the IRI longitudinal evenness, it is necessary to take into account transverse evenness (rutting) as well since this defect affects the steering ability and assignment of repairs (due to pavement wear). Using equation

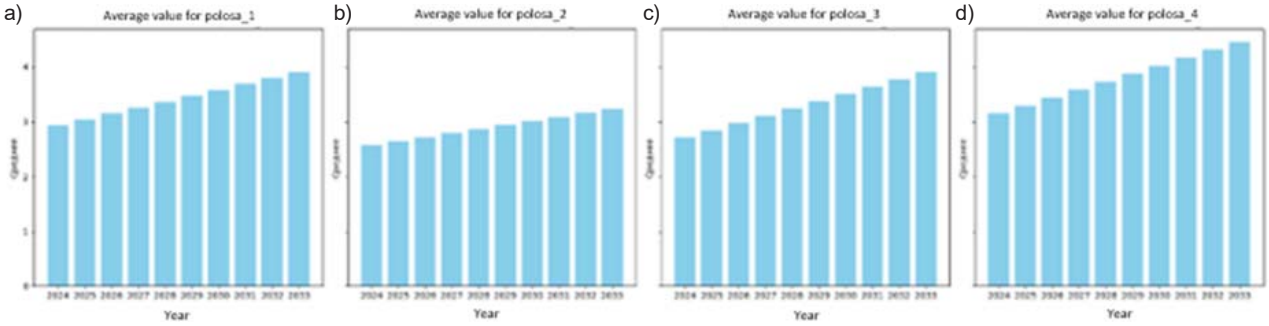

Fig. 13. Predicting the IRI coefficient for 10 years by machine learning

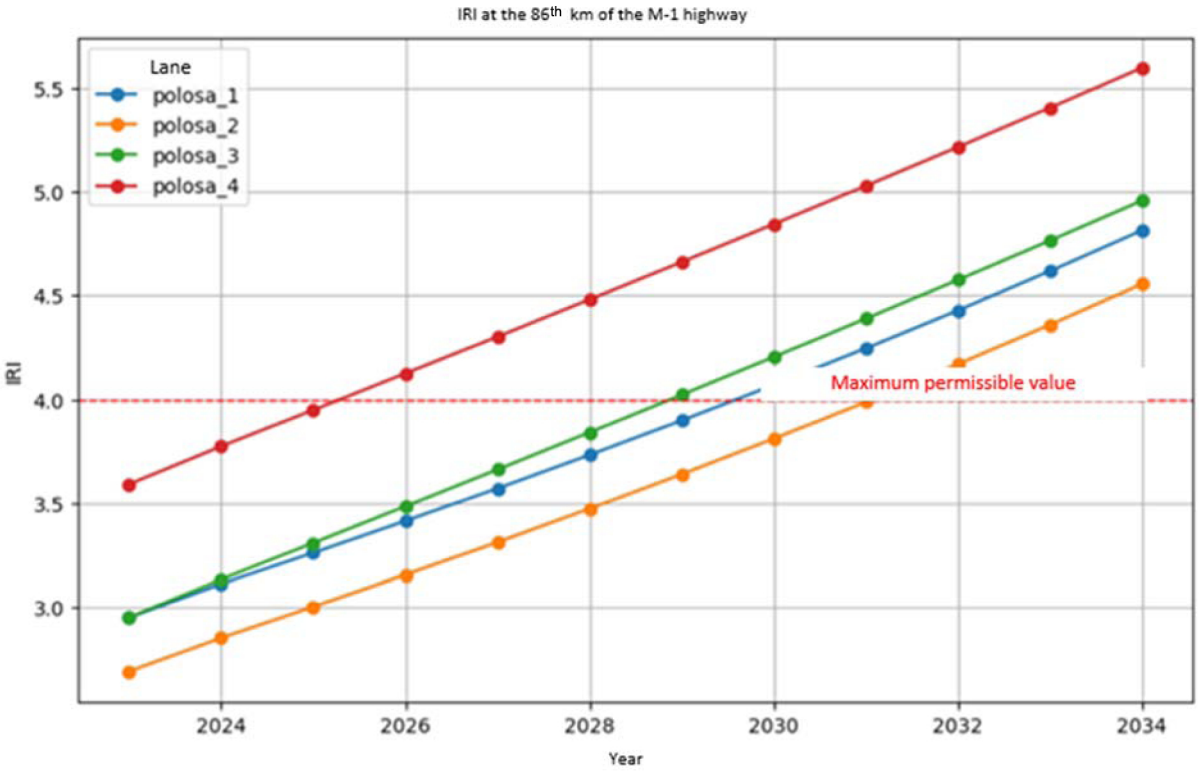

Fig. 14. Traffic intensity prediction: 10-year changes in IRI

6.1 of Organization Standard AVTODOR 2.28-2016 for rutting calculation, changes in transverse evenness (rutting) were forecast (Fig. 15). The graph in Fig. 15 represents a forecast for rutting on the 86 km of the M-1 highway for 10 years into the future. It shows four different lanes, each marked with a different color: blue, orange, green, and red, respectively. The horizontal axis indicates the years from 2024 to 2034, and the vertical axis shows the rutting coefficient in cm. The lines on the graph

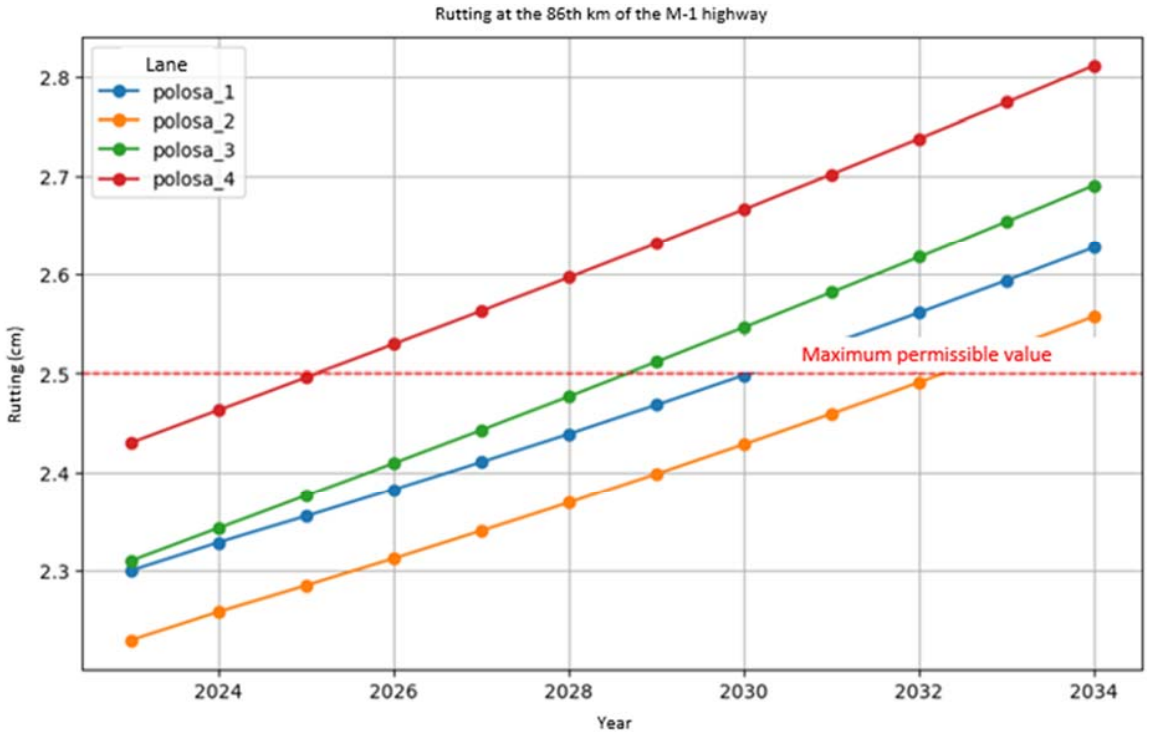

Fig. 15. Forecast of rutting for 10 years

show a linear trend of increasing rutting, indicating continuous pavement deterioration over the forecast period. The fourth lane has the highest level of rutting and shows the greatest rate of increase, which may indicate heavy load or wear. All lanes show a steady increase in rutting over time, indicating a gradual deterioration of the pavement condition.

The first lane (blue line) starts at about 2.4 cm in 2024 and reaches about 2.6 cm by 2032. The second lane (orange line) shows growth from 2.45 cm to just above 2.65 cm over the same period. The third lane (green line) starts around 2.5 cm and grows to about 2.75 cm. The fourth lane (red line) has the highest initial level, about 2.6 cm, and reaches a level of about 2.85 cm by 2032. The red dashed line indicates the maximum permissible rutting value of 2.5 cm. The polosa_4 lane, indicated by the red line, is already exceeding this value by approx. 2025. Lanes 3 and 1, indicated by the green and blue lines, respectively, reach the limit value near the end of the forecast period. Lane 2, indicated by the orange line, remains below the maximum permissible value throughout the forecast period, but also shows a significant increase.

All of the above graphs (Figs. 14–15) emphasize the need for regular pavement monitoring as well as maintenance and repair to slow down the deterioration of the road and ensure safe and comfortable traffic on the M-1 highway. The fourth lane could be out of service in 2025. The first and third lanes expect maintenance in 2029. The second lane will remain intact for ten years.

Conclusion

The relevance of the work is determined by the need to develop an effective strategy for the operation of the road network, ensuring the continuity and safety of traffic. The main objective of the study was to develop an optimal road network repair strategy considering road conditions based on machine learning methods. As a result of this study, the road owner will receive detailed and optimal cost schedules for the planned periods of pavement operation and repair for several years in advance. In addition, the customer will be given the opportunity to make a more accurate calculation of the optimal budget for each stage of repair, allowing for effective financial planning. It can be applied by road authorities to develop a variety of effective solutions that can be easily adapted to new conditions and parameters and will contribute to the rational use of resources and minimize subjective factors in the maintenance planning process. The study has theoretical significance in the development of a road infrastructure condition management strategy model using machine learning methods. Thanks to more accurate and timely diagnostics of the technical condition of the road, it is possible to carry out rehabilitation and repair in advance, which in turn will reduce the cost of overhauls and extend the life of the road.

The implemented deep learning model can be improved, modernized and updated. For instance, one of the development directions could be the use of other neural network architectures or the use of a different type (recurrent or convolutional networks) (Cha et al., 2017) in order to apply other approaches and mathematical algorithms in value prediction tasks (Zari et al., 2015). Besides, this model has the possibility to be extended by adding new class and functional components based on the new assigned tasks and functions in the field of road transportation. These results and basic reasoning show the maximum utility of modern machine learning technologies on real-life examples in the subject area, which once again indicates the importance of developing this direction in the IT sphere in general.

References

Apestin, V. K. (2011). About divergence between design and normative interrepair periods of road pavement service. *Science and Engineering for Highways*, No. 1, pp. 18–20.

Avtodor (2016). *Avtodor State Company Standard. Predicting the condition of operated roads of the Avtodor State Company. Organization Standard AVTODOR 2.28-2016*. Moscow: Avtodor, 26 p.

Cano-Ortiz, S., Pascual-Muñoz, P., and Castro-Fresno, D. (2022). Machine learning algorithms for monitoring pavement performance. *Automation in Construction*. Vol. 139, 104309. DOI: 10.1016/j.autcon.2022.104309.

Cha, Y.-J., Choi, W., and Büyüköztürk, O. (2017). Deep learning-based crack damage detection using convolutional neural networks. *Computer-Aided Civil and Infrastructure Engineering*, Vol. 32, Issue 5, pp. 361–378. DOI: 10.1111/mice.12263.

Gazarov, A. R. (2020). Advantages of using artificial intelligence in the field of construction. *News of the Tula State University. Technical Sciences*, No. 4, pp. 136–139.

Goodfellow, I., Bengio, Y., and Courville, A. (2018). *Deep learning*. 2nd edition. Moscow: DMK Press, 652 p.

Hosmer Jr., D. W., Lemeshov, S., and Sturdivant, R. X. (2013). *Applied logistic regression*. 3rd edition. New York: John Wiley & Sons, 528 p.

Iliopolov, S. K., Seleznev, M. G., and Uglova, Ye. V. (2002). *Dynamics of road structures*. Rostov-on-Don: Rostov State University of Civil Engineering, 258 p.

Interstate Council for Standardization, Metrology and Certification (ISC) (2016). *GOST 33388-2015. Automobile roads of the general use. Requirements to conducting diagnostics and certification*. Moscow: Standartinform, 11 p.

Lasisi, A. and Attoh-Okine, N. (2018). Principal components analysis and track quality index: a machine learning approach. *Transportation Research Part C: Emerging Technologies*, Vol. 91, pp. 230–248. DOI: 10.1016/j.trc.2018.04.001.

Marcelino, P., de Lurdes Antunes, M., Fortunato, E., and Castilho Gomes, M. (2019). Machine learning approach for pavement performance prediction. *International Journal of Pavement Engineering*, Vol. 22, Issue 3, pp. 341–354. DOI: 10.1080/10298436.2019.1609673.

Panthi, K. (2009). *A methodological framework for modeling pavement maintenance costs for projects with performance-based contracts*. PhD Thesis in Civil Engineering. DOI: 10.25148/etd.FI09120824.

Pugachev, I. N., Sheshera, N. G., Grigorov, D. E., and Evtyukov, S. S. (2024). Forecast of traffic flow intensity. Training with a teacher. Random tree method. *T-Comm*, Vol. 18, No. 4, pp. 36–47. DOI: 10.36724/2072-8735-2024-18-4-36-47.

Robinson, R., Danielson, U., and Snaith, M. (1998). *Road maintenance management: concepts and systems*. London: Red Globe Press, 312 p. DOI: 10.1007/978-1-349-14676-5.

Rosavtodor (2018). *Industry road guidance document. Recommendations on diagnostics and assessment of the technical condition of motor roads. ODM 218.4.039-2018*. Moscow: Rosavtodor, 59 p.

Shamraeva, V. V. (2020). Economic efficiency of operation of elements of civil buildings taking into account residual resource: probabilistic-statistical approach. *Modern Science: Actual Problems of Theory and Practice. Series: Economics and Law*, No. 2, pp. 61–68.

Shamraeva, V. V. (2024). Mathematical methods for forecasting stock price changes and their implementation using machine learning methods. *Fundamental Research*, No. 11, pp. 88–96. DOI: 10.17513/fr.43718.

Shamraeva, V. and Savinov, E. (2021). INFRA-BIM for business processes' management in road construction and operation. *Architecture and Engineering*, Vol. 6, No. 3, pp. 19–28. DOI: 10.23968/2500-0055-2021-6-3-19-28.

Stolbov, Yu. V., Stolbova, S. Yu., Pronina, L. A., and Uvarov, A. I. (2017). The provision of the inspections' control accuracy on the IV, V category road basics and coverings by the application of H-3 type niveliers. *Russian Automobile and Highway Industry Journal*, No. 6 (58), pp. 125–132.

Vasilyev, A.P. (2013). *Operation of motor roads*. In 2 volumes. Vol. 2. 3rd edition. Moscow: Academia Publishing Center, 320 p.

Ziari, H., Sobhani, J., Ayoubinejad, J., and Hartmann, T. (2015). Prediction of IRI in short and long terms for flexible pavements: ANN and GMDH methods. *International Journal of Pavement Engineering*, Vol. 17, Issue 9, pp. 776–788. DOI: 10.1080/10298436.2015.1019498.

Znobishchev, S. and Shamraeva, V. (2019). Practical use of BIM modeling for road infrastructure facilities. *Architecture and Engineering*, Vol. 4, No. 3, pp. 49–54. DOI: 10.23968/2500-0055-2019-4-3-49-54.

ОЦЕНКА ТРАНСПОРТНО-ЭКСПЛУАТАЦИОННОГО СОСТОЯНИЯ ДОРОГ НА ОСНОВЕ ДАННЫХ ПЕРЕДВИЖНЫХ ЛАБОРАТОРИЙ МЕТОДАМИ МАШИННОГО ОБУЧЕНИЯ

Виктория Шамраева

Финансовый университет при Правительстве Российской Федерации,
125993, Ленинградский пр-т., 49, Москва, Россия

E-mail: VVShamraeva@fa.ru

Аннотация
Введение. Предметом исследования является прогноз интенсивности движения транспортных средств и состояние дорожного покрытия на линейно протяженном участке автомобильной дороги. В статье рассмотрена модель нейронной сети, посредством которой произведена оценка потребительских свойств участка дороги и его транспортно-эксплуатационных показателей. Объектом исследования является участок дороги М-1 Беларусь, 86-й километр за временной промежуток с 2014 по 2023 годы. **Цель исследования:** описание возможных будущих сценариев состояния дороги, исходя из предсказанных показателей транспортной интенсивности и метрик состояния качества дороги в рамках оценки её потребительских свойств с учётом ровности по показателю International Roughness Index (IRI). **Методы**: Data Science (анализ данных), собранных с передвижных лабораторий, а также алгоритмы машинного обучения (линейная регрессия, градиентный бустинг, случайный лес и нейронные сети на основе Long Short-Term Memory (LSTM)). На выходе создана обученная нейронная сеть, способная спрогнозировать интенсивность транспортного движения на 86 км дороги М-1 Беларусь. Эти методы позволяют выявить скрытые закономерности в данных и обеспечить высокую точность прогнозов. **Результаты:** реализация модели глубокого обучения на примере оценки состояния линейного участка автомобильной дороги позволит решать основные задачи содержания дороги - оптимизировать время и средства при планировании и реализации мероприятий на этапе эксплуатации объектов транспортной инфраструктуры, учитывать возможные риски потери качества состояния дороги при её обновлении и проектировании новых элементов.

Ключевые слова: транспортная инфраструктура; диагностика автомобильных дорог; дефекты; машинное обучение; Data Science; информационная модель дороги.

Guide for Authors
for submitting a manuscript for publication
in the «Architecture and Engineering»

The journal is an electronic media and accepts the manuscripts via the online submission. Please register on the website of the journal http://aej.spbgasu.ru/, log in and press “Submit article” button or send it via email aejeditorialoffice@gmail.com.

Please ensure that the submitted work has neither been previously published nor has been currently submitted for publication in another journal.

Main topics of the journal:

1. Architecture
2. Civil Engineering
3. Geotechnical Engineering and Engineering Geology
4. Urban Planning
5. Technique and Technology of Land Transport in Construction

Title page

The title page should include:

The title of the article in bold (max. 90 characters with spaces, only conventional abbreviations should be used); The name(s) of the author(s); Author’s(s’) affiliation(s); The name of the corresponding author.

Abstract and keywords

Please provide an abstract of 100 to 250 words. The abstract should not contain any undefined abbreviations or unspecified references. Use the IMRAD structure in the abstract (introduction, methods, results, discussion).

Please provide 4 to 6 keywords which can be used for indexing purposes. The keywords should be mentioned in order of relevance.

Main text

It should have the following structure:
1) Introduction,
2) Scope, Objectives and Methodology (with subparagraphs),
3) Results and Discussion (may also include subparagraphs, but should not repeat the previous section or numerical data already presented),
4) Conclusions,
5) Acknowledgements (the section is not obligatory, but should be included in case of participation of people, grants, funds, etc. in preparation of the article. The names of funding organizations should be written in full).

General comments on formatting:

- Subtitles should be printed in Bold,
- Use MathType for equations,
- Tables should be inserted in separate paragraphs. The consecutive number and title of the table should be placed before it in separate paragraphs. The references to the tables should be placed in parentheses (Table 1),
- Use “Top and Bottom” wrapping for figures. Figure captions should be placed in the main text after the image. Figures should be referred to as (Fig. 1) in the text.

References

The journal uses Harvard (author, date) style for references:
- The recent research (Kent and Park, 1990)...
- V. Zhukov (1999) stated that…

Reference list

The list of references should only include works that are cited in the text and that have been published or accepted for publication. Personal communications and unpublished works should only be mentioned in the text. Do not use footnotes or endnotes as a substitute for a proper reference list. All references must be listed in full at the end of the paper in alphabetical order, irrespective of where they are cited in the text. Reference made to sources published in languages other than English or Russian should contain English translation of the original title together with a note of the used language.

Peer Review Process

Articles submitted to the journal undergo a double blind peer-review procedure, which means that the reviewer is not informed about the identity of the author of the article, and the author is not given information about the reviewer.
On average, the review process takes from one to five months.